

# TELEMAC-3D

## Validation Manual

Version v8p3  
December 6, 2021



# Contents

<b>1</b>	<b>Buoyant tracer (Cooper)</b>	<b>11</b>
<b>1.1</b>	<b>Purpose</b>	<b>11</b>
<b>1.2</b>	<b>Description</b>	<b>11</b>
1.2.1	Initial and Boundary Conditions .....	11
1.2.2	Mesh and numerical parameters .....	12
1.2.3	Physical parameters .....	12
<b>1.3</b>	<b>Results</b>	<b>13</b>
<b>1.4</b>	<b>Comments</b>	<b>14</b>
<b>1.5</b>	<b>Conclusion</b>	<b>14</b>
<b>2</b>	<b>Dingemans wave over a bar (NonLinearWave)</b>	<b>15</b>
<b>2.1</b>	<b>Purpose</b>	<b>15</b>
<b>2.2</b>	<b>Description</b>	<b>15</b>
2.2.1	Initial and Boundary Conditions .....	15
2.2.2	Mesh and numerical parameters .....	16
2.2.3	Physical parameters .....	16
<b>2.3</b>	<b>Results</b>	<b>16</b>
<b>2.4</b>	<b>Conclusion</b>	<b>17</b>
<b>3</b>	<b>Non cohesive suspended sediment transport (Rouse)</b>	<b>18</b>
<b>3.1</b>	<b>Purpose</b>	<b>18</b>
<b>3.2</b>	<b>Description</b>	<b>18</b>
3.2.1	Initial and Boundary Conditions .....	18
3.2.2	Mesh and numerical parameters .....	19
3.2.3	Physical parameters .....	20
<b>3.3</b>	<b>Results</b>	<b>20</b>
<b>3.4</b>	<b>Conclusion</b>	<b>21</b>

<b>4</b>	<b>Stability of vertical density in a V-shaped channel (V) . . . . .</b>	<b>22</b>
<b>4.1</b>	<b>Description</b>	<b>22</b>
4.1.1	Initial and boundary conditions . . . . .	22
4.1.2	Mesh and numerical parameters . . . . .	23
<b>4.2</b>	<b>Results</b>	<b>23</b>
<b>5</b>	<b>Violet . . . . .</b>	<b>28</b>
<b>5.1</b>	<b>Purpose</b>	<b>28</b>
<b>5.2</b>	<b>Description</b>	<b>28</b>
5.2.1	Reference . . . . .	28
5.2.2	Geometry and Mesh . . . . .	28
5.2.3	Physical parameters . . . . .	28
5.2.4	Initial and Boundary Conditions . . . . .	29
5.2.5	General parameters . . . . .	29
5.2.6	Numerical parameters . . . . .	29
5.2.7	Comments . . . . .	29
<b>5.3</b>	<b>Results</b>	<b>29</b>
<b>5.4</b>	<b>Conclusion</b>	<b>30</b>
<b>6</b>	<b>Wesel . . . . .</b>	<b>31</b>
<b>6.1</b>	<b>Purpose</b>	<b>31</b>
<b>6.2</b>	<b>Description</b>	<b>31</b>
6.2.1	Geometry and mesh . . . . .	31
6.2.2	Initial condition . . . . .	31
6.2.3	Boundary conditions . . . . .	31
6.2.4	Physical parameters . . . . .	31
6.2.5	Numerical parameters . . . . .	32
<b>6.3</b>	<b>Results</b>	<b>32</b>
<b>6.4</b>	<b>Conclusion</b>	<b>33</b>
<b>7</b>	<b>Automatic Mesh Displacement (amr) . . . . .</b>	<b>36</b>
<b>7.1</b>	<b>Purpose</b>	<b>36</b>
<b>7.2</b>	<b>Description</b>	<b>36</b>
7.2.1	Geometry and Mesh . . . . .	36
7.2.2	Numerical parameters . . . . .	36
<b>7.3</b>	<b>Reference</b>	<b>36</b>
<b>7.4</b>	<b>Results</b>	<b>36</b>
<b>7.5</b>	<b>Conclusion</b>	<b>38</b>
<b>8</b>	<b>Flow along a bend (bendrans) . . . . .</b>	<b>39</b>
<b>8.1</b>	<b>Description</b>	<b>39</b>
8.1.1	Initial and boundary conditions . . . . .	39

8.1.2	Mesh and numerical parameters .....	39
8.1.3	Physical parameters .....	39
<b>8.2</b>	<b>Results</b>	<b>41</b>
<b>8.3</b>	<b>Conclusion</b>	<b>44</b>
<b>9</b>	<b>Bergenmeersen test case .....</b>	<b>45</b>
<b>9.1</b>	<b>Purpose</b>	<b>45</b>
<b>9.2</b>	<b>Description</b>	<b>45</b>
9.2.1	Measurements .....	47
<b>9.3</b>	<b>Computational options</b>	<b>47</b>
9.3.1	Mesh .....	47
9.3.2	Initial and boundary conditions .....	48
9.3.3	Numerical parameters .....	48
9.3.4	Culvert parameters .....	48
<b>9.4</b>	<b>Results</b>	<b>49</b>
<b>10</b>	<b>bottom_bc .....</b>	<b>53</b>
<b>10.1</b>	<b>Purpose</b>	<b>53</b>
<b>10.2</b>	<b>Description of the problem</b>	<b>53</b>
10.2.1	Geometry and Mesh .....	53
10.2.2	Initial and Boundary Conditions .....	53
10.2.3	Numerical parameters .....	53
<b>10.3</b>	<b>Results</b>	<b>54</b>
<b>11</b>	<b>Flow over a bump (bump) .....</b>	<b>55</b>
<b>11.1</b>	<b>Description</b>	<b>55</b>
11.1.1	Initial and boundary conditions .....	55
11.1.2	Mesh and numerical parameters .....	57
<b>11.2</b>	<b>Results</b>	<b>58</b>
<b>11.3</b>	<b>Reference</b>	<b>60</b>
<b>12</b>	<b>Equilibrium of a stratified flow above a bump (bump_static) ...</b>	<b>61</b>
<b>12.1</b>	<b>Purpose</b>	<b>61</b>
<b>12.2</b>	<b>Description</b>	<b>61</b>
<b>12.3</b>	<b>Computational options</b>	<b>62</b>
12.3.1	Mesh .....	62
12.3.2	Physical parameters .....	64
12.3.3	Initial and Boundary Conditions .....	64
12.3.4	General parameters .....	64
12.3.5	Numerical parameters .....	64
<b>12.4</b>	<b>Results</b>	<b>65</b>
<b>12.5</b>	<b>Conclusion</b>	<b>65</b>

<b>13</b>	<b>Flow in a channel with bottom friction (canal) .....</b>	<b>66</b>
<b>13.1</b>	<b>Description</b>	<b>66</b>
13.1.1	Initial and boundary conditions .....	66
13.1.2	Mesh and numerical parameters .....	67
<b>13.2</b>	<b>Results</b>	<b>68</b>
<b>13.3</b>	<b>Conclusion</b>	<b>69</b>
<b>14</b>	<b>Advection of tracers with a rotating cone (cone) .....</b>	<b>70</b>
<b>14.1</b>	<b>Purpose</b>	<b>70</b>
<b>14.2</b>	<b>Description</b>	<b>70</b>
14.2.1	Geometry and mesh .....	70
14.2.2	Initial condition .....	71
14.2.3	Analytic solution .....	71
14.2.4	Physical parameters .....	71
14.2.5	Numerical parameters .....	71
<b>14.3</b>	<b>Results</b>	<b>72</b>
14.3.1	Comparison of schemes .....	72
14.3.2	Maximum principle .....	75
<b>14.4</b>	<b>Conclusion</b>	<b>75</b>
<b>15</b>	<b>Schematic culvert test case (culvert) .....</b>	<b>76</b>
<b>15.1</b>	<b>Purpose</b>	<b>76</b>
<b>15.2</b>	<b>Description</b>	<b>76</b>
<b>15.3</b>	<b>Computational options</b>	<b>76</b>
15.3.1	Mesh .....	76
15.3.2	Initial and boundary conditions .....	76
15.3.3	Numerical parameters .....	77
15.3.4	Culvert characteristics .....	77
<b>15.4</b>	<b>Results</b>	<b>78</b>
<b>16</b>	<b>One way chaining with DELWAQ (delwaq) .....</b>	<b>80</b>
<b>16.1</b>	<b>Description</b>	<b>80</b>
16.1.1	Initial and boundary conditions .....	80
16.1.2	Mesh and numerical parameters .....	81
16.1.3	Physical parameters .....	82
<b>16.2</b>	<b>Results</b>	<b>82</b>
<b>16.3</b>	<b>Conclusion</b>	<b>83</b>
<b>17</b>	<b>depot .....</b>	<b>84</b>
<b>18</b>	<b>erosion_flume .....</b>	<b>85</b>

<b>19</b>	<b>flume_slope .....</b>	<b>86</b>
<b>20</b>	<b>Gaussian water surface with reflecting boundary conditions (gouttedo) .....</b>	<b>87</b>
<b>20.1</b>	<b>Description</b>	<b>87</b>
20.1.1	Initial and boundary conditions .....	87
20.1.2	Mesh and numerical parameters .....	87
<b>20.2</b>	<b>Results</b>	<b>89</b>
<b>21</b>	<b>Gaussian water surface with open boundary conditions (thompson) .....</b>	<b>91</b>
<b>21.1</b>	<b>Description</b>	<b>91</b>
21.1.1	Initial and boundary conditions .....	91
21.1.2	Mesh and numerical parameters .....	91
<b>21.2</b>	<b>Results</b>	<b>93</b>
<b>22</b>	<b>Lock-exchange .....</b>	<b>95</b>
<b>22.1</b>	<b>Purpose</b>	<b>95</b>
<b>22.2</b>	<b>Description</b>	<b>95</b>
<b>22.3</b>	<b>Preamble – an attempt at reproducing Adduce <i>et al.</i>'s experiments</b>	<b>96</b>
<b>22.4</b>	<b>Case setup</b>	<b>96</b>
22.4.1	Geometry and mesh .....	96
22.4.2	Physical parameters .....	97
22.4.3	Initial and Boundary Conditions .....	98
22.4.4	General parameters .....	98
22.4.5	Numerical parameters .....	98
<b>22.5</b>	<b>Reference results</b>	<b>99</b>
<b>22.6</b>	<b>Results</b>	<b>100</b>
22.6.1	Dynamic pressure not included in the wave equation .....	100
22.6.2	Dynamic pressure included in the wave equation .....	105
22.6.3	Hydrostatic hypothesis .....	107
<b>22.7</b>	<b>Conclusion</b>	<b>107</b>
<b>23</b>	<b>Malpasset dambreak (malpasset) .....</b>	<b>109</b>
<b>23.1</b>	<b>Purpose</b>	<b>109</b>
<b>23.2</b>	<b>Description</b>	<b>109</b>
23.2.1	Geometry and Mesh .....	110
23.2.2	Bathymetry .....	111
23.2.3	Numerical parameters .....	111
23.2.4	Initial conditions .....	111
23.2.5	Boundary conditions .....	111
23.2.6	Cases .....	112
23.2.7	Physical parameters .....	112

<b>23.3</b>	<b>Results</b>	<b>112</b>
23.3.1	First observations . . . . .	112
23.3.2	Comparison of schemes . . . . .	116
<b>23.4</b>	<b>Conclusion</b>	<b>121</b>
<b>24</b>	<b>Particles transport (particules)</b> . . . . .	<b>122</b>
<b>24.1</b>	<b>Purpose</b>	<b>122</b>
<b>24.2</b>	<b>Description</b>	<b>122</b>
24.2.1	Initial and boundary conditions . . . . .	122
24.2.2	Mesh and numerical parameters . . . . .	123
24.2.3	Physical parameters . . . . .	123
<b>24.3</b>	<b>Results</b>	<b>124</b>
<b>25</b>	<b>Flow in a channel with 2 bridge piers (pildepon)</b> . . . . .	<b>125</b>
<b>25.1</b>	<b>Purpose</b>	<b>125</b>
<b>25.2</b>	<b>Description</b>	<b>125</b>
25.2.1	Initial and Boundary Conditions . . . . .	125
25.2.2	Mesh and numerical parameters . . . . .	126
25.2.3	Physical parameters . . . . .	127
<b>25.3</b>	<b>Results</b>	<b>127</b>
<b>25.4</b>	<b>Conclusion</b>	<b>129</b>
<b>26</b>	<b>Flow along a beach (plage)</b> . . . . .	<b>130</b>
<b>26.1</b>	<b>Purpose</b>	<b>130</b>
<b>26.2</b>	<b>Description</b>	<b>130</b>
26.2.1	Initial and Boundary Conditions . . . . .	130
26.2.2	Mesh and numerical parameters . . . . .	131
26.2.3	Physical parameters . . . . .	131
<b>26.3</b>	<b>Results</b>	<b>131</b>
<b>27</b>	<b>Salinity during a rain fall (pluie)</b> . . . . .	<b>133</b>
<b>27.1</b>	<b>Description</b>	<b>133</b>
27.1.1	Initial and boundary conditions . . . . .	133
27.1.2	Mesh and numerical parameters . . . . .	133
<b>27.2</b>	<b>Results</b>	<b>135</b>
<b>28</b>	<b>Solitary wave (solit)</b> . . . . .	<b>137</b>
<b>28.1</b>	<b>Purpose</b>	<b>137</b>
<b>28.2</b>	<b>Notations</b>	<b>137</b>
<b>28.3</b>	<b>Theory</b>	<b>137</b>

<b>28.4 Description</b>	<b>138</b>
28.4.1 Geometry and Mesh . . . . .	138
28.4.2 Physical parameters . . . . .	139
28.4.3 Initial and Boundary Conditions . . . . .	139
28.4.4 General parameters . . . . .	139
28.4.5 Numerical parameters . . . . .	139
<b>28.5 Results</b>	<b>140</b>
<b>28.6 Conclusion</b>	<b>141</b>
<b>29 Sources of fluid and tracers (source) . . . . .</b>	<b>142</b>
<b>29.1 Description</b>	<b>142</b>
29.1.1 Initial and boundary conditions . . . . .	142
29.1.2 Mesh and numerical parameters . . . . .	143
<b>29.2 Results</b>	<b>143</b>
<b>30 Wind forced channel flow (stratif_wind) . . . . .</b>	<b>149</b>
<b>30.1 Purpose</b>	<b>149</b>
<b>30.2 Description</b>	<b>149</b>
<b>30.3 Computational options</b>	<b>149</b>
30.3.1 Mesh . . . . .	149
30.3.2 Physical parameters . . . . .	150
30.3.3 Initial and Boundary Conditions . . . . .	151
30.3.4 General parameters . . . . .	151
30.3.5 Numerical parameters . . . . .	151
<b>30.4 Expected results</b>	<b>151</b>
<b>30.5 Results</b>	<b>152</b>
<b>30.6 Conclusion</b>	<b>153</b>
<b>31 Stability of a stratified flow (stratification) . . . . .</b>	<b>154</b>
<b>31.1 Description</b>	<b>154</b>
31.1.1 Initial and Boundary Conditions . . . . .	154
31.1.2 Mesh and numerical parameters . . . . .	157
<b>31.2 Results</b>	<b>157</b>
<b>32 Discretisation with tetrahedra elements (tetra) . . . . .</b>	<b>162</b>
<b>32.1 Purpose</b>	<b>162</b>
<b>32.2 Description</b>	<b>162</b>
32.2.1 Initial and Boundary Conditions . . . . .	162
32.2.2 Mesh and numerical parameters . . . . .	163
32.2.3 Physical parameters . . . . .	163
<b>32.3 Results</b>	<b>164</b>
<b>32.4 Conclusion</b>	<b>165</b>

<b>33</b>	<b>tidal_flats .....</b>	<b>166</b>
<b>34</b>	<b>Propagation of tide prescribed by boundary conditions (tide) .....</b>	<b>167</b>
<b>34.1</b>	<b>Purpose .....</b>	<b>167</b>
<b>34.2</b>	<b>Description .....</b>	<b>167</b>
34.2.1	Geometry and Mesh .....	167
34.2.2	Bathymetry .....	168
34.2.3	Initial conditions .....	168
34.2.4	Boundary conditions .....	168
34.2.5	Physical parameters .....	169
34.2.6	Numerical parameters .....	169
34.2.7	Comments .....	169
<b>34.3</b>	<b>Results .....</b>	<b>169</b>
<b>34.4</b>	<b>Conclusion .....</b>	<b>171</b>
<b>35</b>	<b>Tracer submitted to wetting and drying (tracer_wet_dry) .....</b>	<b>172</b>
<b>35.1</b>	<b>Purpose .....</b>	<b>172</b>
<b>35.2</b>	<b>Description .....</b>	<b>172</b>
35.2.1	Geometry and Mesh .....	172
35.2.2	Bathymetry .....	173
35.2.3	Numerical parameters .....	173
35.2.4	Initial conditions .....	173
35.2.5	Boundary conditions .....	173
35.2.6	Cases .....	173
35.2.7	Physical parameters .....	174
<b>35.3</b>	<b>Results .....</b>	<b>174</b>
35.3.1	First observations .....	174
35.3.2	Comparison of schemes .....	175
<b>35.4</b>	<b>Conclusion .....</b>	<b>179</b>
<b>36</b>	<b>Solitary wave propagation over an uneven bottom (uneven) .....</b>	<b>180</b>
<b>36.1</b>	<b>Purpose .....</b>	<b>180</b>
<b>36.2</b>	<b>Description .....</b>	<b>180</b>
36.2.1	Initial and Boundary Conditions .....	180
36.2.2	Mesh and numerical parameters .....	181
36.2.3	Physical parameters .....	181
<b>36.3</b>	<b>Results .....</b>	<b>182</b>
<b>37</b>	<b>Uncovering of a beach (vasque) .....</b>	<b>183</b>
<b>37.1</b>	<b>Purpose .....</b>	<b>183</b>
<b>37.2</b>	<b>Description .....</b>	<b>183</b>
37.2.1	Geometry and mesh .....	183
37.2.2	Physical parameters .....	184

37.2.3 Initial and boundary conditions . . . . .	184
37.2.4 Numerical parameters . . . . .	185
<b>37.3 Results</b>	<b>185</b>
<b>37.4 Conclusion</b>	<b>185</b>
<b>38 Flow in a channel submitted to wind (vent) . . . . .</b>	<b>186</b>
<b>38.1 Description</b>	<b>186</b>
38.1.1 Initial and Boundary Conditions . . . . .	187
38.1.2 Mesh and numerical parameters . . . . .	187
<b>38.2 Results</b>	<b>187</b>
<b>38.3 Reference</b>	<b>191</b>
<b>Bibliography . . . . .</b>	<b>192</b>

# 1. Buoyant tracer (Cooper)

## 1.1 Purpose

This test demonstrates the ability of TELEMAC-3D to model the buoyancy of an active tracer.

## 1.2 Description

We consider a square channel of 4,000 m side with a flat bottom at  $z = -10$  m with a bump at  $z = -6$  m in the middle ( $x = 2,000$  m;  $y = 2,000$  m) (see Figure 1.1). The source of tracer is located above the bump at  $z = -5$  m.

We observe the buoyancy of the active tracer.

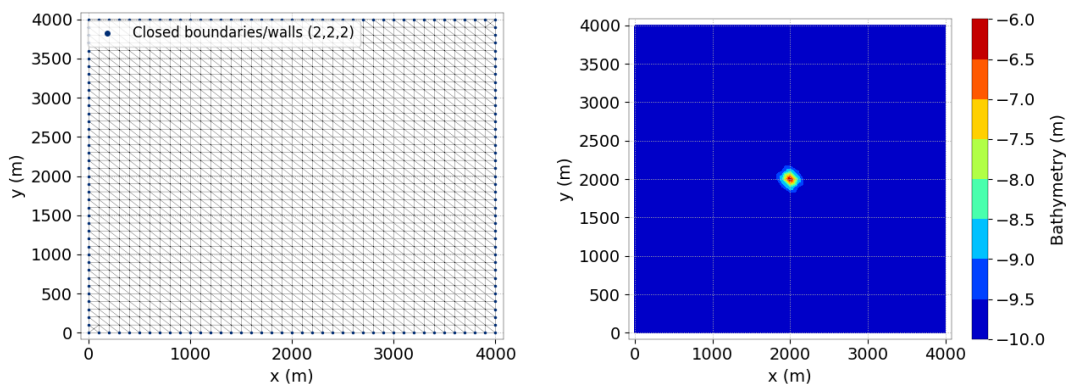


Figure 1.1: Horizontal mesh and bathymetry.

### 1.2.1 Initial and Boundary Conditions

The computation is initialised with a constant elevation equal to 0 m and no velocity. The initial value of tracer is 0 everywhere. See Figure 1.2.

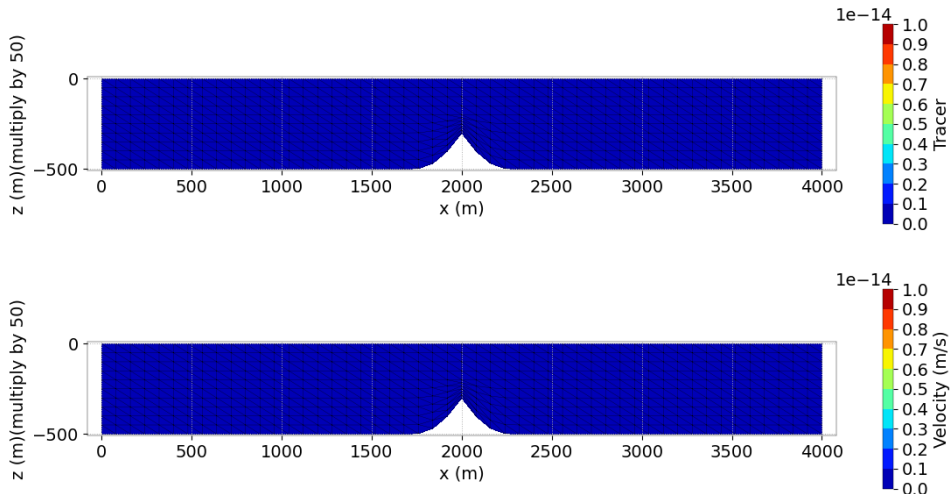


Figure 1.2: Initial state Tracer (up) and velocity (bottom).

The boundary conditions (closed boundaries) are:

- For the solid walls, a slip condition on channel banks is used for the velocities,
- On the bottom, a Nikuradse's formula with asperities of 0.01 m is prescribed.

Tracer discharge at source is equal to  $20.0 \text{ m}^3/\text{s}$  whereas tracer value at source is  $333.33 \text{ g/L}$  or  $\text{kg/m}^3$ .

### 1.2.2 Mesh and numerical parameters

The 2D mesh (Figure 1.1) is made of 3,204 triangular elements (1,683 nodes).

11 fixed planes are regularly spaced in the vertical direction with the 7th plane fixed at -4 m (see Figure 1.3).

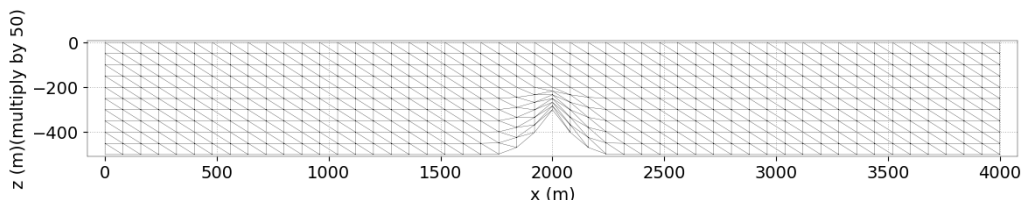


Figure 1.3: Vertical mesh.

The non-hydrostatic version of TELEMAC-3D is used.

To solve the advection, the N-type MURD scheme (scheme #4) is used for both velocities and tracer.

The time step is 5 s for a simulated period of 30 min (= 1,800 s).

### 1.2.3 Physical parameters

Constant diffusion of velocity:

- Horizontal:  $10^{-4} \text{ m}^2/\text{s}$ ,

- Vertical: no.

Constant diffusion of tracer:

- Horizontal: no,
- Vertical:  $0.1 \text{ m}^2/\text{s}$ .

Tracer density law specifying a  $\beta$  spatial expansion coefficient of  $0.0003 \text{ K}^{-1}$  and a standard value of the tracer of 0.0.

### 1.3 Results

Figure 1.5 highlights that the buoyancy of the active tracer generates vertical velocities, thus establishing a large recirculation around the bump. This is not due to the injected flow rate.

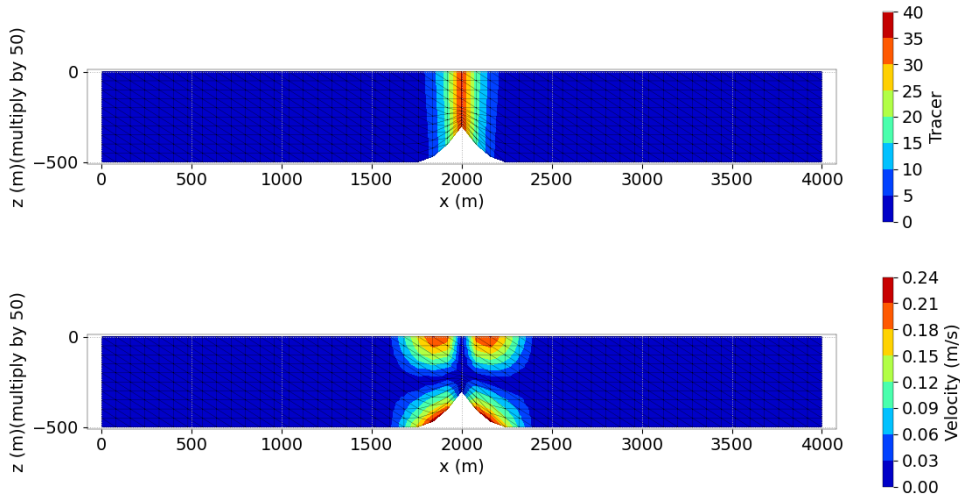


Figure 1.4: Final state Tracer (up) and velocity (bottom).

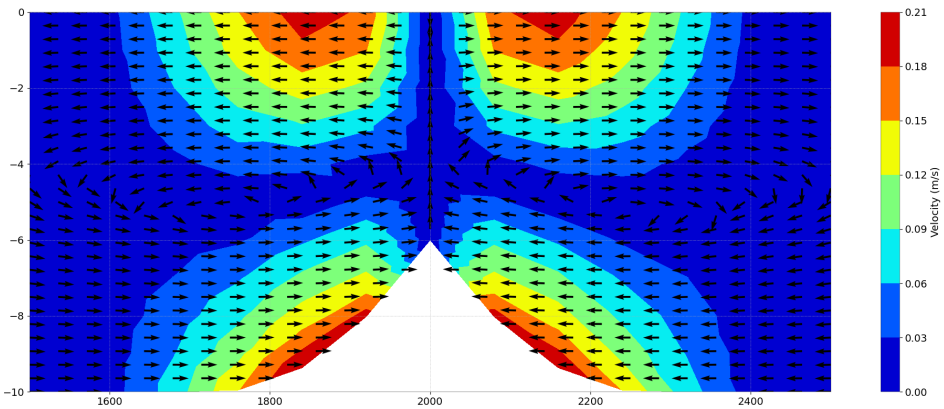


Figure 1.5: Vectorial view of celerity with a zoom.

Mass balance of the log file after 1,800 s:

```

--- WATER ---
INITIAL MASS : 0.1598743E+09
FINAL MASS : 0.1599103E+09
MASS LEAVING THE DOMAIN (OR SOURCE) : -36000.00
MASS LOSS : 0.4833937E-04
--- TRACER 1 ---
INITIAL MASS : 0.000000
FINAL MASS : 0.1199988E+08
MASS EXITING (BOUNDARIES OR SOURCE) : -0.1199988E+08
MASS LOSS : -0.5826335E-03

```

The amount of water injected by the source is correct:  $20 \text{ m}^3/\text{s} \times 1,800 \text{ s} = 36,000 \text{ m}^3$  The amount of tracer injected is correct:  $333.33 \text{ kg/m}^3 \times 20 \text{ m}^3/\text{s} \times 1,800 \text{ s} = 1.19999 \cdot 10^7 \text{ kg}$

## 1.4 Comments

The tested steering file is “t3d\_cooper.cas”. The cases “t3d\_cooper-hyd.cas” & “t3d\_cooper-supg.cas” have been deleted just after the V8P0 release.

## 1.5 Conclusion

TELEMAC-3D simulates correctly the buoyancy of an active tracer.

## 2. Dingemans wave over a bar (NonLinearWave)

### 2.1 Purpose

This test demonstrates the ability of TELEMAC-3D to simulate the evolution of a monochromatic linear wave over a bar. This test case corresponds to a physical model and measurements published by Dingemans (conditions C) [5].

### 2.2 Description

The configuration is a tank 32 m long and 0.3 m wide. The evolution of the topography along the channel is presented in Figure 2.1. It represents a bar. A wave is imposed at the entrance of the channel. The goal is to simulate the evolution of this wave when propagating over the bar.

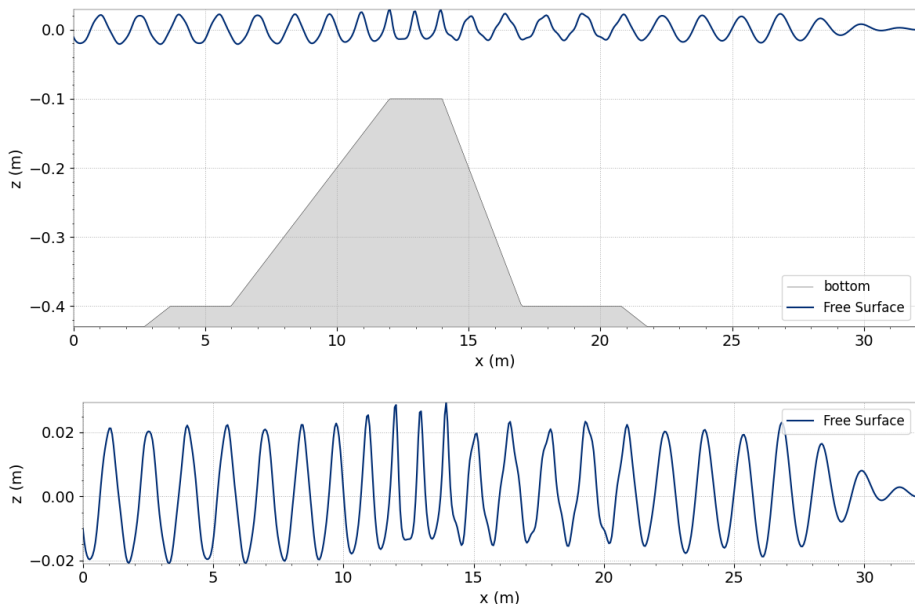


Figure 2.1: Free surface and bottom at the end of simulation.

#### 2.2.1 Initial and Boundary Conditions

The computation is initialised with a constant elevation equal to 0 m and no velocity.

The boundary conditions are only closed lateral boundaries:

- For the solid walls, a slip condition on channel banks is used for the velocities,
- No bottom friction,
- Upstream a wave is imposed at the entrance (amplitude 0.04 m).

### 2.2.2 Mesh and numerical parameters

The 2D mesh is made of 7,680 triangular elements (5,124 nodes).

10 planes are regularly spaced in the vertical direction (see Figure 2.2).

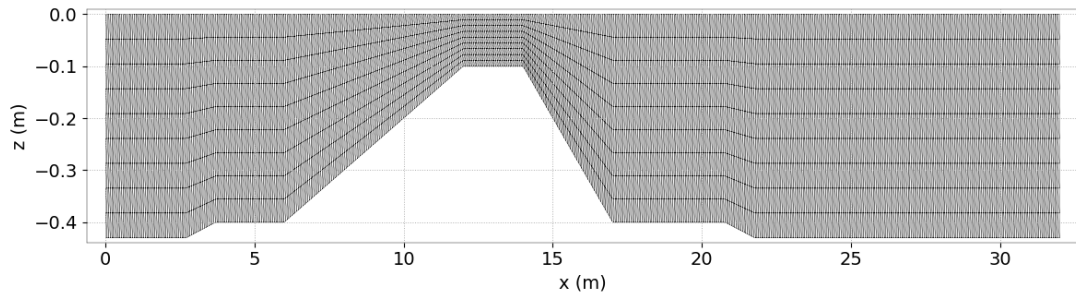


Figure 2.2: Initial vertical mesh along  $y = 0.15$  m.

The non-hydrostatic version of TELEMAC-3D is used.

To solve the advection, the N-type MURD scheme (scheme #4) is used for velocities. The implicitation coefficients for depth and velocities are equal to 0.5 to be accurate.

The time step is 0.0025 s for a simulated period of 33 s.

### 2.2.3 Physical parameters

No diffusion is considered.

## 2.3 Results

Figure 2.1 presents the general shape of the free surface at the end of the simulation.

Figure 2.3 presents a comparison of the TELEMAC simulation and the experimental results at various locations in the channel. This comparison shows a very good agreement between results and measurements which is comparable to the one obtained with 1D Boussinesq models as published in [4].

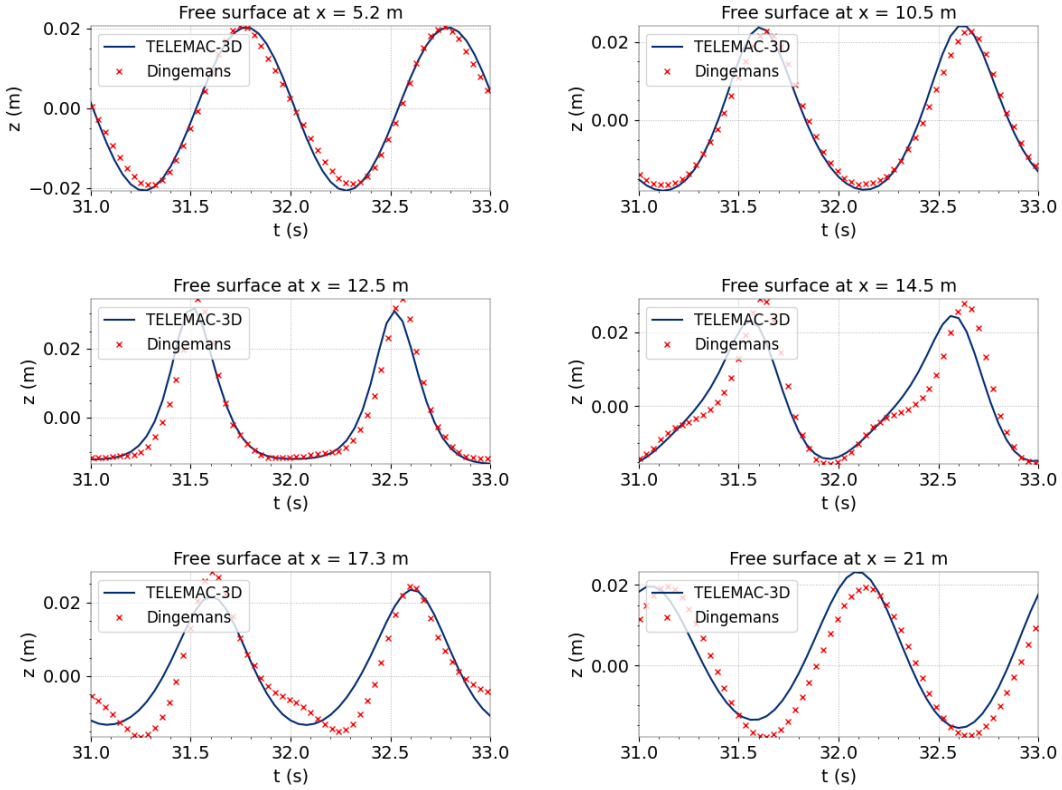


Figure 2.3: Comparison with measurements of Dingemans.

## 2.4 Conclusion

TELEMAC-3D simulates correctly the evolution of a wave on a bar.

### 3. Non cohesive suspended sediment transport (Rouse)

#### 3.1 Purpose

This test validates the modelling of the hydrodynamics and non-cohesive suspended sediment transport, in a permanent and uniform flow. We compare the mean flow velocities to the logarithmic profile and the sediment concentration to an analytical solution derived from the Rouse profile [8].

#### 3.2 Description

It consists of a steady and uniform flow in a rectangular channel ( $500\text{ m} \times 100\text{ m}$ ) with constant slope, without friction on the lateral boundaries, and with friction on the bottom. The turbulence model is chosen to be consistent with the logarithmic velocity profile on the vertical. At the entrance of the channel, sediment is introduced with a constant concentration along the vertical, and an equilibrium profile gradually appears downstream. The constant slope is of  $1.01 \cdot 10^{-3}$  (at  $x = 0\text{ m}$ ,  $z = 0\text{ m}$  and at  $x = 500\text{ m}$ ,  $z = -0.505\text{ m}$ ), designed so as to get a uniform flow with a Strickler coefficient equal to  $50\text{ m}^{1/3}/\text{s}$  when the depth is  $0.5\text{ m}$ .

##### 3.2.1 Initial and Boundary Conditions

The computation is initialised with a constant water depth equal to  $0.5\text{ m}$ , constant sediment concentration equal to  $0.02\text{ g/L}$  velocity and total viscosity field initialised with a logarithmic profile along the vertical (see Figures 3.1 and 3.2).

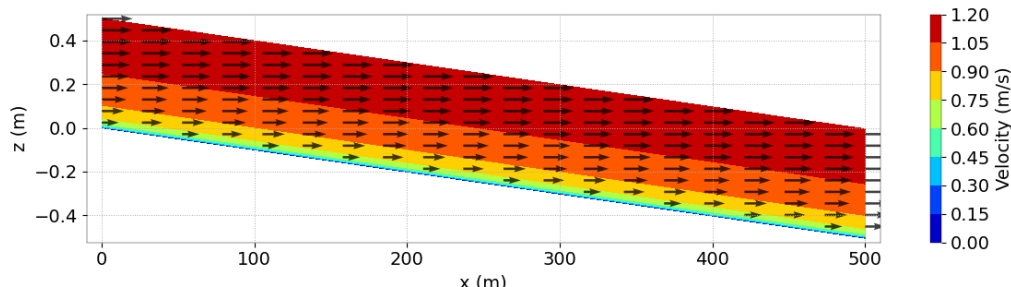


Figure 3.1: Vertical distribution of velocity at initial time step.

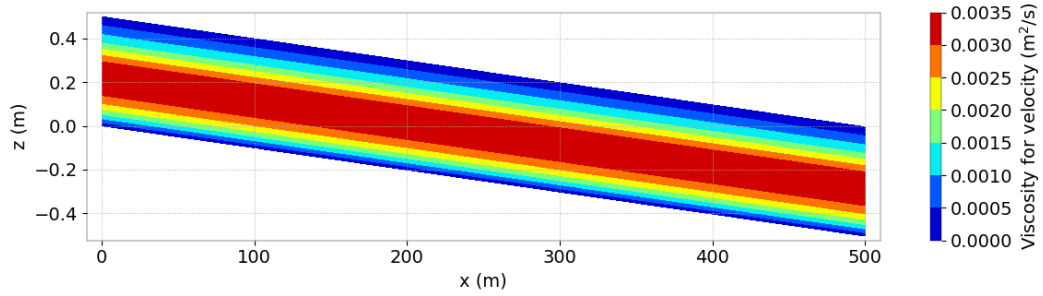


Figure 3.2: Vertical distribution of viscosity at initial time step.

The boundary conditions are:

- For the solid walls, a slip condition on channel banks is used for the velocities,
- On the bottom, a Nikuradse law with bed roughness of  $k_s = 0.0162$  m (equivalent to a Strickler coefficient of  $50 \text{ m}^{1/3}/\text{s}$  at the depth of 0.5 m) is prescribed,
- Upstream a flowrate of  $50 \text{ m}^3/\text{s}$  and constant sediment concentration of 0.02 g/L are prescribed and logarithmic velocity profile,
- Downstream the water level is equal to -0.005 m and logarithmic velocity profile.

### 3.2.2 Mesh and numerical parameters

The 2D mesh (Figure 3.3) is made of 2,204 triangular elements (1,188 nodes). 16 planes are irregularly spaced (zstar) in the vertical direction (see Figure 3.4).

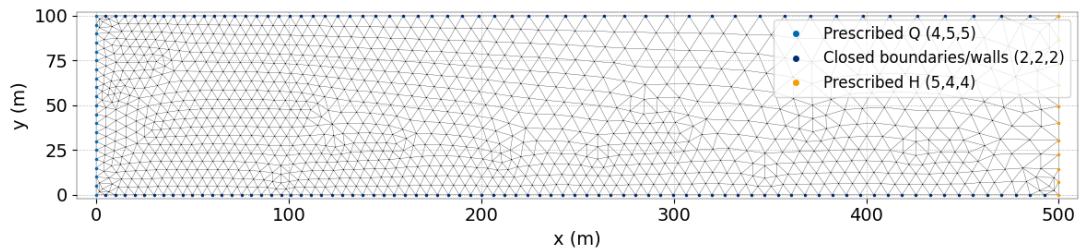


Figure 3.3: Horizontal mesh.

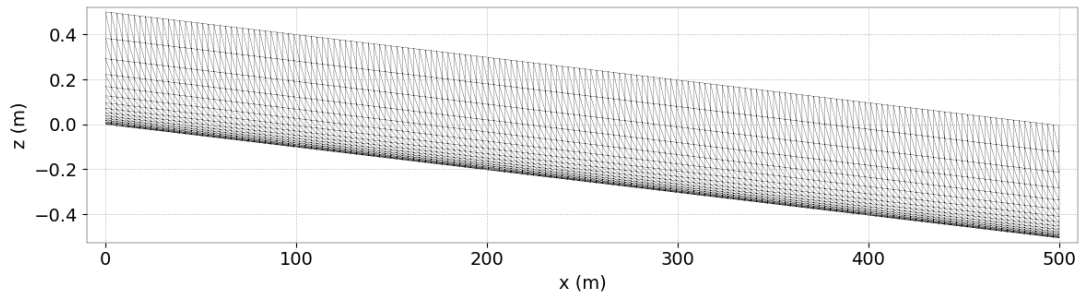


Figure 3.4: Initial vertical mesh along  $y = 1$  m.

The hydrostatic version of TELEMAC-3D is used.

To solve the advection, the method of characteristics is used for velocities and sediment. The time step is 2 s for a simulated period of 2,000 s.

### 3.2.3 Physical parameters

Nezu and Nakagawa mixing length model is used as vertical turbulence model combined with constant horizontal viscosity for velocity equal to  $0.1 \text{ m}^2/\text{s}$ .

Sediment of mean diameter of 6 mm with a settling velocity of -0.01 m/s is modelled with no influence of turbulence on sediment settling velocity. Laminar diffusivity of sediment is equal to  $10^{-4} \text{ m}^2/\text{s}$  for the vertical direction ( $10^{-6} \text{ m}^2/\text{s}$  for the horizontal directions).

## 3.3 Results

Figure 8 (to be drawn!!!) compares the theoretical [8] (i.e. logarithmic) velocity profile with the computed result and shows an excellent agreement. One can see that the point at the first plane above the bottom coincides with the theoretical value, which guarantees that the friction velocity is correct.

Figure 9 (to be drawn!!!) compares the theoretical [8] and the computed turbulent viscosity profiles. The maximum error happens at the first two planes below the surface (perhaps because of the size of the mesh at this level).

Figure 10 (to be drawn!!!) compares the classic theoretical Rouse profile, the modified Rouse profile [8], and the numerical solution obtained with a laminar viscosity of  $10^{-4} \text{ m}^2/\text{s}$ . The numerical solution is close to the modified profile. In theory, the Rouse profile is only valid beyond the viscous layer. The modified profile brings a notable modification only in this viscous layer and is presented here for its interest in software validation.

Figures 3.5, 3.6, 3.7 show the vertical distribution of velocity, viscosity and sediment concentration at final time step.

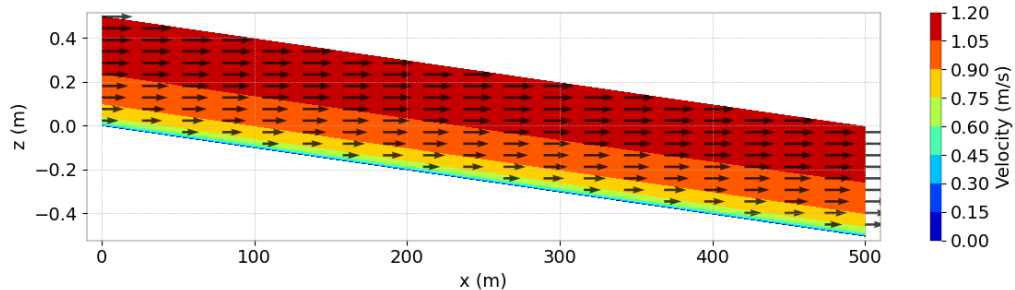


Figure 3.5: Vertical distribution of velocity at final time step.

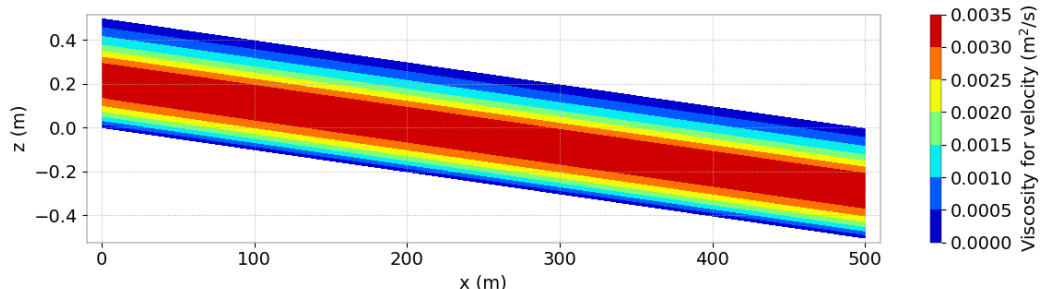


Figure 3.6: Vertical distribution of viscosity at final time step.

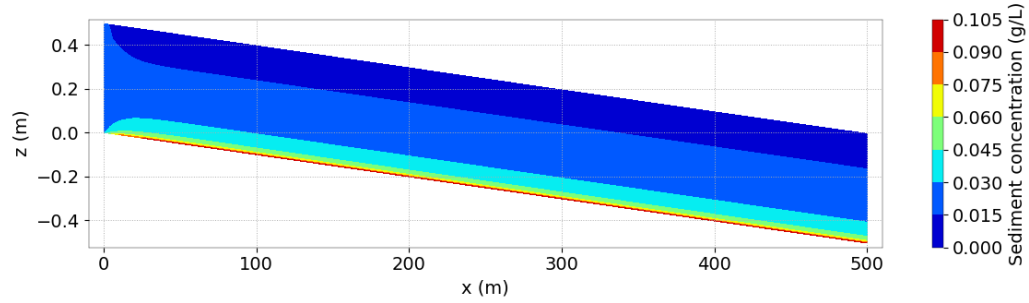


Figure 3.7: Vertical distribution of sediment concentration at final time step.

### 3.4 Conclusion

These comparisons with analytical solutions, in hydrodynamics or suspended sediment transport, thoroughly validate the treatment of diffusion on the vertical in TELEMAC-3D, including a settling velocity. The Nezu and Nakagawa mixing length turbulence model, and the computation of velocity gradients, is also validated.

## 4. Stability of vertical density in a V-shaped channel (V)

### 4.1 Description

This test case presents the stability of the variable vertical density in a V-shaped channel. The purpose of this test is to verify the validity of the diffusion step and the proper treatment of the buoyancy terms. Moreover, this test demonstrates the ability of TELEMAC-3D to model a vertical stratification induced by an active tracer distribution on a non-horizontal topography. A closed rectangular channel is initialised with such vertical tracer distribution without motion. This stratification is stable and the distribution of the tracer should not evolve in time neither generate any flow. The test case is treated with both prism and tetrahedron elements.

The considered domain is a horizontal V-shaped channel. The geometry dimensions of the channel are 100 m wide and 500 m long. The depth is -13 m in the center of the channel, and 0 m on both sides of the channel. The bottom is interpolated linearly between the centre and the banks (observed in Figure 4.1). The horizontal mesh is composed of triangular cells nearly homogenous in size. The test case is first solved using a vertical mesh of prismatic cells fitting the topography, and in a second time using tetrahedron elements. The horizontal and vertical meshes are presented in Figures 4.1 and 4.2.

The active tracer is the temperature with a corresponding value of the thermal expansion coefficient  $\beta = 2.10^{-4} \text{K}^{-1}$  (see the User's Manual). Note that only the horizontal diffusivity is taken into account. It is constant with velocity diffusivity and tracer diffusion equal to  $1 \text{m}^2 \cdot \text{s}^{-1}$ .

#### 4.1.1 Initial and boundary conditions

The initial water level is  $z = 0.1 \text{ m}$  with a null velocity. The temperature is initialised as follows:

$$T(\text{°C}) = 10 + \frac{z}{1.3}.$$

The boundary conditions are:

- All lateral boundaries are solid, i.e., no inlet and no outlet in the domain,
- No flux through the bottom and the free surface for the temperature (or tracer),
- No friction on the bottom and on the channel banks.

### 4.1.2 Mesh and numerical parameters

The mesh (see Figures 4.1 and 4.2) is composed of 648 triangular elements (373 nodes) with 11 planes regularly spaced in the vertical direction, to form prism or tetrahedron elements.

The time step is 0.1 s for a simulated period of 1 s.

This case is computed with the non-hydrostatic version.

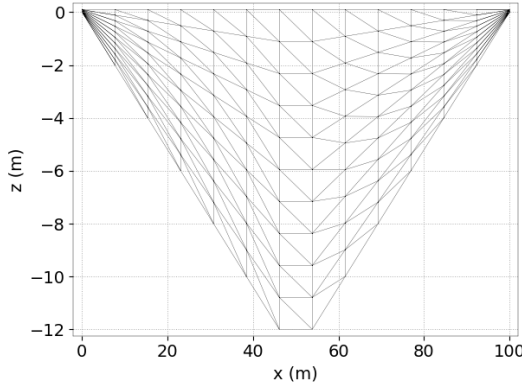


Figure 4.1: Topography and vertical mesh.

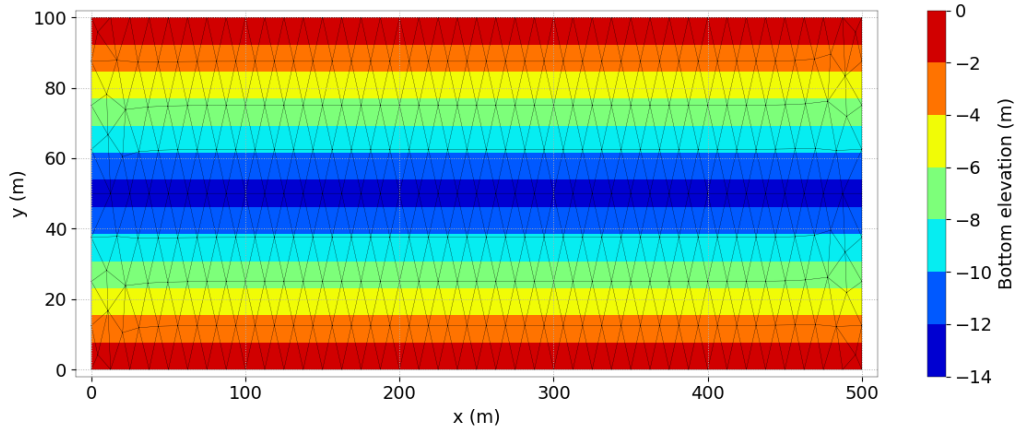


Figure 4.2: Horizontal mesh.

## 4.2 Results

During the simulation, the vertical profile of tracer concentration is stable for both computations. The first computed with prism elements (Figure 4.3) and the second computed with tetrahedron elements (Figure 4.4).

However, at the end of the computation with prism elements, some negligible differences on the temperature field (maximum value for example, up to 0.06 %) are observed. Figure 4.5 shows disturbance of velocity field negligible (of the order of  $10^{-8}$ ) for the prism elements computation. This velocity field is connected to the difficulty to build the diffusion matrix using

prismatic elements. The computation with tetrahedron elements (see Figure 4.6) shows some very negligible (of the order of  $10^{-16}$ ) disturbance of the velocity field. In any case, the situation can be considered as globally stable. The test is done essentially to verify the horizontal diffusion terms, which are estimated in the transformed  $\sigma$ -mesh (buoyancy terms). In this case, the tracer does not induce any flow. The final mass balance of computation using prism elements exposes a very good mass conservation (the mass loss is less than  $0.9 \cdot 10^{-6}$  for the water and 0.1 for the temperature). For the computation using tetrahedron elements, the conservation of mass and temperature is perfect.

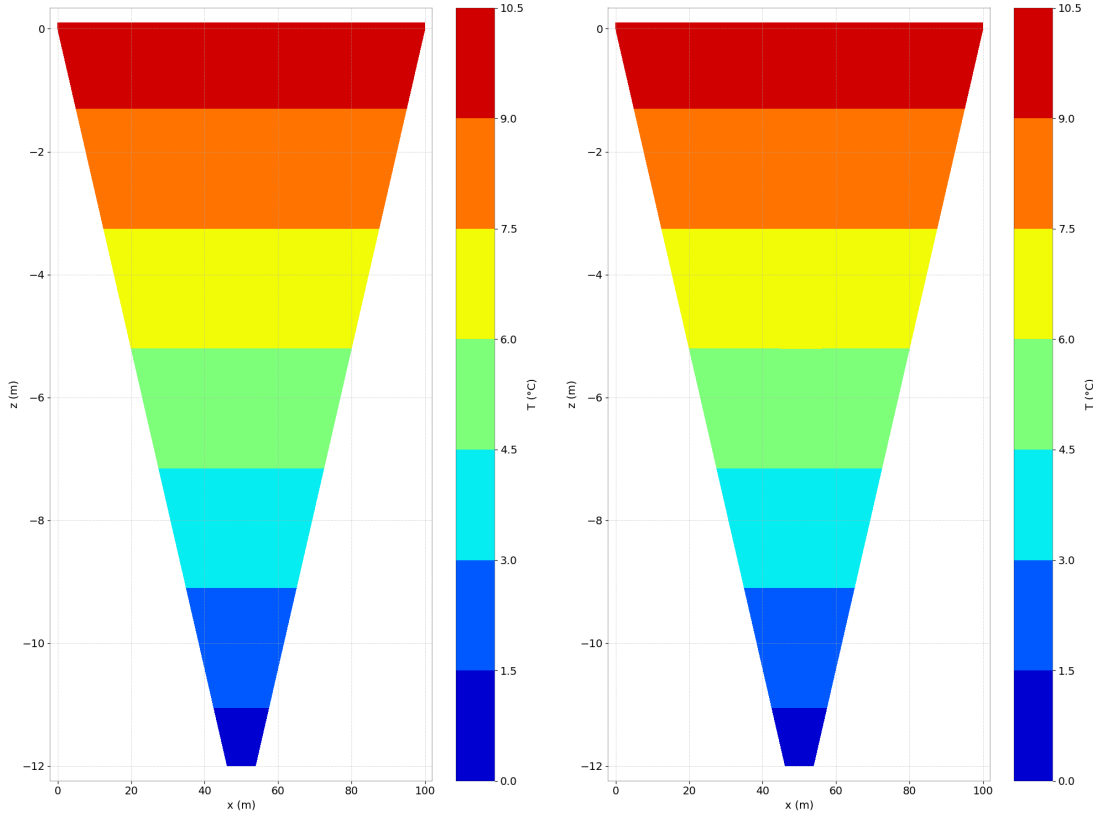


Figure 4.3: Vertical distribution of tracer with prism elements (initial state and end of computation).

To conclude, the diffusion equation of tracers is properly solved by TELEMAC-3D. The buoyancy terms are properly taken into account for a linear vertical tracer distribution. Unlike tetrahedron elements computation, using prism elements generates a small disturbance of the velocity field and some negligible differences on the temperature field. Nevertheless, the generated disturbance is small with respect to the vertical gradient of the tracer and is principally due to machine precision and diffusion matrix treatment. The tracer is still stable at the end of the simulation.

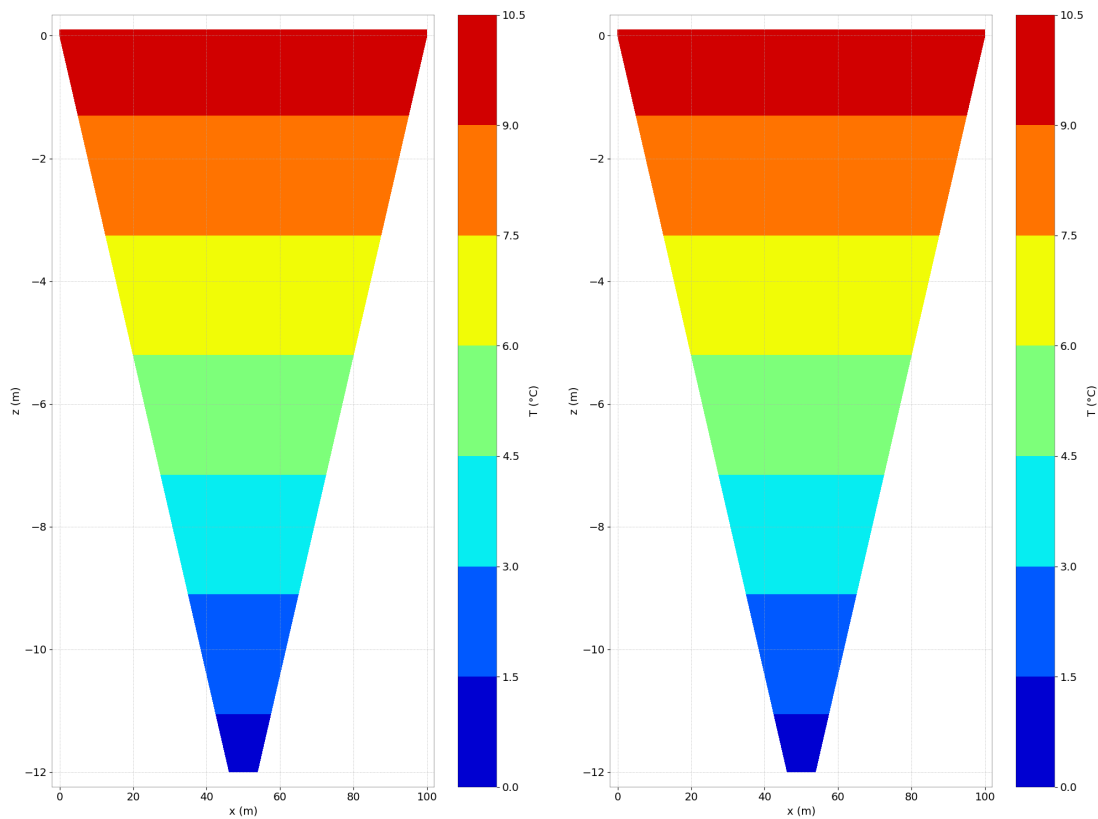


Figure 4.4: Vertical distribution of tracer with tetrahedron elements (initial state and end of computation).

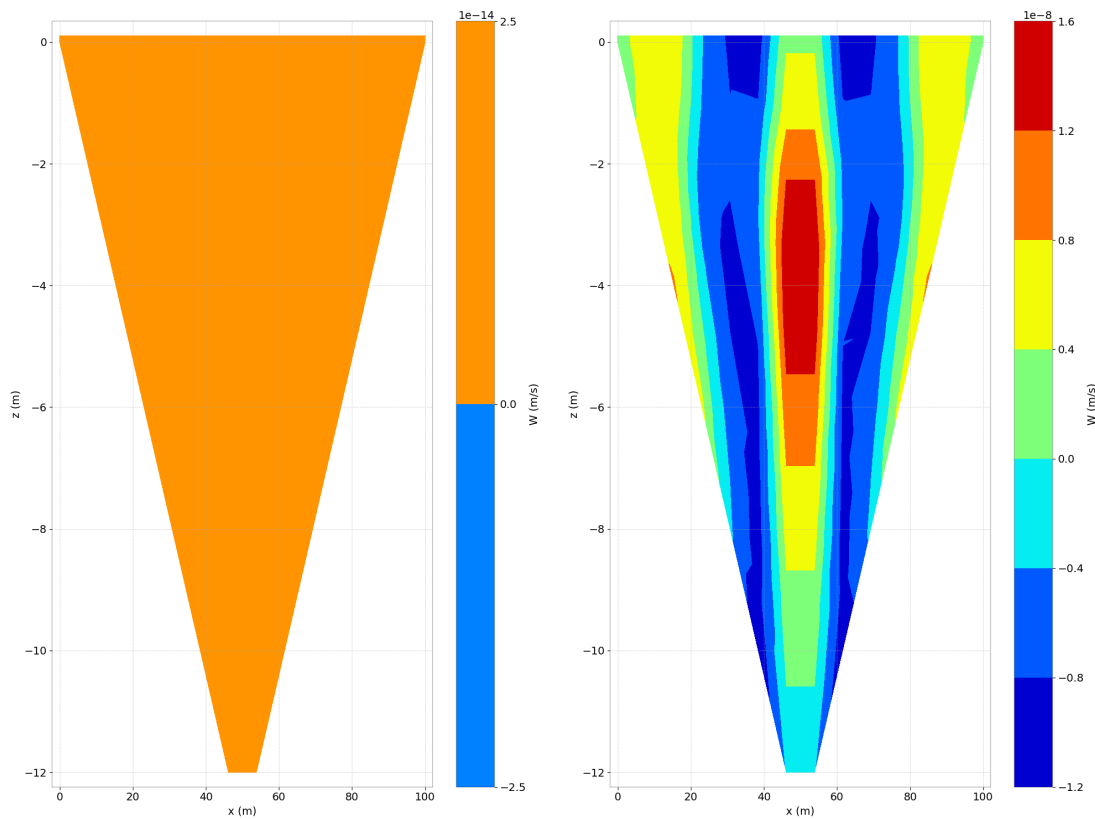


Figure 4.5: Vertical velocities with prism elements (initial state and end of computation).

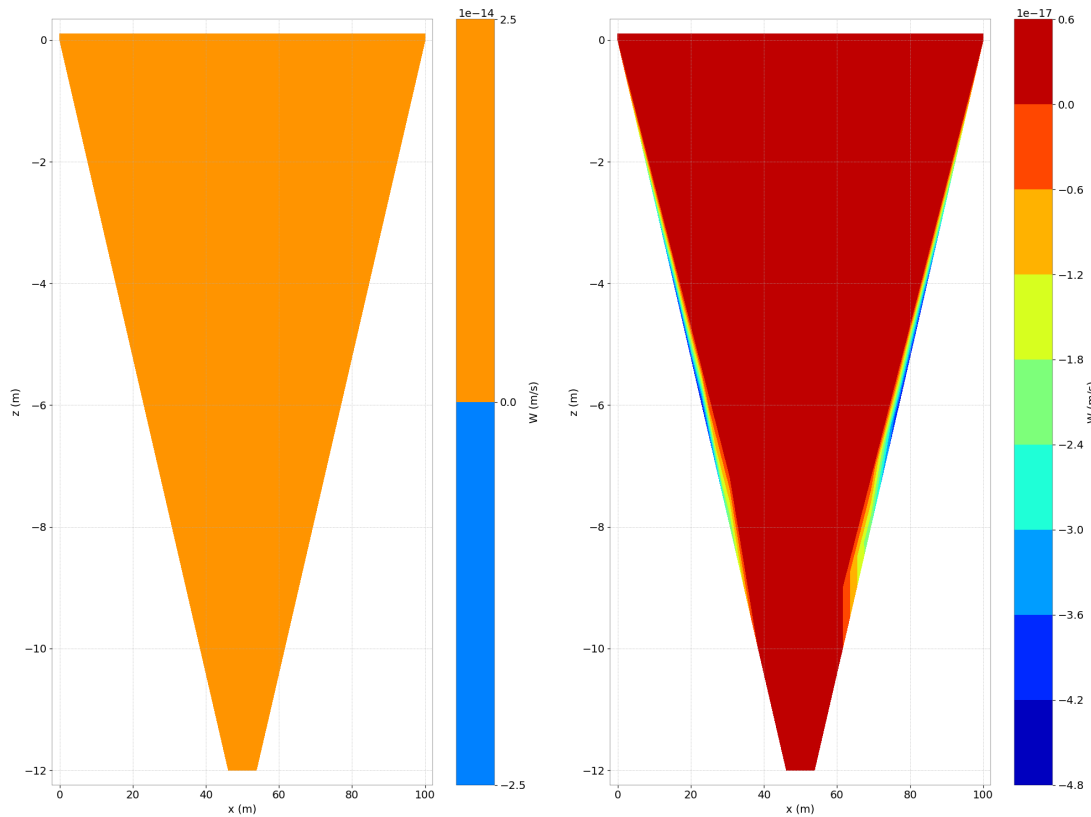


Figure 4.6: Vertical velocities with tetrahedron elements (initial state and end of computation).

## 5. Viollet

### 5.1 Purpose

This test demonstrates the ability of TELEMAC-3D to model thermal and stratified flow.

### 5.2 Description

The test case considers the stable configuration of Pierre-Louis Viollet's experimentation (1980) with a Froude number of 0.9, which consists in a 2 layer flow of same height,  $h = 0.1$  m. The lower layer has a velocity  $U_2$  and a temperature  $T_2$ . The upper layer has a velocity  $U_1 < U_2$  and a temperature  $T_1 > T_2$ .

#### 5.2.1 Reference

#### 5.2.2 Geometry and Mesh

##### Bathymetry

Channel tilt =  $5.30921 \times 10^{-6}$  (see figure 3.18.2)

##### Geometry

Channel length = 10 m ( $100h$ )

Channel width = 1 m ( $10h$ )

##### Mesh

1280 triangular elements (see figure 3.18.2)

697 nodes

27 planes regularly spaced on the vertical ( $\sigma$  transformation).

#### 5.2.3 Physical parameters

Turbulence:  $k-\varepsilon$  in both directions

Prandtl number: 0.71

Karman constant: 0.41

Bottom friction: Haaland law with coefficient equal to 63.4505112

Density law is a function of temperature.

### 5.2.4 Initial and Boundary Conditions

#### Initial conditions

$U_1 = 0.05 \text{ m/s}$   $T_1 = 25.35^\circ\text{C}$

$U_2 = 0.05 \text{ m/s}$   $T_2 = 20^\circ\text{C}$

Constant height of 0.2 m ( $2h$ )

#### Boundary conditions

Closed boundaries on sides.

Upstream prescribed flow rate:  $0.01 \text{ m}^3/\text{s}$

Downstream prescribed water level:  $0.19995 \text{ m}$

A double logarithmic velocity profile is imposed for the lower layer and a logarithmic profile for the upper layer (see figure 3.18.1) according the following formulae defined in the BORD3D subroutine:

where  $z_1$  and  $z_2$  are the levels in upper and lower layers respectively (starting from the lower level of each layer).  $\xi_s = 10^{-4} \text{ m}$  et  $dz$  is the distance between two planes (i.e.  $dz = h/26$  since there are 27 planes).

Upstream  $k$  and  $\varepsilon$  profiles are imposed according the following formulae defined in the KEPCL3 subroutine:

where  $n_{turb} = 5 \times 10^{-3}$ ,  $C_\mu = 0.09$  and  $\delta = 10^{-6}$

Surface and bottom boundary condition for  $\varepsilon$  are defined in the KEPICL subroutine: Neumann at bottom and Dirichlet at surface.

### 5.2.5 General parameters

Time step: 0.1 s

Simulation duration: 500 s (8 min 20 s)

### 5.2.6 Numerical parameters

Non-hydrostatic computation

Advection of velocities, temperature and  $k$ - $\varepsilon$ : N-type MURD scheme

### 5.2.7 Comments

It should be noted that a bias exists in the measures presented: the channel inlet flow does not correspond to the integral of the measured speeds on the section. This comes probably from measurement error of the velocity field. The velocity been the field that is sought to be reproduced, the measured velocity field is corrected by multiplying it by a constant. No correction is applied to temperature measurements.

## 5.3 Results

Figure 3.18.3 presents velocity and temperature profiles comparisons at  $x/h = 10, 30$  and  $100$  between TELEMAC-3D results and corrected experimental measurement of P-L Viollet, for the stable stratification case with  $Fr = 0.9$ .

The comparisons show a good match between simulation results and measurements. The evolution of the velocity and temperature profiles at the different sections of the channel is well reproduced.

#### 5.4 Conclusion

TELEMAC-3D is capable to model thermal and stratified flow.

## 6. Wesel

### 6.1 Purpose

This test case shows a real case application with tidal flats and very large time steps. It was made for comparison with the program UnTRIM from Prof. Casulli (University of Trento). The mesh is compatible with UnTRIM meshes which have restrictions according the orthogonality.

### 6.2 Description

#### 6.2.1 Geometry and mesh

The model area is a 9 km stretch of Lower Rhine River near the towns of Wesel and Xanten (Rh-km 812.5 - 821.5). The resolution is very coarse with mean node distances of about 6 m in the main channel and about 30 m at the floodplains. The vertical is discretised by only 3 sigma layers (see Figure 6.2). The horizontal mesh contains 9,064 nodes and 17,340 elements and can be seen in Figure 6.1. The mesh is compatible to UnTRIM meshes which means that the center of each triangle is inside the triangle. The bathymetry is shown in Figure 6.3.

#### 6.2.2 Initial condition

The initialising of the water level is done with the subroutine **surfini.f** called by **user\_condi3d\_h.f**. From water level measurements in m+NN at low water conditions in 1997 in the file **f01\_wesel.txt** (FORMATTED DATA FILE 1) the initial water level is interpolated (see Figure 6.4). The co-ordinates are given as the left and right hectometer points. The initial velocities are set to zero.

#### 6.2.3 Boundary conditions

At the inlet, the discharge is imposed across the full cross section. In order to avoid instabilities in the beginning the discharge is increased from 0 to 1,061 m<sup>3</sup>/s in 30 min and remains constant afterwards. At the outlet the water depth is fixed to 11.82 m+NN.

#### 6.2.4 Physical parameters

For the time optimisation constant values for the friction and the turbulence are chosen: The Nikuradse friction law is used and an uniform equivalent sand roughness of 3.5 cm is applied. The constant turbulent viscosities are set to 2 m<sup>2</sup>/s for the horizontal dimension and 0.1 m<sup>2</sup>/s for the vertical dimension. This very high horizontal value stabilises the simulation. Typically values of one to two orders of magnitudes lower are applied.

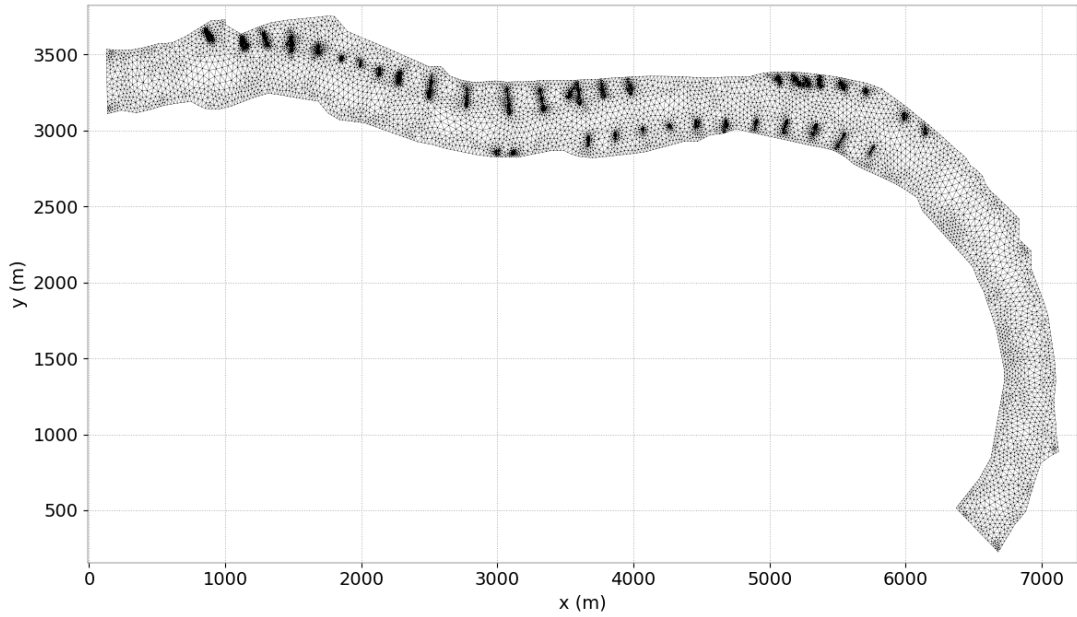


Figure 6.1: Horizontal mesh.

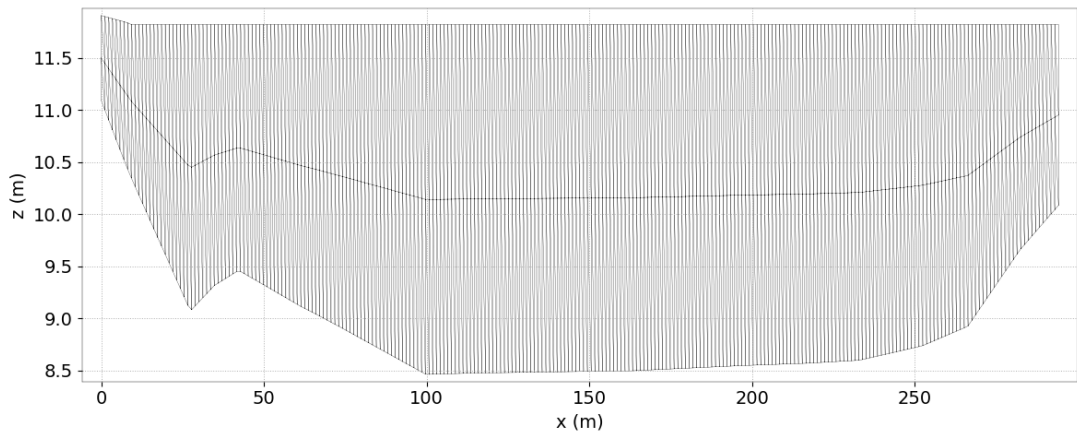


Figure 6.2: Vertical discretisation with 3 planes.

### 6.2.5 Numerical parameters

12 h are simulated with a time step of 50 s to ensure steady state conditions. Figure 6.8 shows that the flux at the outlet equals the flux at the inlet at the end of the simulation time. The non-hydrostatic version is applied and the NERD scheme (# 13) is used for the advection type. Relatively low accuracies of  $10^{-4}$  for propagation and pressure and  $10^{-5}$  for diffusion of velocities are chosen. Full implicit conditions are set for depth and velocities.

## 6.3 Results

The final water levels are shown in Figure 6.5. The difference between the initial and the final water levels are quite small as the initial water levels are calculated from the measurements. The velocity distribution of a typical cross section in the straight part of the river is presented in Figure 6.6. Due to the small number of equally spaced planes, a typical logarithmic profile

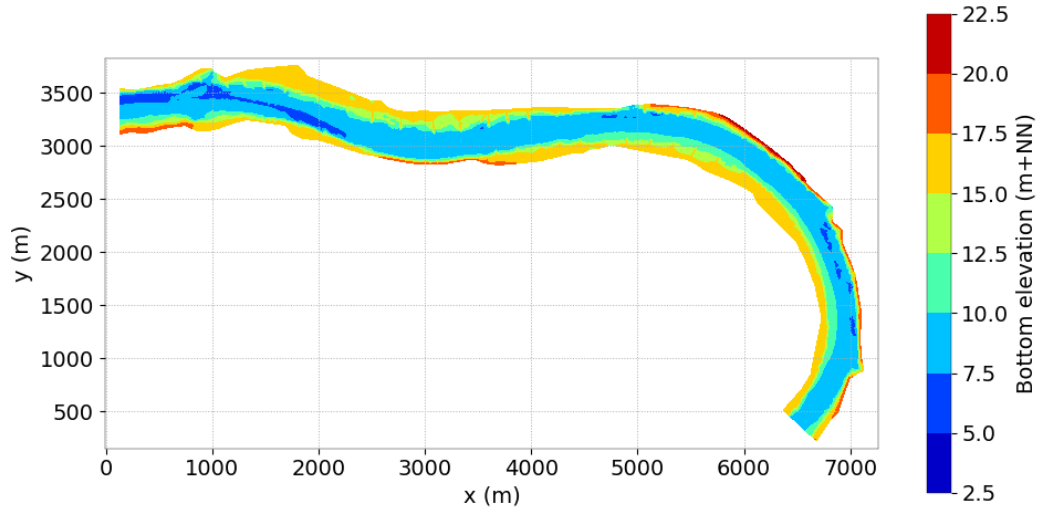


Figure 6.3: Bathymetry.

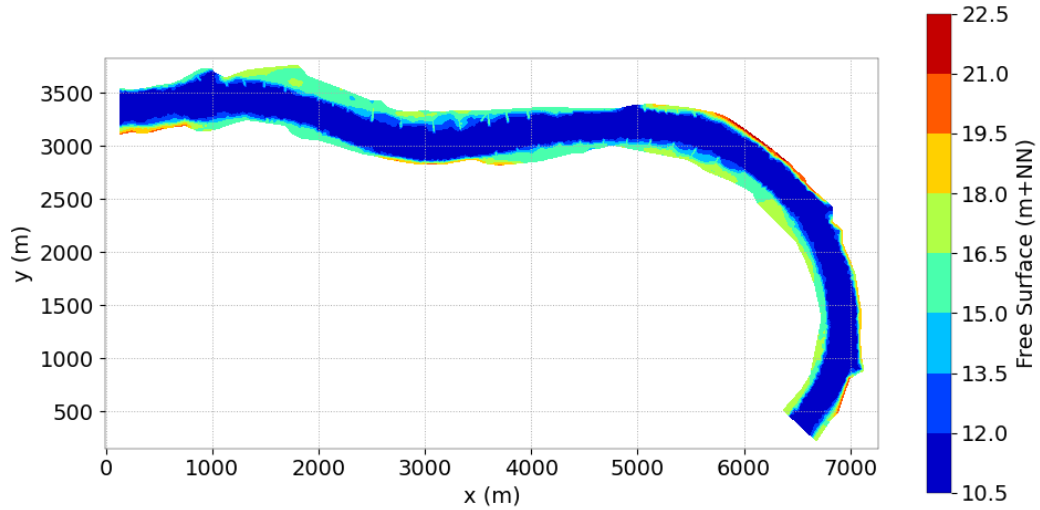


Figure 6.4: Initial water levels.

was not produced. The velocity is nearly constant over the vertical. A comparison along the main channel between the measured water levels and the simulated ones is presented in Figure 6.7. The simulated water levels are a little higher at the inlet, it can be assumed that the friction should be increased for a perfect agreement.

## 6.4 Conclusion

The example shows a successful simulation of low water steady state conditions with tidal flats. The configuration is time optimised by using a coarse mesh, a big time step, a low solver accuracy, a full implicit scheme and a high turbulent viscosity.

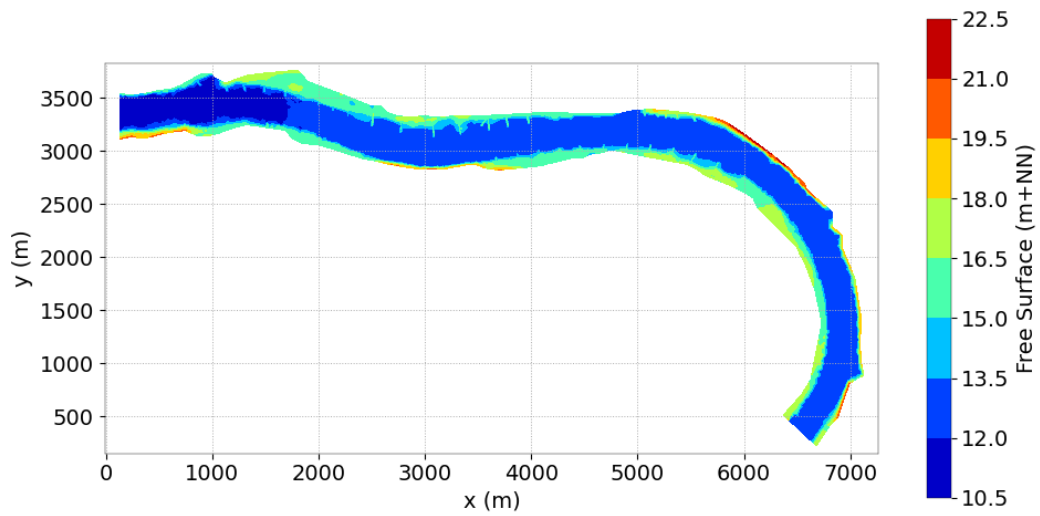


Figure 6.5: Final water levels.

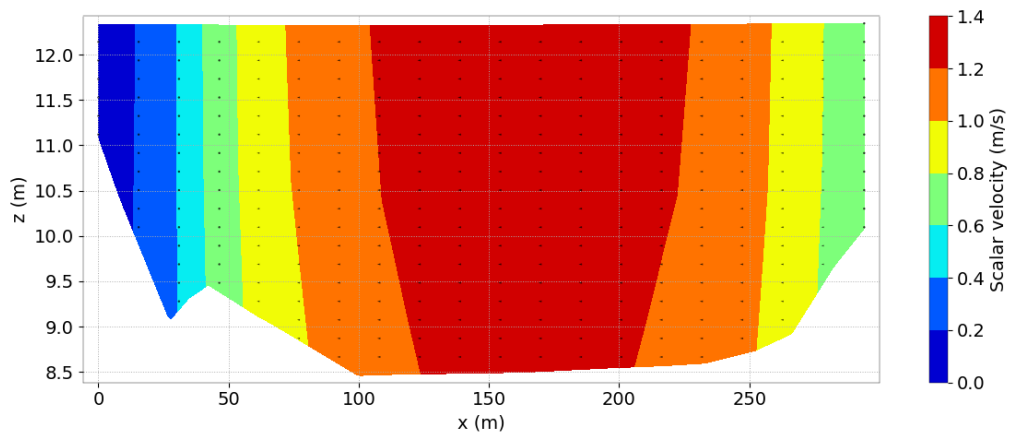


Figure 6.6: Velocities in a cross section at the straight part of the river.

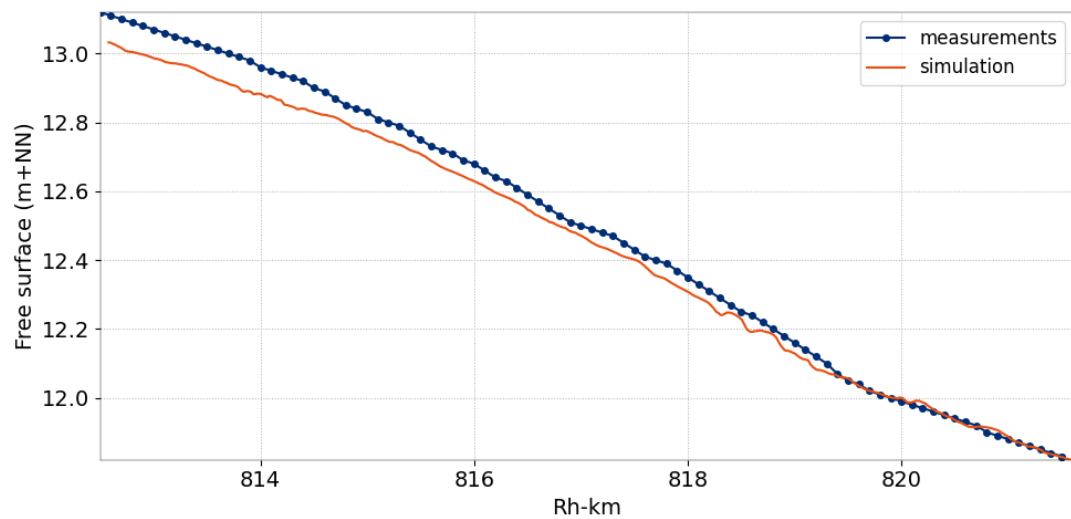


Figure 6.7: Comparison of measured and simulated final water levels along river axis.

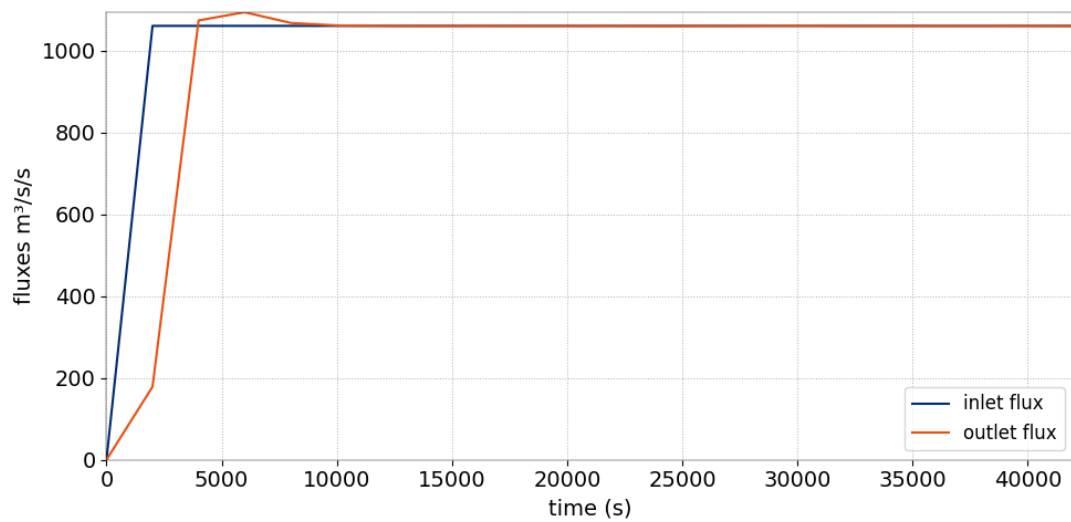


Figure 6.8: Evolution of inlet and outlet fluxes.

## 7. Automatic Mesh Displacement (amr)

### 7.1 Purpose

The AMD (Adaptive Mesh Displacement) method places nodes along the vertical depending on the vertical gradient of a referenced quantity (such as tracer) independently of its horizontal neighbours. In order to reduce the local steepness of the horizontal variations of intermediate surfaces between two neighbouring verticals, a simple low pass filter is used in two dimensions where the average value of one node is combined with half the value of its neighbouring nodes and solved through a Laplace equation. This test case demonstrates the effectiveness of the simple low pass filter. A demonstration of the AMD method itself is presented through the test case “lock-exchange”.

### 7.2 Description

For illustrative purposes we consider a point source of tracer located at the bottom of a straight channel with rectangular cross section with a constant flow in the absence of friction. A depth averaged velocity of 1 m/s is applied at the entrance of the channel. At the source, the tracer concentration is arbitrarily set to 215 units, discharged at a rate of 0.5 m<sup>3</sup>/s.

#### 7.2.1 Geometry and Mesh

The channel is 1 km long, 100 m wide and 10 m deep. The edge length of the mesh is uniform, set at about 10 m.

#### 7.2.2 Numerical parameters

The AMD method is activated with the keyword MESH TRANSFORMATION = 5.

### 7.3 Reference

This test case is based on the work presented within the PhD Thesis of S.E. Bourban [2013, Stratified Shallow Flow Modelling].

### 7.4 Results

The steady state results of the following two test cases are considered:

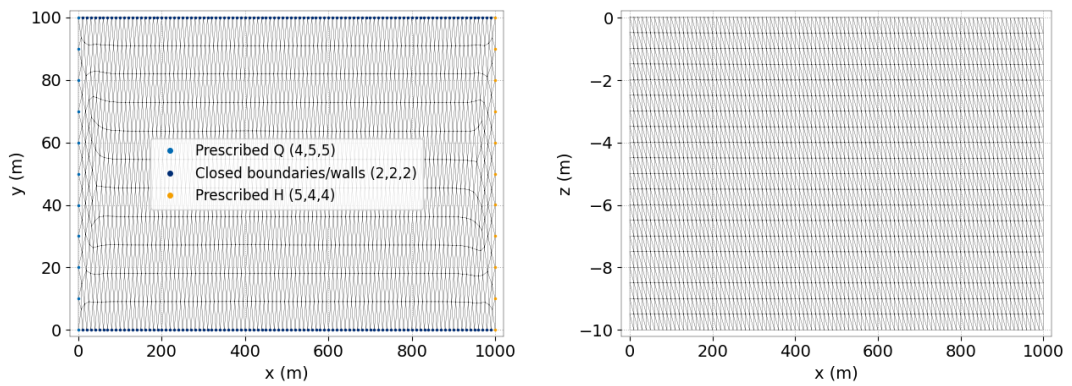


Figure 7.1: Horizontal mesh and initial vertical mesh for the  $\sigma$  computation.

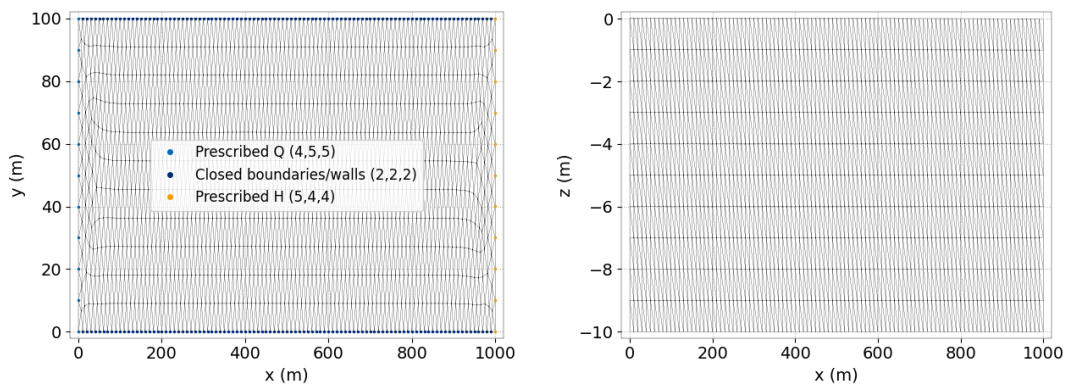


Figure 7.2: Horizontal mesh and initial vertical mesh for the AMD computation.

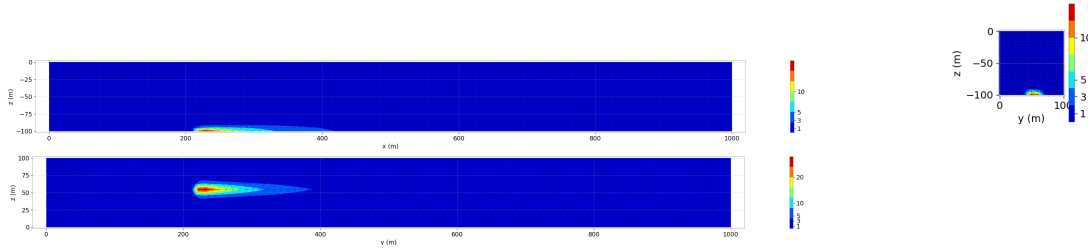


Figure 7.3:  $\sigma$  results.

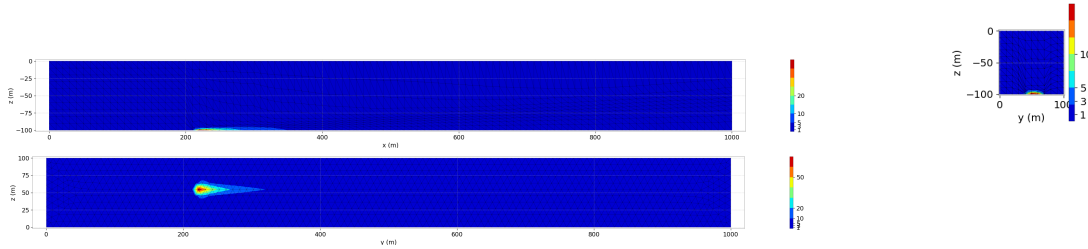


Figure 7.4: AMD results.

- A standard vertical discretisation based on 21 horizontal surfaces, which in this case of a flat bottom and free surface can be associated either to a  $\sigma$ -stretched transformation or a fixed horizontal layering (Figure 7.1).

The top left inset of Figure 7.3 shows the concentration contours of the tracer in a vertical cross section along the  $xz$ -plane, through the middle of the channel. The 21 horizontal lines, from the bottom of the channel at  $z = -10$  m to the top of the channel at  $z = 0$  m highlight, the locations of the 21 surfaces in the 3D mesh. The top right inset also shows a vertical cross section but along the  $yz$ -plane, at  $x = 250$  m. The bottom inset of Figure 7.3 shows a horizontal cross section along the  $xy$ -plane, through the bottom plane of the channel.

- Use of the AMD method based on only 11 surfaces, or half the number of layers.

Again, the top left and right insets of Figure 7.4 show the concentration contours in vertical cross sections along the  $xz$ -plane and  $yz$ -plane respectively. The 11 curvatures of the mesh in the vicinity of the highest gradient of the concentration highlight the successful adaptation of the 3D mesh. The bottom inset of Figure 7.4 shows the concentration contours in a horizontal cross section along the same  $xy$ -plane as in Figure 7.3.

A comparison of the figures shows that using the AMD method allows a better characterisation of the plume horizontally and vertically yet with half the number of intermediate surfaces.

## 7.5 Conclusion

This test case demonstrates the effectiveness of the simple low pass filter combined with the AMD method.

## 8. Flow along a bend (bendrans)

### 8.1 Description

This example shows that TELEMAC-3D is able to simulate a flow along a bend with the Spalart-Allmaras turbulence model,

The configuration is a channel with a rectangular bend. The bottom is flat without slope (at elevation 0 m).

#### 8.1.1 Initial and boundary conditions

The computation is initialised with a constant elevation equal to 0.175 m and no velocity.

The boundary conditions are:

- For the solid walls, a slip condition on channel banks is used for the velocities,
- On the bottom, a Nikuradse law with friction coefficient equal to 0.00188 m is prescribed,
- Upstream a flowrate equal to 0.0295 m<sup>3</sup>/s is prescribed, linearly increasing from 0.0001 to 0.0295 m<sup>3</sup>/s during the first 5 s,
- Downstream the water level is equal to 0.175 m.

#### 8.1.2 Mesh and numerical parameters

The 2D mesh (Figure 8.1) is made of 6,845 triangular elements (3,623 nodes). 5 planes are regularly spaced on the vertical (see Figure 8.2).

The time step is 0.01 s for a simulated period of 100 s.

The non-hydrostatic version is used. To solve the advection, the characteristics are used for both velocities and turbulent variable (scheme 1). GMRES is used for solving the propagation and diffusion of velocities (option 7). Accuracies for every solving of linear system are set to the default value  $10^{-8}$  except for the turbulent variable for which it is set to  $10^{-10}$ . No preconditioning for the diffusion for velocities step is used. The implicitation coefficients for depth and diffusion are both equal to 0.51 to be the more accurate.

#### 8.1.3 Physical parameters

The Spalart-Allmaras model is used for turbulence modelling for both vertical and horizontal directions (VERTICAL TURBULENCE MODEL = HORIZONTAL TURBULENCE MODEL = 5).

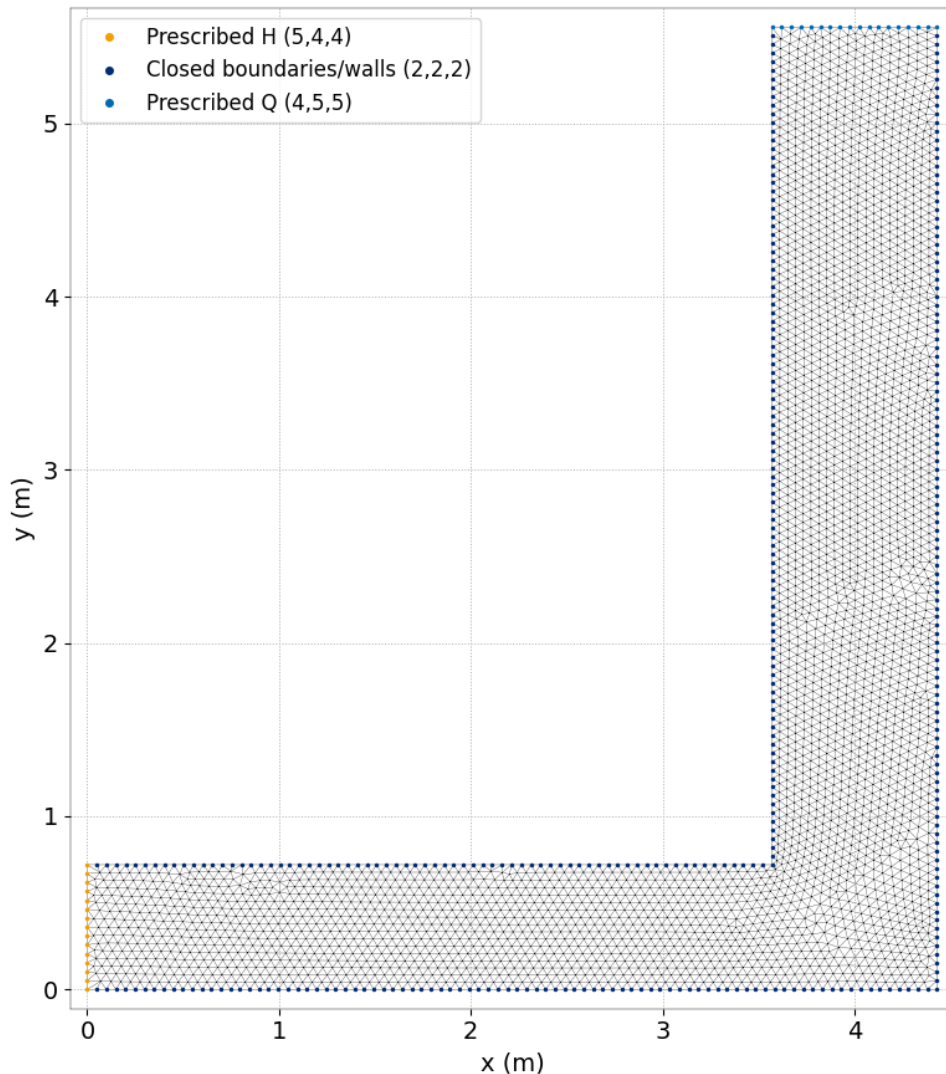


Figure 8.1: Horizontal mesh.

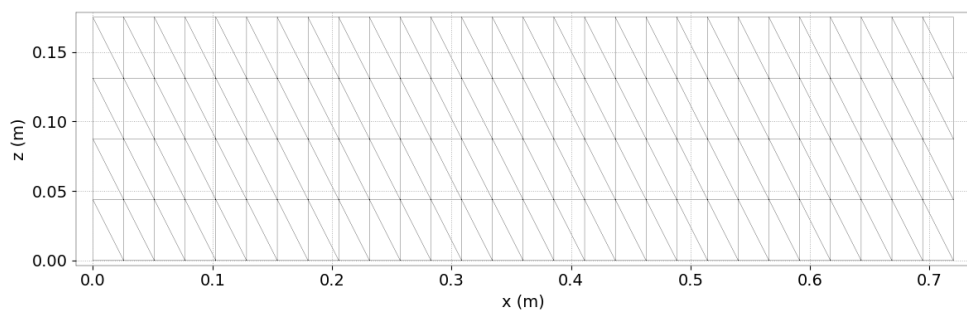


Figure 8.2: Initial vertical mesh.

## 8.2 Results

Figure 8.3 shows the free surface elevation at the end of the computation.

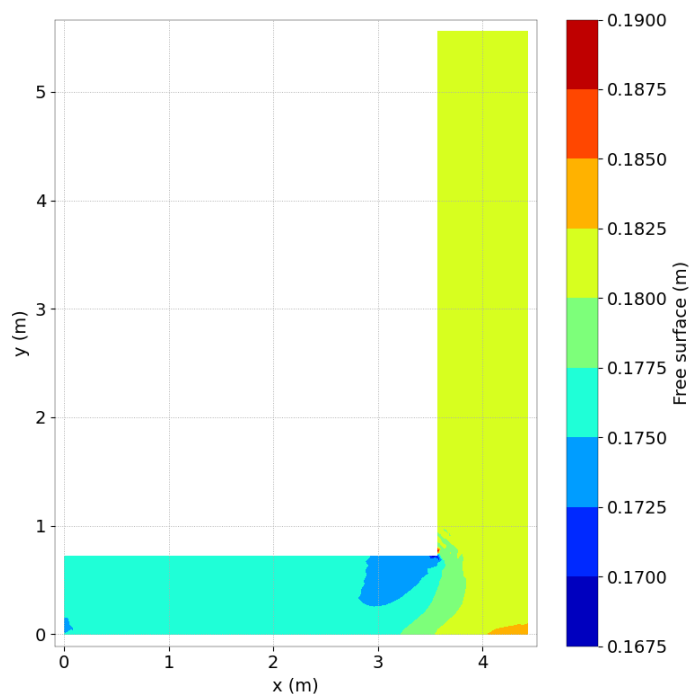


Figure 8.3: Free surface at final time step.

Figure 8.4 shows the magnitude of velocity at the end of the computation. The flow accelerates when turning in the bend and a detachment appears just after the corner at the top.

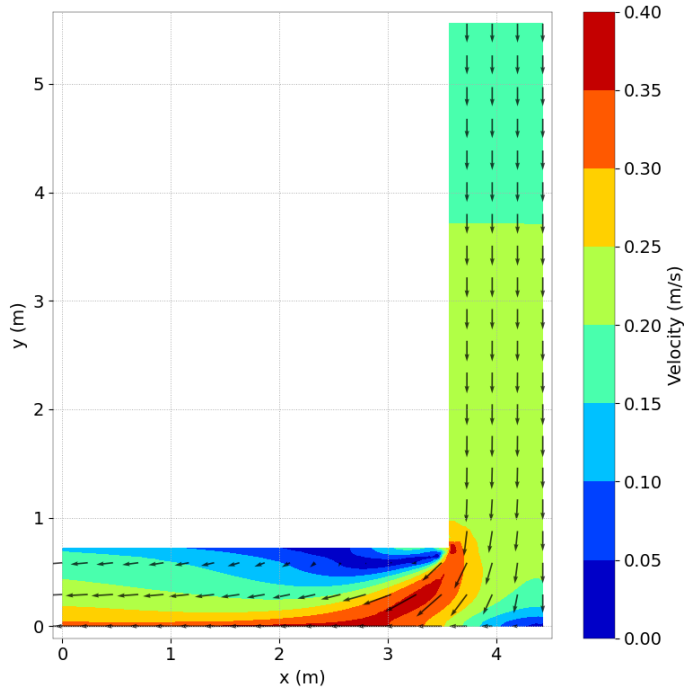


Figure 8.4: Velocity magnitude at the surface at final time step.

Figure 8.5 shows the diffusion along the  $x$  axis for velocity at the end of the computation.

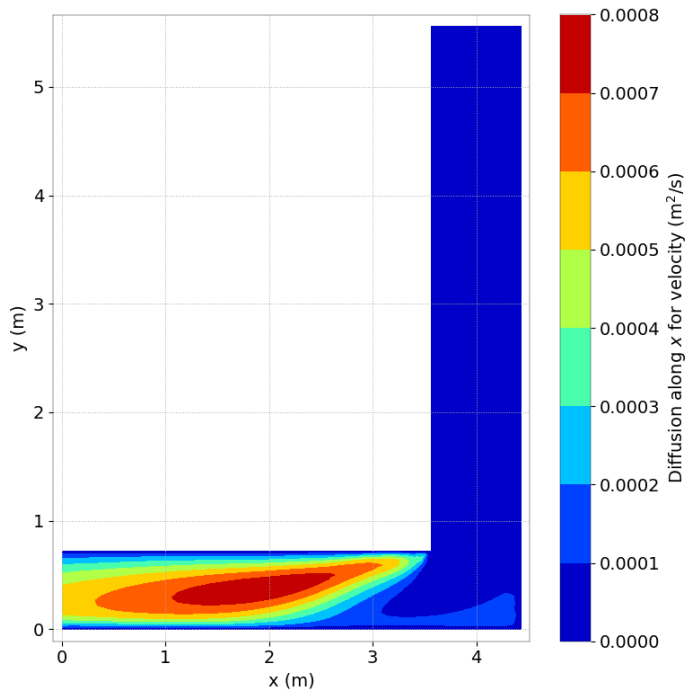


Figure 8.5: Diffusion along  $x$  for velocity at final time step.

Figure 8.6 shows the Turbulent Kinetic Energy at the end of the computation.

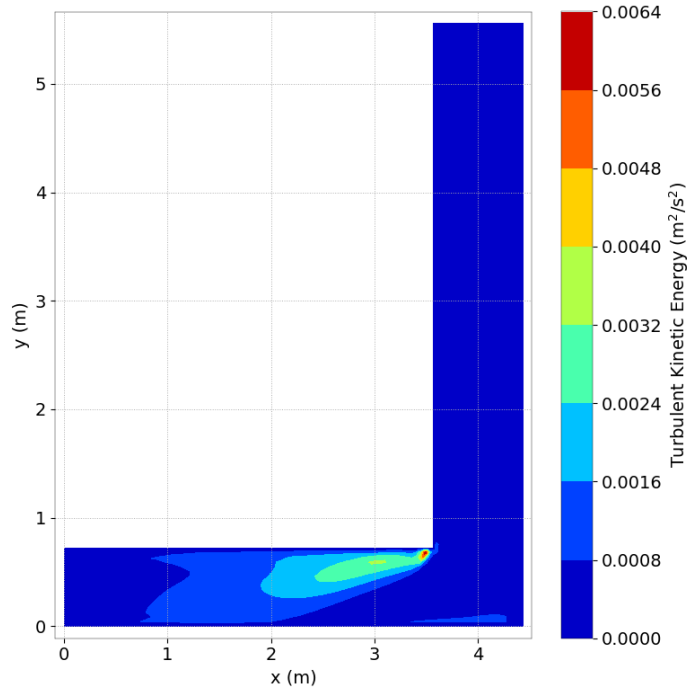


Figure 8.6: Turbulent Kinetic Energy at final time step.

Figure 8.7 shows the dissipation at the end of the computation.

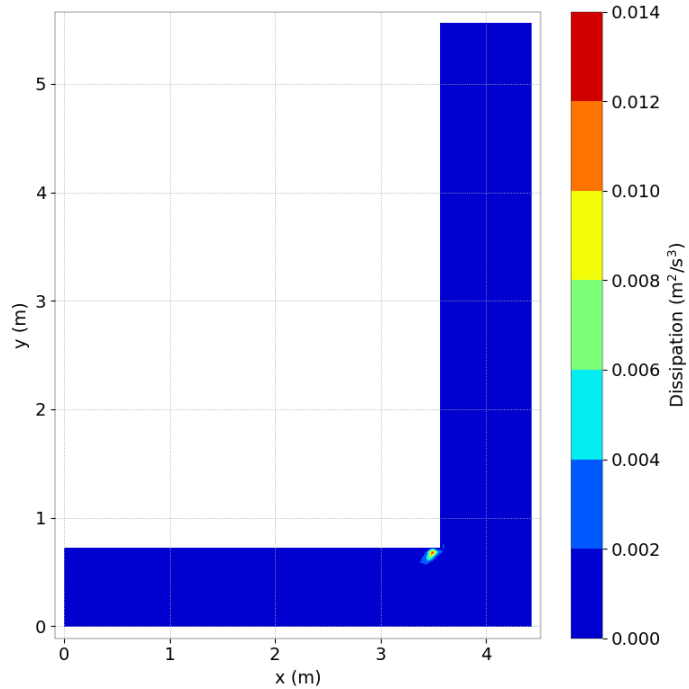


Figure 8.7: Dissipation at final time step.

Diffusion, Kinetic Energy and dissipation are generated after turning in the bend.

### 8.3 Conclusion

This example validates the Spalart-Allmaras turbulence model of TELEMAC-3D.

## 9. Bergenmeersen test case

### 9.1 Purpose

The purpose of this test-case is to test the culvert feature in TELEMAC-3D with a quantitative comparison to measurements of the flow rates through the culverts and the water levels on each side of the culverts.

### 9.2 Description

A recent (2013) example of the implementation of a Flood Control Area (FCA) with a controlled reduced tide (CRT) system is located in Bergenmeersen. The ring dike that surrounds the FCA has a crest level of 8 m TAW (Tweede Algemene Waterpassing, the reference level in Belgium; 0 m TAW corresponds to the average sea level at low water in Ostende port) and the overflow dike has a crest level of 6.8 m TAW. The configuration used for the inlet and outlet culverts is shown in Figure 9.1. Three outlet culverts were built to add to other older three outlet culverts that existed in the area. Above the new outlet culverts, six new inlet culverts were built and at their entrance weirs (i.e. wooden beams) with different heights were added (Figure 9.1 and Figure 9.2). At each inlet and outlet culvert the flow is separated into two parts at the entrance of the culvert by a kind of pilar and then converges again right after this pilar. Figure 9.3 shows an example of the trash screens that are present. Table 9.1 gives an overview of the characteristics of these new inlet and outlet culverts.

To test the culvert feature implemented in TELEMAC-3D, this new configuration of in- and outlet culverts is tested. The quality of the results can be assessed compared to measurements of the mean water levels inside the flood control area, outlet discharges, inlet discharges and mean water levels in the river side.

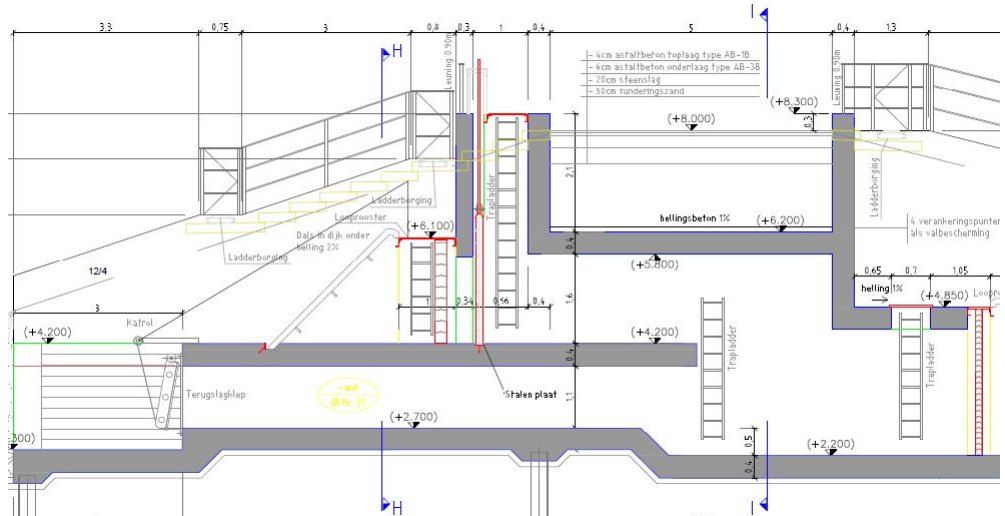


Figure 9.1: Bergenmeersen test case: detail of the side view of the construction of the new inlet and outlet culverts in Bergenmeersen.



Figure 9.2: Bergenmeersen test case: inlet and outlet culvert configuration on the river side (construction phase) (Patrimoniumdatabank W&Z).



Figure 9.3: Bergenmeersen test case: View on the inlet culverts from the river side and inlet and outlet culverts from the FCA side.

Table 9.1: Characteristics of the new inlet and outlet culverts of the new FCA/CRT in Bergenmeersen.

	Inlet (Scheldt side)	Inlet (FCA side)	Outlet (Scheldt side)	Outlet (FCA side)
<b>Number of culverts</b>	6		3	
<b>Culvert width (m)</b>	2.7		3	
<b>Culvert length (m)</b>	9.5		18	
<b>Culvert height (m)</b>	1.6	2.25	1.1	2.25
<b>Level of culvert floor (m TAW)</b>	4.2	2.2	2.7	2.2
<b>Crest level of weirs (m TAW)</b>	4.2/4.2/4.2/ 4.35/4.5/4.5			

### 9.2.1 Measurements

The quality of the numerical results can be assessed compared to measurements of the mean water levels inside the flood control area, outlet discharges, inlet discharges and mean water levels in the river side. Measurements were performed by Flanders Hydraulic Research in Bergenmeersen within a 13 hour campaign during the 10th September, 2013. They obtained water levels in front of the culverts in the Scheldt and in the floodplain sides and discharges for the inlet and outlet culverts. The model results for this period will be compared with the measurements.

## 9.3 Computational options

### 9.3.1 Mesh

The mesh of the computational domain is shown in Figure 9.4. The mesh is cut out of an early version of the Scaldis model. It has a resolution of about 8 m in the river side, and 10 m in the floodplain. Five horizontal layers are uniformly imposed in the model. Detailed bathymetric/topographic data from 2013 is available and used for this model.



Figure 9.4: Planview of the computational domain to model the FCA/CRT in Bergenmeersen. The colour scale represents de bottom values (m TAW).

### 9.3.2 Initial and boundary conditions

The water levels in the Scheldt river are obtained at the Wetteren tidal station. These values are used as the downstream boundary condition for the hydrodynamic model. Upstream a discharge boundary condition is imposed.

### 9.3.3 Numerical parameters

The simulation time is about one day (10th September 2014) corresponding to the time period for which measurements of mean water levels were available. The time step is set to 5 s, providing, together with the chosen mesh resolution, a stable simulation.

The bottom friction is taken into account in the model through the Manning Strickler's parameter  $n$ , set to  $0.02 \text{ s.m}^{-1/3}$ . The horizontal and vertical turbulence viscosity coefficients are both set to  $0.01 \text{ m}^2.\text{s}^{-1}$ , with Smagorinsky turbulence model in the horizontal directions and mixing length model in the vertical direction.

### 9.3.4 Culvert parameters

Table 9.2 shows the file that the user has to give to TELEMAC-3D in order to take into account the culverts for this FCA with CRT in the Bergenmeersen test case. Besides this new structure, there were already in the area three outlet sluices also represented in the input text file as outlet 3 to outlet 6 (information for these outlet sluices is obtained from the Patrimoniumdatabank W&Z). Once again the different head loss coefficients are used to calibrate the model with the experimental data. Most of the parameters are maintained comparatively with the Lippenbroek test case. But there are some exceptions, given the fact that the inlet and outlet culvert configurations are also different. For instance the head loss coefficients at the entrance of the inlet are increased in order to take into account the effect of the flow being split into two parts by a pillar. Following the expression given by Carlier (1972), the head loss due to the presence of pillars is about  $C_p \approx 0.4$  and therefore  $CE_1$  becomes  $CE_1 = C_1 + C_p$ . There is also at the exit of the outlet sluices the separation of the flow into two parts. This effect is taken into account in the head loss due to a valve, increasing the value for  $CV$ . Also during the measurement campaign, the trash screens at the inlet sluices are not cleaned and therefore this coefficient is increased both for the inlet and outlet sluices.

Table 9.2: Input data for the culvert subroutine in TELEMAC-3D to model the Bergenmeersen FCA/CRT.

	<b>CE1</b>	<b>CE2</b>	<b>CS1</b>	<b>CS2</b>	<b>CV</b>	<b>CT</b>	<b>C56</b>	<b>C5</b>	<b>CV5</b>	<b>W</b>	<b>D1</b>	<b>D2</b>	<b>N</b>	<b>L</b>	<b>CP</b>
<b>Inlet 1</b>	0.9	0.5	1	1	0	1	10	6	0	2.7	1.45	2.25	0.015	9.5	0
<b>Inlet 2</b>	0.9	0.5	1	1	0	1	10	6	0	2.7	1.6	2.25	0.015	9.5	0
<b>Inlet 3</b>	0.9	0.5	1	1	0	1	10	6	0	2.7	1.6	2.25	0.015	9.5	0
<b>Inlet 4</b>	0.9	0.5	1	1	0	1	10	6	0	2.7	1.6	2.25	0.015	9.5	0
<b>Inlet 5</b>	0.9	0.5	1	1	0	1	10	6	0	2.7	1.6	2.25	0.015	9.5	0
<b>Inlet 6</b>	0.9	0.5	1	1	0	1	10	6	0	2.7	1.6	2.25	0.015	9.5	0
<b>Outlet 1</b>	0.5	0.5	1	1	12	1	10	6	1.5	3	1.1	2.25	0.015	18.5	2
<b>Outlet 2</b>	0.5	0.5	1	1	12	1	10	6	1.5	3	1.1	2.25	0.015	18.5	2
<b>Outlet 3</b>	0.5	0.5	1	1	12	1	10	6	1.5	3	1.1	2.25	0.015	18.5	2
<b>Outlet 4</b>	0.5	0.5	1	1	12	1	10	6	1.5	1.5	1.8	2.55	0.015	20	2
<b>Outlet 5</b>	0.5	0.5	1	1	12	1	10	6	1.5	1.5	1.8	2.6	0.015	20	2
<b>Outlet 6</b>	0.5	0.5	1	1	12	1	10	6	1.5	1.5	1.8	2.55	0.015	20	2

## 9.4 Results

Figure 9.5 shows the differences in water level in the river in front of the in- and outlet construction of Bergenmeersen. This figure shows that it is difficult to get the water levels in this model correct. The downstream water level boundary of this small model is not located at the same location as the Wetteren tidal measurement station, but more upstream. Keeping this in mind, Figure 9.6 shows the difference between measured and modeled water levels in the floodplain. The water level in the model follows a similar path as the measured water level. Given the complicated construction (in terms of translating this to an equation for discharge) of the in- and outlet structure, these results are a good approximation of reality. In Figure 9.7 we see that the outlet discharge computed by the model fits fairly well the experimental data even if the numerical results overestimate the measurements around 12 h. Regarding the inlet discharge, Figure 9.8 shows that the computed discharges are overestimated by the model, resulting on the overestimation seen in the mean water level in the FCA. A possible explanation for the discrepancies is that the inlet sluices have gates incorporated and in this test case, it is considered that these gates are completely open. We have heard that in reality this is not the case and that the opening of these gates is changed several times over the last two years. The purpose of these gates is to close the area and prevent water from entering. There is no information on the openings of these gates at the time of this 13 h measurement campaign.

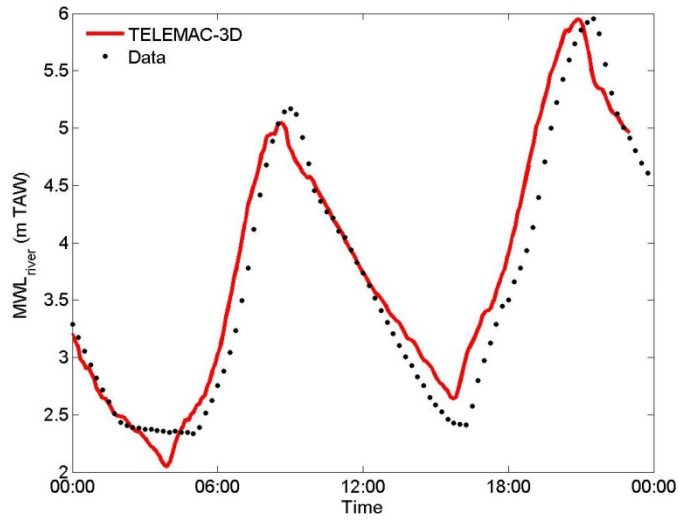


Figure 9.5: Bergenmeersen test case: comparison of the mean water level time evolution in the river between numerical results and measurements.

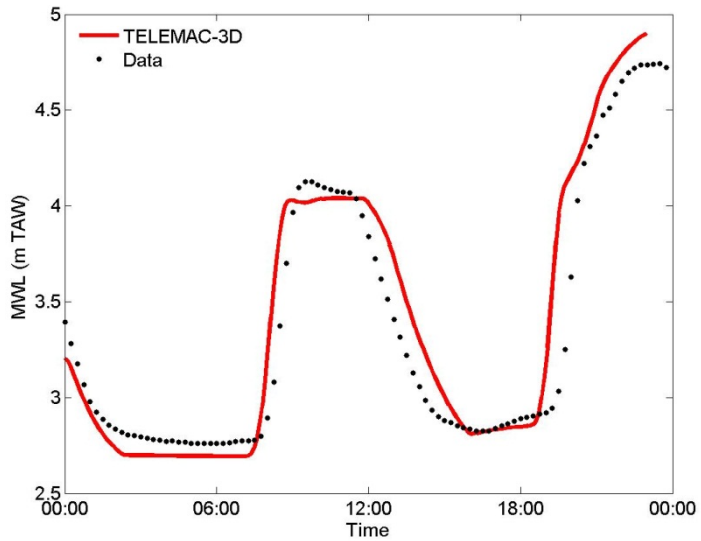


Figure 9.6: Bergenmeersen test case: comparison of the mean water level time evolution in the floodplain between numerical results and measurements.

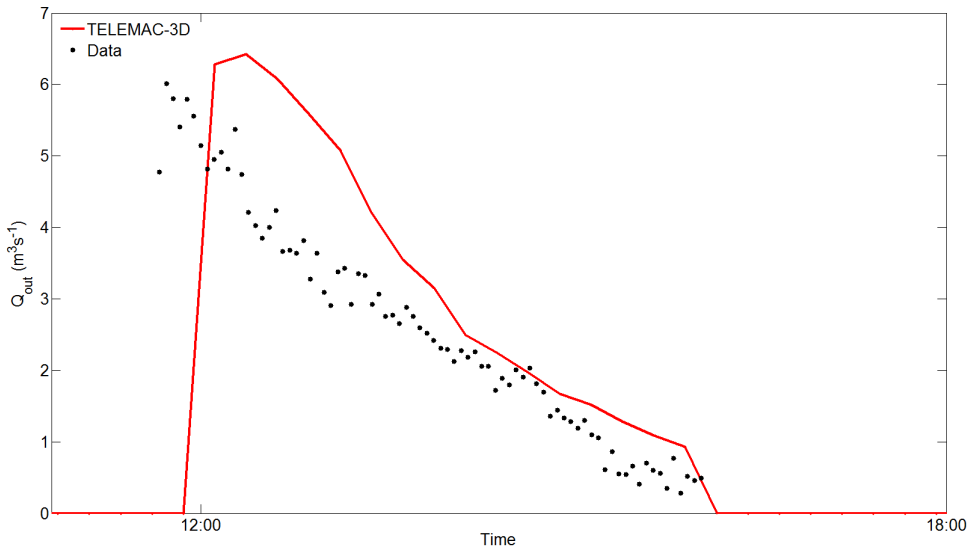


Figure 9.7: Bergenmeersen test case: comparison of outlet culvert discharges time evolution between numerical results and measurements.

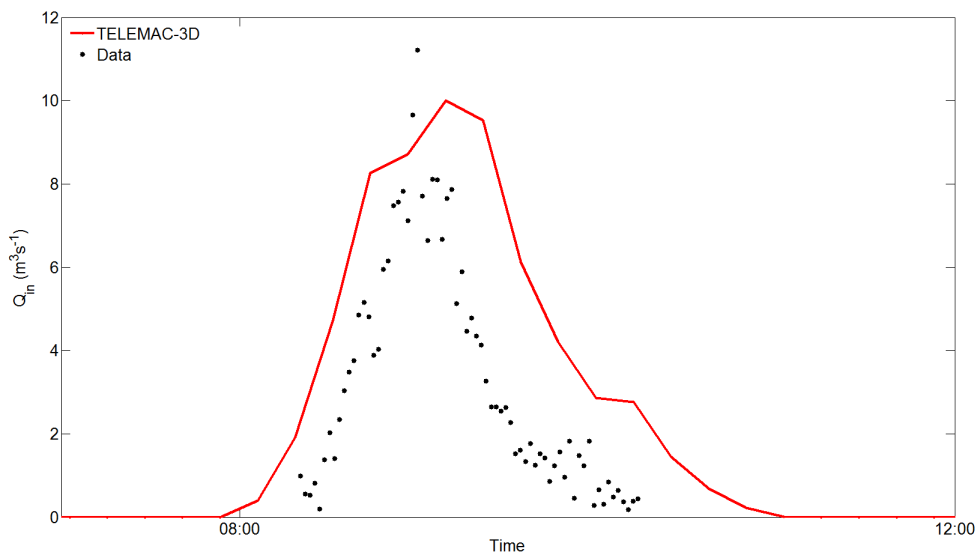


Figure 9.8: Bergenmeersen test case: comparison of inlet culvert discharges time evolution between numerical results and measurements.

The normalized root mean square error is calculated for the mean water levels, outlet and inlet discharges (Table 9.3).

Table 9.3: Normalized root mean square error for the mean water level (MWL\_error), outlet discharge(Qout\_error) and inlet discharge (Qin\_error) in the Bergenmeersen test case.

<b>MWL_error</b>	0.275
<b>Qout_error</b>	0.453
<b>Qin_error</b>	0.538

In Figure 9.9, the flow types that predominate through the inlet and outlet culverts are presented. While for the former, flow types 2, 3 and 4 predominate, for the latter flow types 2 and 4 are the ones that occur the most.

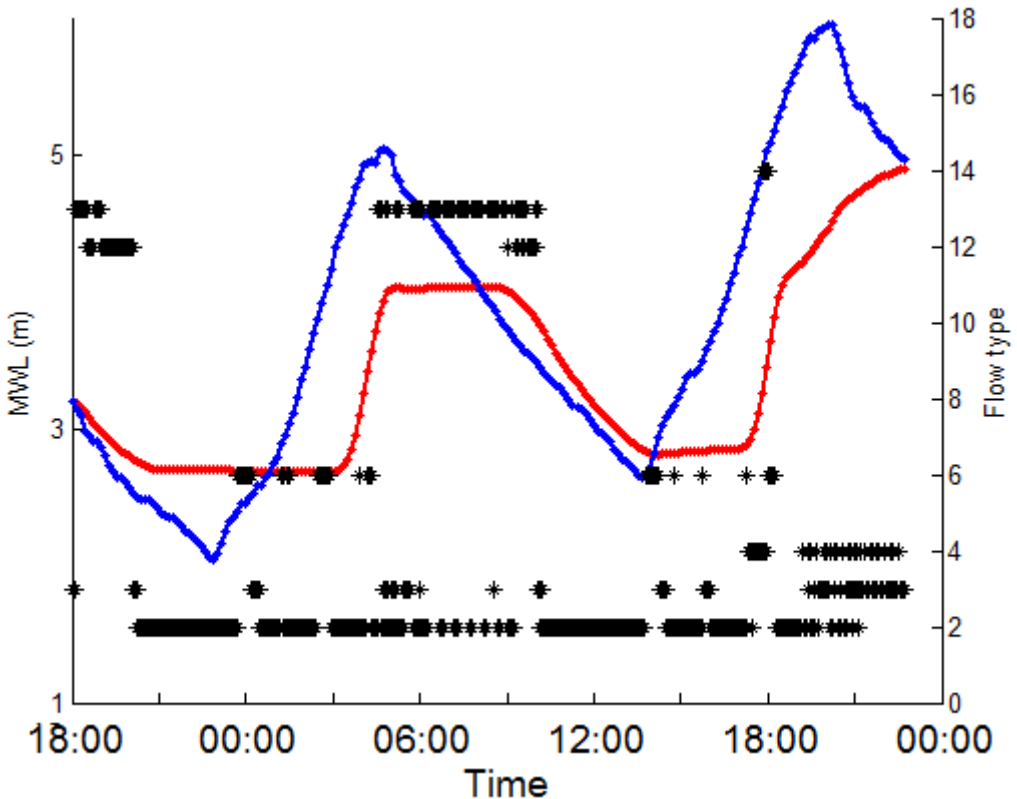


Figure 9.9: Bergenmeersen test case: mean water levels modelled by TELEMAC-3D in the river (blue line) and in the FCA (red line) and the corresponding flow types that occur during the time series. Flow through inlet culvert (type 2 - 6) and through outlet culvert (type 12 - 16).

The results show that given some uncertainty like the representation of ditches and creeks in the topo-bathymetry of the model or the complexity of the in- and outlet structure, numerical results fit fairly well with data, both for the mean water levels and inlet and outlet discharges.

# 10. bottom\_bc

## 10.1 Purpose

This test case is used to validate the boundary conditions on the bed for Telemac-3D simulations

## 10.2 Description of the problem

In this test case two simulations will be run. In `t3d_bottom_inlet.f` a flow rate will be imposed using the boundary conditions on the bed, whereas in `t3d_bottom_source.cas` a source discharge will be imposed on a node on the bed as a source term.

### 10.2.1 Geometry and Mesh

The configuration of this test case is simple, it is a square box of sides 4000 m. The depth is constant, and initially set to 500 m. The geometry of the test case is shown in figure 10.1.

Furthermore, two different meshes will be used, a fine mesh and a coarse mesh. Since source terms are imposed on a node, the coarse mesh is used to impose the inflow on a single node, and it will be used for `t3d_bottom_source.cas`. Since applying a flow rate can be done on several nodes on the bed, the finer mesh will be compared to the coarse mesh for `t3d_bottom_inlet.cas` simulation results. The coarseness of the mesh is also present for the distribution of the planes in the simulation. The fine mesh has a smaller plane spacing near the bed and the free surface, whereas the coarse mesh has the same number of planes, but these are distributed evenly on the bottom half of the domain and the plane spacing decreases towards the free-surface.

### 10.2.2 Initial and Boundary Conditions

A discharge  $Q$  of  $10000 \text{ m}^3\text{s}^{-1}$  will be imposed inside a circle with diameter  $D$  of 100 meters placed at the centre of the bed. All vertical boundaries will be defined as walls, see figure 10.1.

### 10.2.3 Numerical parameters

The key numerical parameters for `t3d_bottom_inlet.f` are:

- OPEN BOUNDARY CONDITIONS ON THE BED = YES
- PRESCRIBED FLOWRATES ON THE BED = 10000.
- NON-HYDROSTATIC VERSION : YES

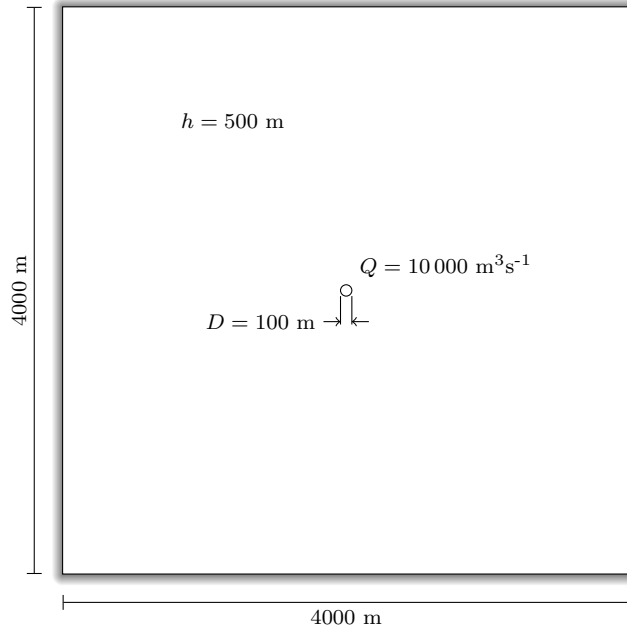


Figure 10.1: Geometrical parameters of the test case.

The key numerical parameters for `t3d_bottom_source.cas` are:

- ABSCISSAE OF SOURCES = 2000.0
- ORDINATES OF SOURCES = 2000.0
- ELEVATIONS OF SOURCES = -500.0
- WATER DISCHARGE OF SOURCES = 10000
- NON-HYDROSTATIC VERSION : YES

### 10.3 Results

At the moment, no post processing is done, however it would be good to have a comparison of the water depth profiles at  $y = 2000 \text{ m}$  and the vertical velocity profiles at  $x = 2000 \text{ m}$  and  $y = 2000 \text{ m}$ . Contour plots of the vertical velocities at  $y = 2000 \text{ m}$  would also be useful.

# 11. Flow over a bump (bump)

## 11.1 Description

This test calculates the fluvial regime in a horizontal straight channel including a topographical singularity (a bump on the bottom). It allows to show that TELEMAC-3D is able to correctly reproduce the hydrodynamic impact of changing bed slopes, vertical flow contractions and expansions. Furthermore, this problem has an analytical solution in 2D. The solution computed by TELEMAC-3D will be compared with this analytical solution. Therefore, it allows also testing the accuracy on the computation of the free-surface, with respect to the bottom gradient.

The geometry dimensions of the channel are 2 m wide and 20.96 m long. The elevation of the flat part of the channel is at -0.2 m (see Figure 11.1). The maximum elevation of the bump in its middle is 0 m (at  $x = 10.0$  m) with the profile of the singularity (Figure 11.2) which is defined by:

$$z_f(x) = \max(-0.2, -0.0246875(x - 10)^2)$$

The studied flow regime provides a transition to super-critical flow conditions located on the bump, and the downstream water level imposes the presence of an hydraulic jump in the downstream reach of the channel. Note that the turbulent viscosity is constant along the horizontal direction and equal to  $10^{-6} \text{ m}^2.\text{s}^{-1}$  (default value) and a mixing length model is applied in the vertical direction (Prandtl formula).

As seen previously, this problem has an analytical solution in 2D. This solution is based on the Bernoulli equations.

For a given discharge per unit length  $q$ , imposed at the upstream boundary and a water depth  $h$  imposed at the downstream boundary, the water line follows the Bernoulli equation written below:

$$\frac{q^2}{2gh^3} + (h + z_f) = H_0$$

where  $H_0$  is specific energy and  $z_f$  is bottom elevation.

### 11.1.1 Initial and boundary conditions

The initial free surface is 0.4 m with a fluid at rest.

The boundary conditions are:

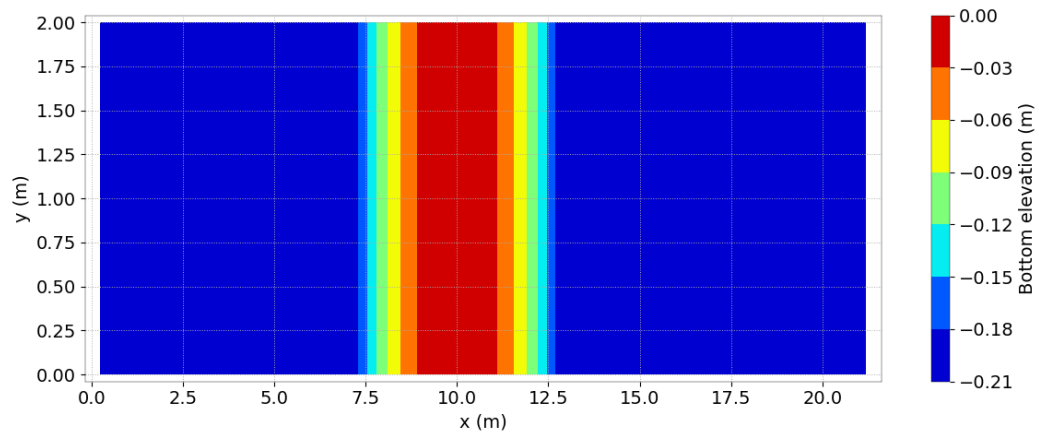


Figure 11.1: Bathymetry.

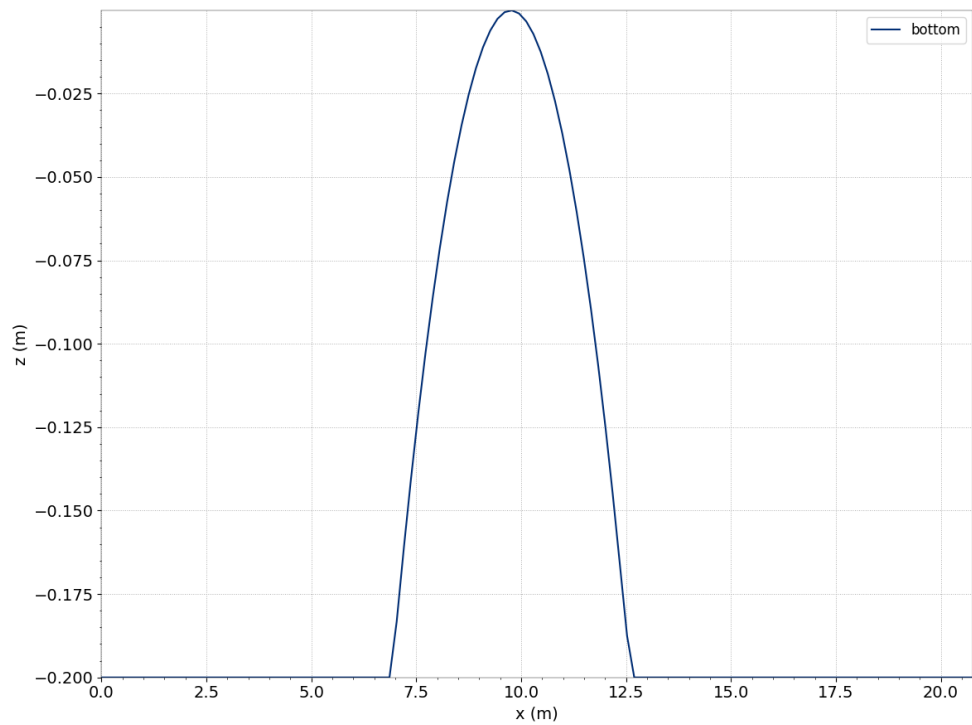


Figure 11.2: Bump profile.

- For the solid walls, a slip condition on channel banks is used for the velocity,
- On the bottom, Strickler law with friction coefficient equal to  $50 \text{ m}^{1/3} \cdot \text{s}^{-1}$  is imposed,
- Upstream a flowrate equal to  $2 \text{ m}^3 \cdot \text{s}^{-1}$  is imposed,
- Downstream the water level is equal to 0.4 m.

### 11.1.2 Mesh and numerical parameters

The mesh (Figures 11.3 and 11.4) is composed of 2,620 triangular elements (1,452 nodes) with 5 planes regularly spaced on the vertical, to form prism elements. Note that the mesh is made up of squares whose sides measure 0.16 m cut into triangles.

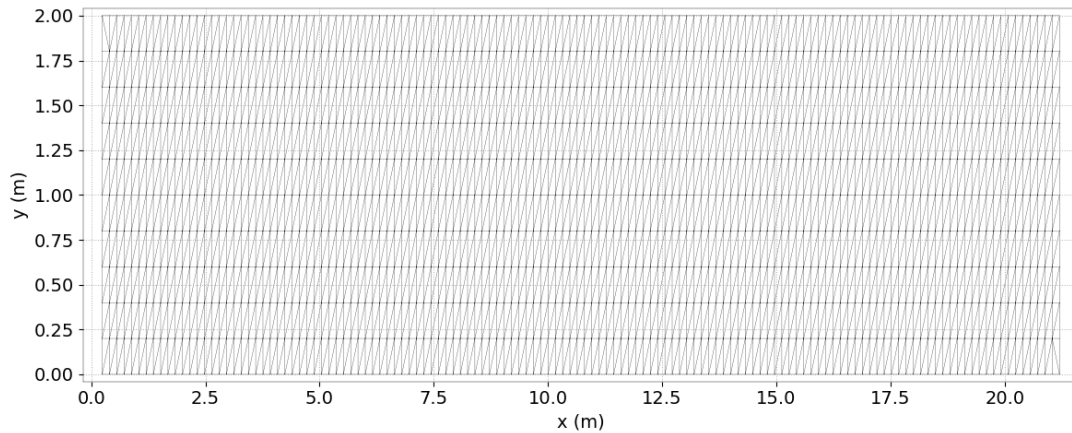


Figure 11.3: Horizontal mesh.

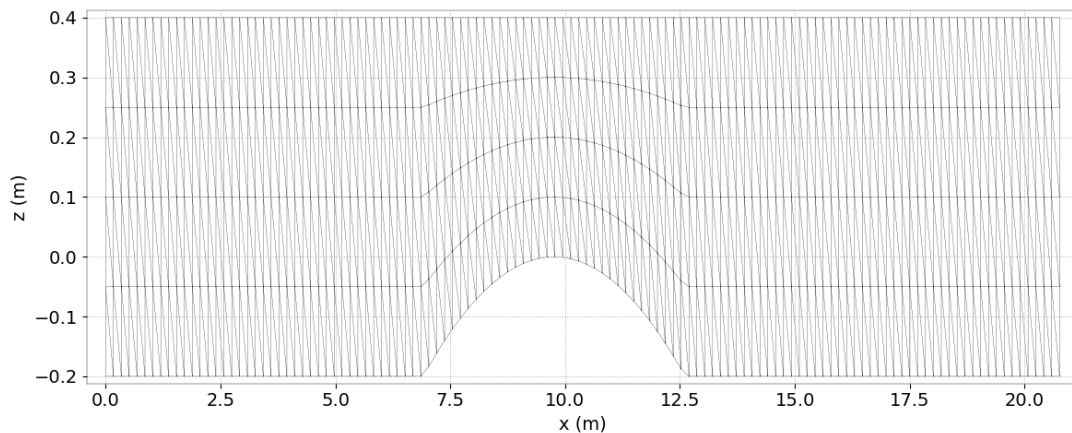


Figure 11.4: Vertical mesh at initial state.

The time step is 0.01 s for a simulated period of 50 s.

This case is computed with the non-hydrostatic version. To solve advection, the method of characteristics is used for the velocities (scheme 1). The GMRES (Generalized Minimal Residual

Method, scheme 7) is used to solve the Pressure Poisson Equation with an accuracy fixed at the default value  $10^{-8}$  (since version 8.1). The implicitation coefficients for depth and velocities are equal to 0.6.

## 11.2 Results

Qualitatively the variation of the velocity field is regular at the surface and vertically in the critical flow area. It follows well the shape of the bump (Figures 11.5 and 11.6). Generally, the results (Figure 11.7) are in good agreement with the analytical solution. This solution is described in details in [1].

Moreover, the position of the hydraulic jump is correctly computed. However, a shift (difference of the free surface at the entrance) is observed on the free surface, which seems to be due to the way to calculate the free surface by TELEMAC-3D.

To conclude, this flow is well reproduced by TELEMAC-3D.

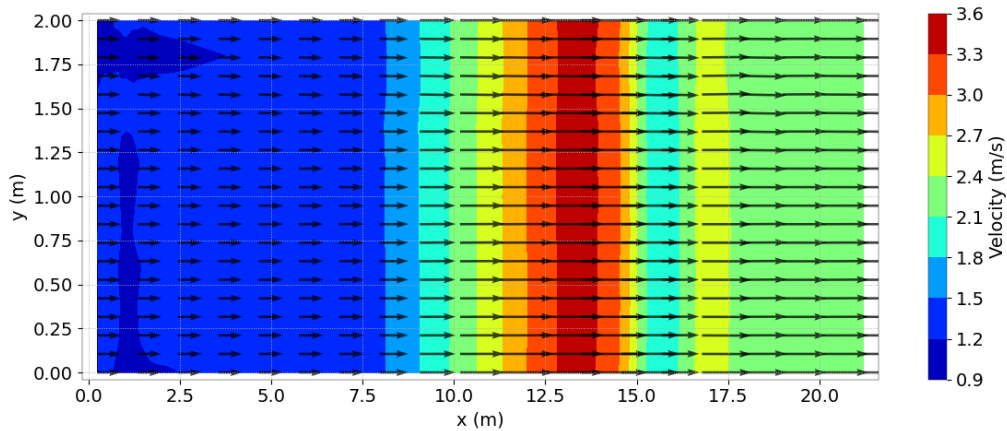


Figure 11.5: Horizontal distribution of velocities at the surface.

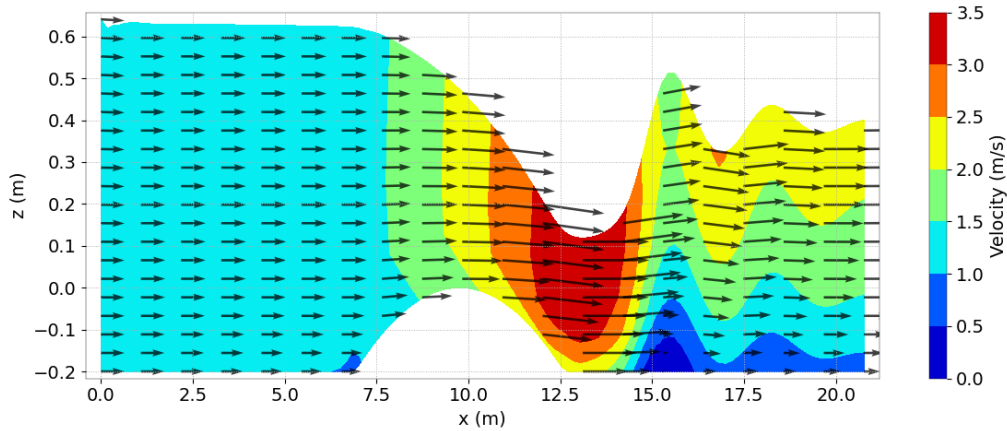


Figure 11.6: Vertical distribution of velocities.

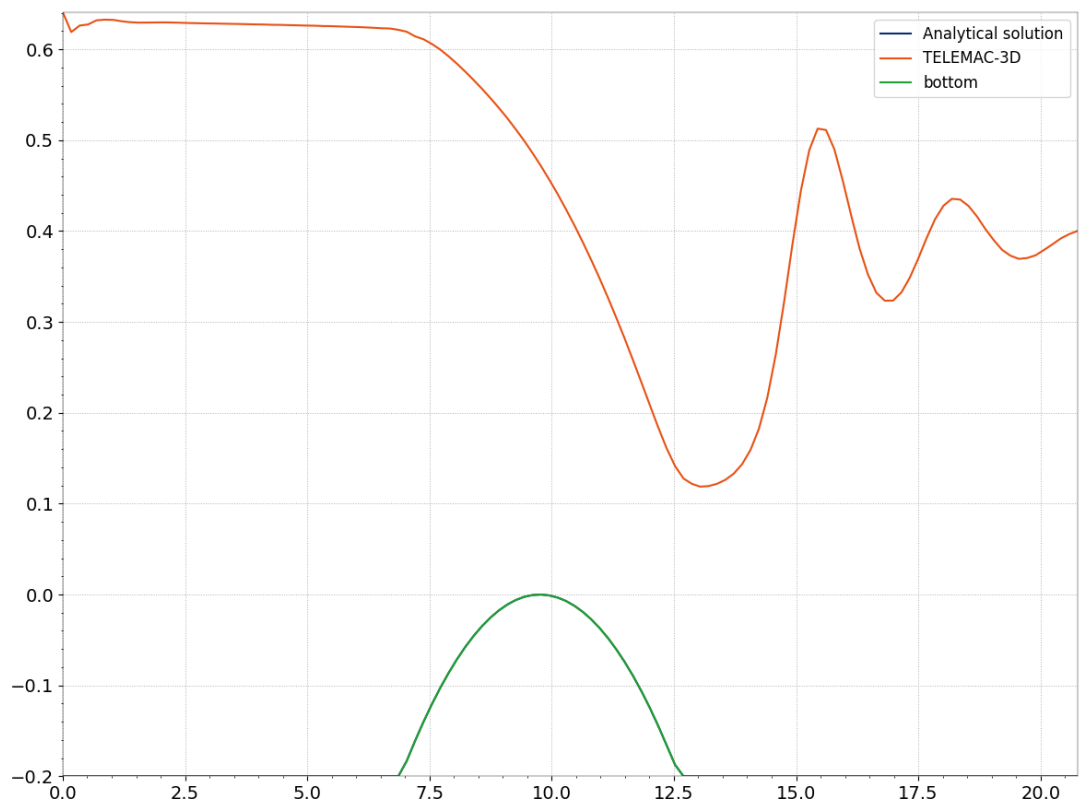


Figure 11.7: Free surface profile comparison between analytical solution and TELEMAC-3D solution.

### 11.3 Reference

- [1] Hydrodynamics of Free Surface Flows modelling with the finite element method. Jean-Michel Hervouet (Wiley, 2007) pp 128-129.

## 12. Equilibrium of a stratified flow above a bump (bump\_static)

### 12.1 Purpose

This test case belongs to a benchmark of CFD codes with analytical solutions. Its aim was to study the behavior of different codes, focusing on situations where the density variations have a crucial influence on the hydrodynamical process. This study was carried out during Lamia Abbas's post-doctoral [10] in 2014-2015.

This test case demonstrates the ability of TELEMAC-3D to preserve equilibria for stratified flows. The example only shows the results for one specific 2D mesh and one distribution of planes over the vertical.

### 12.2 Description

A 3 m long and 2 m wide channel with a specific bottom is considered. The bottom elevation  $z_f$  is defined by a bump at the bottom:

$$z_f(x, y) = \max(0, 0.25 - 1.246(x - 1.2)^2), \quad (12.1)$$

see Figure 12.1.

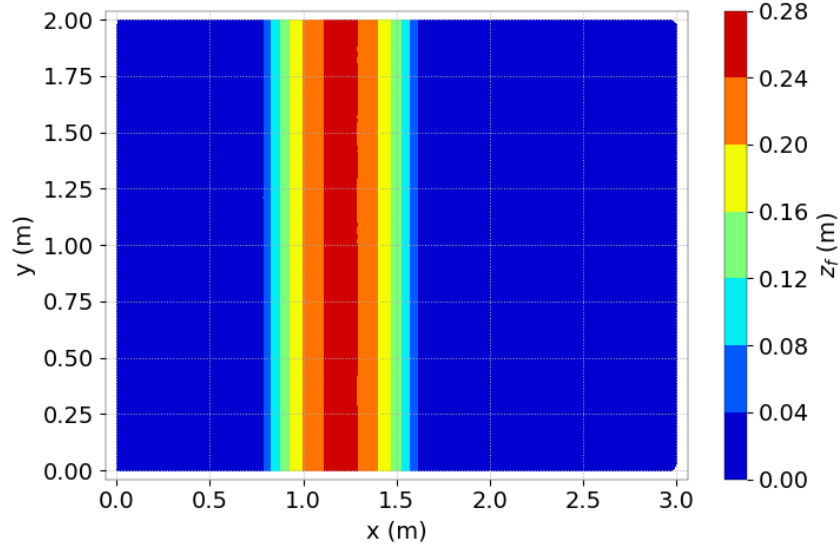


Figure 12.1: Bottom elevation.

The tracer used is temperature. The density is considered as a function of the water temperature:

$$\rho(T) = \rho_0 (1 - \alpha(T - T_0)^2), \quad (12.2)$$

where  $\rho_0 = 999.972 \text{ kg.m}^{-3}$ ,  $T_0 = 4 \text{ }^\circ\text{C}$  and  $\alpha = 7.10^{-6}$ .

There are two layers of water with different temperatures. As the density depends on water temperature, the initial state is chosen nearly stable *i.e.* the heavier fluid is below the lighter. Above the bump, the initial temperature condition follows the bottom elevation as shown in Figure 12.4.

## 12.3 Computational options

### 12.3.1 Mesh

The triangular mesh is composed of 5,250 triangular elements (element size  $\approx 0.05 \text{ m}$ ) and 2,745 nodes (see Figure 12.2).

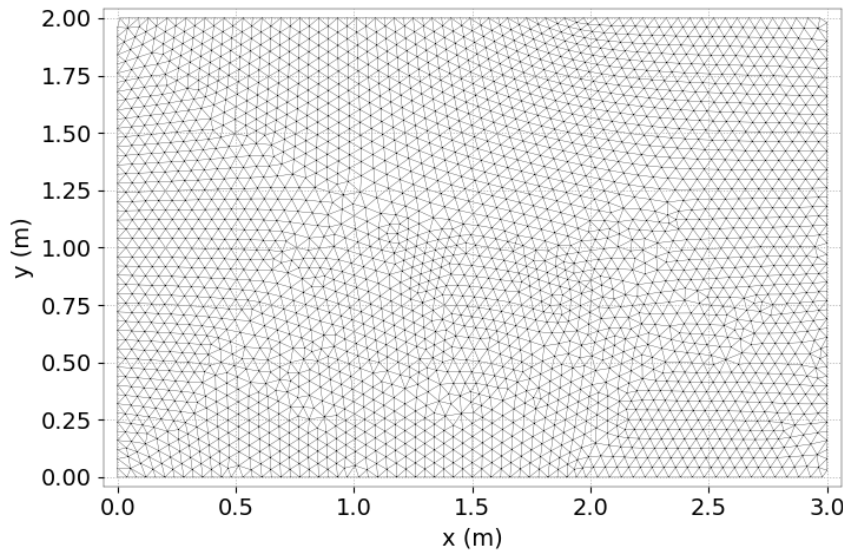


Figure 12.2: Horizontal mesh.

To build the 3D mesh of prisms, 40 planes are regularly spaced over the vertical. The vertical mesh between nodes of coordinates (0 ; 1) to (3 ; 1) can be seen in Figure 12.3.

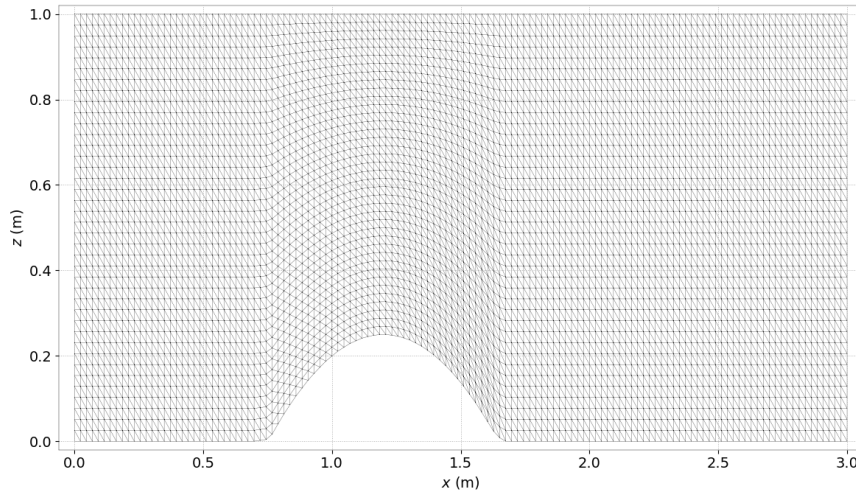


Figure 12.3: Vertical mesh at initial.

The classical  $\sigma$  transformation is used, but as the free surface does not move during the computation, the mesh can be considered as fixed.

During Lamia Abbas's post-doctoral, 3 other 2D grids were used:

- one coarser grid with 1,279 elements (2D) with element size  $\approx 0.1$  m,
- two finer grids with 22,012 resp. 132,876 elements (2D) with element size  $\approx 0.025$  m resp. 0.01 m.

Moreover, 3 different vertical distributions were tested:

- two coarser vertical distributions with 10 resp. 20 horizontal planes leading to  $\approx 0.1$  m resp. 0.05 m vertical height,
- one finer vertical distribution with 100 horizontal planes leading to  $\approx 0.01$  m.

To summarize, the different grids tested during the post-doc were:

N	1	2	3	4	5	6	7	8
$dl$ (m)	0,1	0,05	0,025	0,01	0,1	0,1	0,1	0,05
$dz$ (m)	0,1	0,05	0,025	0,01	0,05	0,025	0,01	0,025
# elements 2D	1,279	5,250	22,012	132,876	1,279	1,279	1,279	5,250
# elements 3D	11,511	99,750	858,468	13,154,724	24,301	49,881	126,621	204,750

### Remarks

Meshes #1, 2, 3 and 4 are isotropic and more and more refined. Meshes #1, 5, 6 and 7 (resp. 2 and 8) have the same horizontal discretisation and a bigger and bigger number of horizontal planes (from 10 to 100).

#### 12.3.2 Physical parameters

The turbulent viscosities for both velocities and tracers are constant, also both for horizontal and vertical directions:  $\nu = 0.003$  m<sup>2</sup>/s and  $\nu_T = 0$ . No wind is taken into account.

#### 12.3.3 Initial and Boundary Conditions

The initial free surface elevation is 1 m with a fluid at rest. The initial temperature depends on elevation, defined as:

$$T_0(x, y, z) = \begin{cases} 25^\circ\text{C} & \text{if } z - z_f > 0.66 \text{ m,} \\ 7^\circ\text{C} & \text{else} \end{cases} \quad (12.3)$$

see Figure 12.4.

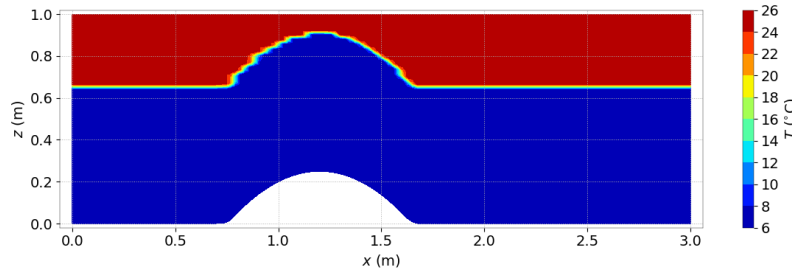


Figure 12.4: Initial condition for temperature.

There are only closed lateral boundaries with free slip condition and no friction at the bottom.

#### 12.3.4 General parameters

The time step is 0.5 s for a simulated period of 100 s.

#### 12.3.5 Numerical parameters

The non-hydrostatic version of TELEMAC-3D is used. To solve the advection steps, the N-type MURD scheme is chosen for the velocities and the PSI-type MURD scheme for the temperature.

## 12.4 Results

If the diffusion of the tracer is not accounted, *i.e.* if  $v_T = 0$  for both horizontal and vertical directions, the system will reach a stable equilibrium characterized by:

$$\frac{\partial T}{\partial x} = 0 \quad \text{and} \quad \frac{\partial T}{\partial y} = 0 \quad \forall x, y, z \in \Omega. \quad (12.4)$$

Then the expected level of the thermocline will be  $H_{eq} = 0.7098$  m (see [10]).

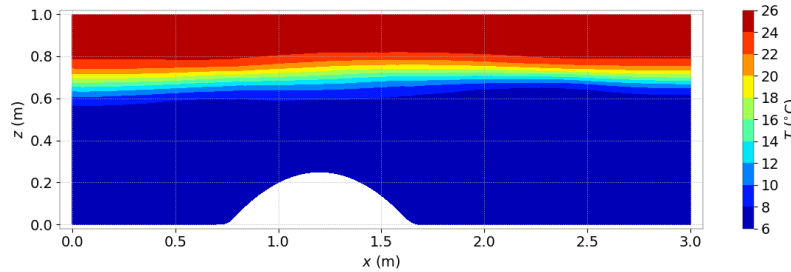


Figure 12.5: Temperature after 100 s.

### Required calculations

A bias exists in the reference solution because the initial quantities of warm and cold waters depend on the 3D mesh. This bias is constant and decreases when refining the mesh.

Moreover, it is difficult to determine the exact location of the thermocline with computations. Indeed, due to numerical diffusion and interpolations done by the code or post-treatment tools, the mixing layer is more or less big. For all these reasons, two points can be investigated:

- A comparison between the distribution of the temperature at the equilibrium and the expected position of the thermocline  $H_{eq}$ ,
- Evaluation of the diffusion by measuring the mixed water defined as:  $Q_m = \int_0^L (Z_2 - Z_1) dx$  with  $Z_1$  and  $Z_2$  defined such as  $T(x, Z_1) = 10$  °C and  $T(x, Z_2) = 22$  °C.

Here, as we do not compare different codes or meshes, we only look at the location of the expected thermocline.

### Planes distribution

Results for the different  $\sigma$  planes distribution are not discussed here, but the user can refer to [10] for more informations.

A suitable distribution of horizontal planes (a  $\sigma$  transformation for the first 3 bottom planes and  $z$  for the ones above so that a maximum number of horizontal planes around the thermocline) enables to greatly improve the results with a reasonable number of elements.

The Automatic Mesh Refinement option (MESH TRANSFORMATION = 5) enables to save the use of some extra planes and may give correct results for such applications.

See [10] for more informations.

## 12.5 Conclusion

TELEMAC-3D is able to preserve equilibria for stratified flows.

# 13. Flow in a channel with bottom friction (canal)

## 13.1 Description

This study case verifies that TELEMAC-3D is able to compute the free surface evolution along a channel with bottom friction.

This example also checks that TELEMAC-3D is able to deal with stage-discharge curves.

The chosen configuration is a straight channel 500 m long and 100 m wide with a flat horizontal bottom without slope. Four different cases are studied:

- A 2D computation using TELEMAC-2D,
- A 3D computation with hydrostatic option,
- A 3D computation with non-hydrostatic option,
- A 3D computation with non-hydrostatic option and a stage-discharge curve  $Z = f(Q)$  at the exit.

In all cases, the flow establishes a steady flow where the free surface is influenced by the friction on the bottom.

Note that the velocity diffusion is constant in horizontal direction and equal to  $0.1 \text{ m}^2.\text{s}^{-1}$  with the non-hydrostatic option and with TELEMAC-2D usage, whereas with the hydrostatic option, it is null. In the vertical direction, the turbulent viscosity uses Nezu and Nakagawa mixing length model for the three TELEMAC-3D computations.

### 13.1.1 Initial and boundary conditions

This test is initialised by a steady flow (3D cases initialised from the 2D case result file, Figures 13.1 and 13.2).

The boundary conditions are:

- For the solid walls, a slip condition on channel banks is used for the velocities,
- On the bottom, Strickler law with friction coefficient equal to  $50 \text{ m}^{1/3}.\text{s}^{-1}$  is imposed,
- Upstream a flowrate equal to  $50 \text{ m}^3.\text{s}^{-1}$  is imposed,

- Downstream the water level is equal to 0.5 m for the first three computations. For the last computation, elevation is also prescribed but by giving a stage-discharge curve  $Z = f(Q)$ .

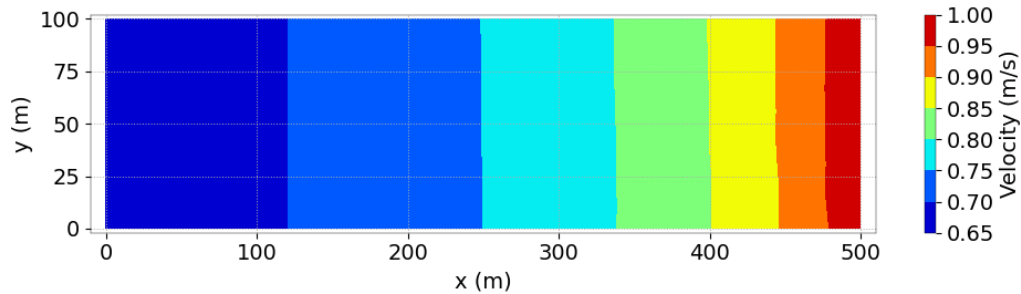


Figure 13.1: Horizontal velocity obtained at the steady state.

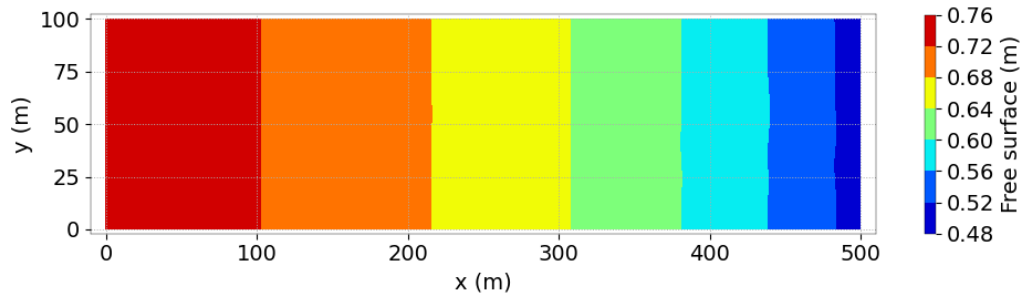


Figure 13.2: Free surface at the steady state.

### 13.1.2 Mesh and numerical parameters

The mesh (Figure 13.3 and 13.4) is composed of 551 triangular elements (319 nodes) with 10 planes regularly spaced on the vertical, to form prism elements.

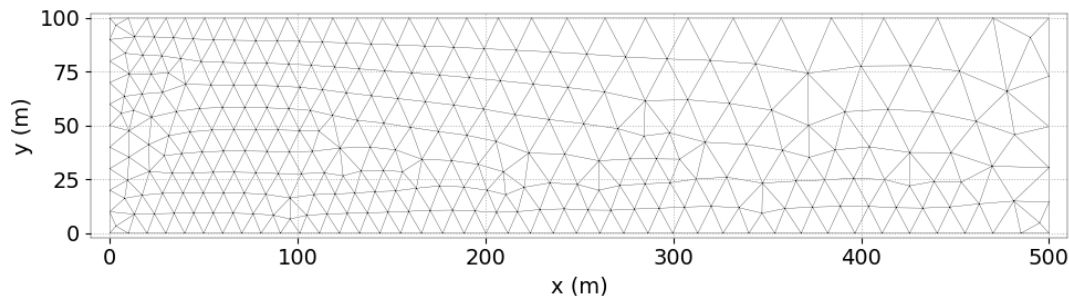


Figure 13.3: Horizontal mesh.

The time step is 2 s for a simulated period of 4,000 s for the 2D computation then 2,000 s more for 3D computations.

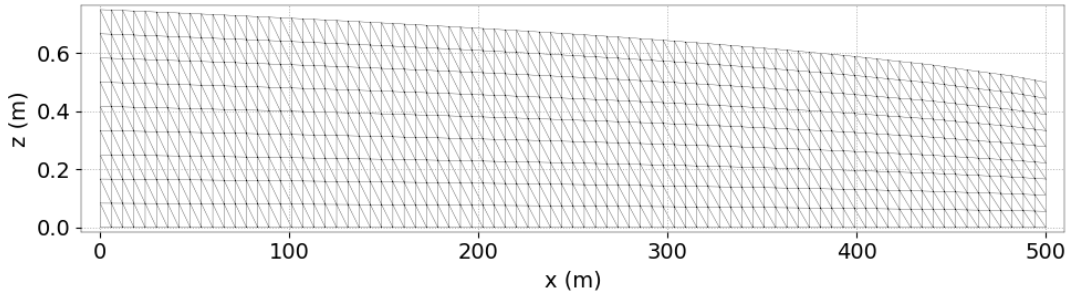


Figure 13.4: Vertical mesh.

This case is computed both with the hydrostatic pressure assumption and the non-hydrostatic version. To solve the advection, the method of characteristics is used for the velocities (scheme 1). The GMRES (Generalized Minimal Residual Method, scheme 7) is used to solve the vertical velocity. The implicitation coefficients for depth and velocities are equal to 0.6.

For the 2D resolution, the conjugate gradient is used for solving the propagation step (option 1) and the implicitation coefficients for depth and velocities are respectively equal to 1 and 0.55.

## 13.2 Results

In Figure 13.5, the three free surface profiles corresponding to the first three simulations are compared. These three results are in good agreement. We can also observe that the flow is completely symmetric without any influence of the space discretisation.

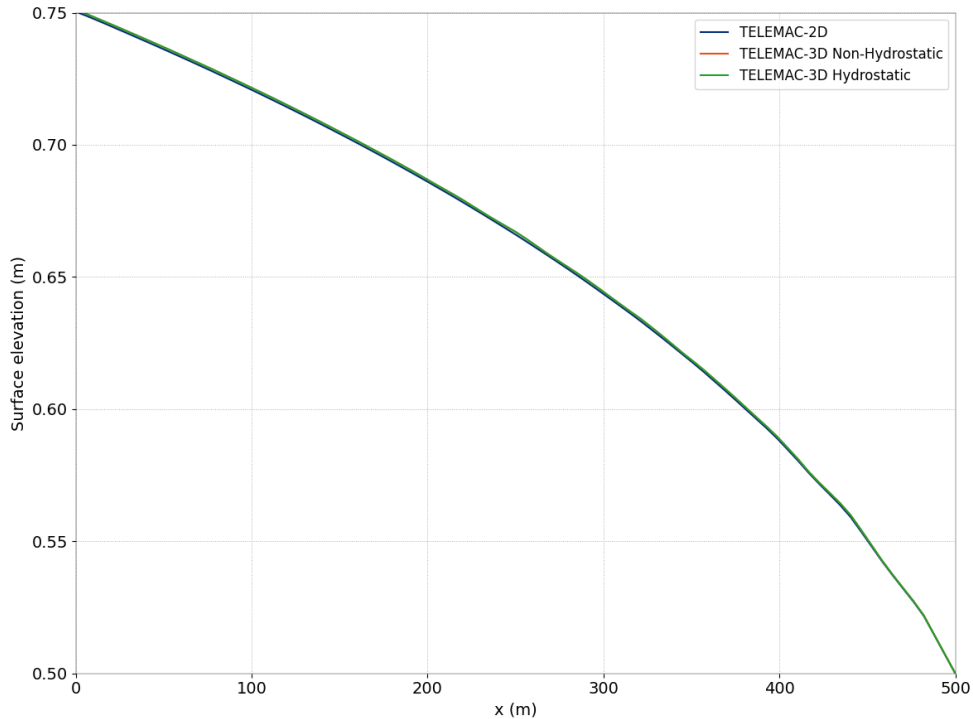


Figure 13.5: Comparison of the free surface profiles between the 2D computation and the 3D computations with hydrostatic and non-hydrostatic options.

The same comments can be done when comparing classical prescribed boundary conditions and boundary conditions with stage-discharge curve, see Figure 13.6.

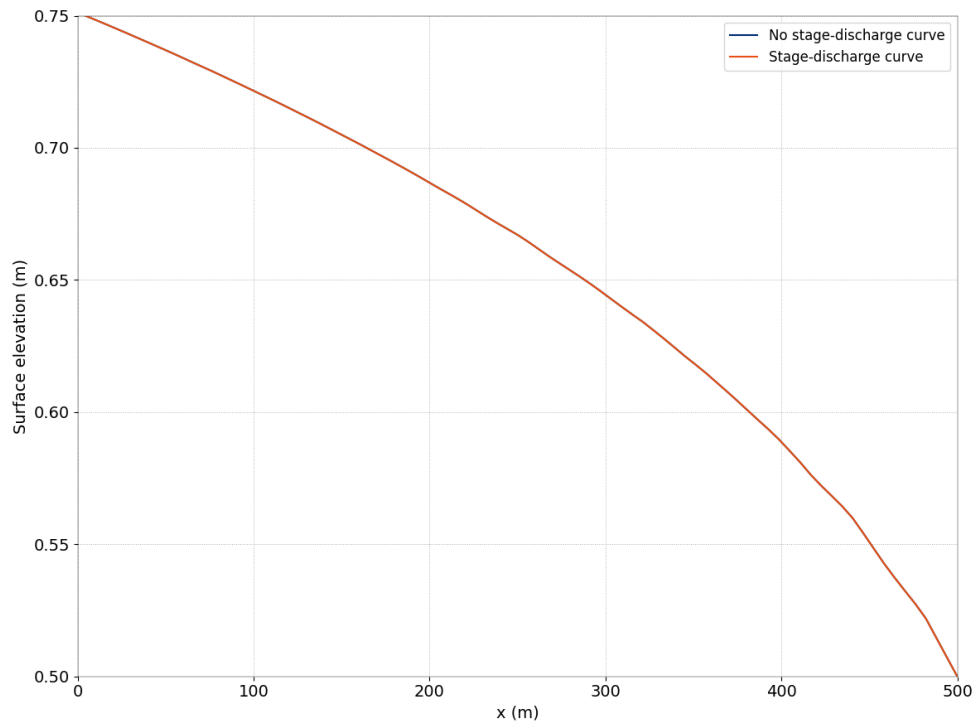


Figure 13.6: Comparison of the free surface profiles between the computations without or with stage-discharge curves.

### 13.3 Conclusion

To conclude, TELEMAC-3D is able to take into account correctly the bottom friction term and stage-discharge curves.

## 14. Advection of tracers with a rotating cone (cone)

### 14.1 Purpose

This test shows the performance of the finite element advection schemes of TELEMAC-3D for passive scalar transport in a time dependent case. It shows the advection of a tracer (or any other passive scalar) in a square basin with flat frictionless bottom.

### 14.2 Description

#### 14.2.1 Geometry and mesh

The domain is a 20.1 m long square. The 2D mesh is made from a regular grid from which every square is cut in half, with 8,978 elements and 4,624 nodes. 6 planes are regularly spaced on the vertical (see Figure 14.2).

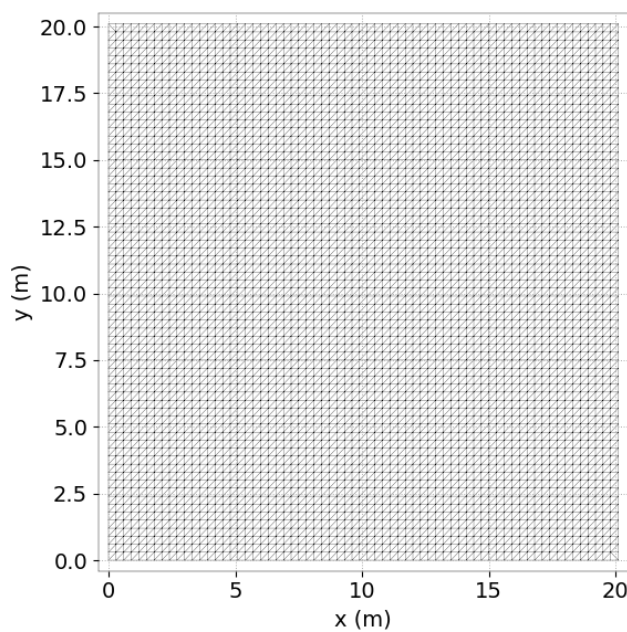


Figure 14.1: 2D domain and mesh of the cone test case.

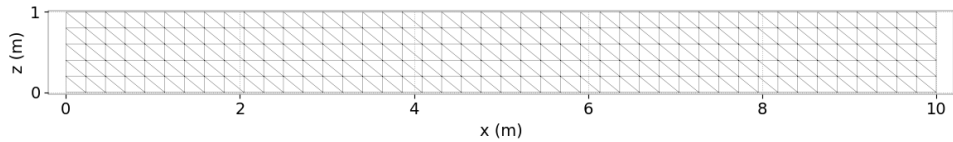


Figure 14.2: Initial vertical mesh.

### 14.2.2 Initial condition

The water depth is constant in time and in space, equal to 1 m. The velocity field is constant in time as well and is divergence free:

$$\mathbf{u} = \begin{cases} u(x, y) = -(y - y_0) \\ v(x, y) = (x - x_0) \end{cases}$$

With  $x_0 = 10.05$  m and  $y_0 = 10.05$  m. The initial value for the tracer is given by the Gaussian function off-centered 4.95 m to the right of  $(x_0, y_0)$ :

$$c^0(x, y) = e^{-\frac{1}{2}[(x-15)^2 + (y-10.2)^2]}$$

### 14.2.3 Analytic solution

The tracer is described by a Gaussian function and is submitted to a rotating velocity field. After one period, we expect that the tracer function has the same position and the same values as the initial condition (i.e. maximum value equal to 1 at the center). The analytical solution for the tracer  $c$  is given by:

$$c(x, y, t) = e^{-\frac{1}{2}[X^2 + Y^2]}$$

with:

$$\begin{cases} X = x - x_0 - R \cos(\omega t) \\ Y = y - y_0 - R \sin(\omega t) \end{cases}$$

where  $R = 4.95$  m.

### 14.2.4 Physical parameters

In this case, the tracer advection equation is solved using fixed hydrodynamic conditions. No bottom friction is imposed and the diffusivities of velocities and tracers are set to zero. Angular velocity of the rotating cone  $\omega$  is equal to 1 rad.s<sup>-1</sup> which gives a rotation period equal to  $T = 2\pi$  (6.2831854820251465 s).

Diffusion for velocities or tracers are both set to 0.

### 14.2.5 Numerical parameters

The simulation time is set to one period of rotation. The time step is chosen in order to do the whole period in 64 steps, so it is equal to 0.098174771 s.

The hydrostatic version is used.

For tracers advection, nearly all the numerical schemes available in TELEMAC-3D are tested (except strong characteristics which are known to be non conservative). For weak characteristics the number of Gauss points is set to the single possible choice: 6. For distributive schemes, like predictor-corrector (PC) schemes (scheme 4 and 5 with options 2 or 3) and locally implicit schemes (LIPS: scheme 4 and 5 with option 4), the number of corrections is set to 5, which is usually sufficient to converge to accurate results. For the locally implicit schemes (scheme 4 and 5 with option 4), the number of sub-steps is equal to 10.

The conjugate gradient is used to solve every linear system except when solving the diffusion of tracers for the SUPG scheme (= 2) for which GMRES is used with Krylov dimension equal to 10. In this last case only diagonal preconditioning is used (2 = default option) whereas the combo 34 (=  $17 \times 2$ ) is possible for other advection schemes (and conjugate gradient).

Accuracy for solving the tracers diffusion step is set to  $10^{-12}$ .

## 14.3 Results

### 14.3.1 Comparison of schemes

The final contour maps after one rotation of the cone are plotted for each scheme in Figures 14.3 and 14.4.

White areas mean the values are outside [0;1]. The shape of the Gaussian function is rather distorted with SUPG (2) and original MURD schemes (PSI, N, Leo Postma, respectively 5, 4 and 3 with scheme option = 1). Using corrections (Predictor-Correction or LIPS) improve the results with less distorted shapes combined to a peak better computed (and closer to 1): i.e. schemes 4 or 5 with scheme option 2, 3 or 4. NERD schemes (13 and 14) give lightly better results than MURD schemes, but are more diffusive than using corrections from MURD schemes. Weak characteristics give the best results for the peak after one period but some values are negative that is a strong drawback for tracers. SUPG also computes many negative values in addition to a quite distorted shape.

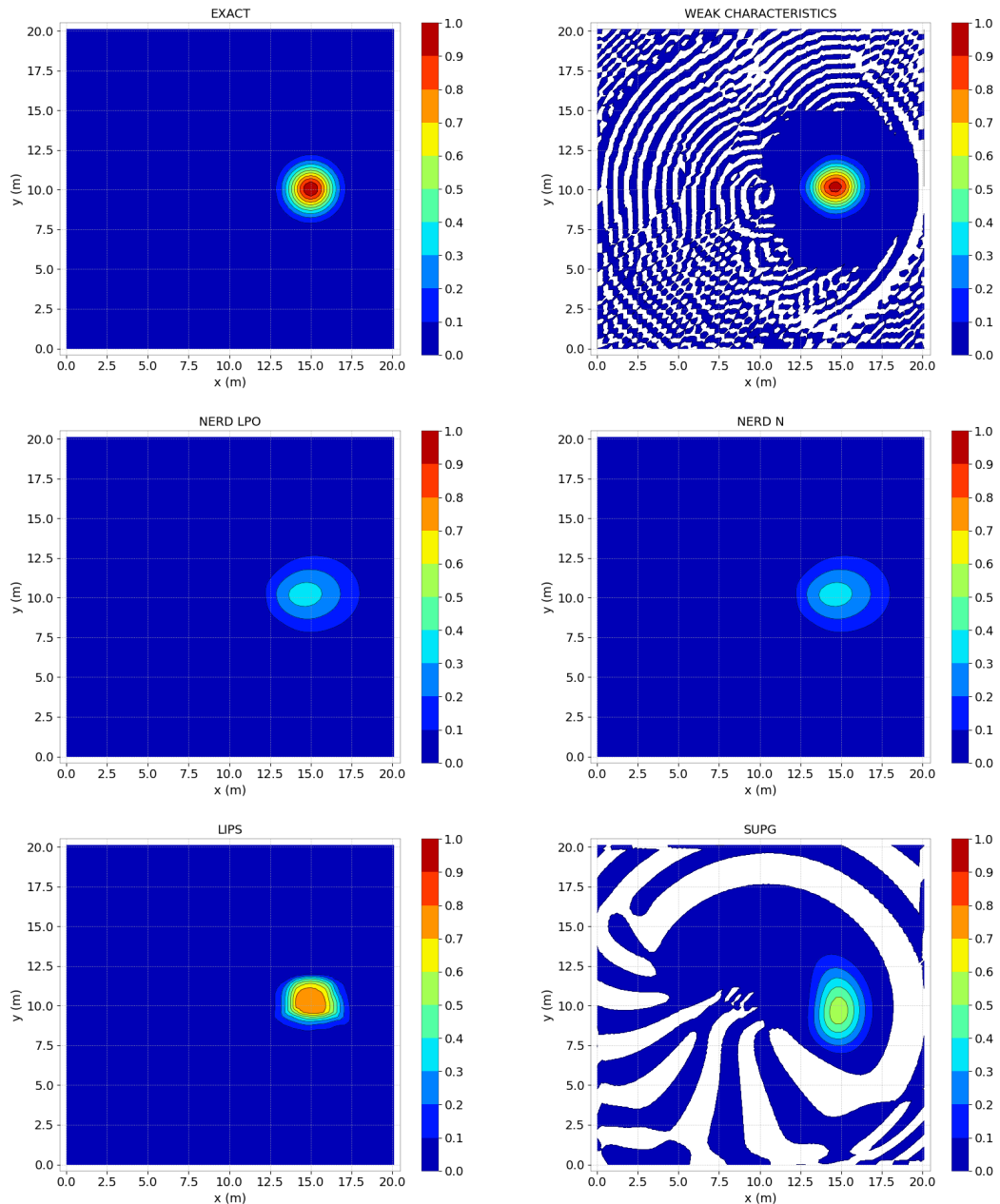


Figure 14.3: Cone test: contour maps of tracer after one period of rotation, for the advection schemes of TELEMAC-3D.

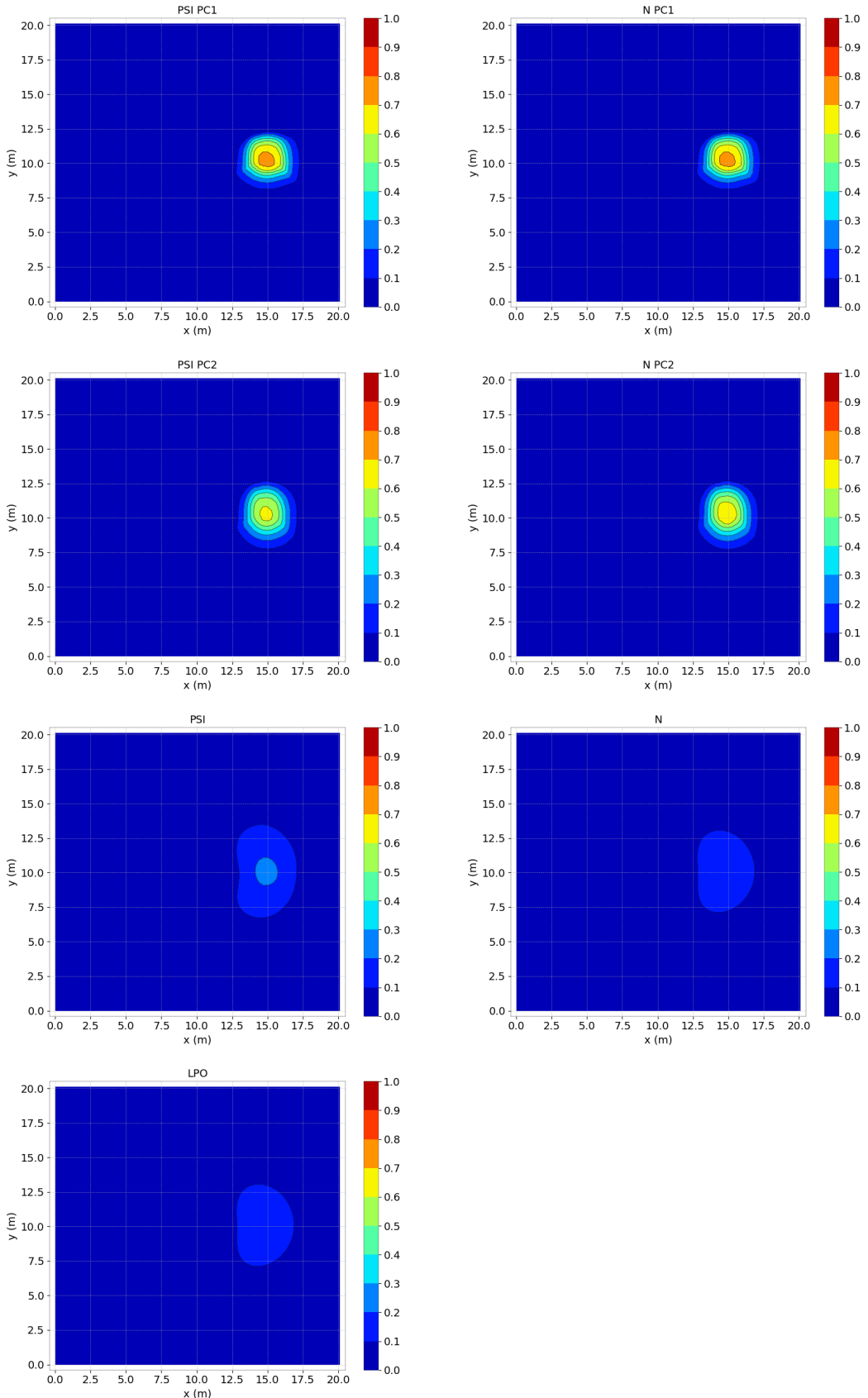


Figure 14.4: Cone test: contour maps of tracer after one period of rotation, for the advection schemes of TELEMAC-3D.

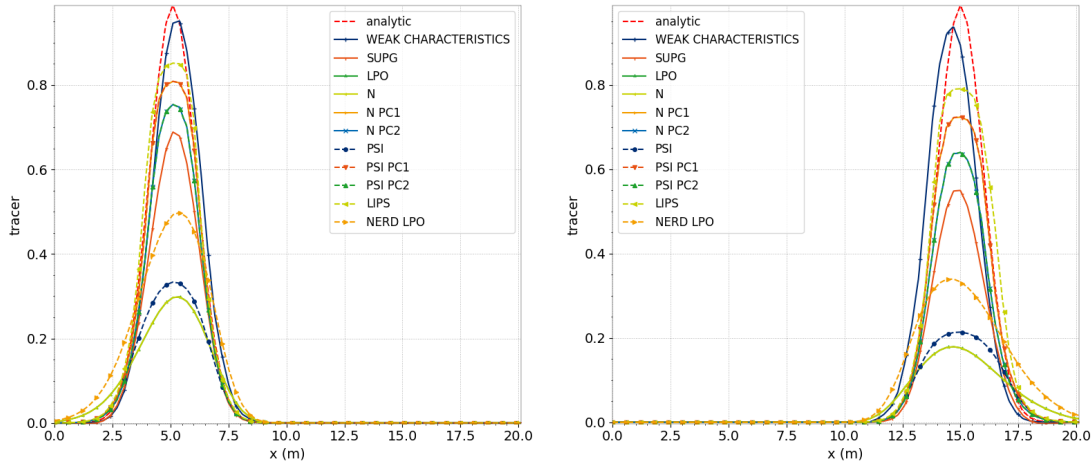


Figure 14.5: 1D solution along slice plane ( $x, y$ ),  $y = 10$  at  $t = T/2$  (left) and  $t = T$  (right).

### 14.3.2 Maximum principle

The minimum value of the Gaussian function is measured after one rotation. The maximum value is computed as well, in order to check the respect of the maximum principle (or monotonicity). Results are shown in Figures 14.6.

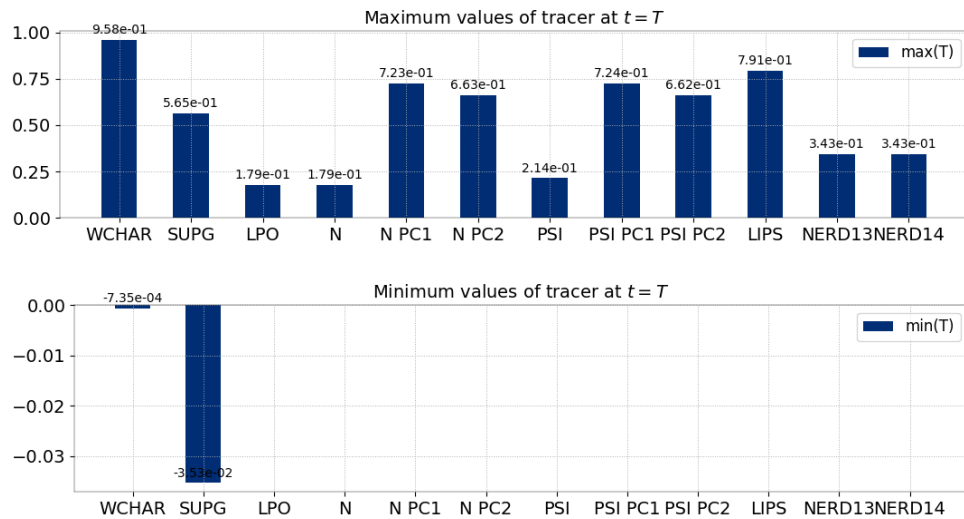


Figure 14.6: Maximum and minimum values of tracer after one rotation of the cone.

As already shown in the previous section, weak characteristics and SUPG compute negative values which is a strong drawback when modelling tracers.

MURD family schemes (all other advection schemes) satisfy the maximum principle as seen in Figures 14.6 (no value outside  $[0, 1]$ ).

## 14.4 Conclusion

TELEMAC-3D is able to model passive scalar transport problems.

## 15. Schematic culvert test case (culvert)

### 15.1 Purpose

The purpose of this case is to test the culvert feature in TELEMAC-3D, qualitatively checking that the behaviour of the flow between a tide-controlled river and a floodplain is consistent.

### 15.2 Description

This schematic test case consists of a piece of flood plain and a piece of tidal river from an estuary and they are separated by a dike. There is water exchange between the floodplain and the estuary through two culverts. In normal tidal conditions, the tide can enter the floodplain and this will create tidal nature like mud flats and marshes. In storm conditions the culverts are closed and the floodplain is used as a buffer to store water. The crest level of the dike between the estuary and the floodplain is a little lower than the other dikes containing the estuary. When extreme high water levels occur inside the estuary, water can flow over the dike into the floodplain. In this schematic test case we only want to simulate the exchange of water between estuary and floodplain through two culverts.

The floodplain has a bed level of 1 m (TAW = Belgian reference level where 0 m is about mean low water level). The dike has a crest level of 6 m and the estuarine river has a bed level of -5 m. An overview of the configuration is given in Figure 15.1. On the right side, the river side, a liquid boundary is set and a tidal signal (i.e. a measured tidal signal from tidal gauge at Schoonaarde, Belgium in the Scheldt estuary) in the form of water levels is applied. Two nodes in the estuary communicate with two nodes in the floodplain to represent the two culverts. One culvert allows flow in both directions and the other culvert only allows flow from the floodplain back to the estuary (this type of culvert in the Scheldt estuary always has a one-way valve and makes sure flood water can return to the estuary after a storm surge).

### 15.3 Computational options

#### 15.3.1 Mesh

#### 15.3.2 Initial and boundary conditions

The water level in the river is prescribed through tidal boundary conditions.

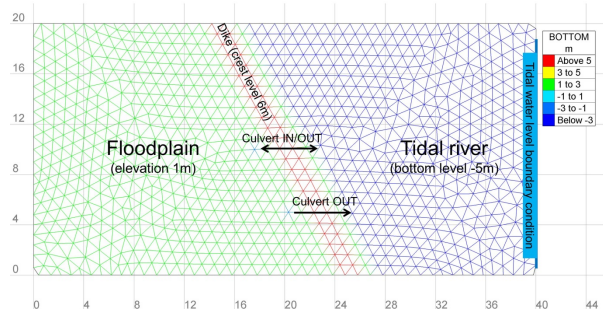


Figure 15.1: Overview of schematic test case for culvert testing.

### 15.3.3 Numerical parameters

The simulation time is about 28 hours. The time step is set to 1 s, providing, together with the chosen mesh resolution, a stable simulation.

The bottom friction is taken into account in the model through the Manning Strickler's parameter  $n$ , set to  $0.02 \text{ s.m}^{-1/3}$ . The horizontal and vertical turbulence viscosity coefficients are both set to  $0.01 \text{ m}^2.\text{s}^{-1}$ , with Smagorinsky turbulence model in the horizontal directions and mixing length model in the vertical direction.

### 15.3.4 Culvert characteristics

The characteristics of the culverts are presented in Table 15.1.

Table 15.1: Culvert specifications (these are as similar to the real field culverts as possible).

	<b>Culvert 1</b>	<b>Culvert 2</b>
<b>I1</b>	583	637
<b>I2</b>	432	497
<b>CE1</b>	0.5	0.5
<b>CE2</b>	0.5	0.5
<b>CS1</b>	1	1
<b>CS2</b>	1	1
<b>LRGbus</b>	1	2
<b>Haut1</b>	1.9	1.5
<b>CLP</b>	0	2
<b>LBUS</b>	0.2	0.2
<b>z1</b>	4	1.5
<b>z2</b>	4.7	1.5
<b>CV</b>	0	1
<b>C56</b>	10	10
<b>CV5</b>	1.5	1.5
<b>C5</b>	6	6
<b>Ctrash</b>	0.8	0.1
<b>Haut2</b>	1.2	1.5
<b>Fric</b>	0.015	0.015
<b>Length</b>	13	40
<b>circ</b>	0	0

## 15.4 Results

Figure 15.2 shows the results of a short simulation with the schematic scenario. The blue line gives the water level in the estuarine river part and the red line gives the water level in the floodplain. From the characteristics of the two culverts, we can see that only culvert 1 allows flow in both directions (**CLP** = 0) and the base level of this culvert ( $\max(z1, z2)$ ) is at 4.7 m. In Figure 15.2, we can see that the flow in the floodplain only starts when the water level in the estuary has reached 4.7 m. Because of the small scale of the schematic model and the real life characteristics of the culverts the outflow of water out of the floodplain follows the estuarine water level one on one.

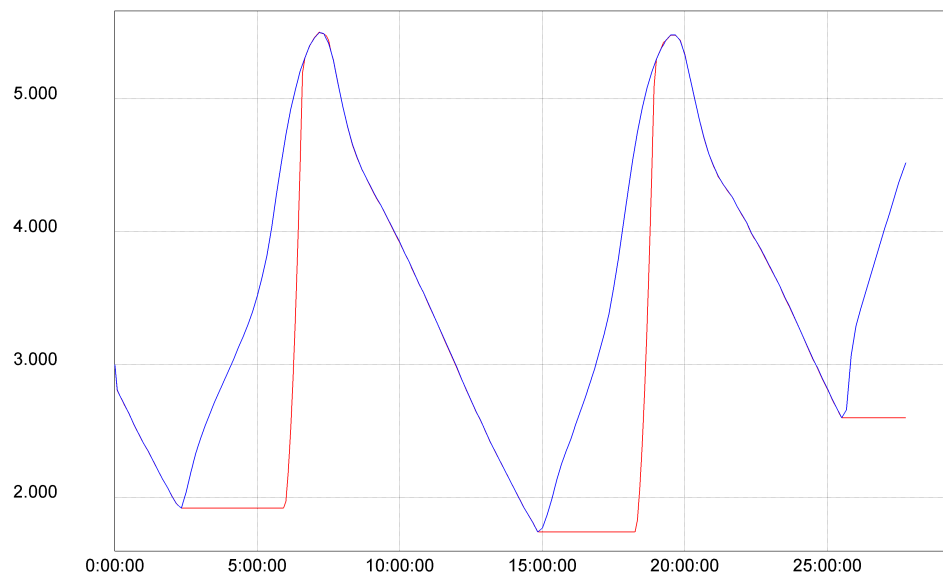


Figure 15.2: Schematic culvert test case: results of two tidal cycles. The blue line gives the water level in the estuarine river part and the red line gives the water level in the floodplain.

## 16. One way chaining with DELWAQ (delwaq)

### 16.1 Description

This test demonstrates the availability of TELEMAC-3D to be chained with DELWAQ, the water quality software from Deltares. This is a one way-chaining by files.

A 20 m wide and 28.5 m long prismatic channel with trapezoidal cross-section contains bridge-like obstacles in one cross-section made of two abutments and two circular 4 m diameter piles (see Figure 16.1).

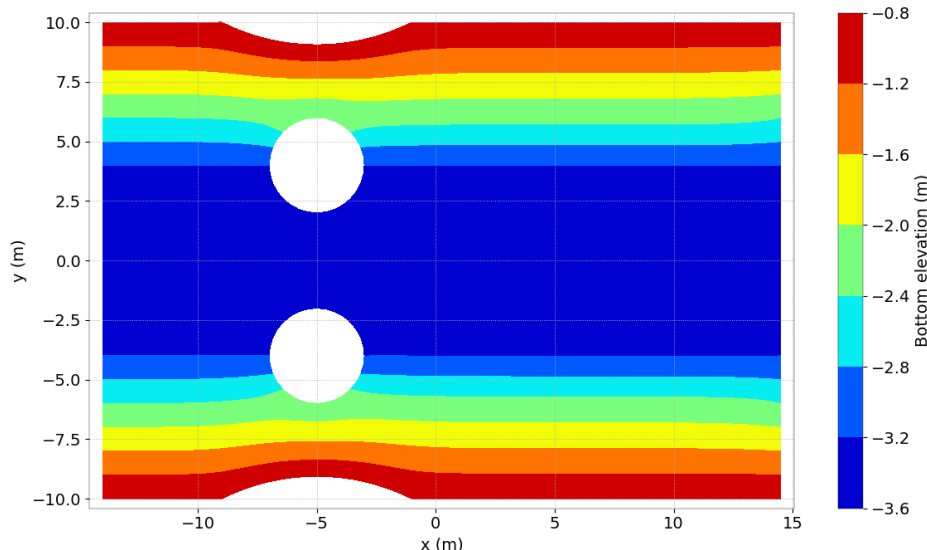


Figure 16.1: Bottom elevation.

The flow resulting from steady state boundary conditions is studied. The deepest water depth is 4 m. The hydrodynamic part is similar to the pildepon test case. The tracer used is temperature.

#### 16.1.1 Initial and boundary conditions

The computation is initialised with a constant elevation equal to 0 m, no velocity and a uniform temperature at 0.

The boundary conditions are:

- For the solid walls, a slip condition on channel banks is used for the velocities,
- On the bottom, a Strickler law with friction coefficient equal to  $40 \text{ m}^{1/3}/\text{s}$  is prescribed and imposed uniform profile of temperature over the vertical along a segment equal to 1,
- Upstream a flowrate equal to  $62 \text{ m}^3/\text{s}$  is prescribed, linearly increasing from 0 to  $62 \text{ m}^3/\text{s}$  during the first 10 s,
- Downstream the water level is equal to 0 m.

### 16.1.2 Mesh and numerical parameters

The 2D mesh (Figure 16.2) is made of 4,304 triangular elements (2,280 nodes). 6 planes are regularly spaced on the vertical (see Figure 16.3).

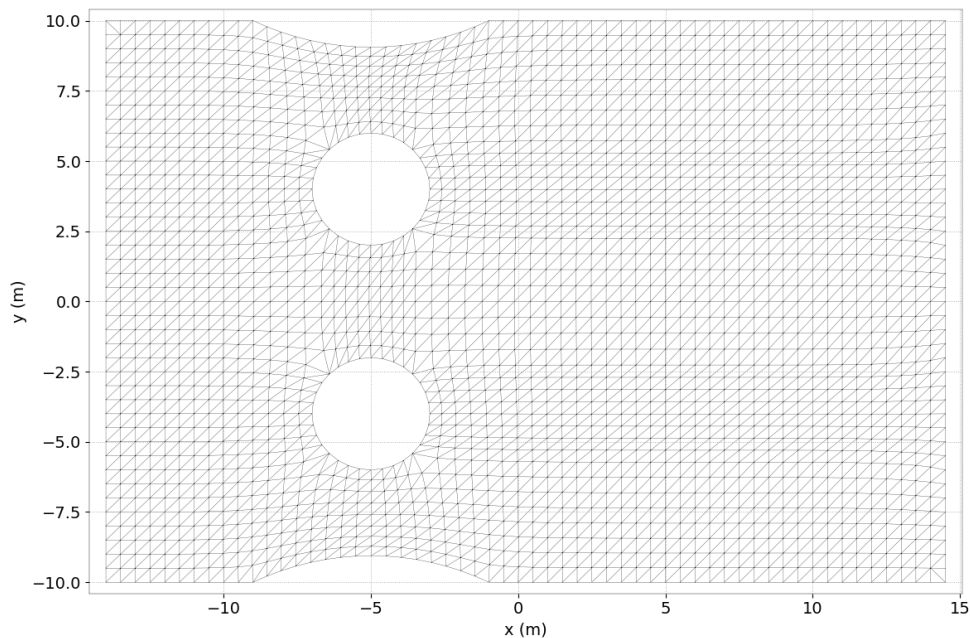


Figure 16.2: Horizontal mesh.

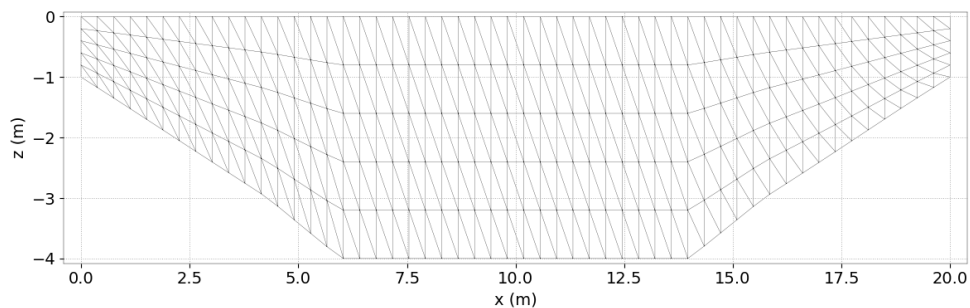


Figure 16.3: Initial vertical mesh.

The time step is 0.1 s for a simulated period of 5 s.

The non-hydrostatic version is used. To solve the advection, the LIPS scheme (default value) is used for the velocities and tracers (scheme 5 + scheme option 4). The conjugate gradient is

used for solving the propagation step (option 1) and the implicitation coefficients for depth and velocities are respectively equal to 0.6 and 0.55 (= default value for velocity).

### 16.1.3 Physical parameters

A mixing length model is used to model turbulence over the vertical while a constant horizontal viscosity for velocity equal to  $0.005 \text{ m}^2/\text{s}$  is chosen.

## 16.2 Results

Figure 16.4 shows the free surface elevation at the end of the computation.

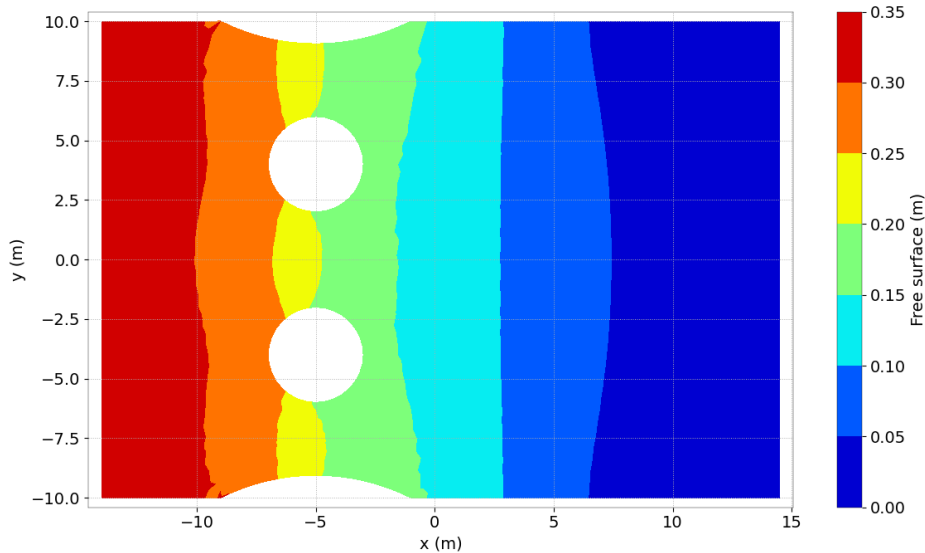


Figure 16.4: Free surface at final time step.

Figure 16.5 shows the magnitude of velocity at the end of the computation.

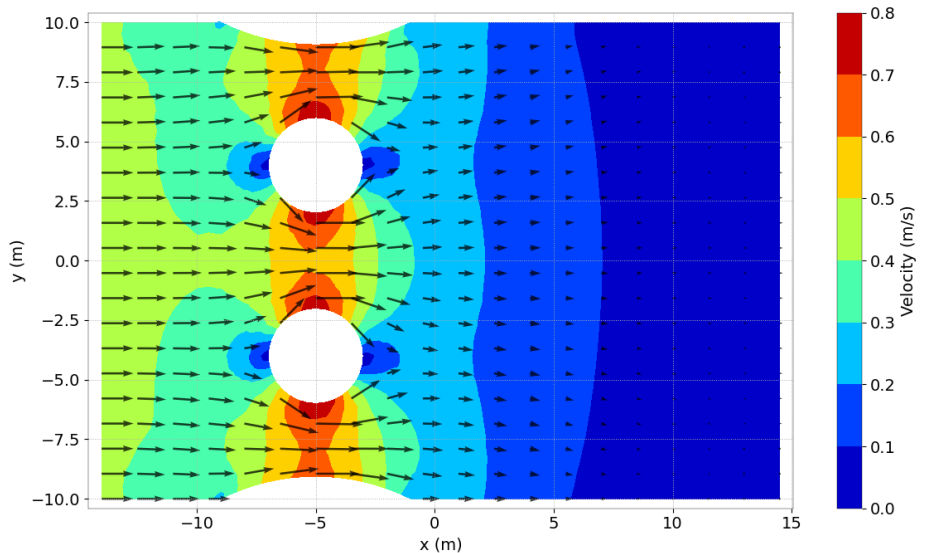


Figure 16.5: Velocity magnitude at the surface at final time step.

If running DELWAQ with the DELWAQ result files written by TELEMAC-3D, the velocity results are similar with both codes.

### 16.3 Conclusion

TELEMAC-3D can be used to chain with DELWAQ.

## 17. depot

This test case validates the coupling of TELEMAC-3D with SISYPHE for bedload transport processes.

Even though this model setup is still valid, new features and bug fixes are now available for the new sediment transport and bed evolution module GAIA of the TELEMAC-MASCARET SYSTEM. Therefore, for newer model implementations, we strongly suggest to use TELEMAC-3D coupled with GAIA for sediment transport and bed evolution processes in 3D.

GAIA test cases “bosse-t3d” and “hippodrome-t3d” provide examples of coupling TELEMAC-3D with GAIA to account for bedload sediment transport.

## 18. erosion\_flume

This test case assesses the capabilities of the TELEMAC-MASCARET SYSTEM at solving sediment transport processes that accounts for mixed sediments (cohesive and non-cohesive) within TELEMAC-3D.

Even though this model setup is still valid, new features and bug fixes are now available for the new sediment transport and bed evolution module GAIA of the TELEMAC-MASCARET SYSTEM. Therefore, for newer model implementations, we strongly suggest to use TELEMAC-3D coupled with GAIA for sediment transport and bed evolution processes in 3D.

GAIA test case “hippodrome-t3d” provides an example of coupling mixed sediment computations using TELEMAC-3D coupled with GAIA.

## 19. flume\_slope

This test case validates the modelling of cohesive sediments with TELEMAC-3D solved with a vertical implicit-advection scheme (tridiagonal matrix solver) for diffusion and settling velocity (ADVECTION-DIFFUSION SCHEME WITH SETTLING VELOCITY = 1).

Even though this model setup is still valid, new features and bug fixes are now available for the new sediment transport and bed evolution module GAIA of the TELEMAC-MASCARET SYSTEM. Therefore, for newer model implementations, we strongly suggest to use TELEMAC-3D coupled with GAIA for sediment transport and bed evolution processes in 3D.

GAIA test cases “hippodrome-t3d“, “rouse-t3d“, “tidal\_flats-t3d“ and “turbidity-t3d“ provide examples of coupling TELEMAC-3D coupled with GAIA to account for cohesive sediment transport processes.

## 20. Gaussian water surface with reflecting boundary conditions (gouttedo)

### 20.1 Description

This test case presents the evolution of a Gaussian water surface centred in a square domain with solid boundaries. It demonstrates that the TELEMAC-3D solution is not polarised because it can simulate the circular spreading of a wave in a square domain. It also shows that the no-flow condition is satisfied on solid boundaries and that the solution remains symmetric after reflection of the circular wave on the boundaries.

The considered domain is a square of 20.1 m length with a flat bottom. The fluid is initially at rest with a Gaussian free surface in the centre of a square domain (see Figure 20.1). The evolution of the surface and the reflection of the wave by the solid boundaries are then calculated during 4 s. Note that the turbulent viscosity is constant in both directions and equal to the water molecular viscosity.

#### 20.1.1 Initial and boundary conditions

The initial water level is a Gaussian-shape, where the water depth is 4.8 m at the centre and 2.4 m at boundary (Figure 20.1). In addition, the velocity is null. Note that the initial free surface elevation is prescribed in the **CONDI3DH** subroutine.

The boundary conditions are:

- For the solid boundaries (or lateral walls), a slip condition is imposed for the velocity,
- On the bottom a Chézy law with a friction coefficient equal to  $60 \text{ m}^{1/2} \cdot \text{s}^{-1}$  is imposed (default value for the friction coefficient until version 8.0).

#### 20.1.2 Mesh and numerical parameters

The mesh (Figures 20.2 and 20.3) is composed of 8,978 triangular elements (4,624 nodes) with 3 planes regularly spaced on the vertical, to form prism elements.

The time step is 0.04 s for a simulated period of 4 s.

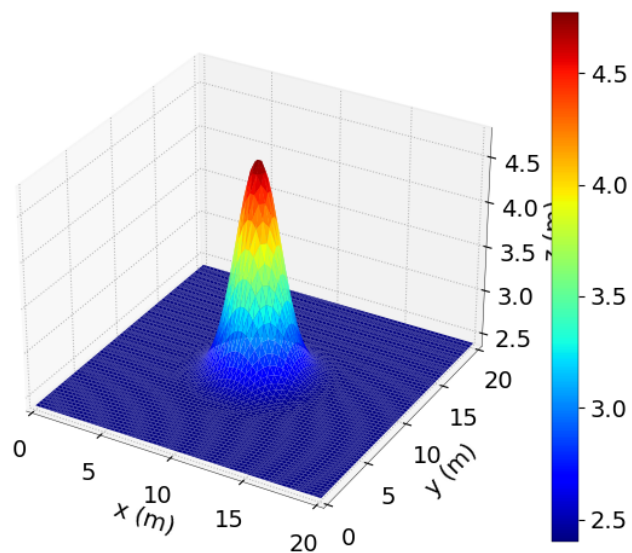


Figure 20.1: Initial free surface.

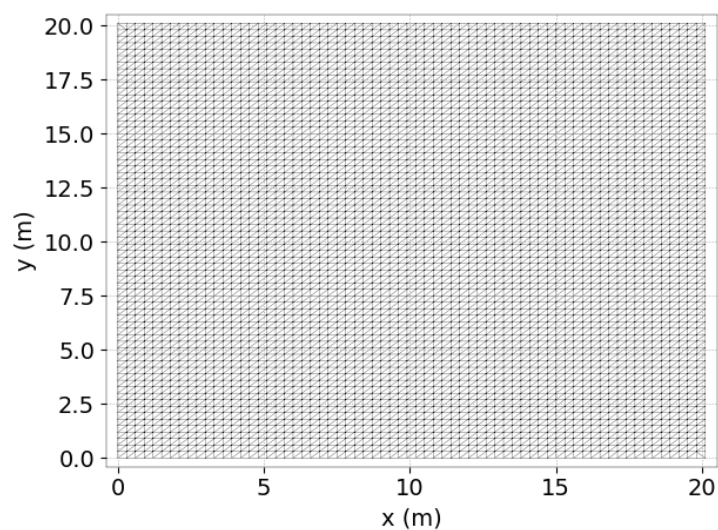


Figure 20.2: Horizontal mesh.

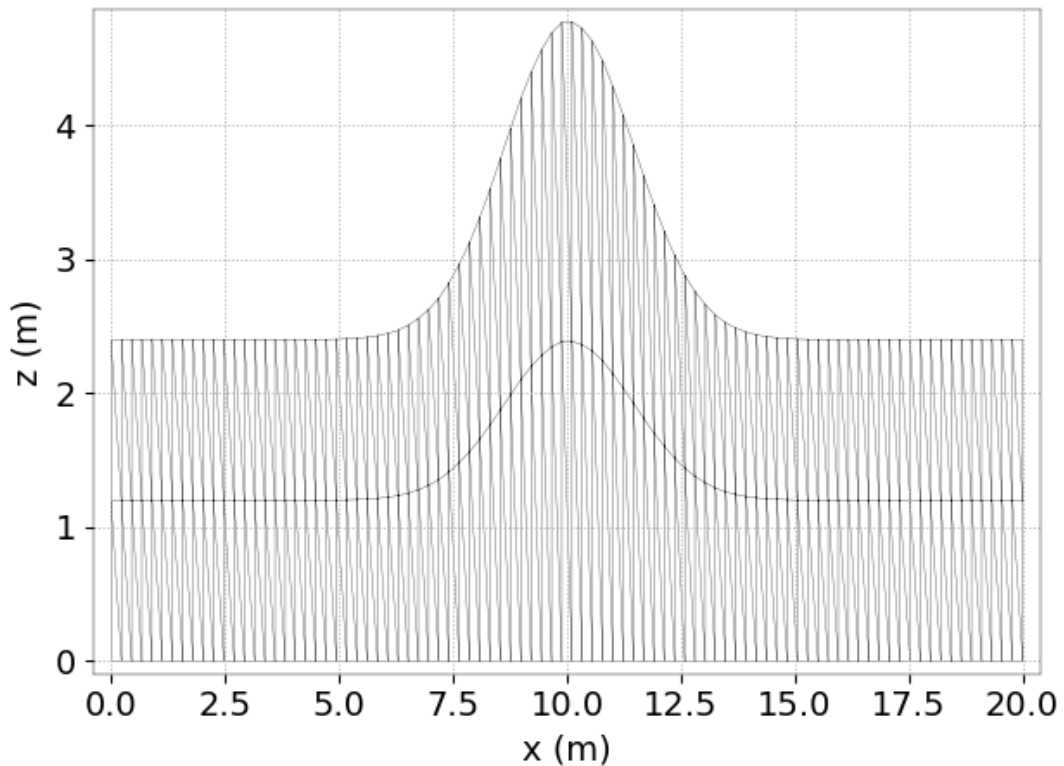


Figure 20.3: Vertical mesh at initial time step.

This case is computed with the non-hydrostatic version. The LIPS scheme is used for the velocities (scheme 5) to solve the advection and the GMRES (Generalized Minimal Residual Method, scheme 7) is used for propagation. The implicitation coefficients for depth and velocities are equal to 0.6.

## 20.2 Results

The wave spreads circularly around the initial water surface peak elevation (Figure 20.4). When it reaches the boundaries, reflection well occurs as expected. The reflected wave is also axi-symmetric. In addition, the final volume in the domain is equal to the initial volume.

Even though the mesh is polarised (along the  $x$  and  $y$  directions and the main diagonal), the solution is not. Solid boundaries are treated properly: no bias occurs in the reflected wave. Water mass is conserved.

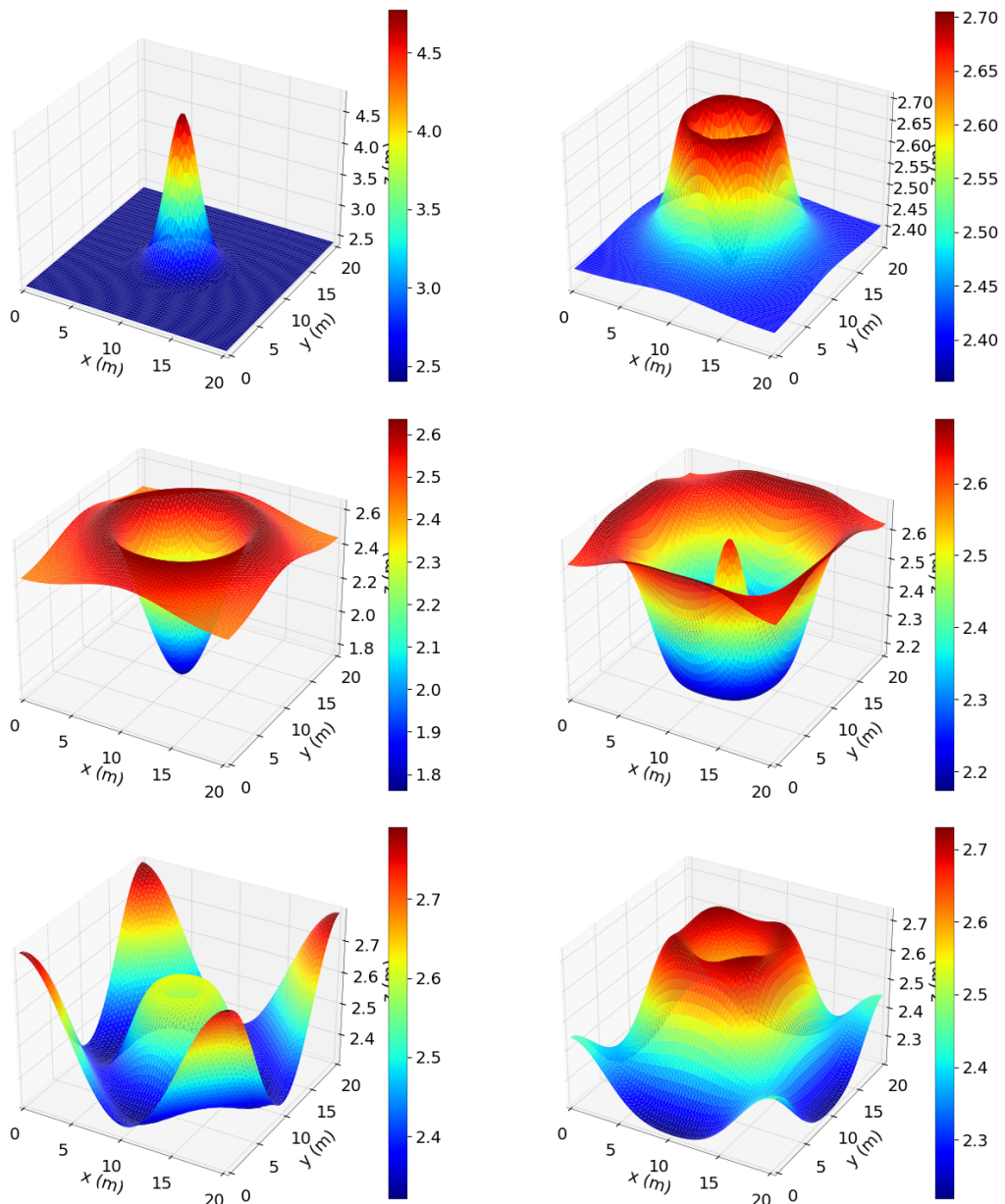


Figure 20.4: Water depth evolution in three dimensions.

## 21. Gaussian water surface with open boundary conditions (thompson)

### 21.1 Description

This test presents the evolution of a Gaussian water surface centred in a square domain. It is identical to validation case 20 but with open boundaries. It shows that the circular wave propagates out of the computational domain freely without any reflection. It demonstrates that the TELEMAC-3D solution is not polarised because it can simulate the circular spreading of a wave in square computation domain. Moreover, it also demonstrates that TELEMAC-3D is capable to deal with open boundaries without prescribing water depth or velocity by using the Thompson method based on characteristic.

The considered domain is a square of 20.1 m length with a flat bottom. The fluid is initially at rest with a Gaussian free surface in the centre of a square domain (see Figure 21.1). The evolution of the surface is then calculated during 4 s.

Note that the turbulent viscosity is constant in both directions and equal to the water molecular viscosity.

#### 21.1.1 Initial and boundary conditions

The initial water level is fixed as a Gaussian-shape, where the water depth is 4.8 m at the centre and 2.4 m at boundary (Figure 21.1). The velocity is null everywhere. Note that the initial free surface elevation is prescribed in the **CONDI3DH** subroutine.

The boundary conditions are:

- On lateral sides, the open boundary with the Thompson method based on characteristic is used,
- On the bottom, Chézy law with friction coefficient equal to  $60 \text{ m}^{1/2} \cdot \text{s}^{-1}$  is imposed (default value for the friction coefficient until version 8.0).

#### 21.1.2 Mesh and numerical parameters

The mesh (Figures 21.2 and 21.3) is composed of 8,978 triangular elements (4,624 nodes) with 3 planes regularly spaced on the vertical, to form prism elements.

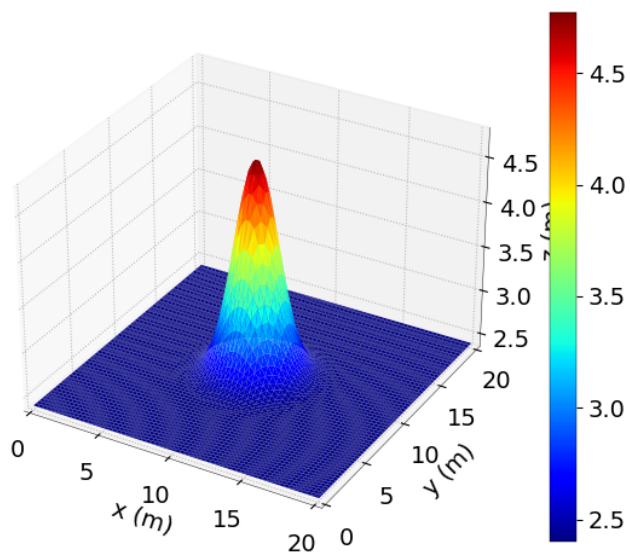


Figure 21.1: Initial free surface.

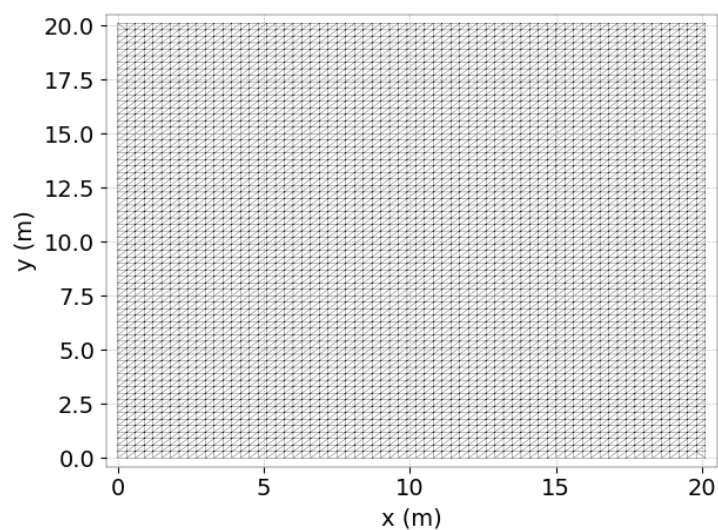


Figure 21.2: Horizontal mesh.

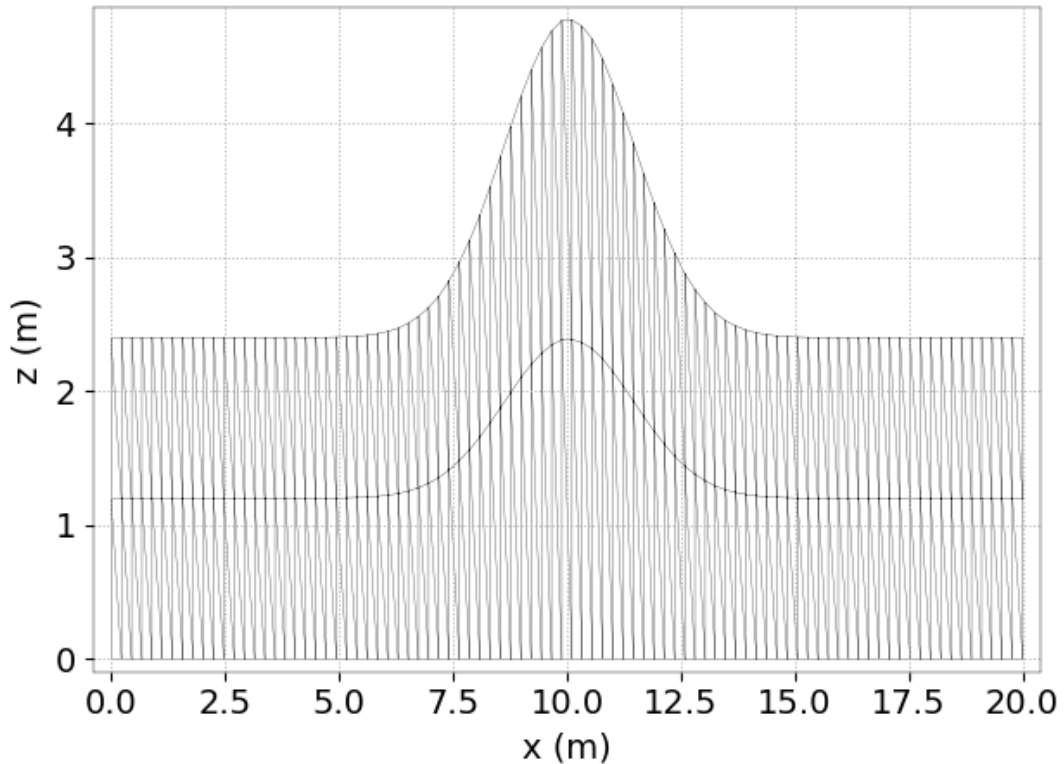


Figure 21.3: Vertical mesh (at initial time step).

The time step is 0.04 s for a simulated period of 4 s.

This case is computed with the non-hydrostatic version. The LIPS scheme is used for the velocities (scheme 5) to solve the advection and the GMRES (Generalized Minimal Residual Method, scheme 7) is used for propagation. The implicitation coefficients for depth and velocities are equal to 0.6. Moreover, the free surface gradient compatibility coefficient is equal to 0.

## 21.2 Results

Figure 21.4 shows that the wave spreads circularly around the initial water surface peak elevation when it reaches the boundaries, the wave goes out of the domain freely, no reflection occurs as expected.

Even though the mesh is polarised (along the  $x$  and  $y$  directions and the main diagonal), the solution is not. Open boundaries are treated properly: no bias occurs. The Thompson method, based on characteristic, enables to use open boundaries (444) without the need to specify water depth or velocity at the boundary.

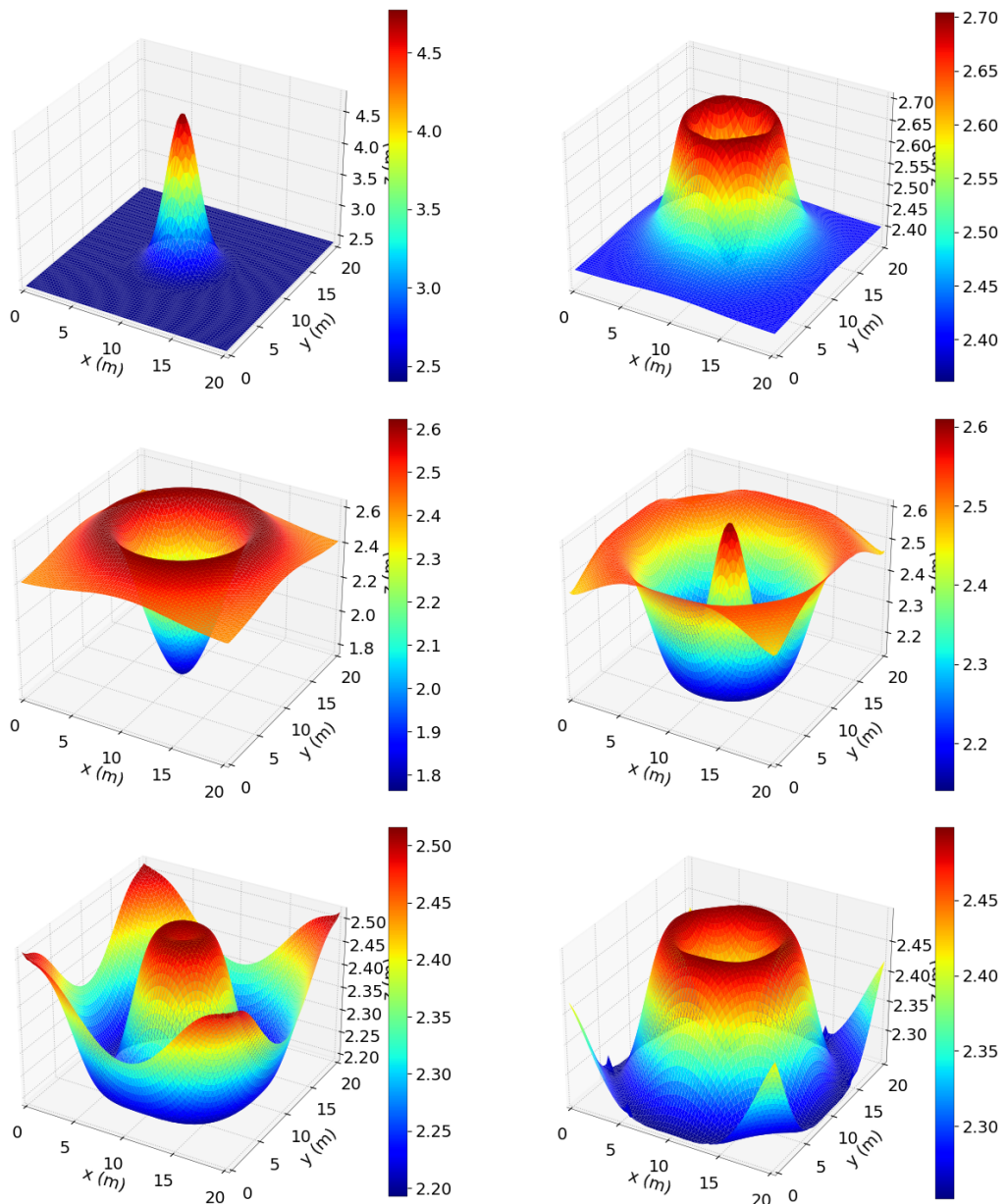


Figure 21.4: Water depth evolution in three dimensions.

## 22. Lock-exchange

### 22.1 Purpose

This test demonstrates the ability of TELEMAC-3D to model the motion of two fluids with different densities.

### 22.2 Description

This validation case consists of a lock-exchange flow in a rectangular cavity of height  $L$  and length  $7.5L$ . The width of the cavity is equal to  $0.3L$ . The flow consists of fresh water (on the right) and saline water (on the left) separated at  $t = 0$  and suddenly released. The heavy fluid sinks below the lighter one by forming a saline wedge which, according to the observations, makes an angle of about  $\pi/3$  with the bottom [3]. For this test-case, the dimensionless time is defined by:

$$t^+ = \frac{tU}{L}, \quad (22.1)$$

with:

$$U = \sqrt{|\beta|SgL}. \quad (22.2)$$

Where  $S$  is the salinity in the left-side of the cavity at  $t = 0$  and  $\beta$  the coefficient of haline dilatation.  $U$  is an estimation of the front velocity. Considering that the whole potential energy of the initial conditions is transformed into kinetic energy, it can be estimated that the front velocity is equal to  $0.5U$ . Measurements actually show that the velocity of the lower front is about equal to  $0.47U$ , while that of the upper front is about equal to  $0.59U$  for a free-surface lock exchange flow [2]. The dimensionless numbers describing the flow are the Grashof number and the Schmidt number, defined by:

$$Gr = \frac{U^2 L^2}{\nu^2}, \quad (22.3)$$

and:

$$Sc = \frac{\nu}{K}, \quad (22.4)$$

where  $\nu$  is the molecular dynamic viscosity and  $K$  is the molecular haline diffusion coefficient. The density law depending on salinity used in TELEMAC-3D reads:

$$\rho = \rho_0(1 + 750.10^{-6}S), \text{ with } \rho_0 = 999.972 \text{ kg/m}^3 \quad (22.5)$$

so that  $\beta$  is equal to  $-7.5.10^{-4} (\text{g/L})^{-1}$ .

## 22.3 Preamble – an attempt at reproducing Adduce *et al.*'s experiments

In order to compare the shape of the simulated flow to experimental results, we first considered the case studied experimentally by Adduce *et al.* [1]. At  $t^+ = 0$ , the separation between the fresh and saline water is now located at  $L$  from the left side of the cavity. The Schmidt number is still equal to 1 but the Grashof number is now equal to  $7.3 \cdot 10^8$  (the salinity is set to 9 g/L in the left part and 0 g/L on the right part, the molecular dynamic viscosity is set to  $2.7 \cdot 10^{-5} \text{ m}^2 \cdot \text{s}^{-1}$ ). The non-hydrostatic version of TELEMAC-3D was used, using an N advection scheme with the option 2 and 5 corrections. The dynamic pressure is calculated before the resolution of the wave equation and no turbulence model is used. Figure 22.1 shows the results obtained at  $t^+ = 7.3$  and 16.4 compared to the experiments. The velocity of the front seems correctly reproduced by the numerical model, but the shape of the flow is quite different from the experimental one. The simulation was run without using any turbulence model, which may explain why there is less diffusion than in the experiment.

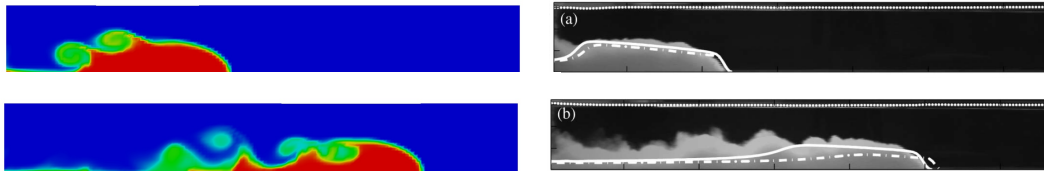


Figure 22.1: Lock-exchange: comparison of the experimental results by Adduce *et al.* [1] (right) at  $t^+ = 7.3$  and 16.4 with the simulation results (left), using a N advection scheme with the option 2 and 5 corrections. The dynamic pressure is calculated before the resolution of the wave equation.

The same simulation was then run with the  $k - \epsilon$  turbulence model applied in all directions, but there is no visible impact on the results because this is a case of transition between a laminar and a turbulent flow. In these conditions, it is hard to compare the various advection schemes or numerical options on this case: different flow shapes are obtained but there is never enough diffusion to match the turbulent diffusion observed in the experiments. We did not find reference data regarding a less turbulent experimental setup where the shape of the free-surface flow is displayed. Thus, we chose to simulate a case without available experimental data but with a lower Grashof number.

## 22.4 Case setup

### 22.4.1 Geometry and mesh

Given the difficulties in reproducing a free-surface experimental setup, the case simulated here is the one described in J. Jankowski's PhD thesis [9]. The flow consists of fresh water (on the right) and saline water (on the left) separated at  $t^+ = 0$  at the half-width of the domain. The Schmidt number is equal to 1 and the Grashof number is equal to  $8 \cdot 10^7$  (the salinity is set to 1 g/L in the left part and 0 g/L on the right part, the molecular dynamic viscosity is set to  $2.7 \cdot 10^{-5} \text{ m}^2 \cdot \text{s}^{-1}$ ).

#### Bathymetry

The bed of the cavity is flat at the elevation  $z = -4$  m.

### Geometry

The cavity is 30 m long and 1.2 m wide.

### Mesh

The mesh consists of 1,806 triangular elements, which corresponds to 1,060 nodes. Along the vertical, 24 regularly spaced planes are used. Figure 22.2 shows a vertical and a horizontal section of the mesh.



Figure 22.2: Lock-exchange: vertical (top) and a horizontal (bottom) sections of the mesh.

#### 22.4.2 Physical parameters

The influence of the Coriolis force and meteorological forcings are not taken into account.

### 22.4.3 Initial and Boundary Conditions

#### Initial conditions

- Constant water depth = 4 m
- No velocity
- Initial salinity: 1 g/L on the left half part and 0 g/L in the other part (defined in the subroutine **USER\_CONDI3D\_TRAC** and the keyword INITIAL VALUES OF TRACERS) – see Figure 22.3.

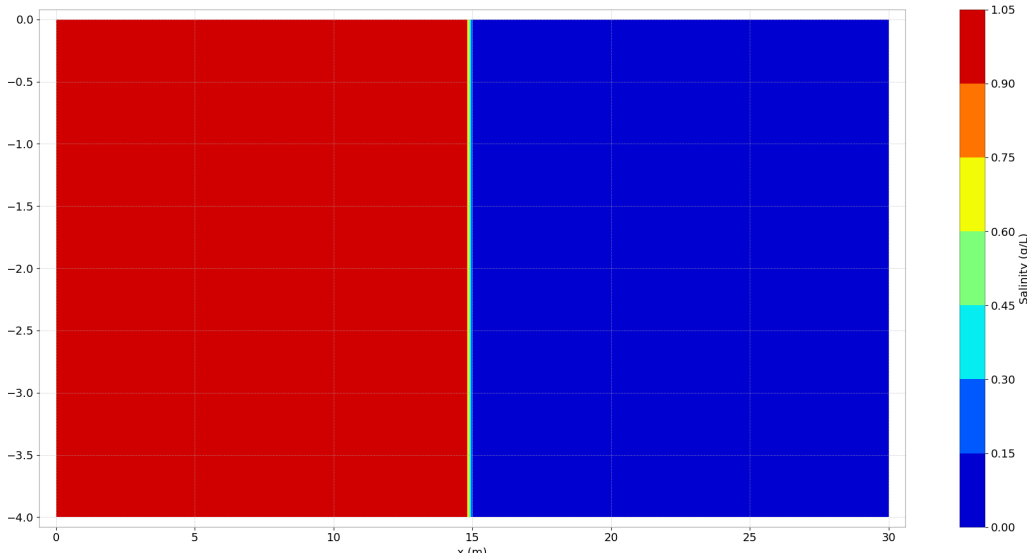


Figure 22.3: Lock-exchange: initial salinity distribution, ranging from 0 (blue) to 1 (red).

#### Boundary conditions

- Closed boundaries
- No bottom friction

### 22.4.4 General parameters

- Time step: 0.5 s
- Simulation duration: 100 s

### 22.4.5 Numerical parameters

- Advection of velocities and tracers: tests with the characteristics scheme, SUPG, the Leo Postma scheme and the N and PSI-type MURD schemes with options 1, 2 and 3 and several numbers of corrections
- DYNAMIC PRESSURE IN WAVE EQUATION: runs with this keyword set to YES and NO (dynamic pressure calculated before and after the wave equation resolution, respectively)
- Linear solver: solver 7 (GMRES) used with a precision of  $10^{-10}$  and a maximum of 2,000 iterations for all the matrix inversions
- Implicitation coefficients on the velocity and depth : 0.5
- Non-hydrostatic version: used to test the advection schemes and dynamic pressure option, one hydrostatic run also performed to compare to the non-hydrostatic version

## 22.5 Reference results

There is no available experimental data regarding the shape of the flow for this specific case, but we have an estimation of the angle between the wedge and the bottom and the front velocity values. The angle should be about equal to  $\pi/3$  and the lower front velocity should be about equal to 0.081 m/s. On this case, it is also expected that Rayleigh-Taylor instability cells will form at the interface between the two fluids. In order to have an idea what these instabilities should look like, fine simulations were run with the second order predictor-corrector PSI MURD-type advection scheme (the most accurate advection solver in TELEMAC-3D at the moment – SCHEME OPTION FOR THE ADVECTION = 3). The triangle size in the horizontal mesh is 0.025 m and 80 planes are used, so that the horizontal and vertical discretisations are equal. The 3D mesh contains about 9 million points. The time step size is equal to 0.2 s and the simulation duration is 100 s ( $t^+ = 4.29$ ). Figures 22.4 and 22.5 show the results at  $t^+ = 4.29$  when using 5, 10 and 15 corrections, calculating the dynamic pressure after or before the resolution of the wave equation. We observed that this option has a visible influence on the results.

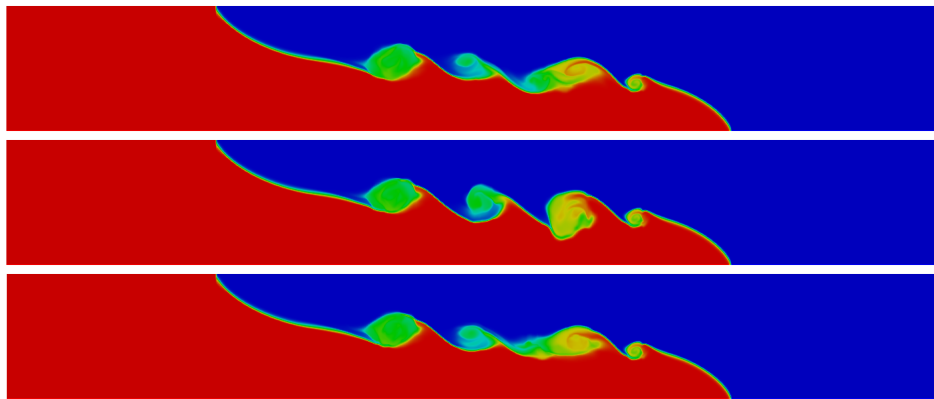


Figure 22.4: Lock-exchange: fine simulation results at  $t^+ = 4.29$  with a PSI advection scheme with the option 3, using 5, 10 and 15 corrections (from top to bottom). The dynamic pressure is calculated after the resolution of the wave equation.

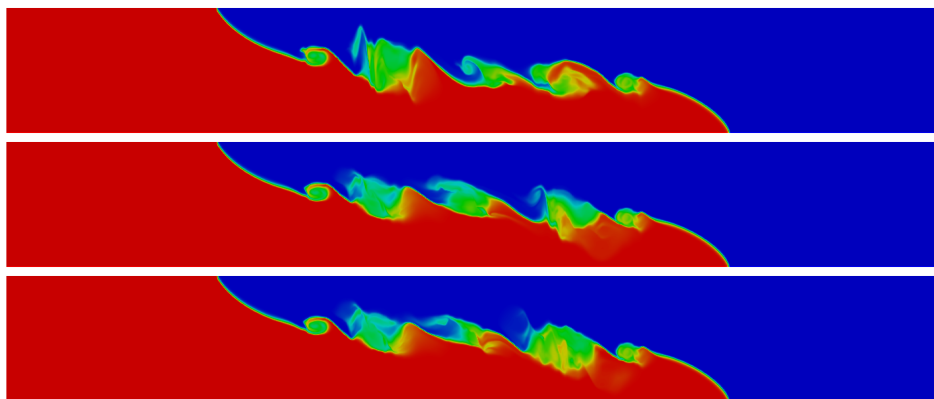


Figure 22.5: Lock-exchange: fine simulation results at  $t^+ = 4.29$  with a PSI advection scheme with the option 3, using 5, 10 and 15 corrections (from top to bottom). The dynamic pressure is calculated before the resolution of the wave equation.

The mean velocity of the lower front is equal to 0.084 m/s and the angle between the wedge front

and the vertical is about equal to  $\pi/3$ , which matches experimental observations on this type of flows. It is also visible that several instability cells appear in the simulations. At least three cells appear at the interface, and one or two more depending on the numerical options. The shape of the instability cells is influenced by the option DYNAMIC PRESSURE IN WAVE EQUATION and by the number of corrections in the distributive scheme. These results show that this case is very sensitive to slight numerical changes. In what follows, we will compare the various advection schemes, the DYNAMIC PRESSURE IN WAVE EQUATION option and the hydrostatic version of TELEMAC-3D on this case: for a given discretisation, we will observe whether the main instability cells appear or not, and check the value of the angle to the bottom and of the front velocity.

## 22.6 Results

### 22.6.1 Dynamic pressure not included in the wave equation

#### Characteristics

Figure 22.6 shows the results obtained with the characteristics advection scheme at  $t^+ = 4.29$ . The lower front velocity is equal to 0.072 m/s in the simulation (as compared to 0.081 m/s) and the angle of the wedge is well captured by the model but it is so diffusive that the Rayleigh-Taylor instabilities do not trigger.

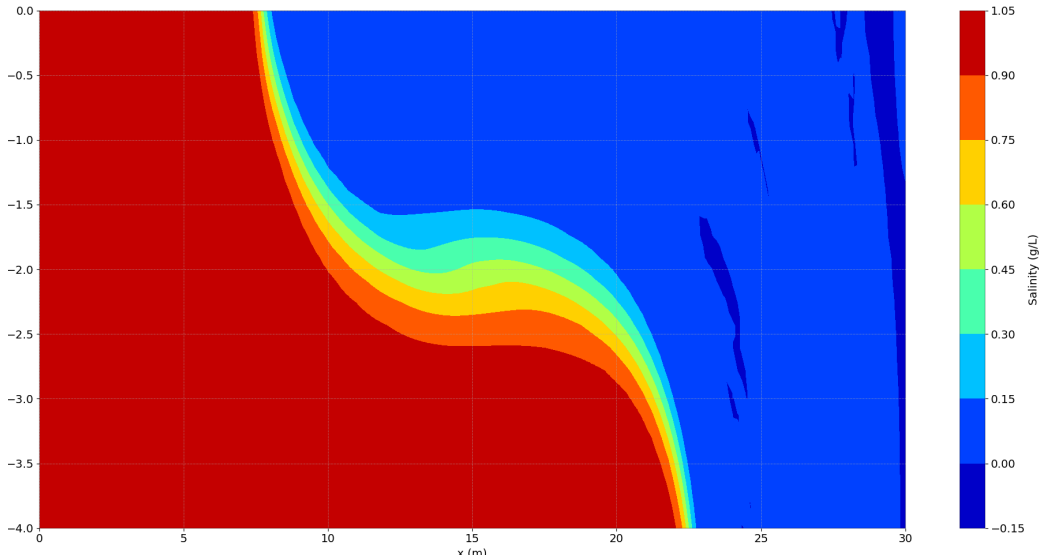


Figure 22.6: Lock-exchange: simulation result at  $t^+ = 4.29$  with the characteristics advection scheme. The dynamic pressure is calculated after the resolution of the wave equation.

#### SUPG

Figure 22.7 shows the results obtained with the SUPG advection scheme, with the option 2 on the velocity and tracer and the option 0 on the water depth, at  $t^+ = 4.29$ . It is visible that the maximum principle is not fulfilled with this scheme since the final tracer values are outside the initial bounds. The spurious behaviour mostly occurs at the upper and lower fronts, in the white zones of the plot. On the other hand, the lower front velocity is equal to 0.082 m/s in the simulation (as compared to 0.081 m/s) and the angle of the wedge is well captured by the model. It is however too diffusive to let instabilities develop during the simulation. They are slightly visible in the results, but still very diffused.

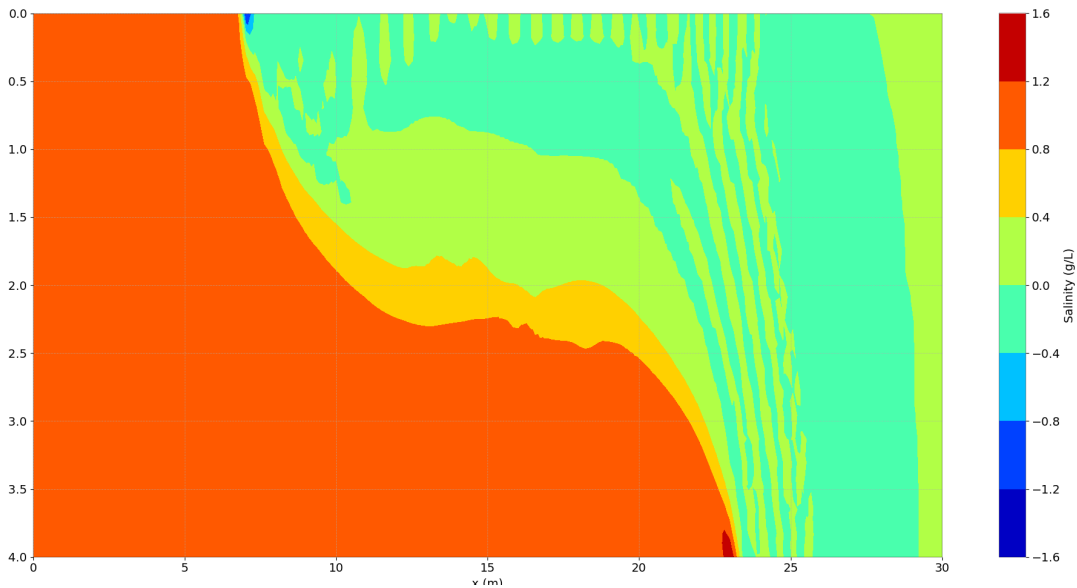


Figure 22.7: Lock-exchange: simulation result at  $t^+ = 4.29$  with the SUPG advection scheme with the salinity ranging from -0.1 (dark blue) to 1.1 (dark red) on the top and from -1.4 (blue) to 2 (red) on the bottom. The dynamic pressure is calculated after the resolution of the wave equation.

### Leo Postma scheme

Figure 22.8 shows the results obtained with the Leo Postma advection scheme at  $t^+ = 4.29$ . The lower front velocity is equal to 0.074 m/s in the simulation (as compared to 0.081 m/s) and the angle of the wedge is well captured by the model. But it is too diffusive, so that the Rayleigh-Taylor instabilities do not trigger in the simulation.

### PSI (or N) scheme

Figures 22.9 to 22.11 show the results obtained with the options 1, 2 and 3 with the PSI scheme, using two to five corrections, at  $t^+ = 4.29$ . We recall that the option 1 corresponds to the classical scheme, the option 2 is the first order predictor-corrector scheme and the option 3 is the second-order predictor corrector scheme. The results obtained with the N scheme are very similar so they are not shown here. It appears in the results that for this discretisation the first order predictor-corrector scheme provides better results than the second-order one since they present more instability cells. Both have converged after about 4 corrections. The lower front velocity is equal to ??m/s in the simulations (as compared to 0.081 m/s).

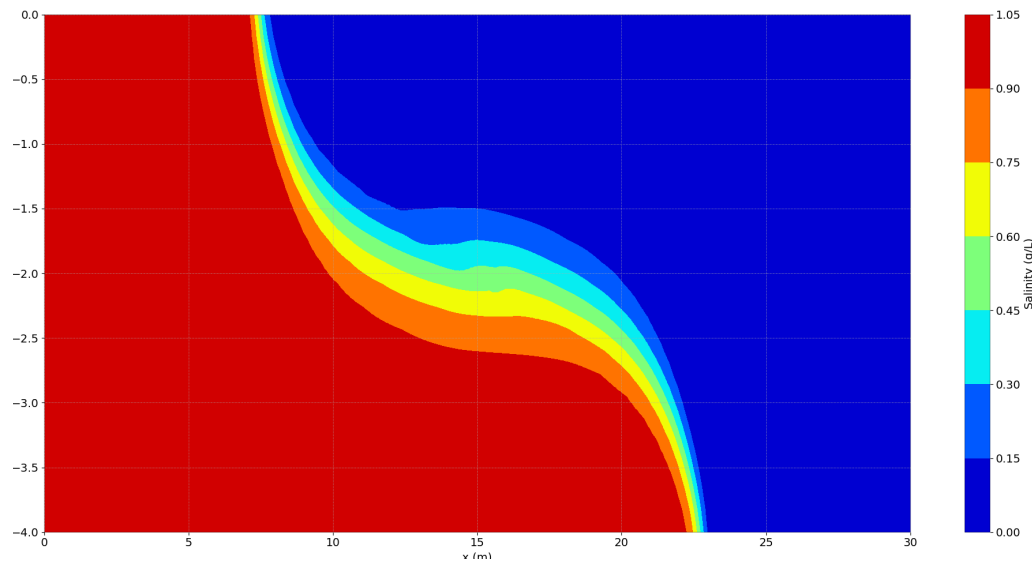


Figure 22.8: Lock-exchange: simulation result at  $t^+ = 4.29$  with the Leo Postma advection scheme. The dynamic pressure is calculated after the resolution of the wave equation.

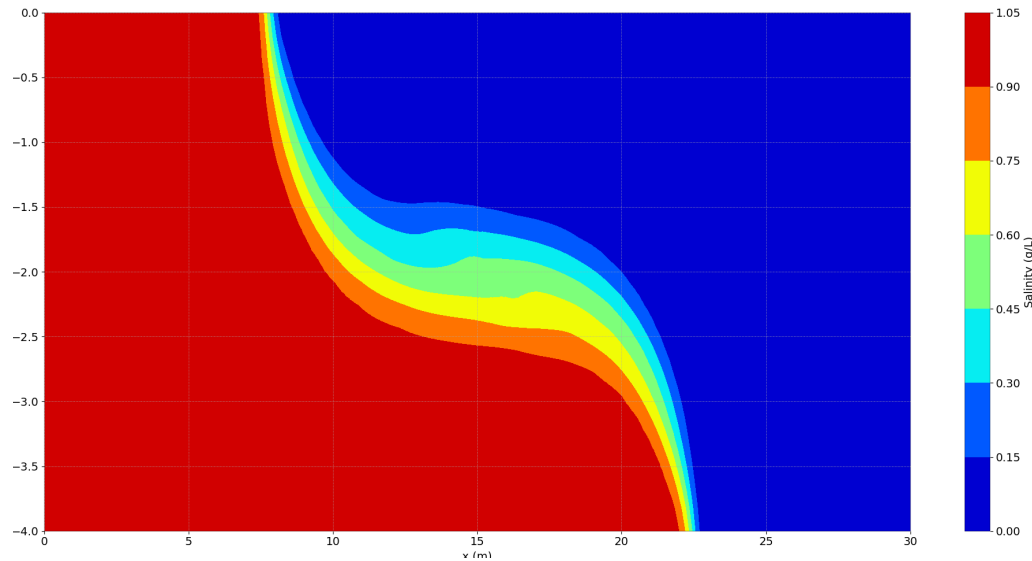


Figure 22.9: Lock-exchange: simulation result at  $t^+ = 4.29$  with a PSI advection scheme with the option 1. The dynamic pressure is calculated after the resolution of the wave equation.

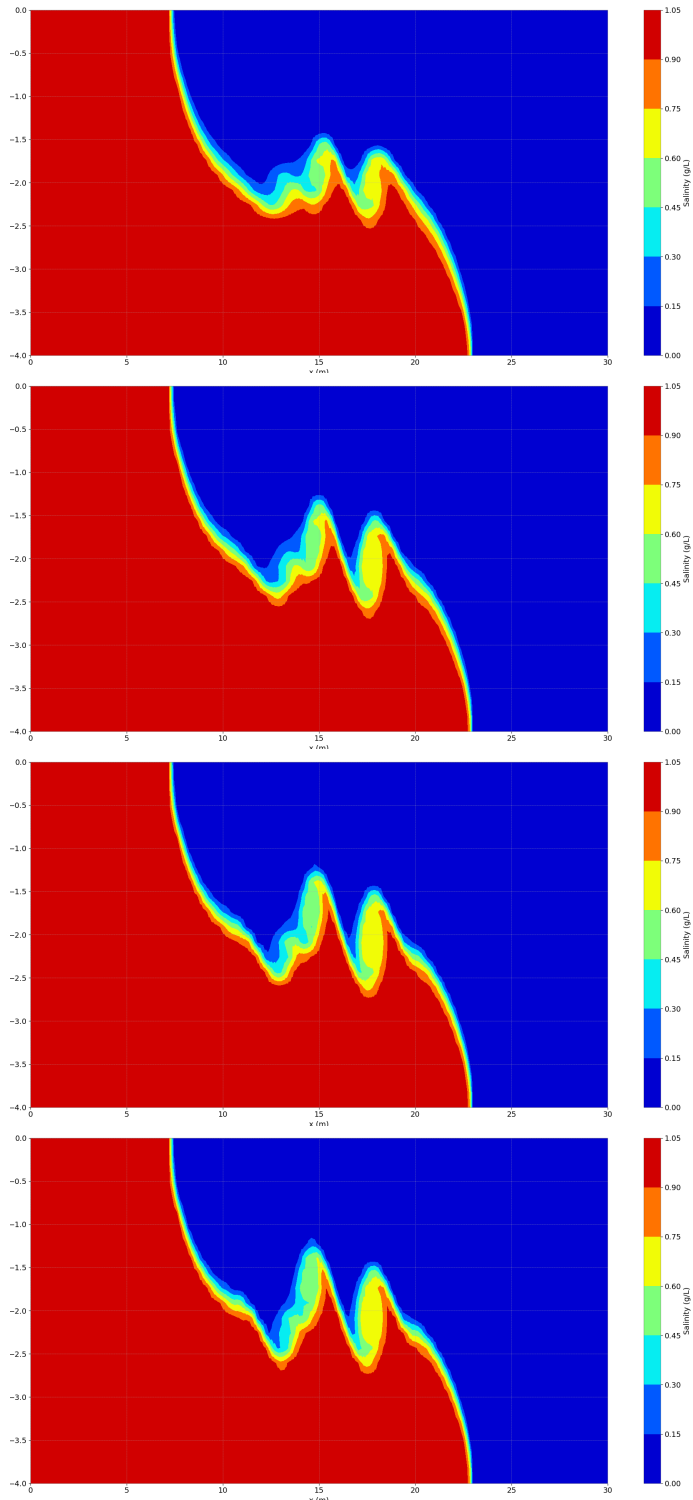


Figure 22.10: Lock-exchange: simulation result at  $t^+ = 4.29$  with a PSI advection scheme with the option 2, using 2, 3, 4 and 5 corrections (from top to bottom). The dynamic pressure is calculated after the resolution of the wave equation.

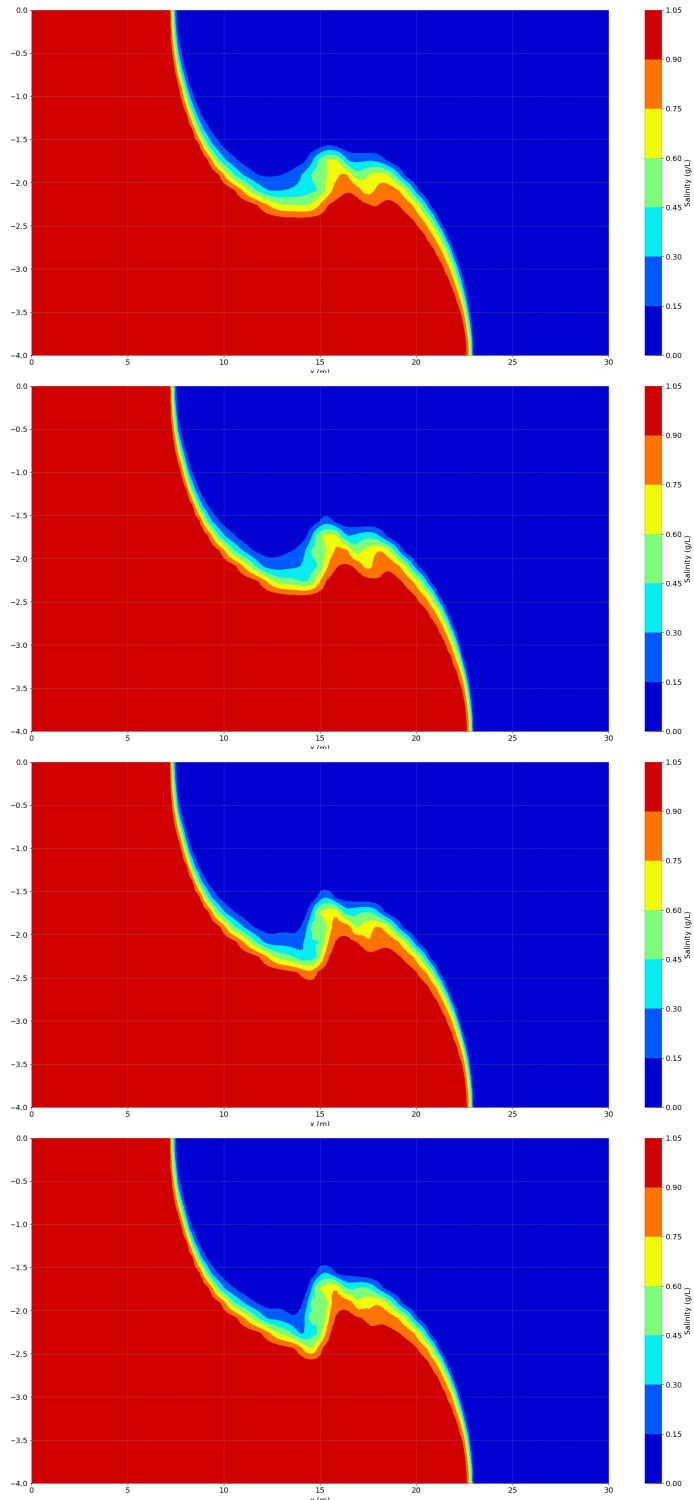


Figure 22.11: Lock-exchange: simulation result at  $t^+ = 4.29$  with a PSI advection scheme with the option 3, using 2, 3, 4 and 5 corrections (from top to bottom). The dynamic pressure is calculated after the resolution of the wave equation.

### 22.6.2 Dynamic pressure included in the wave equation

In this section we show the results obtained when the dynamic pressure is calculated before the resolution of the wave equation (thus, before the hydrostatic pressure). This change does not impact the results obtained with the characteristics, SUPG and Leo Postma schemes because they are so diffusive that for this discretisation the instability cells do not appear. However, the results obtained with the predictor-corrector PSI scheme are influenced by this option. The same holds for the N scheme, but once again the results obtained with the N and PSI schemes were so close that we chose to show only the results of the PSI scheme, which were even slightly improved compared to the results of the N scheme. Here we only show the results obtained with the first-order predictor-corrector PSI scheme since we saw previously that it provides the best results for this mesh discretisation.

#### PSI scheme

Figure 22.12 shows the results obtained with the option 2 for the PSI scheme, using two to five corrections, at  $t^+ = 4.29$ .

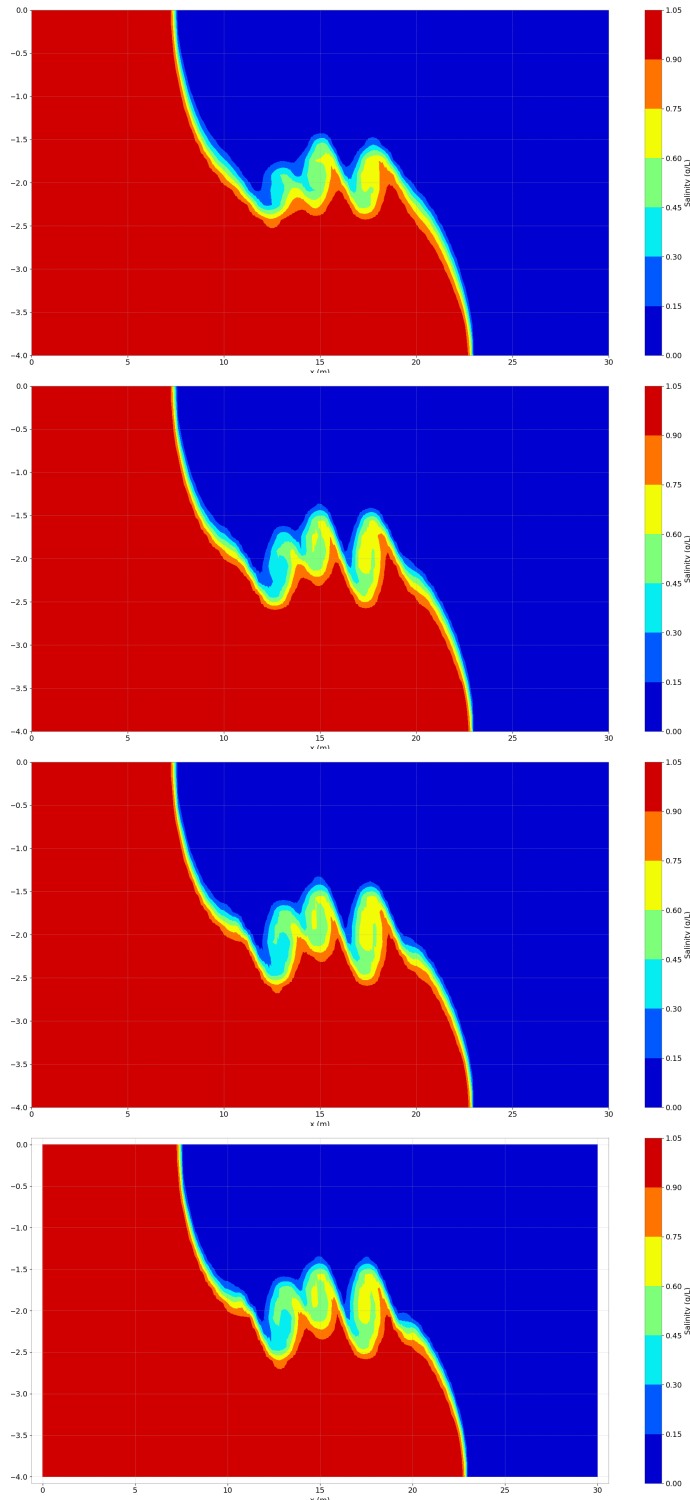


Figure 22.12: Lock-exchange: simulation result at  $t^+ = 4.29$  with a PSI advection scheme with the option 2, using 2, 3, 4 and 5 corrections (from top to bottom). The dynamic pressure is calculated before the resolution of the wave equation.

### 22.6.3 Hydrostatic hypothesis

The results of the hydrostatic computation are presented in Figure 22.13. The average velocity of the lower front is approximately 0.068 m/s and the angle of the wedge compared to the bottom is close to  $90^\circ$ . Besides, the instability cells do not appear in the results. This shows that the hydrostatic hypothesis is not valid for this type of case.

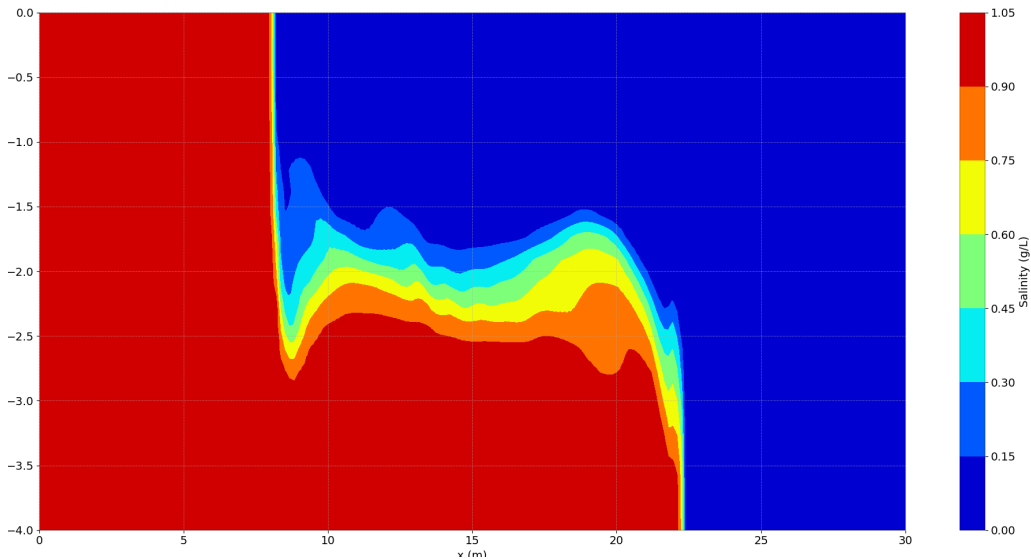


Figure 22.13: Lock exchange test: results with the hydrostatic hypothesis.

## 22.7 Conclusion

In this document, a sensitivity analysis on the lock-exchange case was performed. First, we tried to reproduce an experimental setup, but realized we could not correctly reproduce the flow shape with TELEMAC-3D: without a turbulence closure, there is not enough diffusion in the numerical result whereas using the  $k - \varepsilon$  turbulence model is way too diffusive. Thus, we chose a less turbulent setup, which is actually the one proposed in J. Jankowski's PhD thesis and was already used as a TELEMAC-3D example. We used twice as many planes as in the original simulation, using the non-hydrostatic version of TELEMAC-3D and testing the various advection schemes and the option DYNAMIC PRESSURE IN WAVE EQUATION. We also compared the hydrostatic and non-hydrostatic versions. In order to have a reference solution, fine simulations for this case were run, with a space discretisation of 0.025 m (9 million points in 3D). The results of the fine simulations showed that Rayleigh-Taylor instabilities appear at the interface between the two fluids. There are three major central cells and, depending on the options, one or two smaller external cells. Their shape is influenced by the number of corrections used in the distributive scheme and the choice for the option DYNAMIC PRESSURE IN WAVE EQUATION.

In the coarser simulations, we observed that only the N or PSI MURD-type advection schemes with the option 2 (1st order predictor-corrector) or 3 (2nd order predictor-corrector) are accurate enough to reproduce the instability cells with this discretisation (0.2 m). The 2nd order predictor-corrector PSI or N schemes have a higher order of convergence than the 1st order one, but for this discretisation the latter provide better results. The three main instability cells only appear when setting the option DYNAMIC PRESSURE IN WAVE EQUATION to YES and with the 1st order predictor-corrector N or PSI schemes. The results thus seem to be improved

by calculating the dynamic pressure before the resolution of the wave equation. We can also conclude that the options 2 or 3 for the MURD-type advection schemes greatly improve the quality of the numerical solution provided by TELEMAC-3D compared to all the other advection schemes. However, it seems difficult for the user to choose the number of corrections to apply in the distributive schemes and a possible improvement would be to let TELEMAC-3D decide when the algorithm has converged based on a convergence criterion.

On the other hand, the results show that the hydrostatic hypothesis is not valid for this type of case: the shape of the flow is not correctly reproduced with the hydrostatic option.

Finally, it is important to keep in mind that this test-case is very sensitive due to its unstable nature, and that slight changes to the schemes might lead to significant differences when it comes to the shape of the instabilities.

## 23. Malpasset dambreak (malpasset)

### 23.1 Purpose

This test illustrates that TELEMAC-3D is able to simulate a real dam break flow on an initially dry domain. It also shows the propagation of the wave front and the evolution in time of the water surface and velocities in the valley downstream. It was used as a test case in the program ESPRIT for the european project PCECOWATER (Parallel Computing of Environment COastal and lake shallow WATER dynamics).

### 23.2 Description

This case is the simulation of the propagation of the wave following the break of the Malpasset dam (South-East of France). This accident occurred in December 1959. The model represents the reservoir upstream from the dam and the valley and flood plain downstream. The entire valley is approximately 18 km long and between 200 m (valley) and 7 km wide (flood plain). The complete study is described in details in [7]. The simulation is performed using 2 or 6 vertical planes (cases MURD P2 and MURD P6) using the treatment of negative depths introduced since TELEMAC-3D 7.0. The historical simulation using 2 vertical planes and the method of characteristics (named CHAR P2) has been kept. Nevertheless, the recommended advection scheme for velocities for such applications is now the N-type MURD scheme (14). A simulation using 2 vertical planes with a large mesh (FINE P2) is also performed, but only in parallel to save CPU time. The characteristics of the case are the following:

- Observed mean wave velocity  $U_0 = 27 \text{ km.h}^{-1} = 7.5 \text{ m.s}^{-1}$ ,
- Initial water depth upstream of the dam  $H_0 = 55 \text{ m}$ ,
- Total duration of the event  $T = 4,000 \text{ s}$ ,
- Valley length  $L = 18 \text{ km}$ ,
- Maximum valley width  $l_M = 7 \text{ km}$ ,
- Reynolds Number  $R_e = \frac{U_0 \times H_0}{\nu} = 4.12 \times 10^8$  where  $\nu$  is the kinematic viscosity of water,
- Froude Number  $F_r = \frac{U_0}{\sqrt{g \times H_0}} = 0.32$  where  $g$  is the gravity acceleration.

### 23.2.1 Geometry and Mesh

The size of the model is approximately  $17 \text{ km} \times 9 \text{ km}$ . The mesh is refined in the river valley (downstream from the dam) and on the banks. Two 2D triangular meshes are tested:

**Regular mesh (Figure 23.1 - a):**

- 26,000 triangular elements,
- 13,541 nodes,
- Maximum size range is from 17 to 313 m.

**Fine mesh (Figure 23.1 - b):**

- 104,000 triangular elements,
- 53,081 nodes,
- Maximum size range is from 8.5 to 156.5 m.

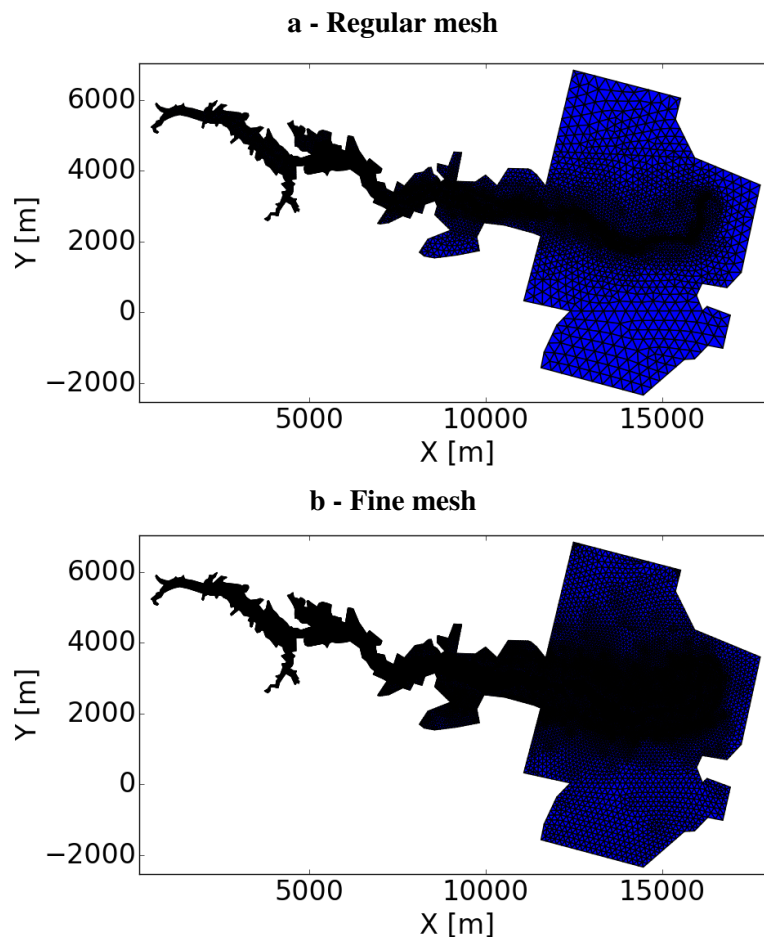


Figure 23.1: Malpasset case meshes.

In this 2D mesh, the dam is modelled by a straight line between the points of coordinates (4,701.18 m ; 4,143.10 m) and (4,655.50 m ; 4,392.10 m). Its location is shown in Figure 23.2. For the construction of the 3D mesh, two discretizations with 2 or 6 layers regularly spaced on the vertical are tested.

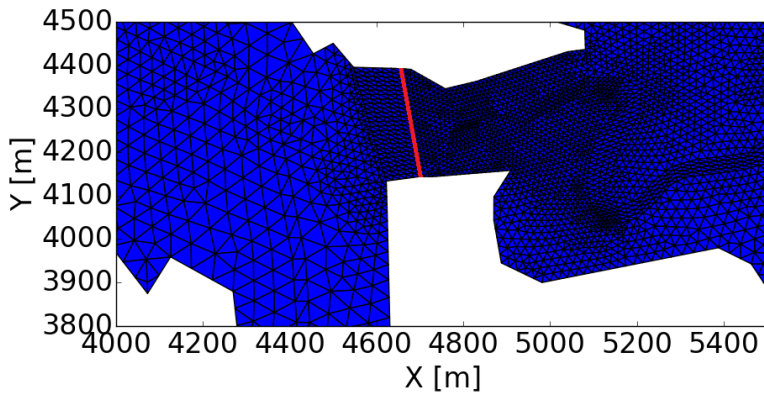


Figure 23.2: Dam location on the Malpasset case.

### 23.2.2 Bathymetry

Old maps have been used to deduce the topography of the domain (Figure 23.3). In fact, the topography after the accident could not be used because of the dramatic changes that occurred. Therefore, the IGN map of Saint-Tropez, Number 3, of year 1931, was used.

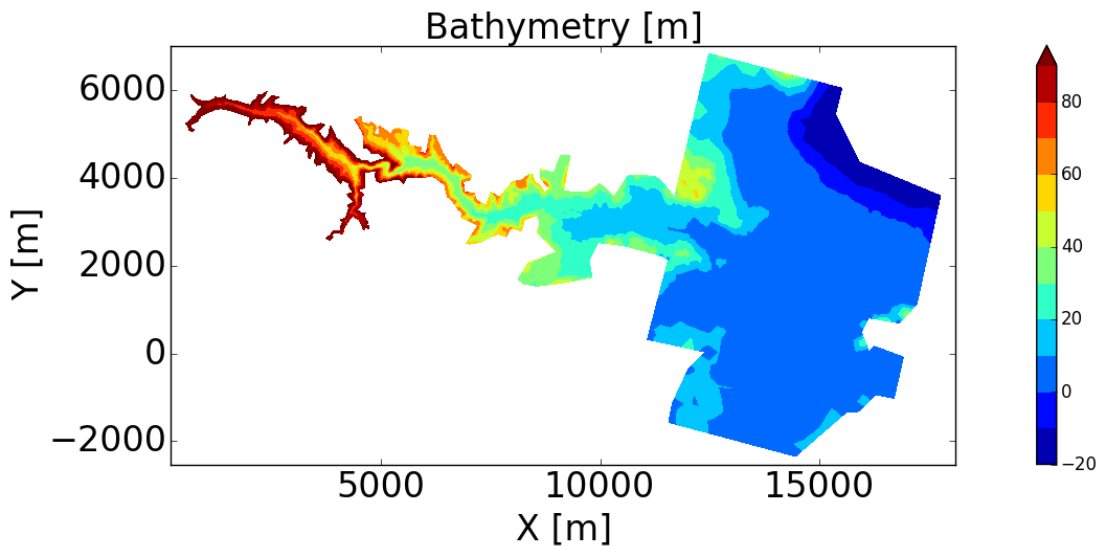


Figure 23.3: Bottom levels in the domain of the Malpasset case.

### 23.2.3 Numerical parameters

#### 23.2.4 Initial conditions

At the beginning of the simulation, the dam is assumed undamaged and the reservoir is full. There is no water in the downstream valley, and no velocity in all the domain.

#### 23.2.5 Boundary conditions

The boundaries are solid everywhere and the channel banks considered as solid walls. There is no friction on the solid walls. The bottom is considered as a solid boundary with roughness. The Strickler formula with friction coefficient =  $30 \text{ m}^{1/3}/\text{s}$  is used.

### 23.2.6 Cases

For this test case, four different simulations are run. The following characteristics are common to all cases:

- Type of computation: Non-hydrostatic,
- Duration: 4,000 s.

The simulation parameters specific to each case are summed up in Table 23.1.

Case	Name	Mesh	Number of vertical planes	Advection scheme for velocities	Time step
1	MURD P2	Regular	2	N-type MURD	4.0 s
2	CHAR P2	Regular	2	Characteristics	4.0 s
3	MURD P6	Regular	6	N-type MURD	4.0 s
4	FINE P2	Fine	2	N-type MURD	1.0 s

Table 23.1: List of the simulation parameters used for the four cases tested in the Malpasset example.

### 23.2.7 Physical parameters

In the simulations, the Coriolis force and the wind effect are not taken into account. Besides, the viscosity is set as constant and equal to  $1 \text{ m}^2/\text{s}$  on horizontal directions.

## 23.3 Results

### 23.3.1 First observations

Figure 23.4 illustrates the progression of the flood wave after the dam break (simulation MURD P2 with scheme N-type MURD using the treatment of negative depths that smoothes the results on tidal flats).

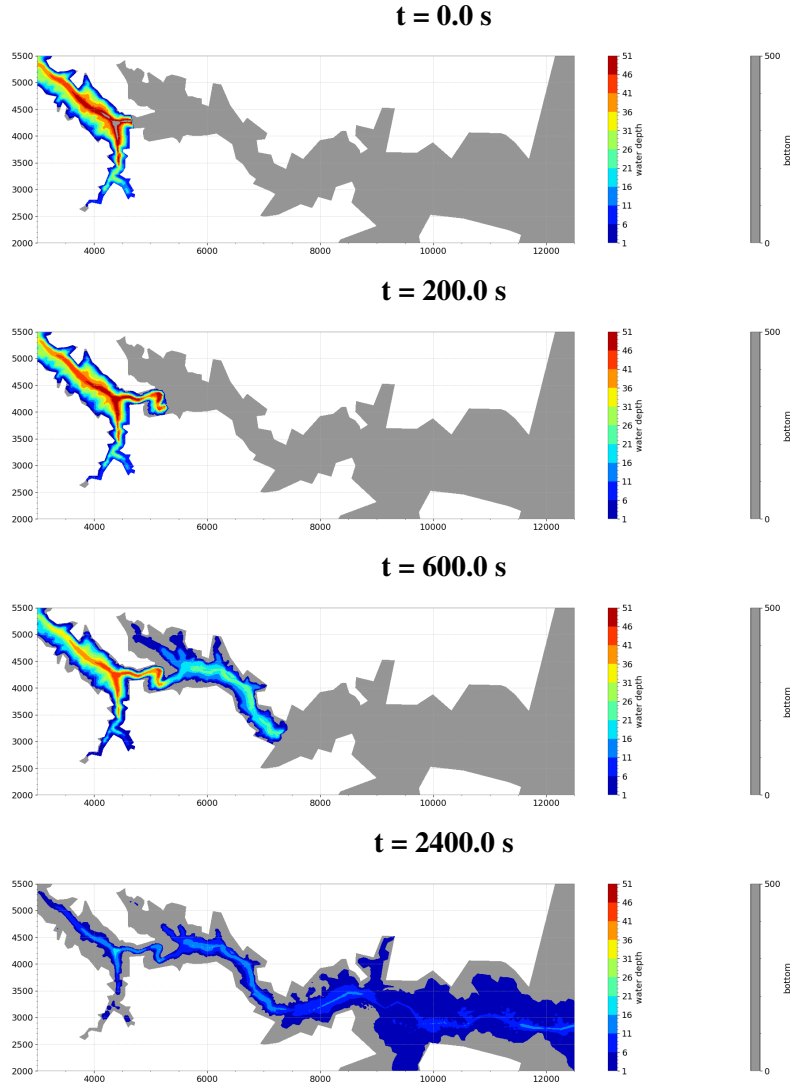


Figure 23.4: Evolution of the water depth in time for Case MURD P2 on the Malpasset example.

Figure 23.5 shows the water depth at time 400 s obtained with 2 planes (MURD P2), 6 planes (MURD P6) and the treatment of negative depths, 2 planes using the method of characteristics (CHAR P2) and 2 planes using the fine mesh (FINE P2) calculations. The results are similar for simulations using the MURD scheme with 2 and 6 planes. The characteristics scheme gives comparable results. The wave seems to propagate faster with the fine mesh. Figures 23.6 show the velocity field after 100 s in the vicinity of the dam for 3 XY planes of case MURD P6.

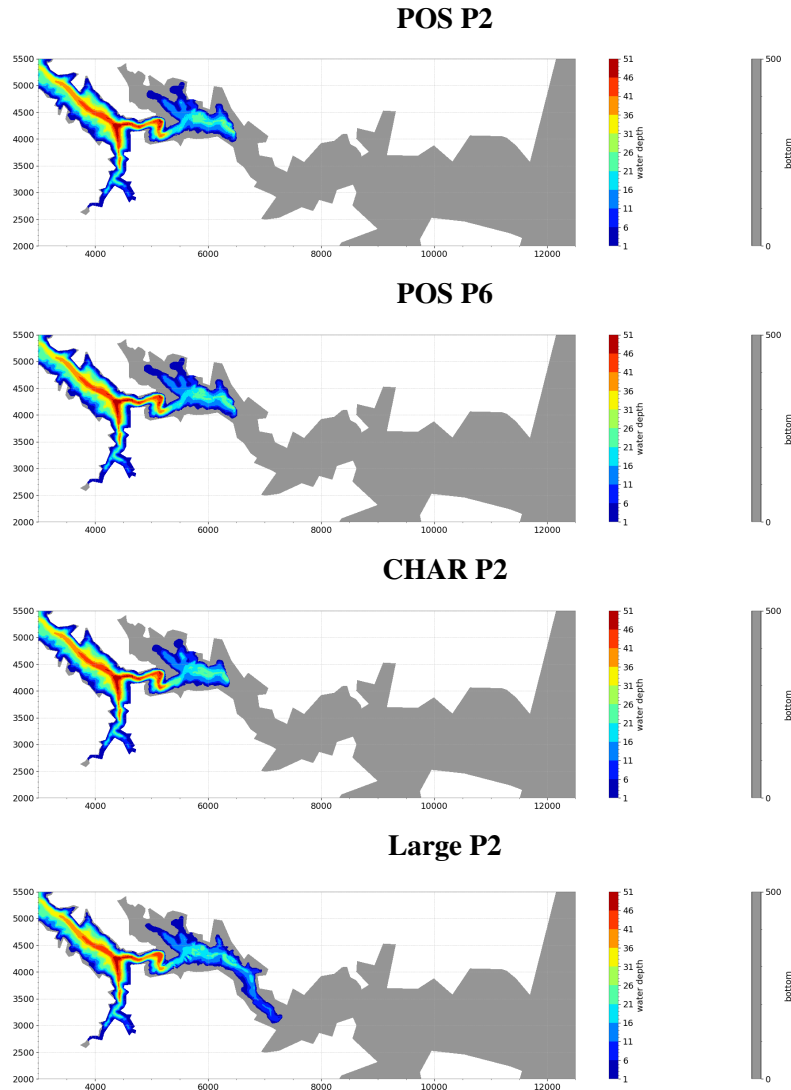


Figure 23.5: Water depth at 400 s for the studied cases on the Malpasset example.

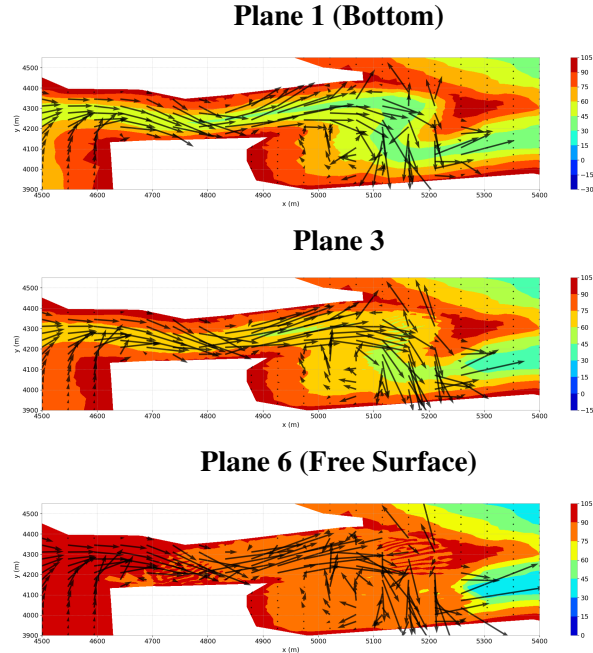


Figure 23.6: Velocity field for case POS P6 after 100 s on the Malpasset example.

The effect of the bend is noticeable even in this early stage of the simulation for all the planes. In fact, a recirculation can be observed on the right bank in the three figures.

Velocity values are compared in Figure 23.7 for the same three planes. The free surface velocity values are slightly higher than near the bottom.

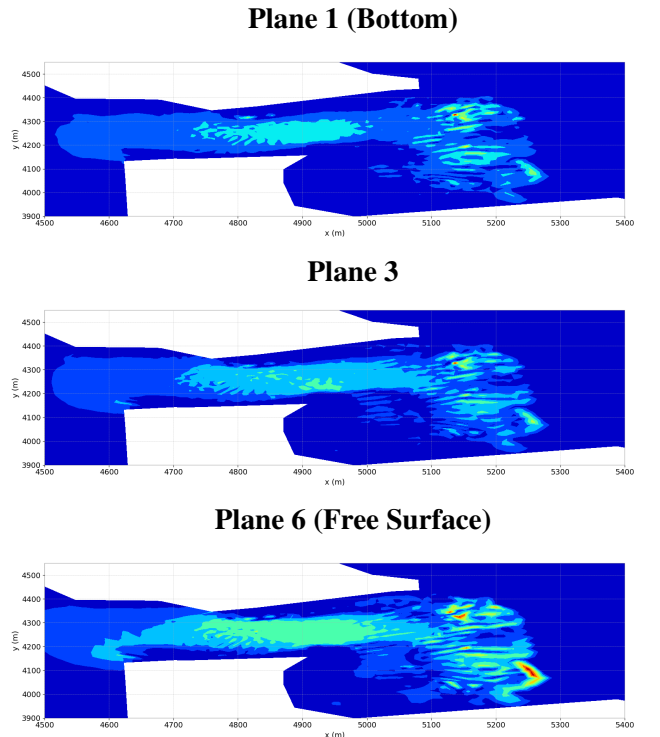


Figure 23.7: Velocity values for case POS P6 after 100 s on the Malpasset example.

### 23.3.2 Comparison of schemes

#### Performance

Performance tests are conducted on the cases. The studied variable here is the water depth.

Times of simulation for each of these cases with sequential and parallel runs (using 4 processors) are shown in Table 23.2<sup>1</sup>. Remember that the computation with the fine mesh is only run in parallel to save CPU time and no result is shown in sequential for it.

CPU Time	MURD P2	CHAR P2	MURD P6	FINE P2
Sequential	1 M 48 S	1 M 27 S	9 M 26 S	7 M 52 S
Parallel	0 M 33 S	0 M 24 S	2 M 41 S	7 M 52 S

Table 23.2: Time of simulation for different cases of the Malpasset example.

With the regular 2D mesh and 2 planes on the vertical, the fastest scheme is the characteristics. Nevertheless, the MURD scheme simulation time is only few seconds longer.

Obviously, increasing the number of planes or the number of 2D elements makes the simulation much longer. Further more, parallel runs using 4 processors considerably decrease simulation times.

Sequential and parallel simulations results are compared for each case in Table 23.3. That allows to quantify the loss of information that goes along with the partitioning of the mesh.

	$\ \varepsilon\ _{L^1}$	$\ \varepsilon\ _{L^2}$	$\ \varepsilon\ _{L^\infty}$
MURD P2			
CHAR P2			
MURD P6			

Table 23.3: Sequential VS Parallel - Errors on water depth values on the Malpasset case.

#### Accuracy

In order to evaluate the precision of the tested schemes, the results are compared to data obtained from:

- A physical model (see [7]) (Non-distorted, 1/400 scale) that was built in LNHE (EDF) in 1964, from which measurements of the free surface were taken using gauges put in different locations,
- Reality. In fact, three electric transformers (called A, B and C from upstream to downstream) were destroyed by the wave and the the times of electric shutdowns were precisely recorded.

The locations of these observation points are shown in Figure 23.8.

---

<sup>1</sup>Keep in mind that these times are specific to the validation run and the type of the processors that were used for this purpose.

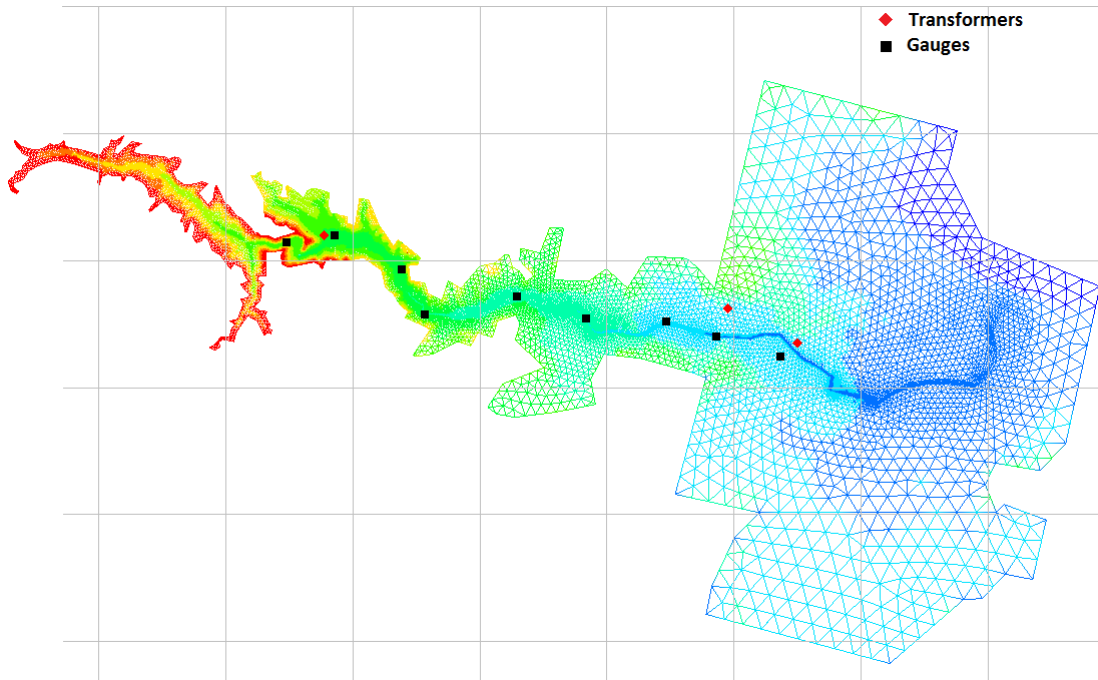


Figure 23.8: location of gauges (physical model) and transformers (field) represented on the mesh of the Malpasset case.

The measured data used in this document are the following:

- Recorded time from A (5,550 m ; 4,400 m) to B (11,900 m ; 3,250 m) : 1,140.0 s,
- Recorded time from A to C (13,000 m ; 2,700 m): 1,320.0 s,
- Maximum free surface elevations obtained from gauges. The values are converted to water depths (by deducing the bathymetry values) and summed up in Table 23.4.

Point Name	x-coordinate	y-coordinate	Distance to dam	Measured Max water depth
P6	4,947	4,289	336	40.3
P7	5,717	4,407	1,320	14.6
P8	6,775	3,869	2,160	24.0
P9	7,128	3,162	3,420	12.8
P10	8,585	3,443	4,840	11.8
P11	9,674	3,085	6,000	8.3
P12	10,939	3,044	7,220	10.1
P13	11,724	2,810	7,980	6.8
P14	12,723	2,485	8,960	5.4

Table 23.4: Maximum values of water depth on measurement points of the Malpasset case (m).

These data are used to calculate the relative gap percentage between the physical model results and numerical model results. This error percentage is calculated as a  $L^1$ -type relative error given by  $100 \times \frac{H_{telemac3d} - H_{gauge}}{H_{gauge}}$ . The maximum values of water depth are extracted for each gauge for all the schemes and summed up in Table 23.5. Negative values of error percentage are colored in red and correspond to a numerical estimation lower than the observed one.

Point	MURD P2	CHAR P2	MURD P6	FINE P2
P6	55.54 (37.82%)	49.04 (21.69%)	55.35 (37.34%)	54.16 (34.39%)
P7	30.77 (110.75%)	28.62 (96.03%)	31.04 (112.60%)	24.17 (65.55%)
P8	27.17 (13.21%)	23.22 (-3.25%)	25.22 (5.08%)	24.87 (3.63%)
P9	21.57 (68.52%)	20.13 (57.27%)	22.23 (73.67%)	18.93 (47.89%)
P10	15.75 (33.47%)	14.62 (23.90%)	15.45 (30.93%)	15.50 (31.36%)
P11	8.85 (6.63%)	5.76 (-30.60%)	8.99 (8.31%)	7.39 (-10.96%)
P12	8.77 (-13.17%)	8.82 (-12.67%)	8.80 (-12.87%)	8.06 (-20.20%)
P13	14.73 (116.62%)	13.86 (103.82%)	14.78 (117.35%)	14.86 (118.53%)
P14	5.20 (-3.70%)	4.91 (-9.07%)	5.16 (-4.44%)	4.56 (-15.56%)

Table 23.5: Maximum values of water depth on measurement points for different schemes on the Malpasset case - relative errors.

First deduction is that the number of planes does not seem to influence the results much (comparison between MURD P2 and MURD P6). The fine mesh improves the results for points 6 to 10, but the error percentages rise for points 11 to 14.

In general, for all the schemes, some points (eg. P14) seem to result with very high discrepancies in comparison with observed results. The following interpretation can be found in reference [7].

« *The discrepancies on the free surface elevation at the nine gauges, between 1-D and 2-D solutions, and the physical model, remain large and are questionable. However, the results are good as soon as the wave reaches the floodplain, the difference at gauge 14 being 14 cm with a total depth of 5.4 m. It is clear from the sensitivity study done with TELEMAC-2D that the differences are not entirely due to an inaccurate solution of the Shallow water equations. As a matter of fact, numerical and physical parameters have little influence on the maximum free surface elevation, but not in a range that would allow a possible perfect match. Several other factors could be responsible for the error such as:*

- *the physical model itself, because a 1/400 scale gives a 4 m difference for a 1cm error on measurements,*
- *the Shallow Water equations are an approximation and their assumptions, such as the hydrostatics pressure, cannot be fully verified in this case - a test with Boussinesq or Serre equations would be of the utmost interest to clarify this point,*
- *the dam failure scenario, which was probably not absolutely instantaneous,*
- *the debris flow and sediment transport, which was not taken into account in this study»*

Next, the propagation time of the wave recorded in TELEMAC-3D is compared to reality in Table 23.6. Negative values of error percentage are colored in red and correspond to a numerical estimation lower than the observed one.

Distance	MURD P2	CHAR P2	MURD P6	FINE P2
A to B	1024.0 (-10.2%)	1308.0 (14.7%)	1012.0 (-11.2%)	1070.0 (-6.1%)
A to C	1184.0 (-10.3%)	1500.0 (13.6%)	1168.0 (-11.5%)	1186.0 (-10.2%)

Table 23.6: Propagation time of the wave for different schemes on the Malpasset case - relative error.

The errors here have the same magnitude for the first three cases. The use of 6 planes does not improve the results. Nevertheless, the finer mesh gives better estimation of the A-B transit time.

### Comparison on profiles

Here, the schemes are compared on profiles upstream (Figure 23.9) and downstream (Figure 23.10) of the dam. The locations of these profiles are the following:

- Upstream of the dam: (4,634.0 ; 4,132.84) (4,589.81 ; 4,393.22),
- Downstream of the dam: (4,884.95 ; 4,161.82) (4,846.39 ; 4,362.44).

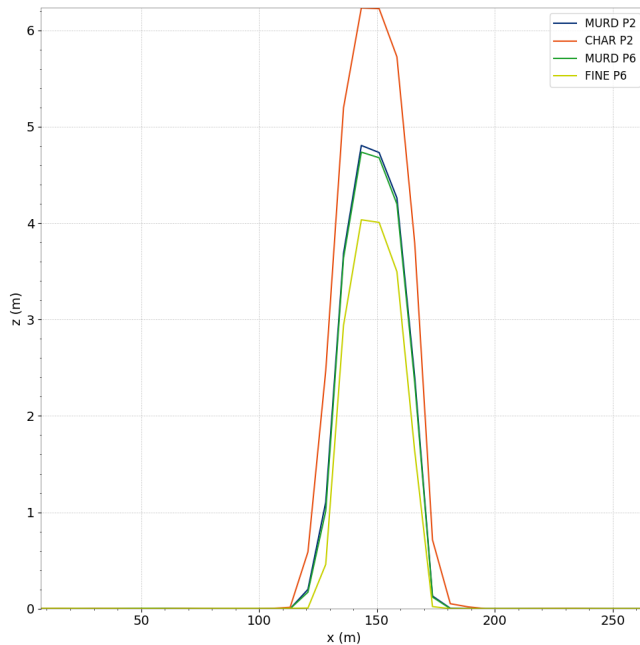


Figure 23.9: Profiles of water depth upstream of the dam at last iteration of the Malpasset case.

These figures show the following:

- The number of planes does not seem to influence the water depth profile,
- The refinement of the 2D mesh has considerable influence,
- The characteristics scheme seems to overestimate the values of the water depth as compared to the MURD scheme.

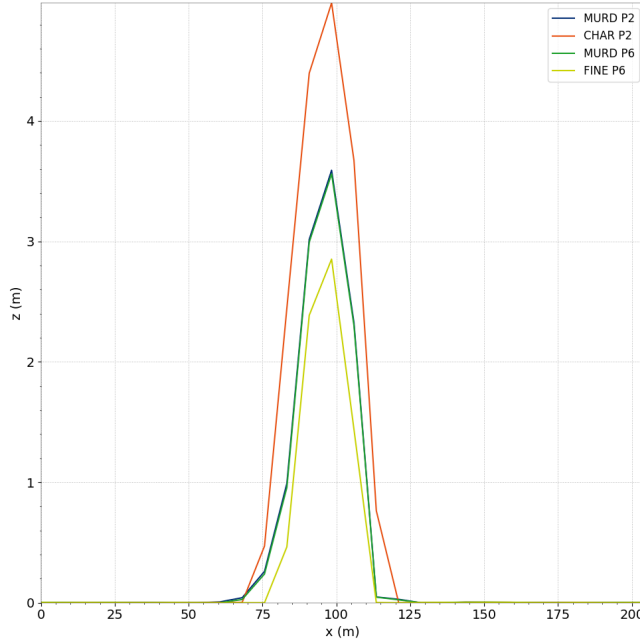


Figure 23.10: Profiles of water depth downstream of the dam at last iteration of the Malpasset case.

### Positivity

Further more, the positivity of the used schemes can be checked for all cases. In order to achieve this, the minimum value of the water depth during the whole simulation, and on all the points of the mesh, is transcribed in Table 23.7.

Schemes	MURD P2	CHAR P2	MURD P6	FINE P2
Minimum $H$ [m]				

Table 23.7: Minimum value of water depth through the simulation for each case of the Malpasset example.

### Mass conservation

Mass conservation can be checked by calculating the volume in the domain during time (as the density is constant in time and space). Lost volume is calculated as  $V_{initial} - V_{final}$ .

		MURD P2	CHAR P2	MURD P6	FINE P2
<b>Sequential</b>	Lost volume [ $\text{m}^3$ ]	2.98E-08	-1.94E-07	2.24E-07	
	Relative error	<b>3.08E-16</b>	<b>-2.00E-15</b>	<b>2.31E-15</b>	
<b>Parallel</b>	Lost volume [ $\text{m}^3$ ]	-4.47E-08	-1.19E-07	1.49E-08	-1.49E-08
	Relative error	<b>-4.62E-16</b>	<b>-1.23E-15</b>	<b>1.54E-16</b>	<b>-1.54E-16</b>

Table 23.8: Volume loss and relative error for different schemes of the Malpasset case.

Table 23.8 shows that the schemes are conservative. Mass conservation is equivalent between sequential and parallel runs. The evolution of volume through time for each of the schemes is shown in Figure 23.11 and vizually confirms the previous conclusion.

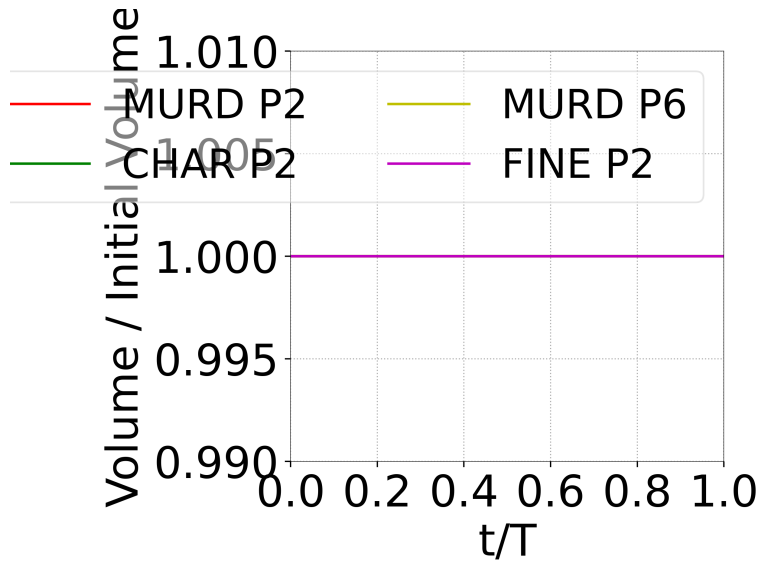


Figure 23.11: Evolution of water volume through time for the tested schemes on the Malpasset case.

## 23.4 Conclusion

TELEMAC-3D is capable of simulating the propagation of a dam break wave in a river valley initially dry. The recommended scheme here is the N-type MURD scheme, as it gives a good approximation with the observed data, specially for the wave speed. Further more, the simulation time with the MURD scheme is equivalent to that with the characteristics scheme. Moreover, in this test case, a higher number of planes does not improve the results, but a refinement of the 2D mesh does. Unfortunately, for the latter, simulation time increases considerably.

## 24. Particles transport (particles)

### 24.1 Purpose

This test demonstrates the ability of TELEMAC-3D to track the transport of particles which are released into the fluid from discharge points.

### 24.2 Description

The configuration is a section of river (around 1,700 m long and 300 m wide) with realistic bottom. The geometric data include a groyne in the transversal direction and an island (see Figure 24.1).

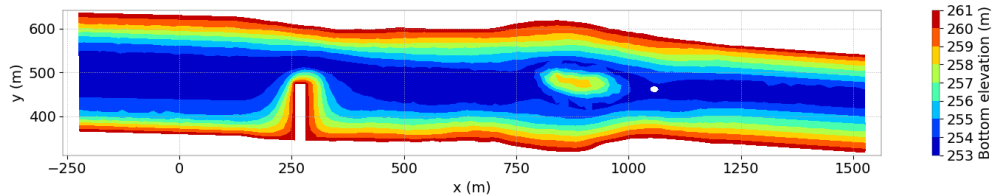


Figure 24.1: Bottom elevation.

#### 24.2.1 Initial and boundary conditions

The initialisation of the computation is done from a 2D result file (water depth and horizontal velocity components).

The boundary conditions are:

- For the solid walls, a slip condition on channel banks is used for the velocities,
- On the bottom, a Strickler law with friction coefficient equal to  $55 \text{ m}^{1/3}/\text{s}$  is prescribed,
- Upstream a flowrate equal to  $700 \text{ m}^3/\text{s}$  is prescribed,
- Downstream the water level is equal to 265 m.

Drogues are released every 10 time steps until the 600<sup>th</sup> time step (= 3,000 s). Thus a maximum of 61 drogues are released, each time at  $x = -200 \text{ m}$ .

### 24.2.2 Mesh and numerical parameters

The mesh (Figure 24.2) is made of 3,780 triangular elements (2,039 nodes). It is refined around the island and in front of the groyne. 10 planes regularly spaced on the vertical (Figures 24.4 along  $y$  axis and Figures 24.3 along  $x$  axis).

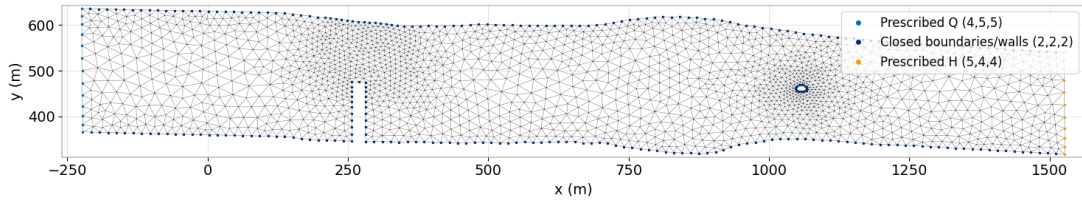


Figure 24.2: Horizontal mesh.

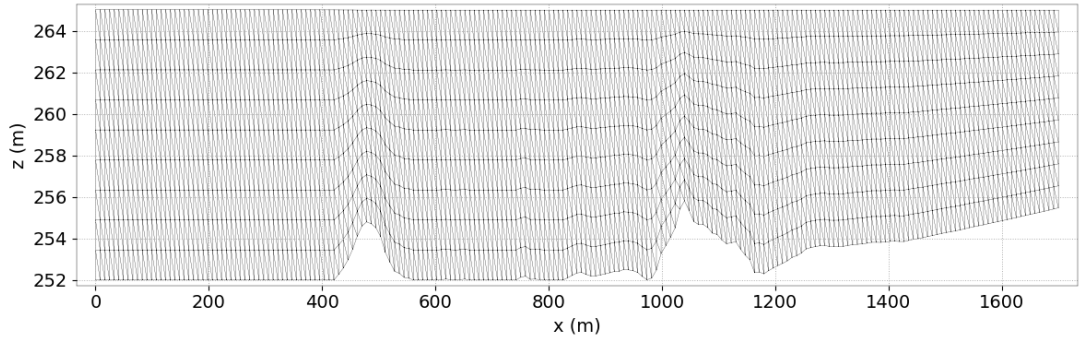


Figure 24.3: Vertical mesh at initial time step along  $x$  axis for  $y = 500$  m.

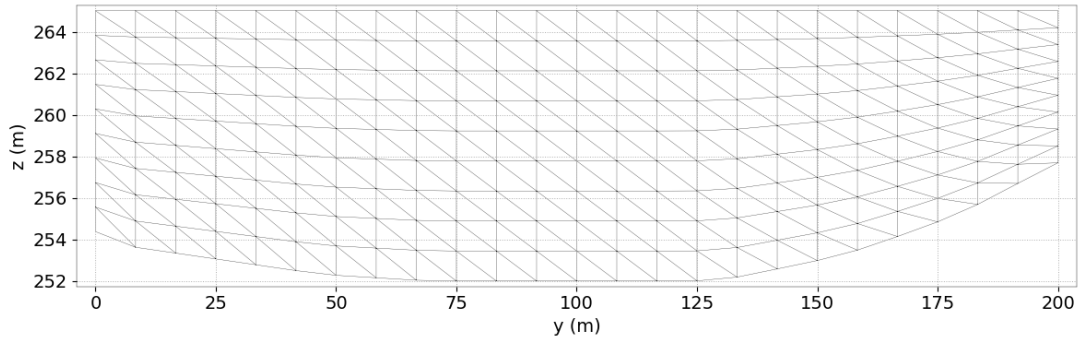


Figure 24.4: Vertical mesh at initial time step along  $y$  axis for  $x = 0$  m.

The time step is 5 s for a simulated period of 2 h (= 7,200 s).

The non-hydrostatic version is used.

To solve the advection, the method of characteristics is used for the velocities (scheme 1). The GMRES is used for solving the propagation and PPE steps (option 7).

A maximum of 100 drogues are released.

### 24.2.3 Physical parameters

Turbulence is modelled with a mixing length model over the vertical and a horizontal constant viscosity equal to  $10^{-2}$  m<sup>2</sup>/s.

### 24.3 Results

The flow establishes a steady flow where the free surface is lightly higher before the groyne than after (see Figure 24.5). The flow accelerates in front of the groyne due to the restriction of section. A recirculation appears just after the groyne.

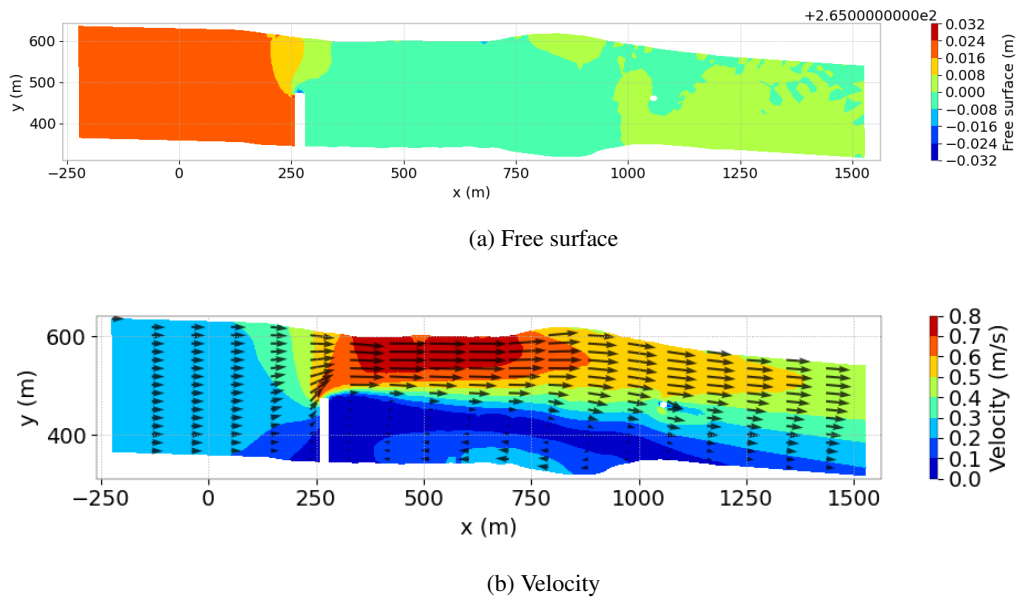


Figure 24.5: Results.

## 25. Flow in a channel with 2 bridge piers (pildepon)

### 25.1 Purpose

This example demonstrates the ability of TELEMAC-3D to represent the impact of an obstacle on a channel flow. It also demonstrates the capability to represent unsteady eddies in a model with steady state boundary.

### 25.2 Description

The configuration is a 28.5 m long and 20 m wide prismatic channel with trapezoidal cross-section contains bridge-like obstacles in one cross-section made of two abutments and two circular 4 m diameter piles (See Figure 25.1). The flow resulting from steady state boundary conditions is studied. The deepest water depth is 4 m.

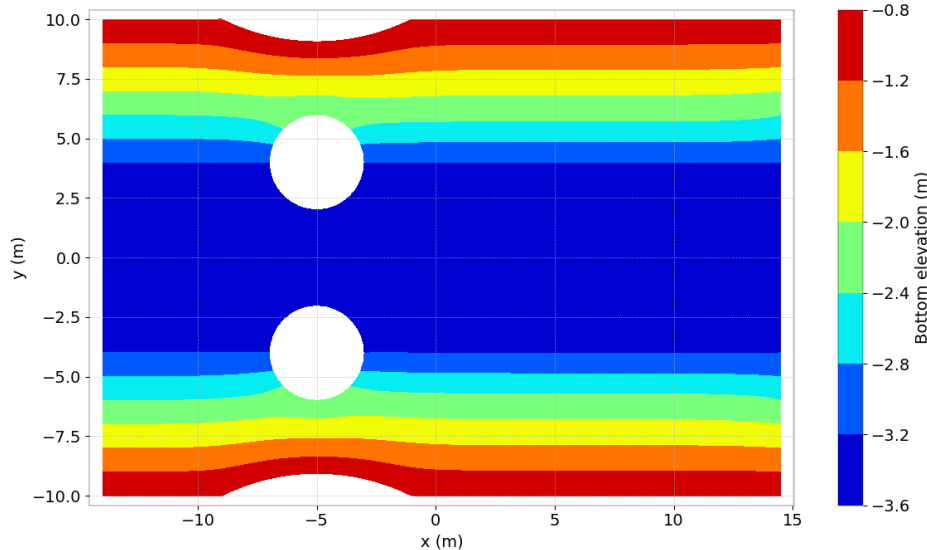


Figure 25.1: Bottom elevation.

#### 25.2.1 Initial and Boundary Conditions

The computation is initialised with a constant elevation equal to 0 m and no velocity.

The boundary conditions are:

- For the solid walls, a slip condition on channel banks is used for the velocities,
- On the bottom, a Strickler law with friction coefficient equal to  $40 \text{ m}^{1/3}/\text{s}$  is prescribed,
- Upstream a flowrate equal to  $62 \text{ m}^3/\text{s}$  is prescribed, linearly increasing from 0 to  $62 \text{ m}^3/\text{s}$  during the first 20 s,
- Downstream the water level is equal to 0. m (= initial elevation).

### 25.2.2 Mesh and numerical parameters

The 2D mesh (Figure 25.2) is made of 4,304 triangular elements (2,280 nodes). 6 planes are regularly spaced on the vertical (see Figure 25.3).

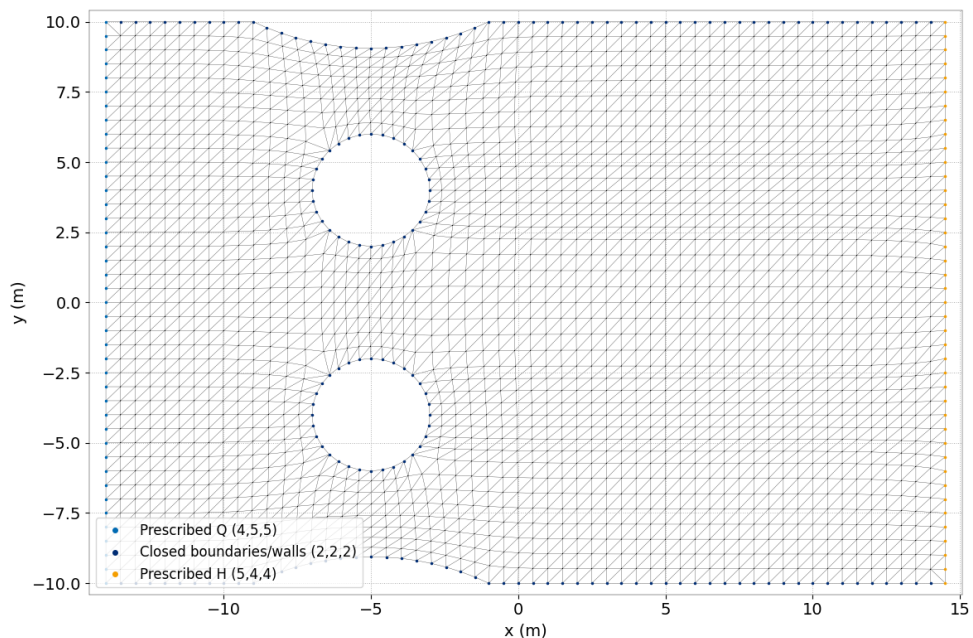


Figure 25.2: Horizontal mesh.

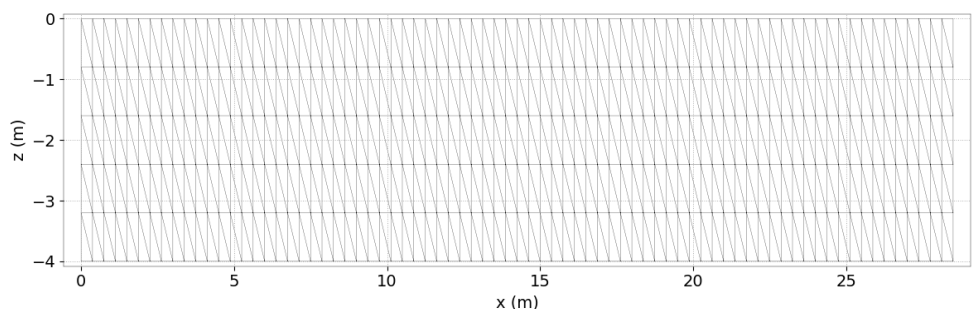


Figure 25.3: Initial vertical mesh.

2 computations are run: one with the hydrostatic hypothesis and one with non-hydrostatic version.

To solve the advection, the method of characteristics is used for velocities.

GMRES is used for solving the propagation and diffusion of velocities (option 7). The implicitation coefficients for depth and velocities are respectively equal to 0.6 and 1.

The time step is 0.1 s for the hydrostatic version, 0.4 s for the non-hydrostatic version. The simulated period is 80 s for both cases.

### 25.2.3 Physical parameters

A mixing length model is used as vertical turbulence model combined with constant horizontal viscosity for velocity equal to  $0.005 \text{ m}^2/\text{s}$ .

## 25.3 Results

The obstacles create a contraction of the streamlines, and Karman vortices are observed behind the piers. The Karman vortices produce an asymmetry of the velocity field. This velocity field is unsteady behind the piers in the Karman vortices (see top of Figures 25.4 and 25.5, where surface velocities are shown for the hydrostatic and non-hydrostatic simulations respectively).

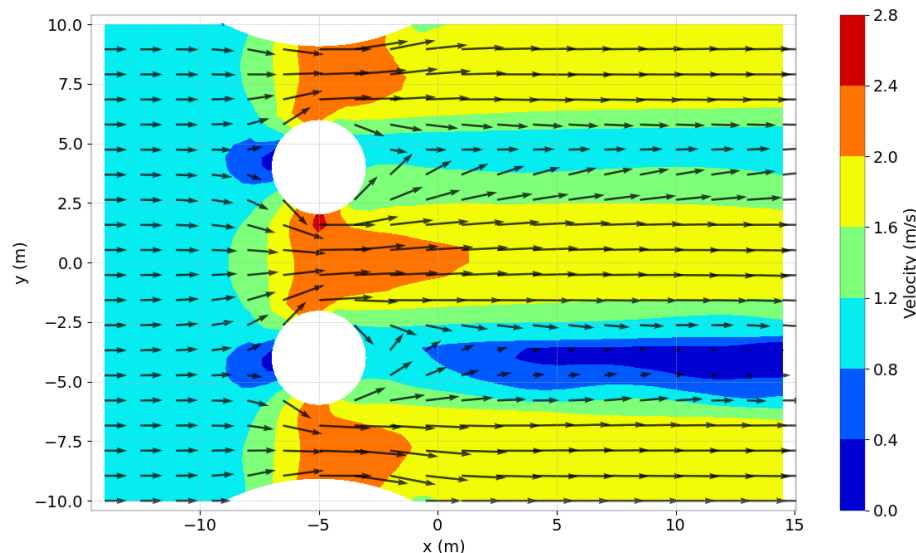


Figure 25.4: Velocity magnitude at the surface at final time step for the hydrostatic case.

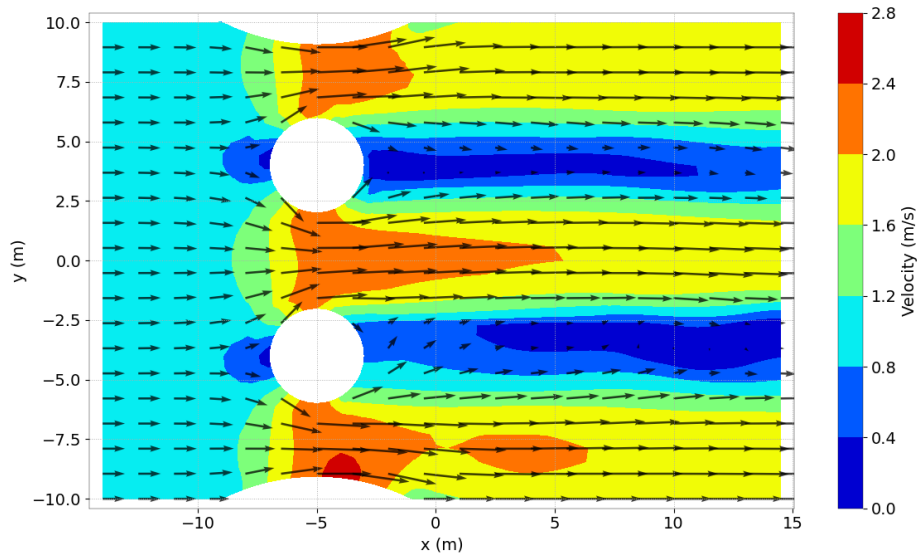


Figure 25.5: Velocity magnitude at the surface at final time step for the non-hydrostatic case.

Figures 25.6 and 25.7 show the free surface at final time step ( $= 80$  s) for the hydrostatic and non-hydrostatic computations.

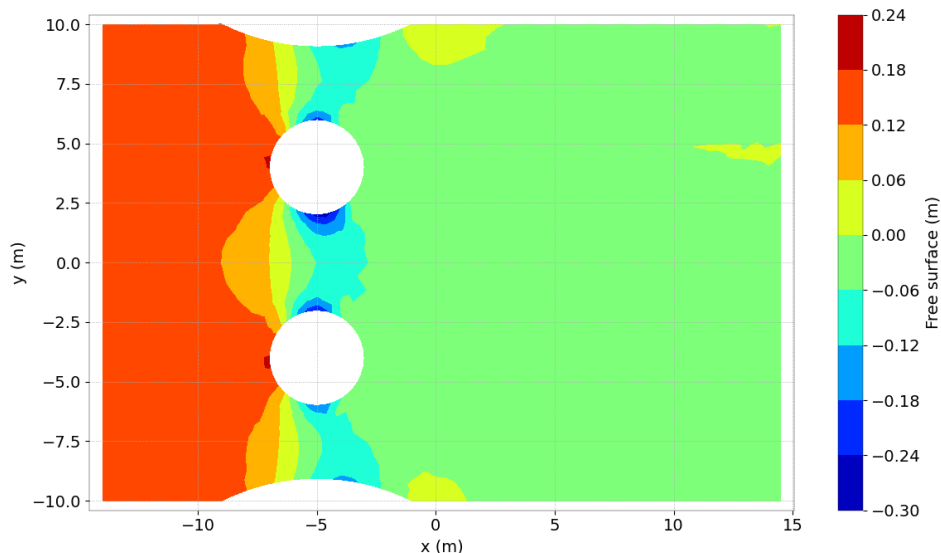


Figure 25.6: Free surface at final time step for the hydrostatic case.

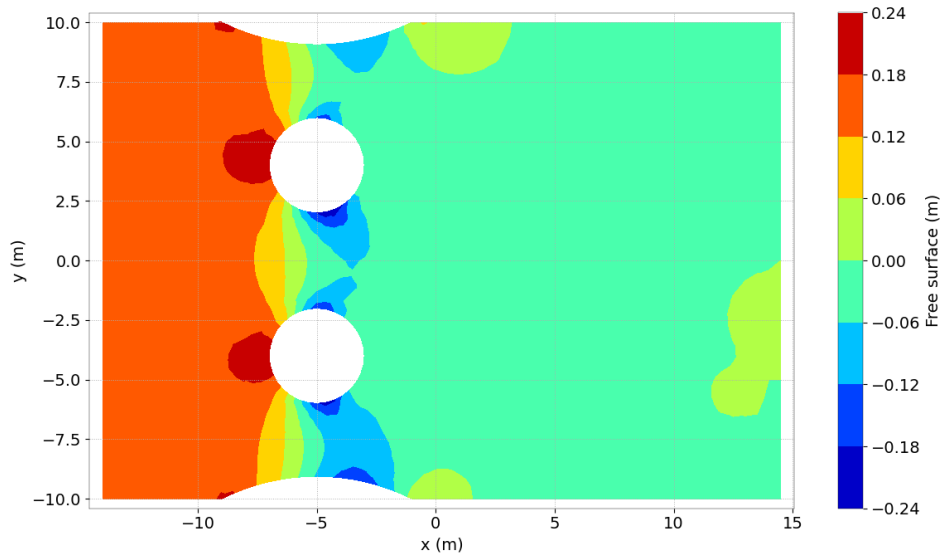


Figure 25.7: Free surface at final time step for the non-hydrostatic case.

## 25.4 Conclusion

TELEMAC-3D can be used to study the hydrodynamic impact of engineering works (like bridge piers), and to analyse unsteady flow, such as the Karman vortices.

## 26. Flow along a beach (plage)

### 26.1 Purpose

This example tests the  $k - \omega$  model of TELEMAC-3D.

### 26.2 Description

The configuration is a flat channel ( $z = -0.43$  m) with a kind of cavity and a beach where the bathymetry is increasing from -0.43 m to 0 m in the cavity (see Figure 26.1).

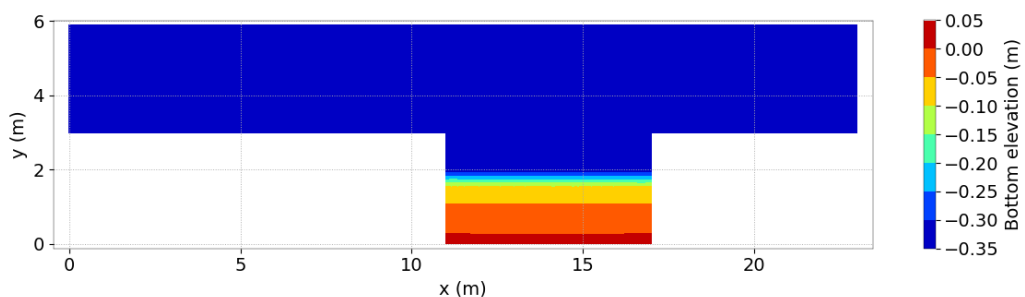


Figure 26.1: Bottom elevation.

#### 26.2.1 Initial and Boundary Conditions

The computation is initialised with a constant elevation equal to 0.1 m and no velocity.  
The boundary conditions are:

- For the solid walls, a slip condition on channel banks is used for the velocities,
- On the bottom, a Strickler law with friction coefficient equal to  $60 \text{ m}^{1/3}/\text{s}$  is prescribed,
- Upstream a flowrate equal to  $0.155 \text{ m}^3/\text{s}$  is prescribed,
- Downstream the water level is equal to 0.1 m (= initial elevation).

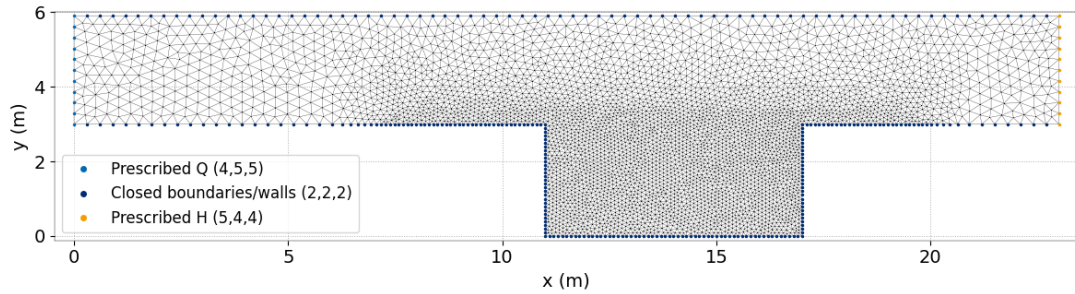
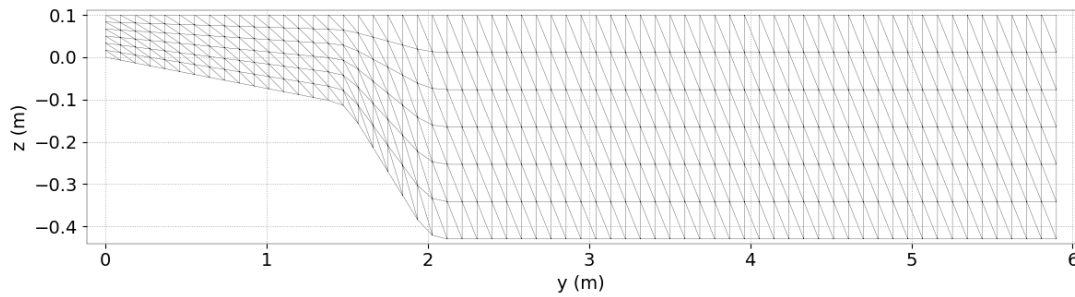


Figure 26.2: Horizontal mesh.

Figure 26.3: Initial vertical mesh along  $x = 15$  m.

### 26.2.2 Mesh and numerical parameters

The 2D mesh (Figure 26.2) is made of 8,796 triangular elements (4,561 nodes). 7 planes are regularly spaced on the vertical (Figure 26.3).

The hydrostatic version of TELEMAC-3D is used.

To solve the advection, the method of characteristics is used for velocities and  $k - \omega$  variables. The time step is 0.2 s for a simulated period of 200 s.

### 26.2.3 Physical parameters

Turbulence is modelled with the  $k - \omega$  model of TELEMAC-3D.

## 26.3 Results

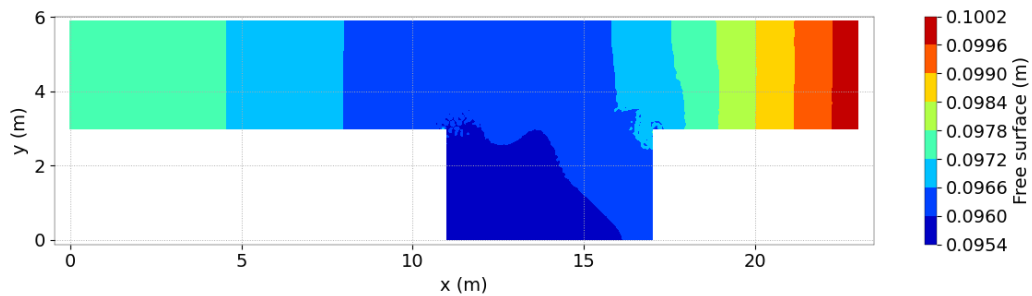


Figure 26.4: Free surface at final time step.

A recirculation can be seen in the cavity representing the beach (Figure 26.5).

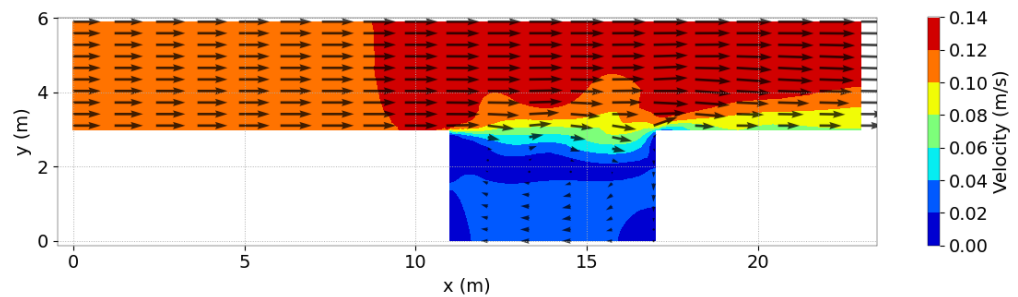


Figure 26.5: Velocity magnitude at the surface at final time step.

## 27. Salinity during a rain fall (pluie)

### 27.1 Description

This test illustrates that TELEMAC-3D is able simulating a rain fall (addition of fresh water on the sea water surface). It allows to show that transport by advection and diffusion of active and passive tracers are correctly represented by TELEMAC-3D.

We consider a square basin of side 10 m. The bottom is flat with a water depth equal to 10 m. An initial salinity is imposed in the basin, as well as a fictive rain of 864,000 mm per day.

Note that the turbulent viscosity is constant in horizontal direction and equal to  $0.1 \text{ m}^2.\text{s}^{-1}$  and a mixing length model is used in the vertical direction (Nezu-Nakagawa formula).

#### 27.1.1 Initial and boundary conditions

The water is initially at rest with a constant initial salinity equal to  $32 \text{ kg.m}^{-3}$  (or  $\text{g.L}^{-1}$ ) and the water depth is equal to 10 m.

The boundary conditions are:

- Solid boundaries everywhere on the basin banks with a slip condition on velocity,
- On the bottom, Nikuradse law with friction coefficient equal to 0.0162 m is imposed,
- At the surface, a fictive rain of 864,000 mm per day ( $10 \text{ mm.s}^{-1}$ ) is taken into account.

#### 27.1.2 Mesh and numerical parameters

The mesh (Figures 27.1 and 27.2) is composed of 272 triangular elements (159 nodes) with 21 planes regularly spaced on the vertical, to form prism elements.

The time step is 1 s for a simulated period of 3 s.

This case is computed with the hydrostatic pressure assumption. The method of characteristics scheme is used for the velocities (scheme 1) to solve the advection and a direct solver (scheme 8) is used for propagation. The implicitation coefficients for depth and velocities are equal to 0.6.

For the tracer (or salinity), the PSI-type MURD scheme is used to solve the advection (scheme 5) and a direct solver (scheme 8) is used for the diffusion.

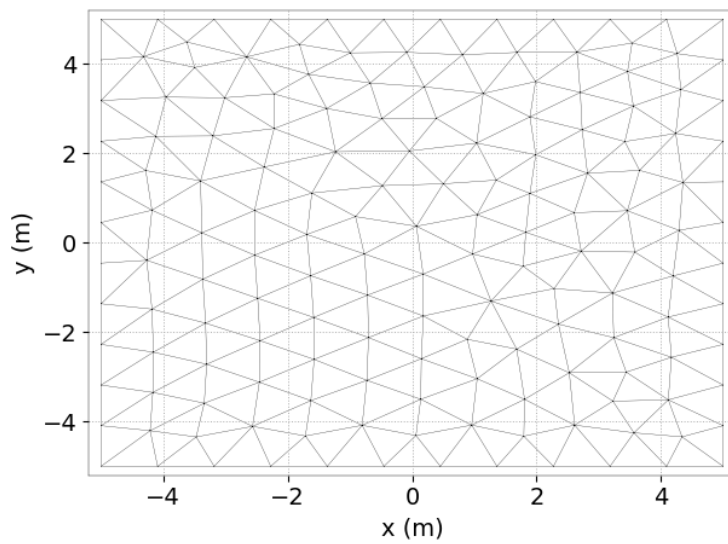


Figure 27.1: Horizontal mesh.

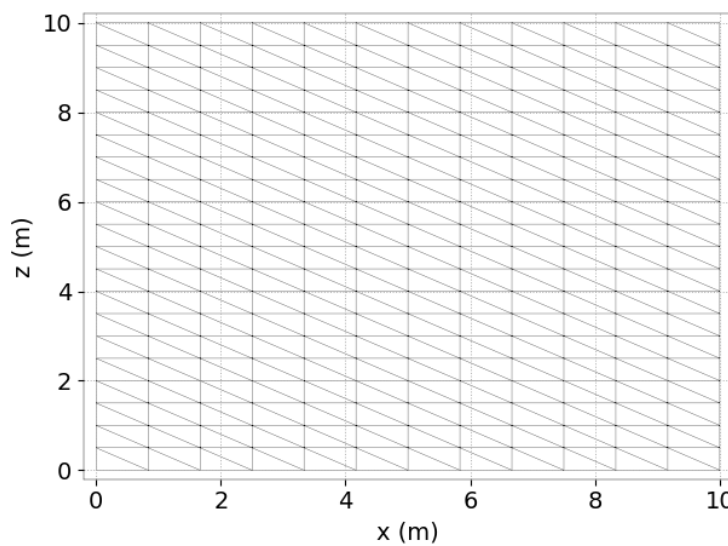


Figure 27.2: Vertical Mesh.

## 27.2 Results

The mass balance is the following:

```
-- WATER --
INITIAL MASS : 1000.000
FINAL MASS : 1003.000
MASS LEAVING THE DOMAIN (OR SOURCE) : -3.000000
MASS LOSS : -0.3397282E-12
```

The water mass balance is excellent (of the order of  $10^{-12}$ ). The quantity of rain during the total simulation is 30 mm. Taking into account the surface of the basin ( $100 \text{ m}^2$ ), the quantity of supplied fresh water is equal to  $3 \text{ m}^3$ . The final mass is well computed and equal to  $1,003 \text{ m}^3$ . In addition, the total tracer (salinity) remains well constant (with a mass loss of the order of  $10^{-8}$ ).

As expected, the salinity at the surface decreases during the simulation (see Figure 27.3), due to the rain. The salinity profile on the vertical at the end of the simulation is so presented in Figure 27.4.

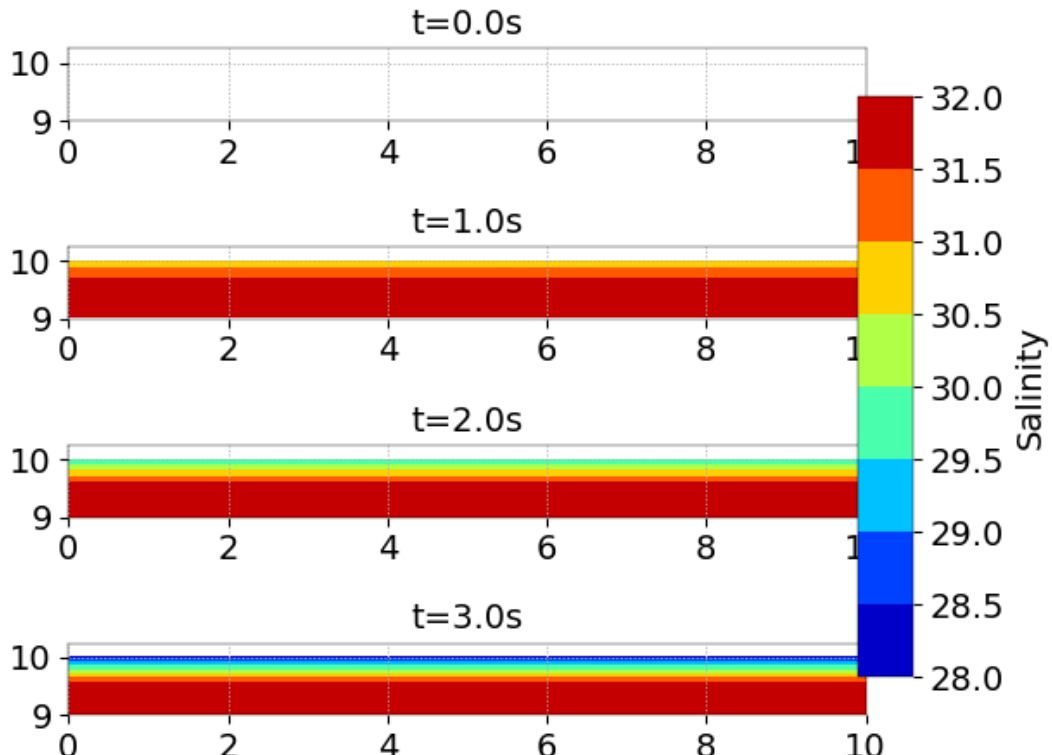


Figure 27.3: Salinity evolution in three dimensions.

Therefore, TELEMAC-3D is capable of simulating the supply of water on the free surface due to the rain.

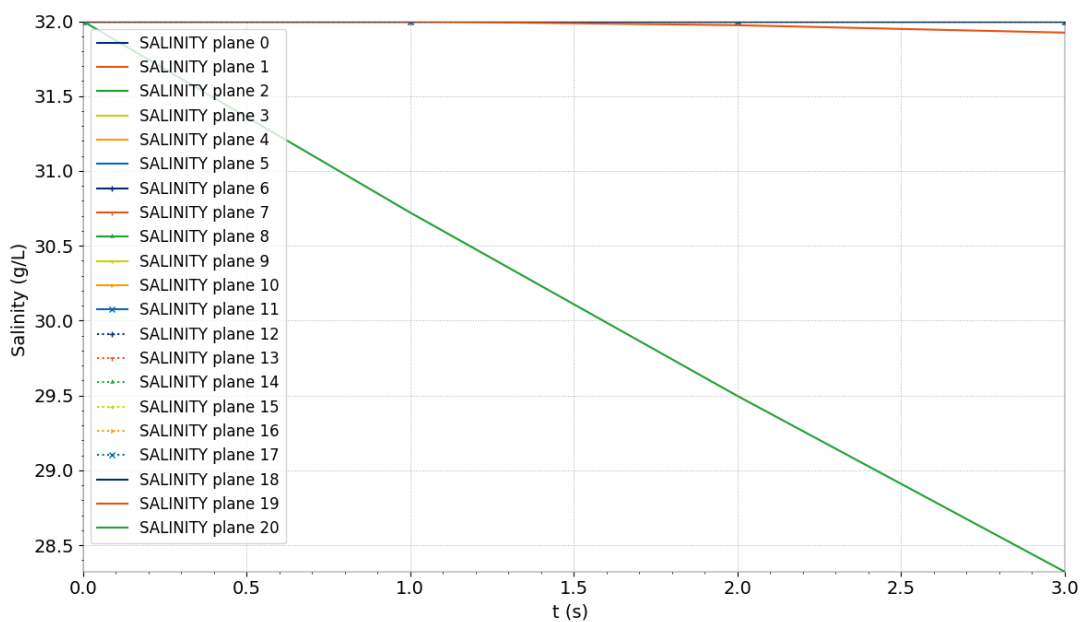


Figure 27.4: Salinity profile on the vertical at the last time step.

## 28. Solitary wave (solit)

### 28.1 Purpose

This test demonstrates the ability of TELEMAC-3D to model the propagation of a solitary wave with only 2, 3 or 4 vertical levels. In an ideal case, the wave should travel without changing its shape and amplitude. This study demonstrates the necessity of using the non-hydrostatic version of the software to simulate non-linear waves propagation.

### 28.2 Notations

This test-case is the same as described in [9]. The notations are illustrated in Figure 28.1.

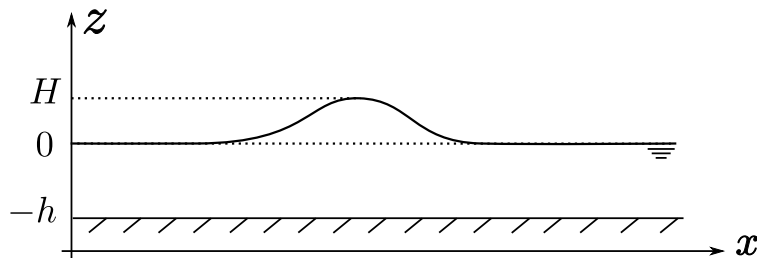


Figure 28.1: Solitary wave propagation over a flat bottom: description of the notations.

### 28.3 Theory

#### Authorship

The following description is extracted from the PhD thesis of Jacek A. Jankowski [9]. Only slight changes were done to the text.

A solitary wave is a single elevation of the water surface above an undisturbed surrounding, which is neither preceded nor followed by any free surface disturbances. Neglecting dissipation, as well as bottom and lateral boundary shear, a solitary wave travels over a horizontal bottom without changing its shape and velocity. The accuracy of the model can be evaluated by comparing the amplitude and celerity of the wave with its theoretical values, as well as the

deformation of the wave as it travels.

There are several theories that aim at giving an approximation of the free-surface and velocity field for this form of non-linear finite-amplitude wave. The most known ones are the Stokes and cnoidal waves theories. The latter is used here, based on Laitone [11]. According to [9], it is the most frequently used for comparative studies. It provides approximate formulae for the velocity components  $u, w$ , free surface elevation  $\eta$  defined as  $\eta = z + h$ , pressure  $p$  and wave celerity  $c$  of a solitary wave with a height of  $H$ , on a vertical section of an infinitely long channel of an undisturbed depth  $h$  ( $z = 0$  at the free-surface, see Figure 28.1). They read:

$$\left\{ \begin{array}{l} u = \sqrt{gh} \frac{H}{h} \operatorname{sech}^2 \left[ \sqrt{\frac{3}{4} \frac{H}{h^3}} (x - ct) \right] \\ w = \left( \sqrt{3gh} \sqrt{\frac{H}{h^3}} \frac{z+h}{h} \right) \operatorname{sech}^2 \left[ \sqrt{\frac{3}{4} \frac{H}{h^3}} (x - ct) \right] \tanh \left[ \sqrt{\frac{3}{4} \frac{H}{h^3}} (x - ct) \right] \\ \eta = h + H \operatorname{sech}^2 \left[ \sqrt{\frac{3}{4} \frac{H}{h^3}} (x - ct) \right] \\ p = \rho g (\eta + z) \\ c = \sqrt{g(H+h)} \end{array} \right. \quad (28.1)$$

It is interesting that in this analytical approximation the vertical velocity component is not treated as small, as commonly taken, but the pressure can be assumed hydrostatic (fourth line of (28.1)) at the same level of exactness as the horizontal velocity (with  $\mathcal{O}((H/h)^2)$ )[11]. Therefore, this initial condition is suitable for fair comparisons between models with and without hydrostatic approximation and the initial value of zero hydrodynamic pressure is assumed. Although the initial velocity field (first two lines of (28.1)) is perfectly divergence-free, larger values of the hydrodynamic pressure appear immediately after the first time step (60% of the value of the hydrostatic pressure at the bottom).

Following the test cases provided by Ramaswamy [13], a solitary wave described by (28.1) is applied in a long channel as an initial condition, and the behaviour of the solution is observed thereafter. Due to the fact that the simulation is performed in a finite domain, and Laitone's formulae are valid for an indefinitely long channel, care must be taken choosing the initial position of the wave crest. In order to deal with it, the use of the effective wave length  $\lambda$  concept is made.  $\lambda$  is equal to the doubled length between the wave crest and a point, where the free surface elevation is  $\eta(x) = 0.01H$ . According to Laitone:

$$\lambda = 6.9 \sqrt{\frac{h^3}{H}}. \quad (28.2)$$

For example, when  $H/h = 0.1$ ,  $\lambda/2 \approx 11h$ , and for a channel of 10 m depth, the initial distance between the solitary wave crest and a boundary should be at least 110 m.

## 28.4 Description

### 28.4.1 Geometry and Mesh

#### Geometry

A long channel of 600 m long and 6 m wide is considered, with a constant depth  $h = 10$  m. The bottom is flat, at the elevation  $z = -10$  m.

### Mesh

The mesh is composed of 6 elements on the width and 600 on the length, with a resolution in the direction parallel to the channel axis of 1 m (see Figure 28.2). This corresponds to 7,206 triangular elements and 4,210 nodes. Various numbers of planes on the vertical are considered: 2, 3 and 4.

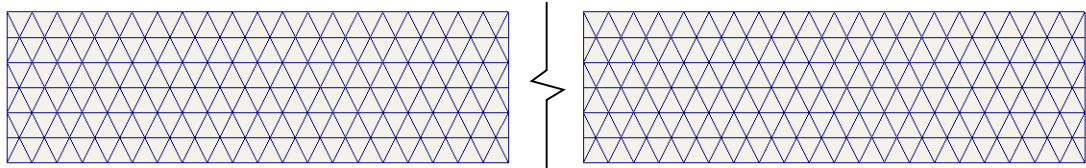


Figure 28.2: Solitary wave propagation over a flat bottom: mesh of the case in the  $(x, y)$  plane.

#### 28.4.2 Physical parameters

The flow is assumed to be inviscid, without shear on the lateral boundaries and on the bottom.

#### 28.4.3 Initial and Boundary Conditions

##### Initial conditions

As the initial condition the hydrostatic approximation given by (28.1) is applied, with a wave height of  $H = 1$  m, and the initial crest position at  $x = 150$  m. The velocity field and the free-surface elevation are given by (28.1).

##### Boundary conditions

The lateral boundaries and the bottom are impervious, there is no friction.

#### 28.4.4 General parameters

The time step size is constant, equal to  $\Delta t = 0.1$  s (the Courant number in the direction of wave propagation varies from 0.2 to about 1.0 at the wave crest). The simulation time is 30 s.

#### 28.4.5 Numerical parameters

The non-hydrostatic version is used. Advection of velocities is done with the method of characteristics. The solver for the pressure is the GMRES (Generalized Minimal Residual Method, scheme 7) with diagonal preconditionning, an accuracy of  $10^{-6}$  is asked for.

A coefficient of implicitation for the depth and velocities of 0.51 is used. A mass-lumping is used on the depth, with a coefficient of 1. There are no tidal flats in this case.

## 28.5 Results

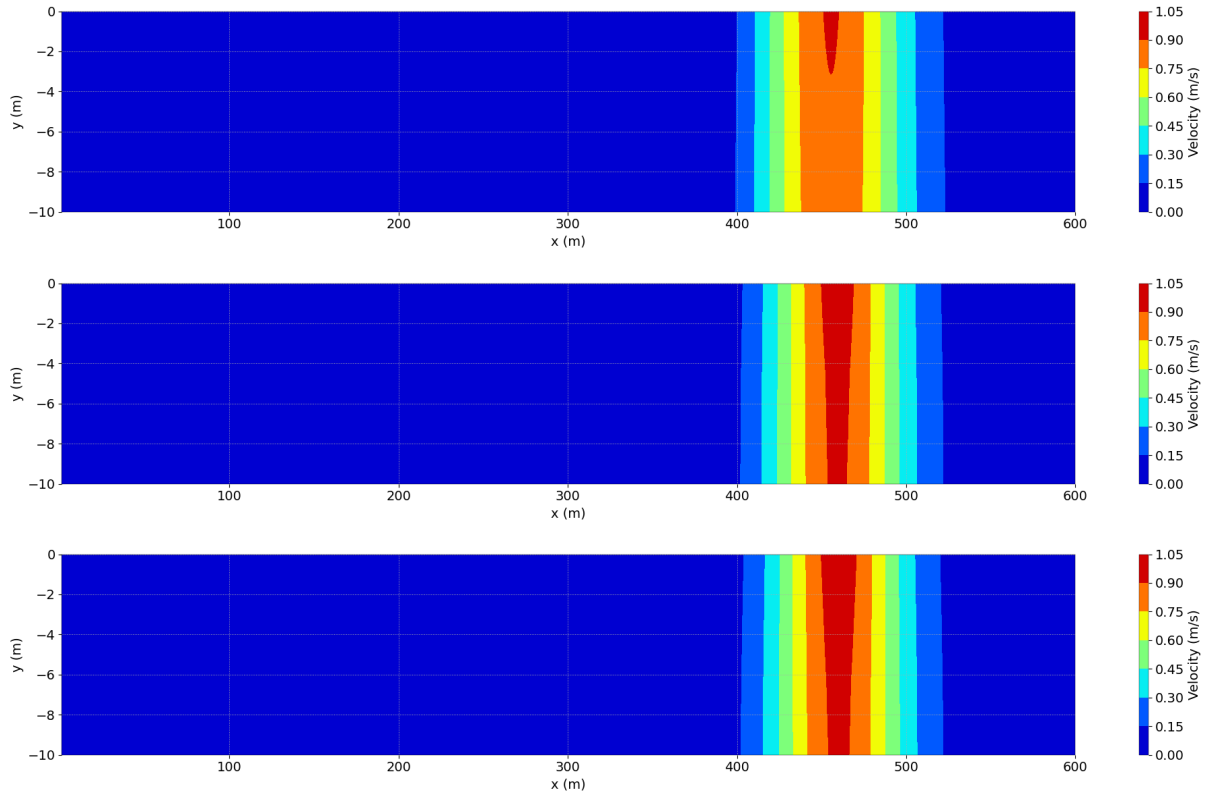


Figure 28.3: Solitary wave propagation over a flat bottom: simulation results using 2, 3 and 4 planes: the colours represent the velocity magnitude, from 0 (blue) to 1 (red).

Figure 28.3 presents a longitudinal cross profile of the free surface at different times of the simulation and for the various configurations on vertical discretisation. The amplitude of the wave remains nearly constant in all cases. The relative error on the wave amplitude after 30 s is of 4.8 % with 2 planes and about 0.01 % with 3 and 4 planes (see the Table 28.1). On the other hand, the theoretical celerity of the propagation is equal to  $\sqrt{g(h+H)}$ . With a water level  $h = 10$  m and a wave height  $H = 1$  m, the theoretical celerity is equal to  $10.38 \text{ m.s}^{-1}$ . Table 28.1 shows the values of the wave displacement and celerity on the numerical models (using 2, 3 and 4 planes). The error on the celerity is also displayed, showing a maximum error of 1.9 % (using two planes) and less than 1 % when refining on the vertical.

Table 28.1: Solitary wave propagation over a flat bottom: values of the wave height and displacement after 30 s in the simulation, together with the values of wave celerity and relative error on the celerity using 2, 3 and 4 planes in the mesh.

	<b>2 planes</b>	<b>3 planes</b>	<b>4 planes</b>
<b>Final wave height (m)</b>	0.952	0.999875	1.0002
<b>Final displacement (m)</b>	305.5	309	310
<b>Wave celerity (<math>\text{m.s}^{-1}</math>)</b>	10.18	10.3	10.33
<b>Relative error on the celerity (%)</b>	1.9	0.8	0.5

**Results using the hydrostatic version of TELEMAC-3D**

The users should be aware that when using the hydrostatic version on this test-case, the results are not in good agreement with the approximate theoretical solution: the shape of the velocity field is deteriorated, the error on the wave celerity is of about 10 % and the error on the wave height after 30 s of propagation is of 15 %.

## 28.6 Conclusion

TELEMAC-3D correctly simulates the propagation of a solitary wave when using the non-hydrostatic formulation.

# 29. Sources of fluid and tracers (source)

## 29.1 Description

This test shows the capability of TELEMAC-3D to manage multiple sources of fluid and tracers. It also demonstrates the ability to compute injection and conservation of multiple tracers.

A 100 m long and 40 m wide flat bottom basin with a constant water depth of 1 m is considered (the bottom being  $z = -1$  m). The fluid is at rest. Sources are specified at two points of the mesh. Three tracers are used, one is the sum of the two others (tracer 2).

Note that the turbulent viscosity is constant in both directions and equal to the water molecular viscosity ( $10^{-6} \text{ m}^2 \cdot \text{s}^{-1}$ , default value).

### 29.1.1 Initial and boundary conditions

Initially, the fluid is at rest and the water level is null.

The boundary conditions are:

- Solid boundaries without roughness (slip conditions) everywhere, i.e., no entrance and no outlet in the domain,
- On the bottom, Chézy law with friction coefficient equal to  $60 \text{ m}^{1/2} \cdot \text{s}^{-1}$  is imposed (default value for the friction coefficient until version 8.0).

The sources are defined at following positions:

- Position source 1:  $x \approx -21.6 \text{ m}$ ,  $y \approx 5.3 \text{ m}$ ,  $z = -0.5 \text{ m}$ ,
- Position source 2:  $x \approx -0.8 \text{ m}$ ,  $y \approx -10. \text{ m}$ ,  $z = -0.5 \text{ m}$

A constant discharge of  $1 \text{ m}^3 \cdot \text{s}^{-1}$  is imposed at both sources. The source 1 diffuses without any velocity in every direction , whereas source 2 has an initial velocity:  $U = 0.5 \text{ m.s}^{-1}$ ,  $V = 2 \text{ m.s}^{-1}$ . At source 1, the tracers 1 and 2 are discharged. At source 2, the tracers 2 and 3 are discharged with a concentration of  $10 \text{ kg.m}^{-3}$  (or  $\text{g.L}^{-1}$ ) for all tracers.

Note that the definition of the discharges and tracer concentrations at sources has been done in the SOURCES FILE. As this last file is present in the examples directory, the keyword VALUES OF THE TRACERS AT THE SOURCES is ignored but is given as an example coherent with what is done in the SOURCES FILE.

### 29.1.2 Mesh and numerical parameters

Figure 29.1 shows the horizontal mesh and sources positions. The mesh is composed of 674 triangular elements (373 nodes) with 5 planes regularly spaced on the vertical, to form prism elements.

The time step is 1.1 s for a simulated period of 1,100 s.

This case is computed with the hydrostatic pressure assumption. To solve the advection, the method of characteristics is used for the velocities (scheme 1, default until version 8.0) and the explicit finite volume Leo Postma scheme for tidal flats is used for the tracer (scheme 13).

## 29.2 Results

Figure 29.2 highlights the influence of the initial velocity of source 2 on the horizontal velocity field at mid depth at 550 s. Additionally, it shows tracer 2 spreads in every direction at source 1, unlike at source 2 where tracer 2 diffuses in the initial velocity direction.

The horizontal and vertical plumes of each tracer at 1,100 s, in Figures 29.3 and 29.4 respectively, allow verifying that the plume of tracer 2 is the combination of the plumes of tracer 1 and 3.

Moreover, the following mass balance of the TELEMAC-3D simulation shows that the amount of water injected by the sources is very good ( $2,200 \text{ m}^3 = 2 \text{ sources} \times 1 \text{ m}^3 \cdot \text{s}^{-1} \times 1,100 \text{ s}$  with an error lower than  $10^{-6} \text{ m}^3$ , thus a relative error lower than  $10^{-9}$ ). If the keywords for accuracy for propagation and diffusion of tracers are equal to  $10^{-14}$ , the error becomes lower than  $10^{-12} \text{ m}^3$ , thus a relative error lower than the machine accuracy  $10^{-15}$ .

The mass balance also shows the conservation and the amount of discharged tracer 1, 2 and 3 is good (e.g. for tracer 2:  $10 \text{ kg} \cdot \text{m}^{-3} \times 2 \text{ sources} \times 1,100 \text{ s} \times 1 \text{ m}^3 \cdot \text{s}^{-1} = 22,000 \text{ kg}$  with an error lower than  $10^{-5} \text{ kg}$ , so a relative error lower than  $10^{-9}$ ). To get an error lower than  $2.10^{-8} \text{ kg}$ , so a relative error lower than  $2.10^{-12}$ , an accuracy of  $10^{-14}$  is required for the diffusion of tracers and propagation. Otherwise, the mass balances may be worse but sufficient enough, depending on the accuracy the user wishes.

Balance for ACCURACY FOR PROPAGATION =  $10^{-8}$  and ACCURACY FOR DIFFUSION OF TRACERS =  $10^{-9}$  in serial:

FINAL MASS BALANCE		
T =	1100.0000	
 --- WATER ---		
INITIAL MASS	:	4000.000
FINAL MASS	:	6200.000
MASS LEAVING THE DOMAIN (OR SOURCE)	:	-2200.000
MASS LOSS	:	0.2391803E-06
 --- TRACER 1: TRACER 1 , UNIT : ?? * M3)		
INITIAL MASS	:	0.000000
FINAL MASS	:	11000.00
MASS EXITING (BOUNDARIES OR SOURCE)	:	-11000.00
MASS LOSS	:	0.5897147E-05
 --- TRACER 2: TRACER 2 , UNIT : ?? * M3)		

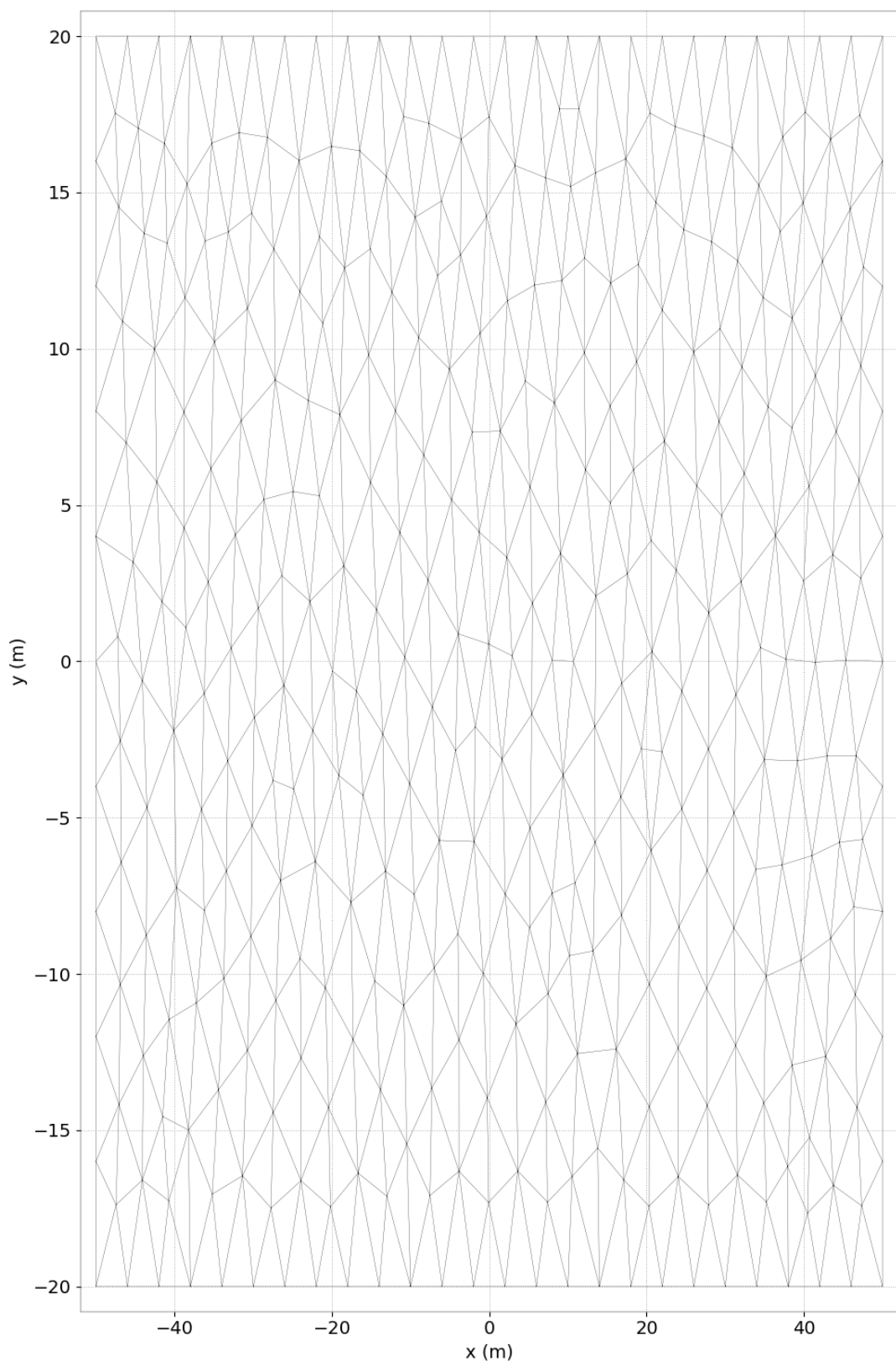


Figure 29.1: Horizontal mesh.

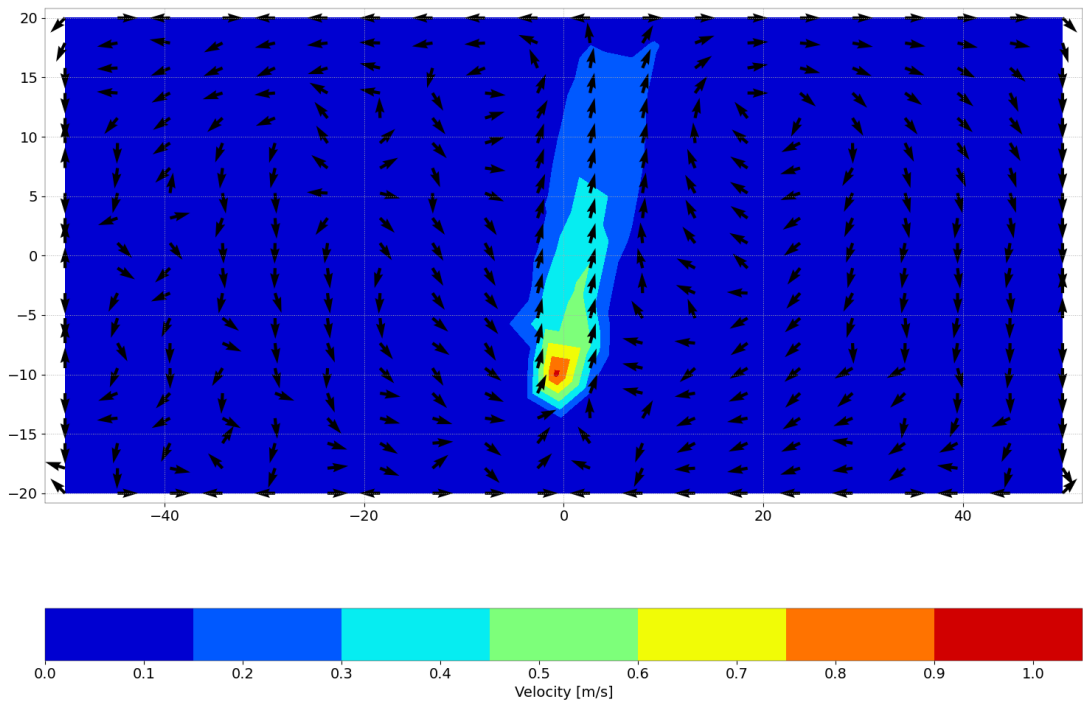


Figure 29.2: Horizontal velocity field at mid depth at 550 s.

```

INITIAL MASS : 0.000000
FINAL MASS : 22000.00
MASS EXITING (BOUNDARIES OR SOURCE) : -22000.00
MASS LOSS : 0.2584195E-05

--- TRACER 3: TRACER 3 , UNIT : ?? * M3)
INITIAL MASS : 0.000000
FINAL MASS : 11000.00
MASS EXITING (BOUNDARIES OR SOURCE) : -11000.00
MASS LOSS : -0.3261903E-05

```

Balance for ACCURACY FOR PROPAGATION =  $10^{-8}$  and ACCURACY FOR DIFFUSION OF TRACERS =  $10^{-9}$  in parallel (4 processors):

```

FINAL MASS BALANCE
T = 1100.0000

--- WATER ---
INITIAL MASS : 4000.000
FINAL MASS : 6200.000
MASS LEAVING THE DOMAIN (OR SOURCE) : -2200.000
MASS LOSS : 0.2391880E-06

--- TRACER 1: TRACER 1 , UNIT : ?? * M3)
INITIAL MASS : 0.000000
FINAL MASS : 11000.00
MASS EXITING (BOUNDARIES OR SOURCE) : -11000.00
MASS LOSS : 0.5897129E-05

```

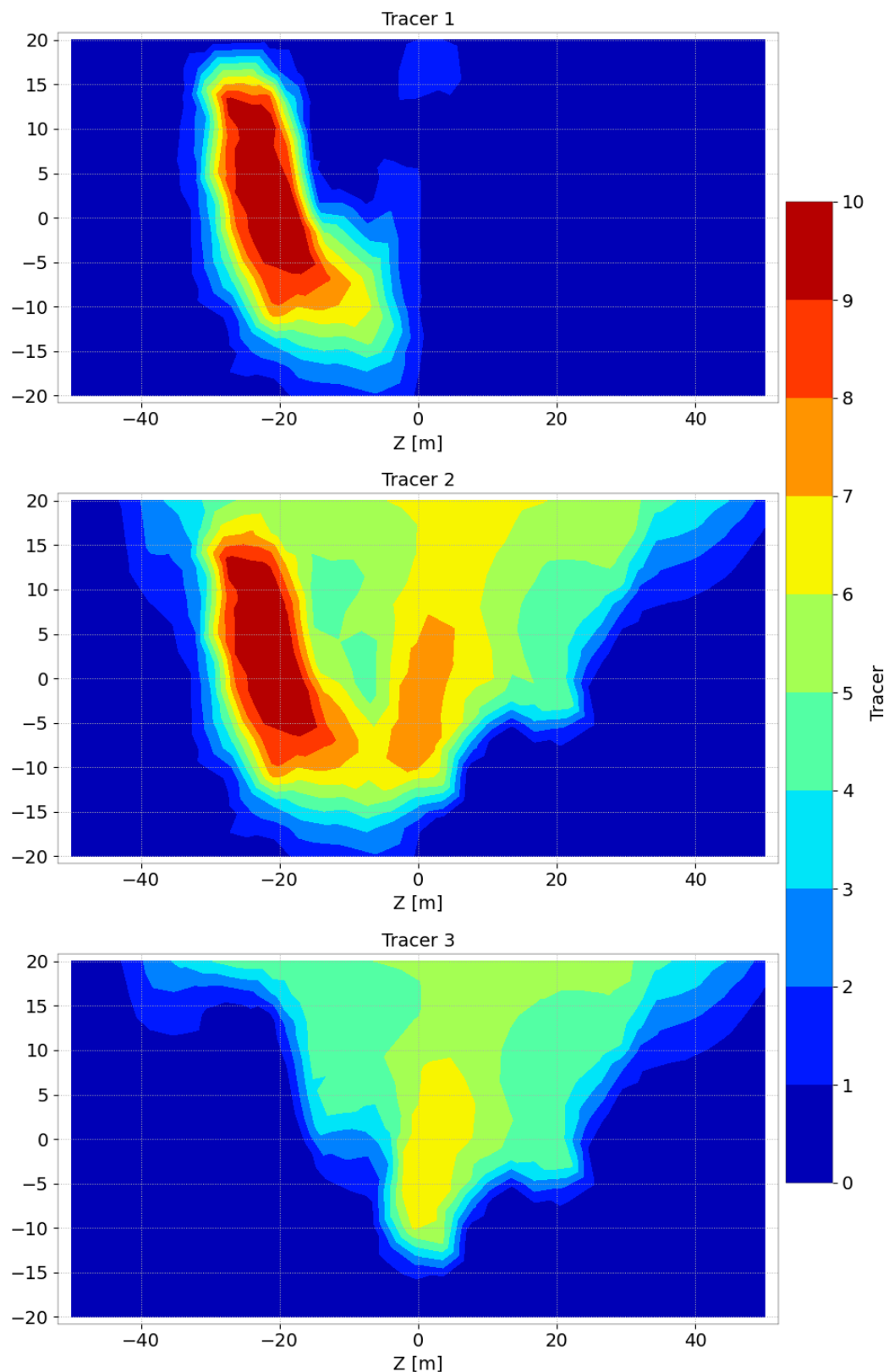


Figure 29.3: Horizontal shape of the plumes for each tracers.

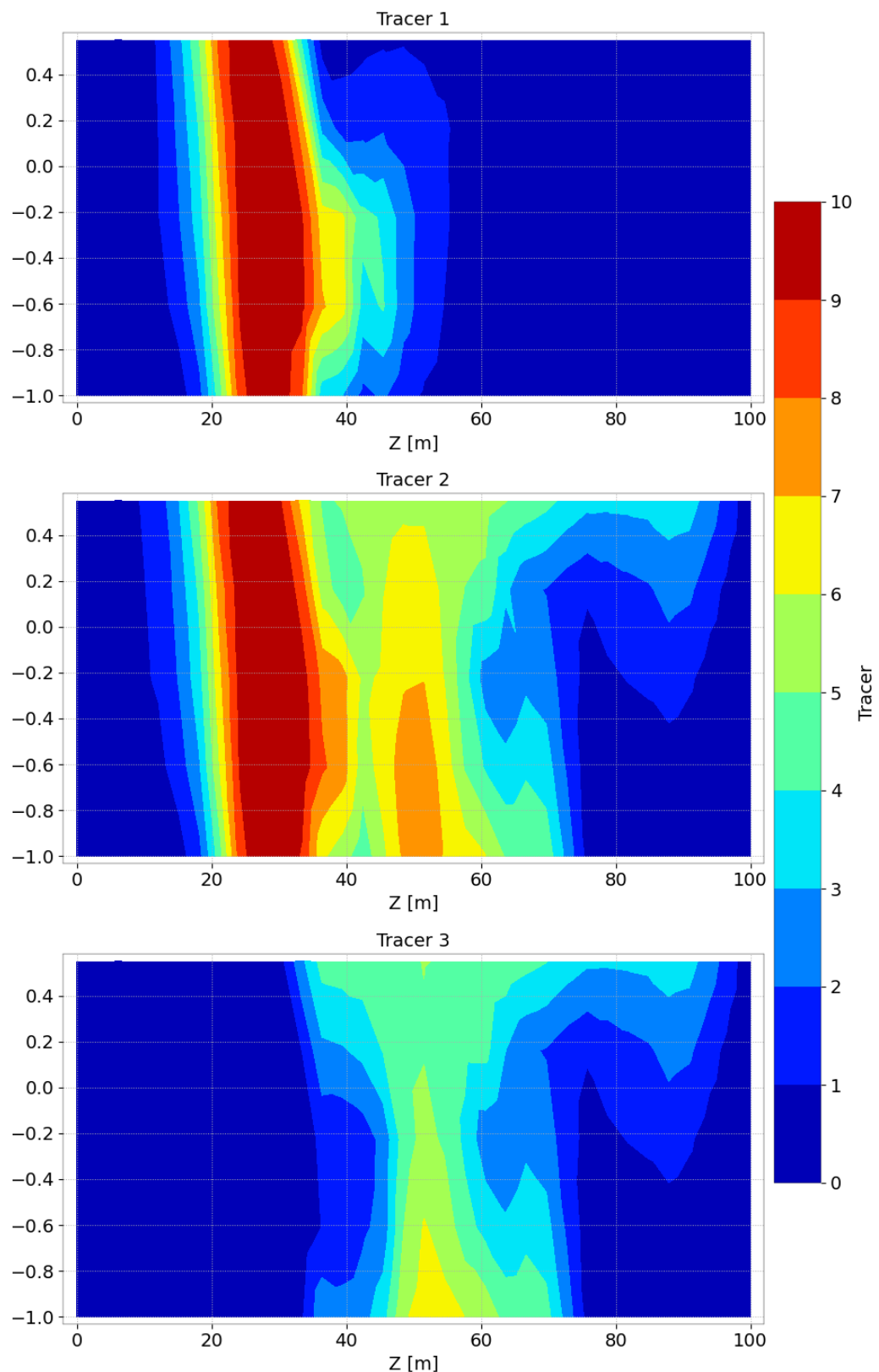


Figure 29.4: Vertical shape of the plumes for each tracers.

```

--- TRACER 2: TRACER 2      , UNIT : ??          * M3)
INITIAL MASS                 : 0.000000
FINAL MASS                   : 22000.00
MASS EXITING (BOUNDARIES OR SOURCE) : -22000.00
MASS LOSS                     : 0.2584253E-05

--- TRACER 3: TRACER 3      , UNIT : ??          * M3)
INITIAL MASS                 : 0.000000
FINAL MASS                   : 11000.00
MASS EXITING (BOUNDARIES OR SOURCE) : -11000.00
MASS LOSS                     : -0.3261830E-05

```

Balance for ACCURACY FOR PROPAGATION =  $10^{-14}$  and ACCURACY FOR DIFFUSION OF TRACERS =  $10^{-14}$  in serial:

```

FINAL MASS BALANCE
T =           1100.0000

--- WATER ---
INITIAL MASS                 : 4000.000
FINAL MASS                   : 6200.000
MASS LEAVING THE DOMAIN (OR SOURCE) : -2200.000
MASS LOSS                     : 0.4547474E-12

--- TRACER 1: TRACER 1      , UNIT : ??          * M3)
INITIAL MASS                 : 0.000000
FINAL MASS                   : 11000.00
MASS EXITING (BOUNDARIES OR SOURCE) : -11000.00
MASS LOSS                     : -0.1768058E-07

--- TRACER 2: TRACER 2      , UNIT : ??          * M3)
INITIAL MASS                 : 0.000000
FINAL MASS                   : 22000.00
MASS EXITING (BOUNDARIES OR SOURCE) : -22000.00
MASS LOSS                     : -0.1020817E-07

--- TRACER 3: TRACER 3      , UNIT : ??          * M3)
INITIAL MASS                 : 0.000000
FINAL MASS                   : 11000.00
MASS EXITING (BOUNDARIES OR SOURCE) : -11000.00
MASS LOSS                     : 0.7525159E-08

```

To conclude, TELEMAC-3D is able to compute the evolution and the conservation of tracers discharged by sources.

## 30. Wind forced channel flow (stratif\_wind)

### 30.1 Purpose

This test case belongs to a benchmark of CFD codes with analytical solutions. Its aim was to study the behavior of different codes, focusing on situations where the density variations have a crucial influence on the hydrodynamical process. This study was carried out during Lamia Abbas's post-doctoral [10] in 2014-2015.

This test case demonstrates the ability of TELEMAC-3D to simulate the response of a density-stratified water to wind stress. It is inspired by [6] and [12]. It models the wind blowing on a stratified lake. The wind generates the deflection of the thermocline and 2 recirculations. The example only shows the results for one specific 2D mesh and one distribution of planes over the vertical.

### 30.2 Description

A 10 m long and 2 m wide channel with flat bottom (elevation  $z = 0$  m) is considered.

The tracer used is temperature. The density is considered as a function of the water temperature:

$$\rho(T) = \rho_0 (1 - \alpha(T - T_0)^2), \quad (30.1)$$

where  $\rho_0 = 999.972 \text{ kg.m}^{-3}$ ,  $T_0 = 4^\circ\text{C}$  and  $\alpha = 7.10^{-6}$ .

There are two layers of water with different temperatures. As the density depends on water temperature, the initial state is chosen nearly stable *i.e.* the heavier fluid is below the lighter as shown in Figure 30.3.

### 30.3 Computational options

#### 30.3.1 Mesh

The triangular mesh is made of 4,548 triangular elements (element size  $\approx 0.1$  m) and 2,409 nodes (see Figure 30.1).

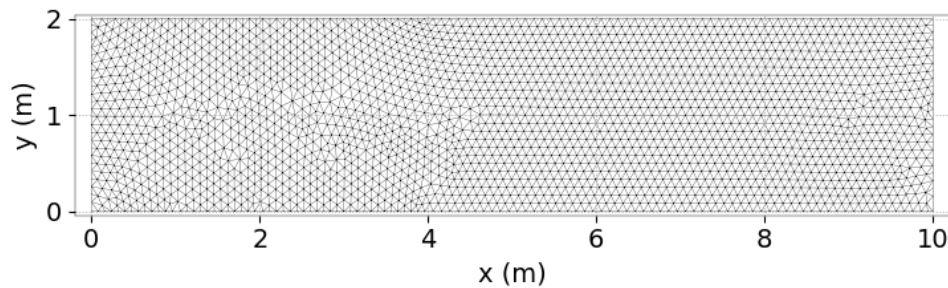


Figure 30.1: Horizontal mesh.

To build the 3D mesh of prisms, 40 planes are regularly spaced over the vertical (classical  $\sigma$  transformation). The vertical mesh between nodes of coordinates  $(0 ; 1)$  to  $(10 ; 1)$  can be seen in Figure 30.2.

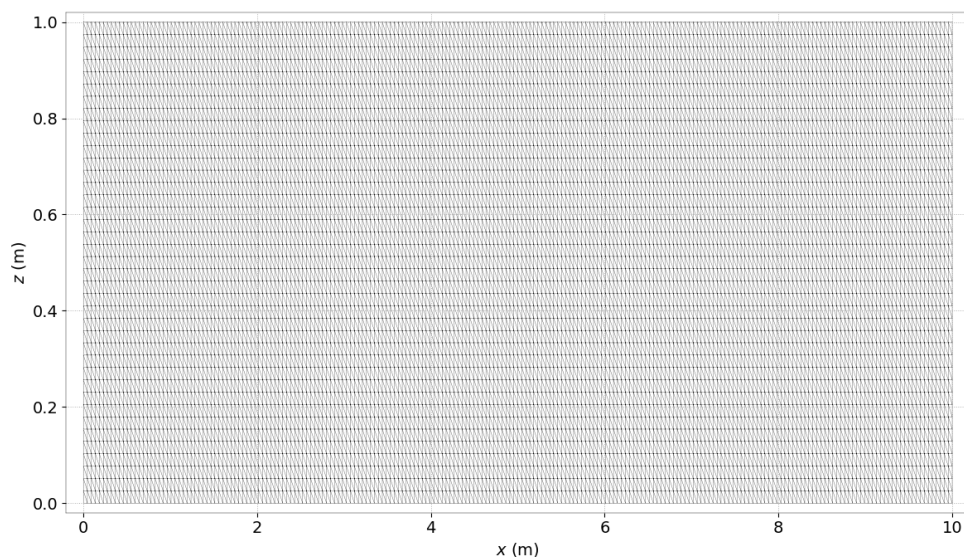


Figure 30.2: Vertical mesh.

During Lamia Abbas's post-doctoral, one finer 2D grid was also used ( $dl \approx 0.05$  m) with 18,922 triangular elements and 9,721 nodes.

Moreover, 2 different vertical distributions were tested:

- one coarser vertical distribution with 20 horizontal planes leading to  $\approx 0.05$  m vertical height,
- one finer vertical distribution with 80 horizontal planes leading to  $\approx 0.0125$  m vertical height.

### 30.3.2 Physical parameters

The turbulent viscosities for both velocities and tracers are constant, also both for horizontal and vertical directions.  $v_z = 0.01$  m<sup>2</sup>/s but no diffusion for velocity along horizontal directions.  $v_T = 0$  for both horizontal and vertical directions.

A constant wind blows with a wind magnitude = 10 m/s along  $x$  with COEFFICIENT OF WIND INFLUENCE =  $1.25 \cdot 10^{-6}$ . THRESHOLD DEPTH FOR WIND = 0.1 m as the vertical planes are close just below the free surface.

### 30.3.3 Initial and Boundary Conditions

The initial free surface elevation is 1 m with a fluid at rest. The initial temperature depends on elevation, defined by:

$$T_0(x, y, z) = \begin{cases} 25^\circ\text{C} & \text{if } z \geq 0.5 \text{ m}, \\ 8^\circ\text{C} & \text{else} \end{cases} \quad (30.2)$$

see Figure 30.3.

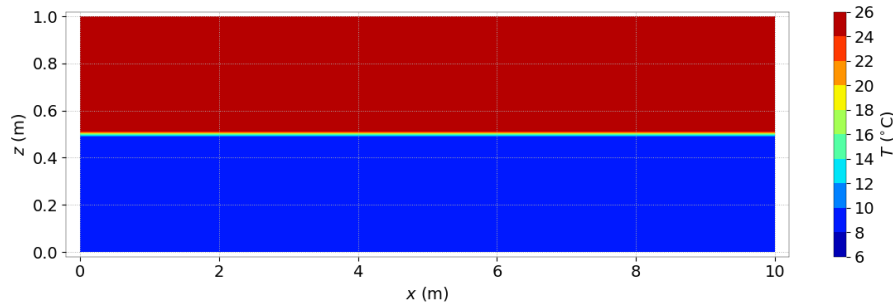


Figure 30.3: Initial condition for temperature.

There are only closed lateral boundaries with free slip condition and no friction at the bottom.

### 30.3.4 General parameters

The time step is 0.25 s for a simulated period of 1,200 s.

### 30.3.5 Numerical parameters

The non-hydrostatic version of TELEMAC-3D is used. To solve the advection steps, the method of characteristics is chosen for the velocities and the PSI-type MURD scheme for the temperature. Other advection schemes give similar results with TELEMAC-3D.

## 30.4 Expected results

Audusse and al. [6] derive an analytical solution at the stationary regime under the following hypotheses:

- Hydrostatic pressure assumption,
- Stationary equilibrium state,
- $v_T = 0, v_H = 0, v_z \neq 0$ ,
- Near the mid-length of the basin it is assumed:

$$\frac{\partial u}{\partial x} = 0, \quad \frac{\partial^2 u}{\partial x^2} = 0 \quad \text{and} \quad w = 0. \quad (30.3)$$

Under these hypotheses, two recirculations with counter directions will appear, see Figure 30.4.

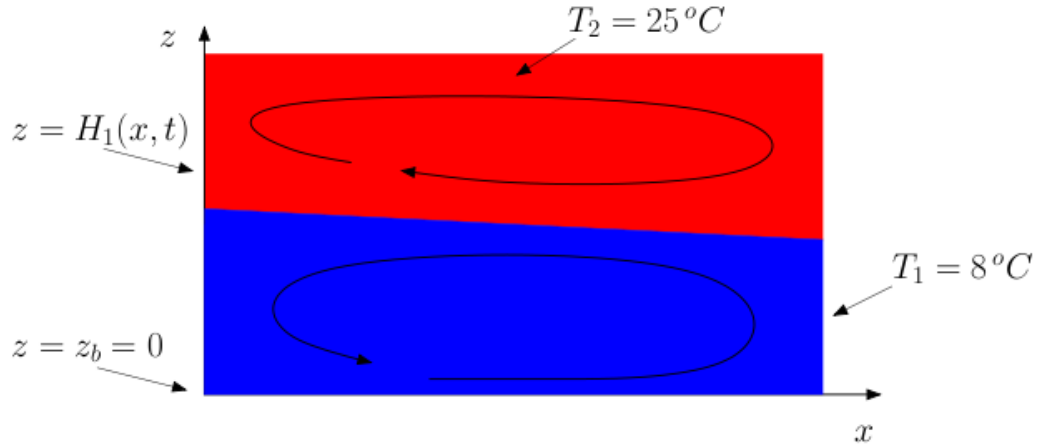


Figure 30.4: A schematical description of the solution (source [10]).

Moreover, the case where the initial location of the thermocline is  $H_1 = H/2$ . Then, the velocities at the mid-length are:

$$U_1(z) = \frac{H_1^2 - 3z^2}{12\mu_1 H} \tau_s, \quad (30.4)$$

$$U_2(z) = \frac{15z^2 + 36H_1z + 19H_1^2}{12\mu_2 H} \tau_s, \quad (30.5)$$

and the deflection of the thermocline is:

$$\frac{\partial H_1}{\partial x} = \frac{\tau_s}{H(\rho_1 - \rho_2)}. \quad (30.6)$$

## 30.5 Results

Figure 30.5 shows the final temperature distribution (after 1,200 s) and the thermocline deflection. As expected, the thermocline slope has the good sign, but due to the big diffusion, it is difficult to compute it with accuracy.

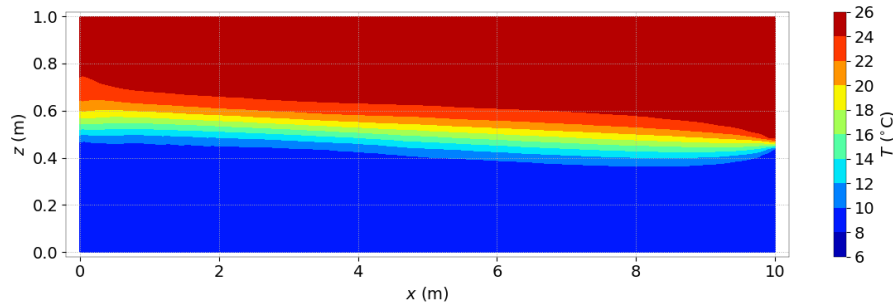


Figure 30.5: Temperature distribution after 1,200 s.

Figure 30.6 shows the final velocity vectors (after 1,200 s) and the opposite circulations in the upper and the lower layers.

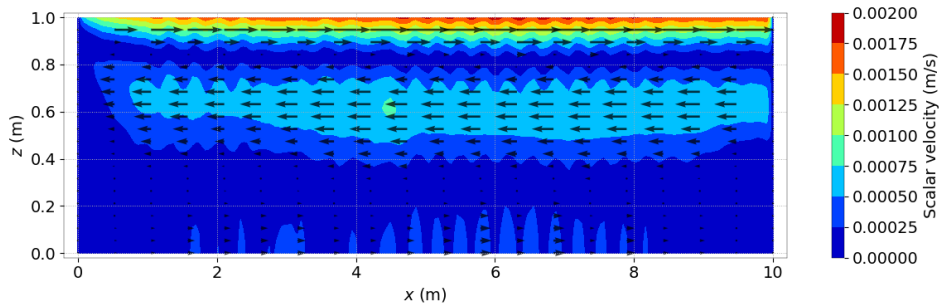


Figure 30.6: Velocity field and vectors after 1,200 s.

See [10] for more informations, in particular the results for different meshes and the comparison between the analytical and computed velocities.

## 30.6 Conclusion

TELEMAC-3D is able to simulate the response of a density-stratified water to wind stress.

# 31. Stability of a stratified flow (stratification)

## 31.1 Description

This test is a flat channel with saline stratification. It demonstrates the ability of TELEMAC-3D to model stratified flow with a special focus on the stability of the stratification. This case also demonstrates the capacity of the  $k$ - $\varepsilon$  model to reproduce turbulent phenomena.

The domain is a rectangular channel with 2,000 m long and 100 m wide (see Figure 31.1). The bottom of this channel has a mild slope (0 m at the entrance, -0.019 m at the output). The general water depth is 10 m and the constant velocity along the channel is imposed. Salinity (or tracer) is prescribed as shown in Figure 31.2. Density law depends then on salinity ( $S_{al}$ ):

$$\rho = \rho_{ref}(1 + 750 \cdot 10^{-6} \cdot S_{al}), \text{ with } \rho_{ref} = 999.972 \text{ kg.m}^{-3}$$

Note that the turbulent viscosity is constant in horizontal direction and equal to  $0.1 \text{ m}^2.\text{s}^{-1}$ . The  $k$ - $\varepsilon$  model is only used in the vertical direction.

### 31.1.1 Initial and Boundary Conditions

The initial water depth is 10 m with a constant longitudinal velocity equal to  $1 \text{ m.s}^{-1}$ . The tracer (or salinity) is equal to  $38 \text{ kg.m}^{-3}$  ( $\text{g.L}^{-1}$ ) at the bottom below the plane number 18 (i.e. at 2.5 m of the water surface) and  $28 \text{ kg.m}^{-3}$  at the top above the plane number 18 (Figure 31.2). Note that the tracer and velocity field are directly initialised in the new (since V7P3) **CONDI3DUVV** and **CONDI3DTRAC** subroutines.

The boundary conditions are:

- For the solid lateral walls, a slip condition on the channel banks is used for the velocity,
- On the bottom, Strickler law with friction coefficient equal to  $70 \text{ m}^{1/3}.\text{s}^{-1}$  is imposed,
- Upstream, a flow rate equal to  $1,000 \text{ m}^3.\text{s}^{-1}$  is imposed and a tracer equal to the initial repartition,
- Downstream, the water depth is imposed at 9.981054 m.

Note that the tracer and velocity field are directly prescribed on the liquid boundaries in the new (since V7P3) **USER\_BORD3D** subroutine.

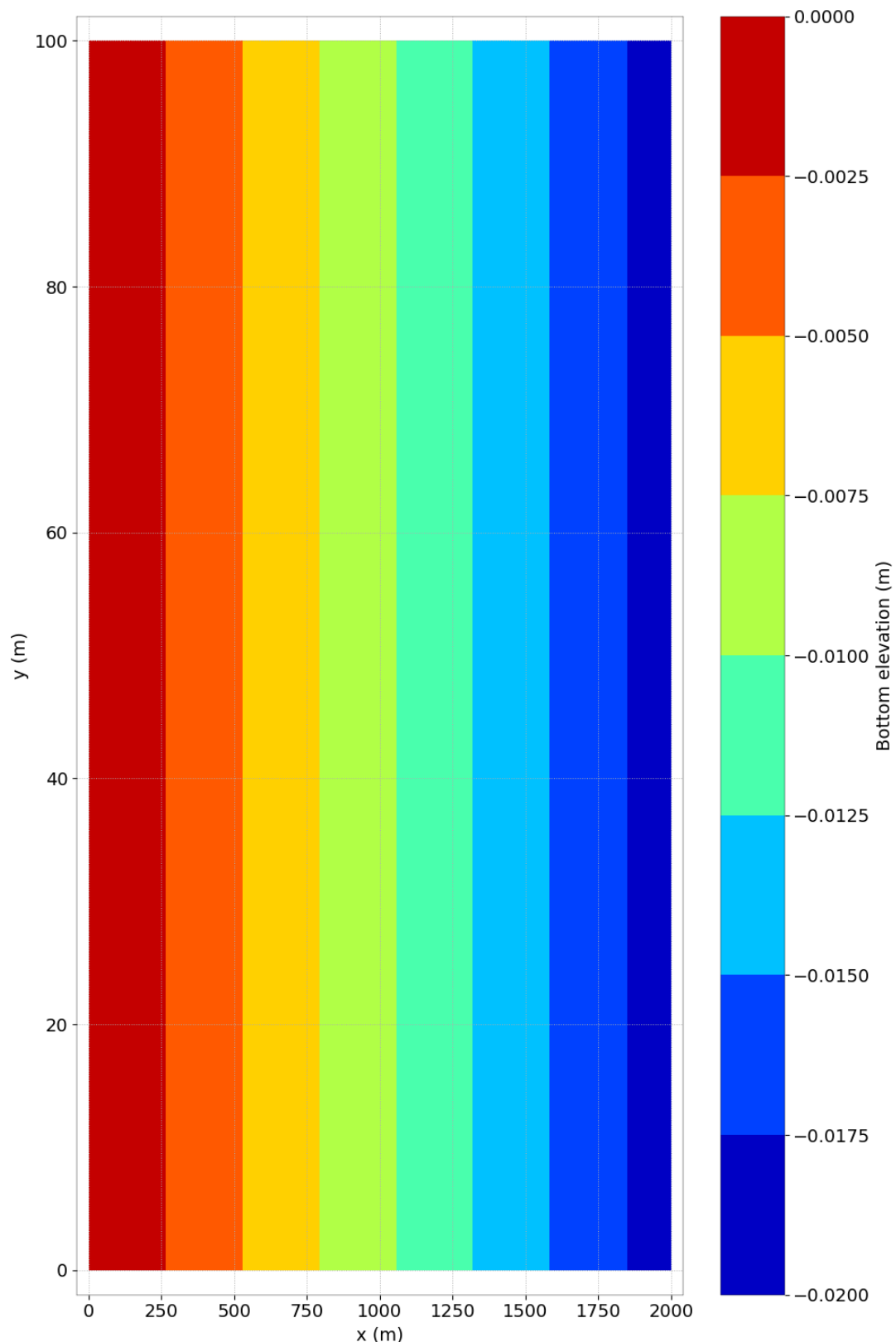


Figure 31.1: Bottom topography.

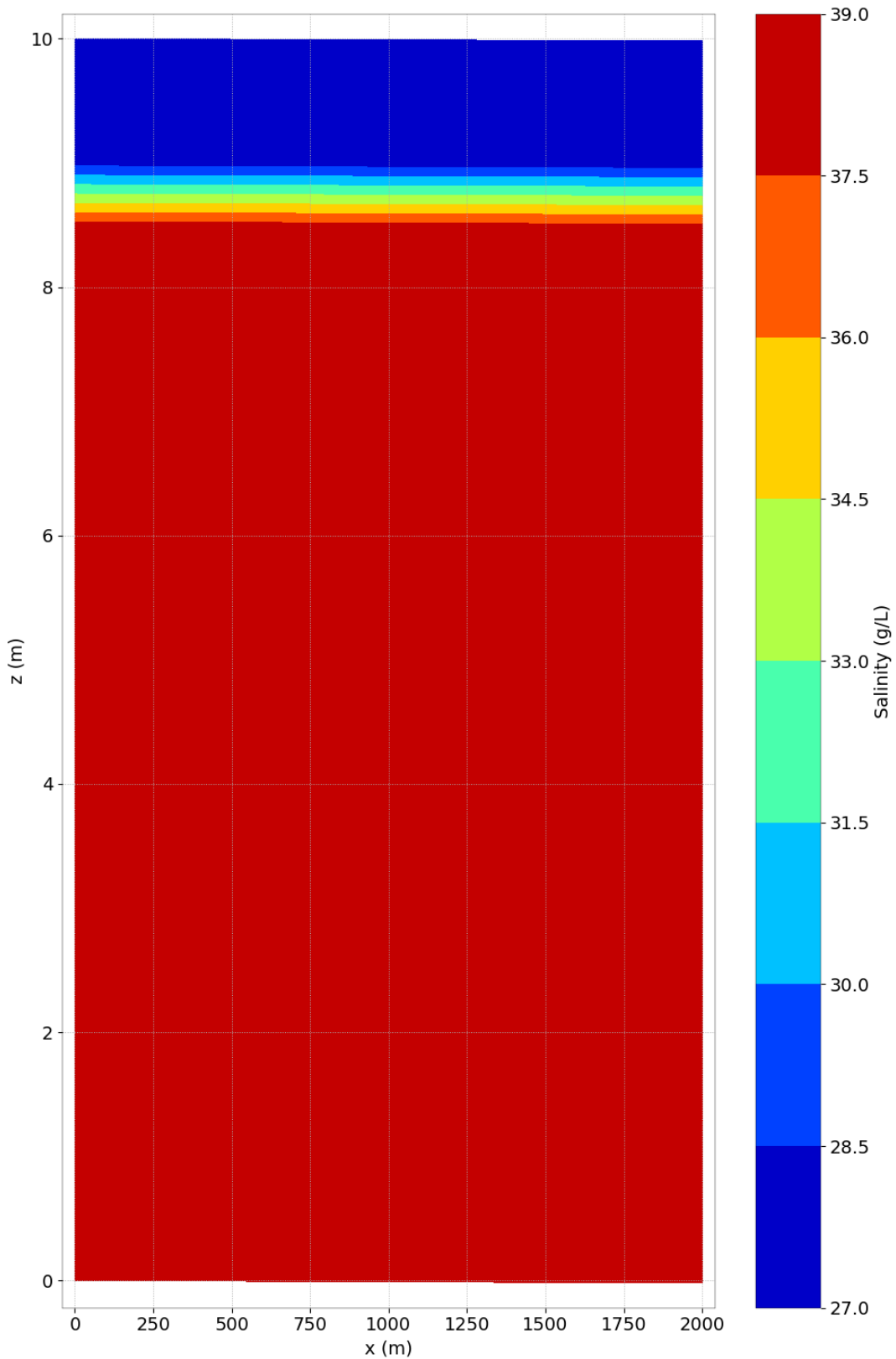


Figure 31.2: Initial salinity along the channel.

### 31.1.2 Mesh and numerical parameters

The mesh (Figure 31.3 and 31.4) is composed of 2,204 triangular elements (1,188 nodes) with 21 planes regularly spaced on the vertical, to form prism elements.

The time step is 2 s for a simulated period of 2,000 s.

This case is computed with the hydrostatic pressure hypothesis. To solve advection, the N-type MURD scheme (scheme 4) is used for the velocities,  $k$ - $\varepsilon$  model and the tracer (or salinity). The implicitation coefficients for depth and velocities are equal to 1.

## 31.2 Results

As expected, the vertical gradient of salinity remains well stable, see Figures 31.2 and 31.5.

In Figure 31.6, we can observe the turbulence phenomenon modelled by the  $k$ - $\varepsilon$  model. This turbulence is created at the bottom and is developing on the vertical column of water. However, the turbulence is clearly blocked by the saline stratification (see Figure 31.7).

To conclude, TELEMAC-3D is able to represent correctly stratified flows. In addition, the  $k$ - $\varepsilon$  model is able to simulate turbulence generated by bottom friction.

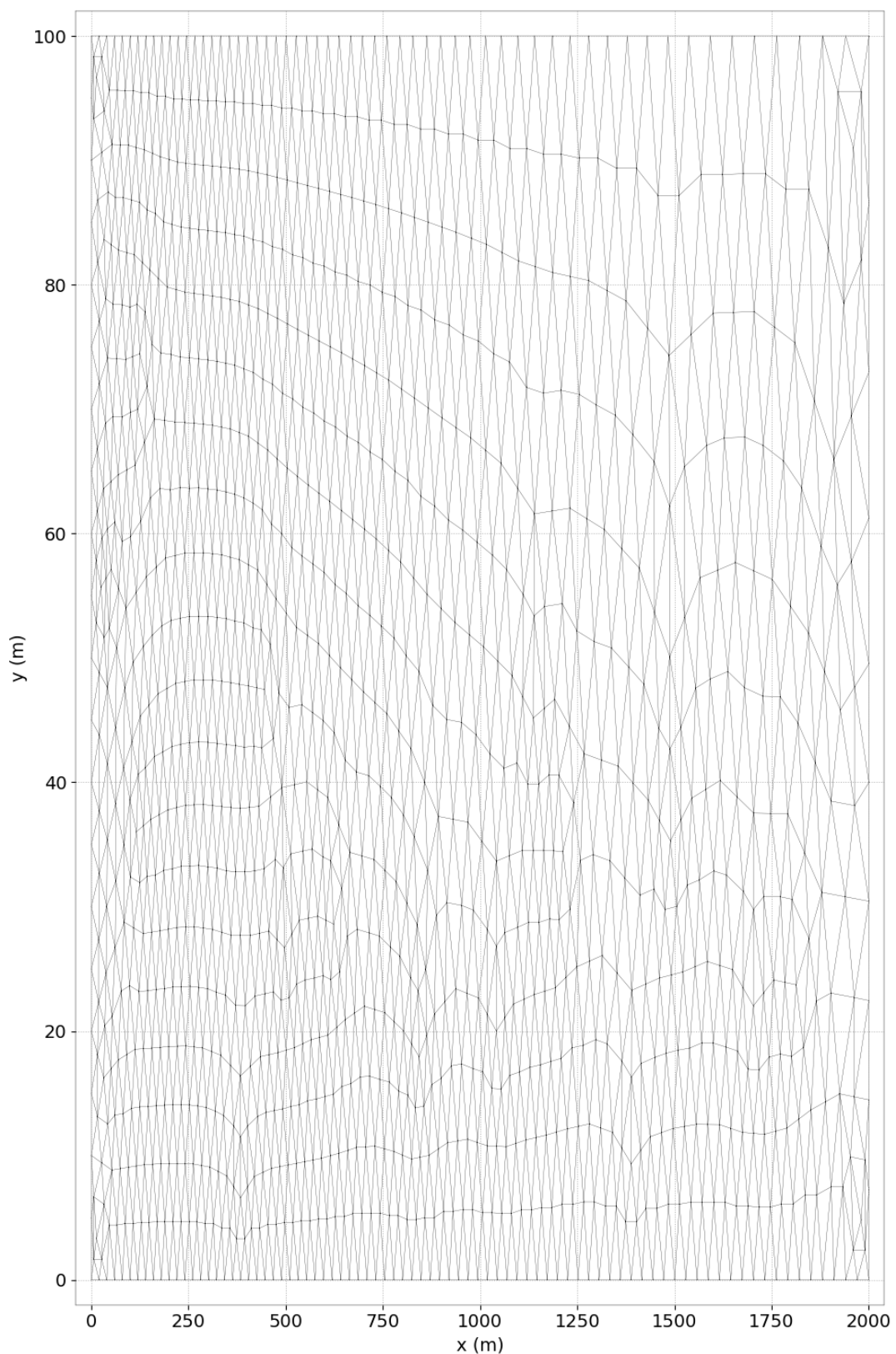


Figure 31.3: Horizontal mesh.

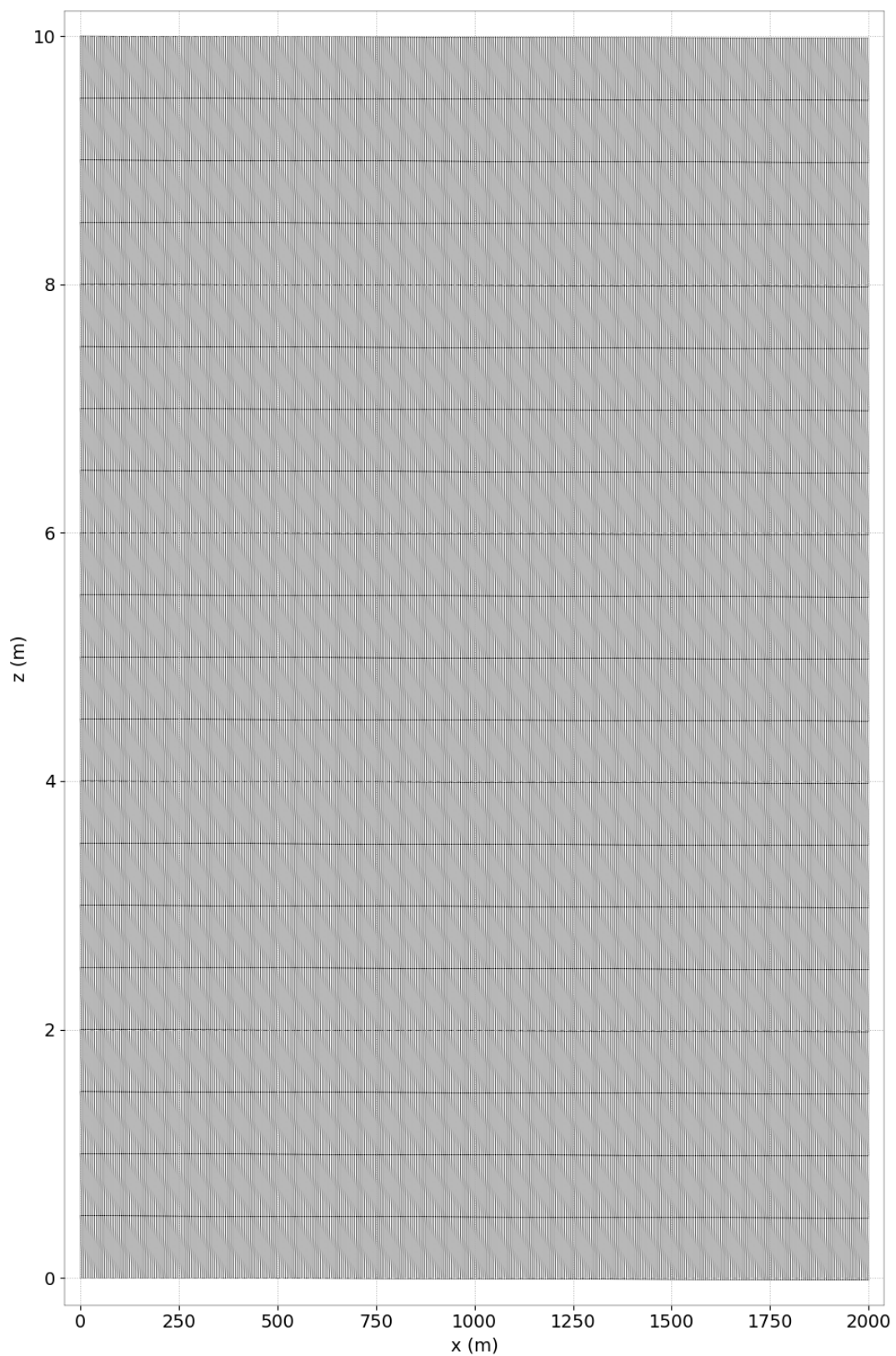


Figure 31.4: Vertical mesh.

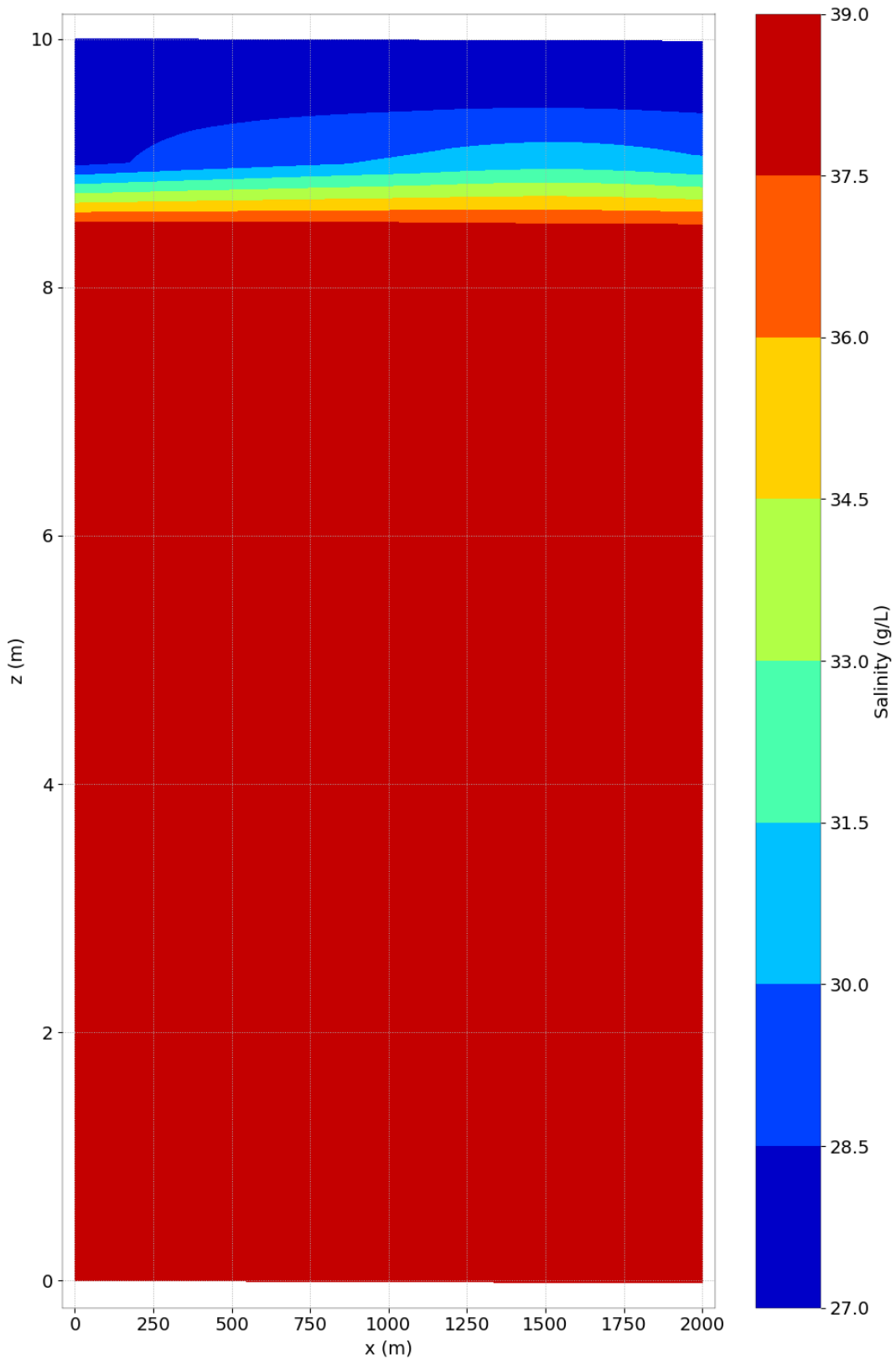


Figure 31.5: Final salinity along the channel at 2,000 s.

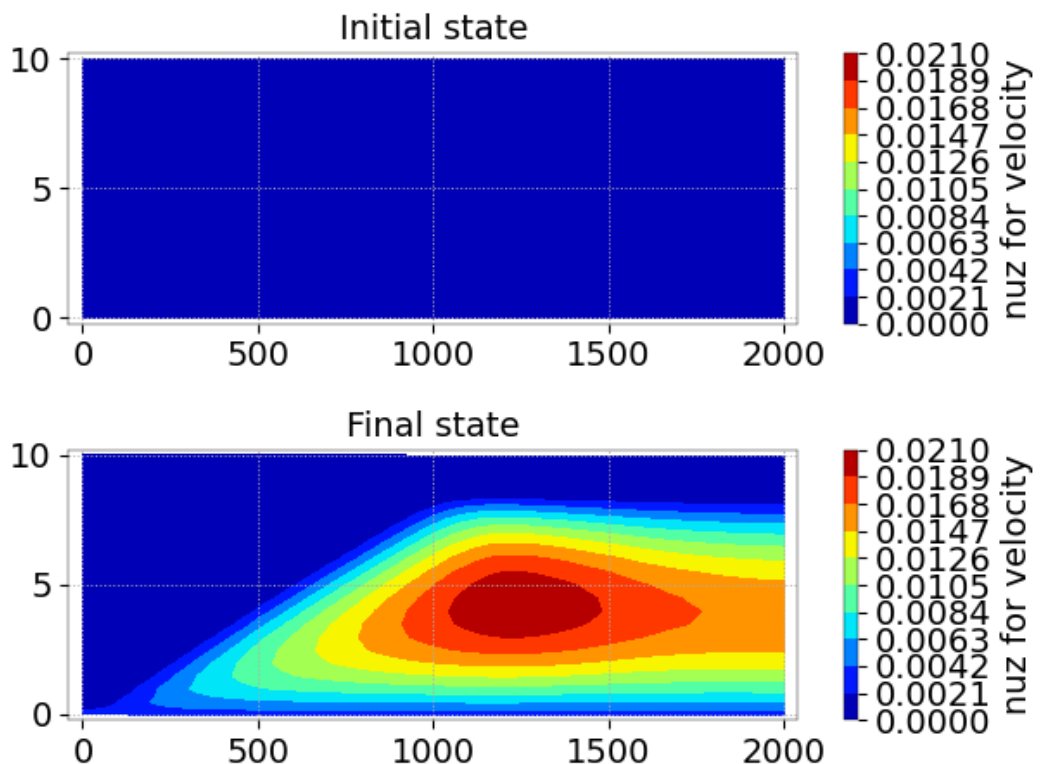


Figure 31.6: Evolution of turbulence on the vertical along the channel.

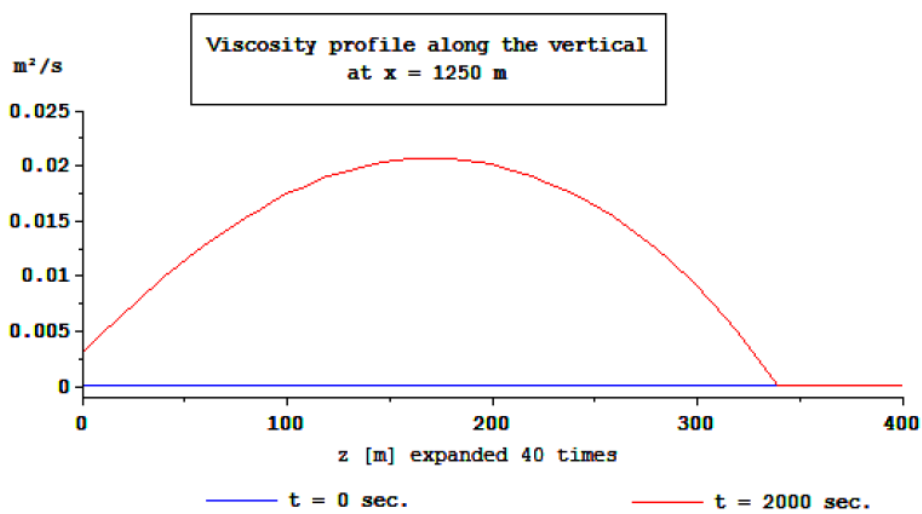


Figure 31.7: Viscosity profile along the vertical at 1,250 m.

## 32. Discretisation with tetrahedra elements (tetra)

### 32.1 Purpose

This test demonstrates the ability of TELEMAC-3D to be discretised with prisms split into tetrahedra.

### 32.2 Description

The configuration is a frictionless channel presenting an idealised bump on the bottom. The channel is horizontal with a 4 m long bump in its middle. The maximum elevation of the bump is 20 cm. The flow regime is sub-critical. It is the same geometry as the TELEMAC-2D test case “bumflu”.

The tracer used is salinity (considered as active with the 2nd density law).

The bottom elevation is defined by (see Figure 32.1):

$$\begin{cases} \text{if } x \geq 2.5, & z = \max(-0.0246875(x-10)^2, -0.3) \\ \text{if } x < 2.5, & z = \max(-0.2 - 0.3(\frac{x}{2.5})^2, -0.3) \end{cases}$$

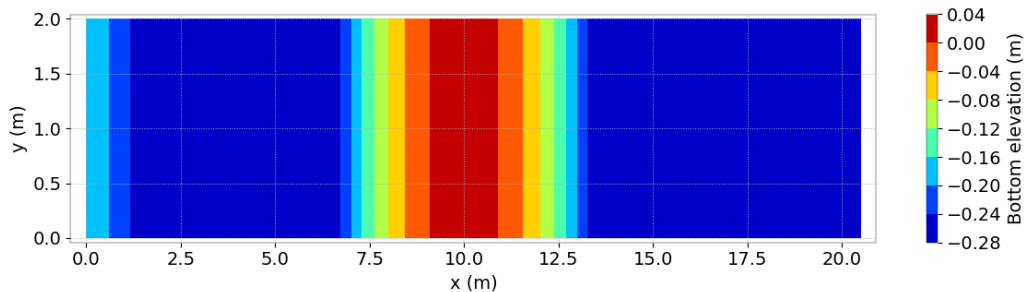


Figure 32.1: Bottom elevation.

#### 32.2.1 Initial and Boundary Conditions

The computation is initialised with a constant elevation equal to 1.8 m and no velocity. The initial value of salinity is 30 g/L everywhere.

The boundary conditions are:

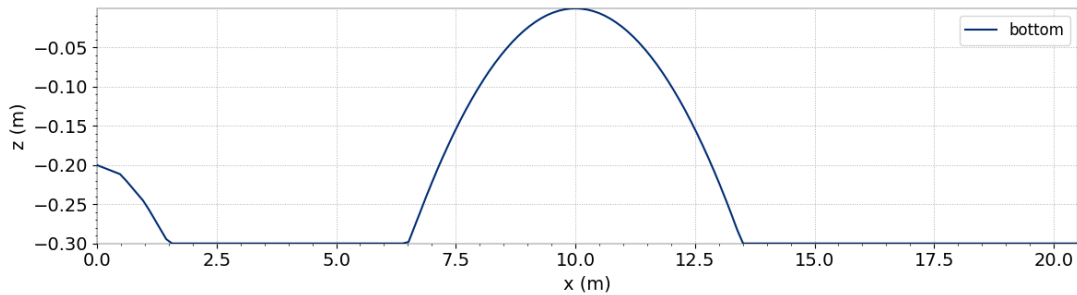


Figure 32.2: Bump profile.

- For the solid walls, a slip condition on channel banks is used for the velocities,
- On the bottom, a Strickler law with friction coefficient equal to  $30 \text{ m}^{1/3}/\text{s}$  is prescribed,
- Upstream a flowrate and salinity are prescribed. Flowrate is equal to  $4 \text{ m}^3/\text{s}$ , linearly increasing from 0 to  $4 \text{ m}^3/\text{s}$  during the first 10 s. Imposed salinity is equal to  $40 \text{ g/L}$  if  $z \leq -0.2 \text{ m}$  or  $30 \text{ g/L}$  if  $z > -0.2 \text{ m}$ ,
- Downstream the water level is equal to 1.8 m (= initial elevation), so that the water depth is 2 m.

### 32.2.2 Mesh and numerical parameters

The 2D mesh (Figure 32.3) is made of 2,620 triangular elements (1,452 nodes).

10 planes are regularly spaced in the vertical direction except one fixed plane with the elevation -0.2 m (plane number 4), see Figure 32.4.

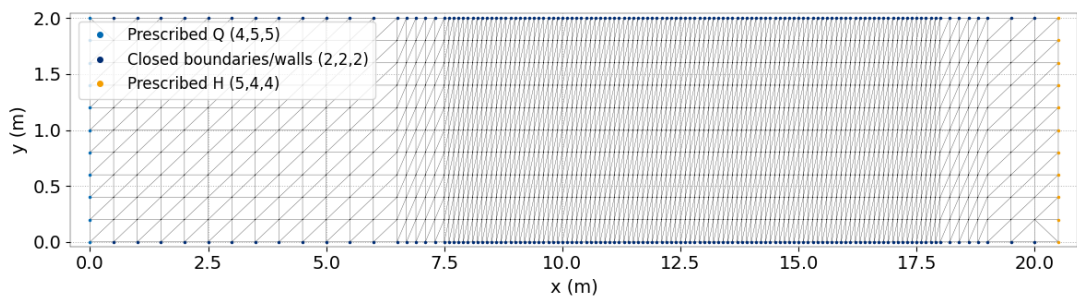


Figure 32.3: Horizontal mesh.

Tetrahedra elements (split prisms) are chosen for discretisation.

The non-hydrostatic version of TELEMAC-3D is used.

To solve the advection, the edge by edge explicit finite volume Leo Postma (scheme #13) is used for every variable (velocities, salinity,  $k$  and  $\varepsilon$ ).

The time step is 0.04 s for a simulated period of 40 s.

### 32.2.3 Physical parameters

Turbulence is modelled with the  $k - \varepsilon$  model of TELEMAC-3D.

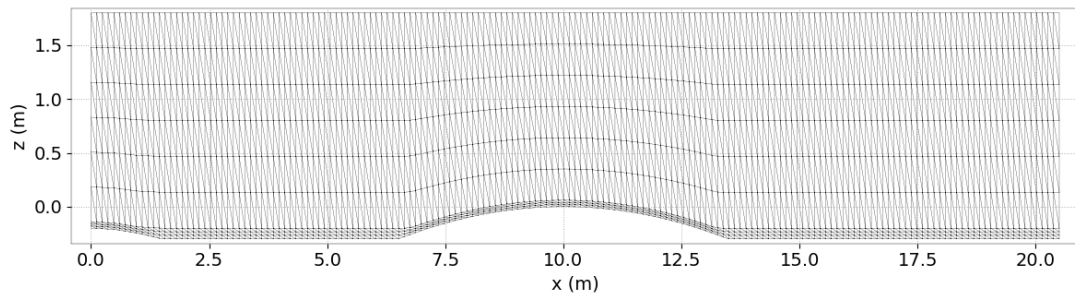


Figure 32.4: Initial vertical mesh along  $y = 1$  m.

### 32.3 Results

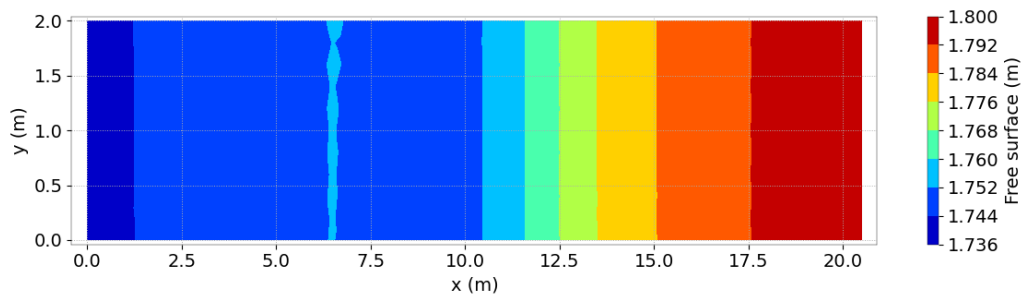


Figure 32.5: Free surface at final time step.

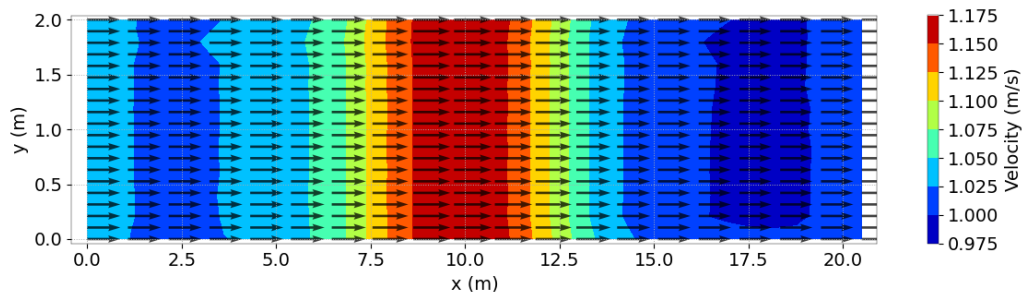


Figure 32.6: Velocity magnitude at the surface at final time step.

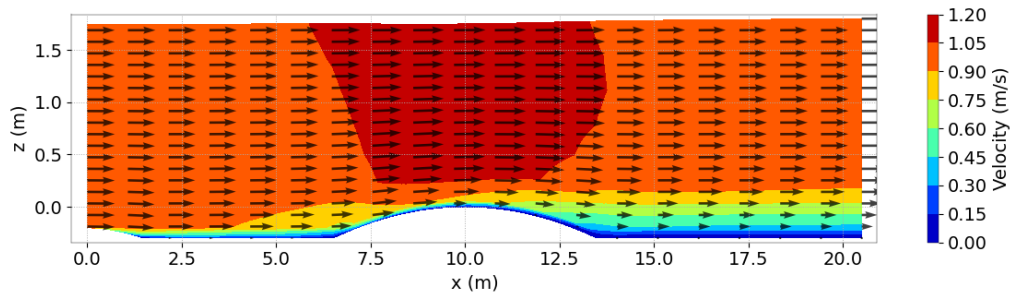


Figure 32.7: Vertical distribution of velocity magnitude at the surface at final time step.

**32.4 Conclusion**

TELEMAC-3D is able to be discretised with prisms split into tetrahedra.

## 33. tidal\_flats

This test case validates the modelling of cohesive sediments with TELEMAC-3D solved with a vertical implicit-advection scheme (tridiagonal matrix solver) for diffusion and settling velocity (ADVECTION-DIFFUSION SCHEME WITH SETTLING VELOCITY = 1). In particular, this example deals with sediment transport processes with wetting and drying zones.

Even though this model setup is still valid, new features and bug fixes are now available for the new sediment transport and bed evolution module GAIA of the TELEMAC-MASCARET SYSTEM. Therefore, for newer model implementations, we strongly suggest to use TELEMAC-3D coupled with GAIA for sediment transport and bed evolution processes in 3D.

GAIA test cases “hippodrome-t3d“, “rouse-t3d“, “tidal\_flats-t3d“ and “turbidity-t3d“ provide examples of coupling TELEMAC-3D coupled with GAIA to account for cohesive sediment transport processes.

## 34. Propagation of tide prescribed by boundary conditions (tide)

### 34.1 Purpose

This test demonstrates the availability of TELEMAC-3D to model the propagation of tide in a maritime domain by computing tidal boundary conditions. A coastal area located in the English Channel off the coast of Brittany (in France) close to the real location of the Paimpol-Bréhat tidal farm is modelled to simulate the tide and the tidal currents over this area. Time and space varying boundary conditions are prescribed over liquid boundaries.

### 34.2 Description

#### 34.2.1 Geometry and Mesh

The geometry of the domain is almost a rectangle with the French coasts on one side (22 km  $\times$  24 km). The triangular mesh is composed of 4,385 triangular elements and 2,386 nodes (see Figure 34.1).

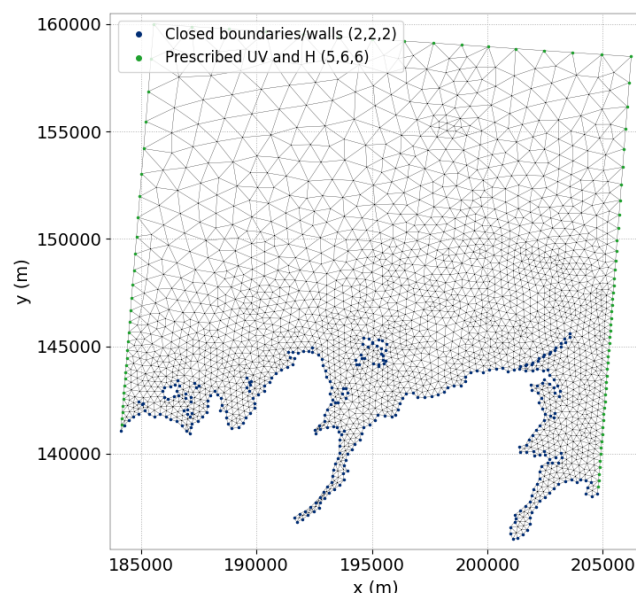


Figure 34.1: Horizontal mesh.

To build the 3D mesh of prisms, 11 planes are regularly spaced over the vertical. A slice of 3D mesh between nodes of coordinates (185,500 ; 150,000) to (200,500 ; 150,000) can be seen in Figure 34.2.

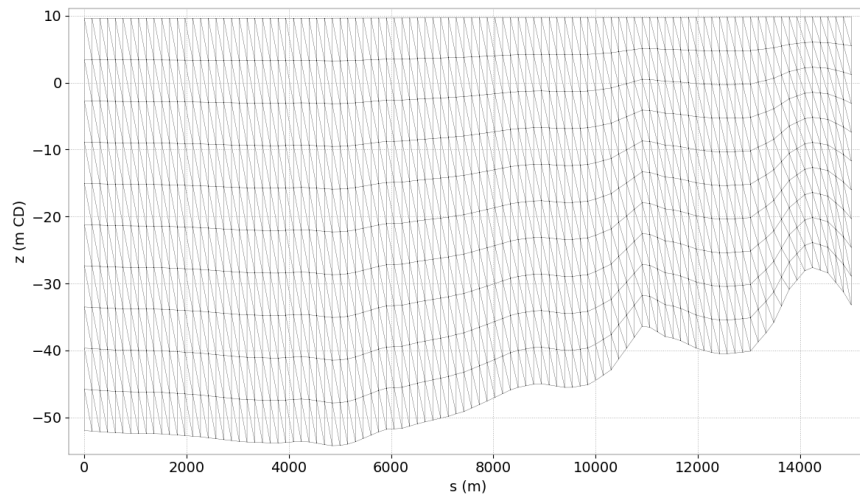


Figure 34.2: Slice of 3D mesh.

### 34.2.2 Bathymetry

A real bathymetry of the area bought from the SHOM (French Navy Hydrographic and Oceanographic Service) is used. ©Copyright 2007 SHOM. Produced with the permission of SHOM. Contract number 67/2007

### 34.2.3 Initial conditions

Initial conditions are defined by a constant elevation and no velocity.

### 34.2.4 Boundary conditions

Several databases of harmonic constants are interfaced with TELEMAC-3D:

- The JMJ database resulting from the LNH Atlantic coast TELEMAC model by Jean-Marc JANIN,
- The global TPXO database and its regional and local variants from the Oregon State University (OSU),
- The regional North-East Atlantic atlas (NEA) and the global atlas FES (e.g. FES2004 or FES2012...) coming from the works of Laboratoire d'Etudes en Géophysique et Océanographie Spatiales (LEGOS),
- The PREVIMER atlases.

In the tide test case, only the JMJ database is used as example. The user can read the TELEMAC-2D validation document and the TELEMAC-2D examples to see how it is done with NEA atlas or TPXO-like tidal solutions, and of course the TELEMAC-3D or TELEMAC-2D user manuals. Elevation and horizontal velocity boundary conditions are computed by TELEMAC-3D from an harmonic constants database (JMJ from LNH). If a tidal solution from OSU has been downloaded (e.g. TPXO, European Shelf), it can be used to compute elevation and horizontal velocity boundary conditions as well.

### 34.2.5 Physical parameters

Vertical turbulence model: mixing length model

Horizontal viscosity for velocity:  $10^{-4} \text{ m}^2/\text{s}$

Coriolis: yes (constant coefficient over the domain =  $1.10 \times 10^{-4} \text{ rad/s}$ )

No wind, no atmospheric pressure, no surge and nor waves

### 34.2.6 Numerical parameters

Time step: 20 s

Simulation duration: 90,000 s = 25 h

Non-hydrostatic version

Advection for velocities: Characteristics method

Thompson method with calculation of characteristics for open boundary conditions

Free Surface Gradient Compatibility = 0.5 (not 0.9) to prevent on wiggles

Tidal flats with correction of Free Surface by elements, treatments to have  $h \geq 0$

### 34.2.7 Comments

If a tidal solution from OSU has been downloaded (e.g. TPXO, European Shelf), it can be used to compute initial conditions with the keyword INITIAL CONDITIONS set to TPXO SATELLITE ALTIMETRY. Thus, both initial water levels and horizontal components of velocity can be calculated and may vary in space.

## 34.3 Results

Tidal range, sea levels and tidal velocities are well reproduced compared to data coming from the SHOM or at sea measurements. In Figure 34.3 the water depth and free surface elevation at final time are shown in the case of the JMJ database. In Figure 34.4 the surface velocity magnitude, vectors and streamlines are plotted from the 3D RESULT FILE. If using the 2D RESULT FILE, a mask for tidal flats could be added for variable fields.

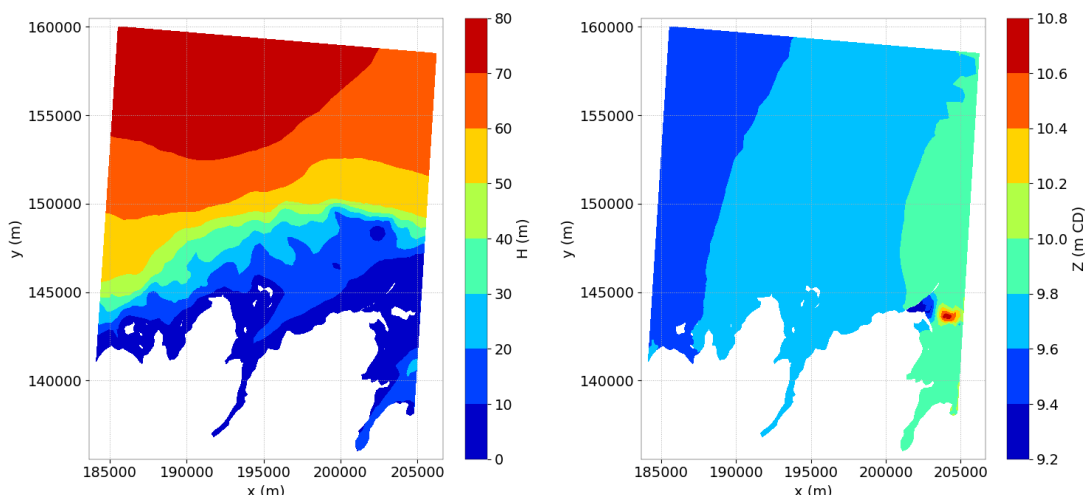


Figure 34.3: Water depth (in m) and free surface elevation (in m CD) at final time.

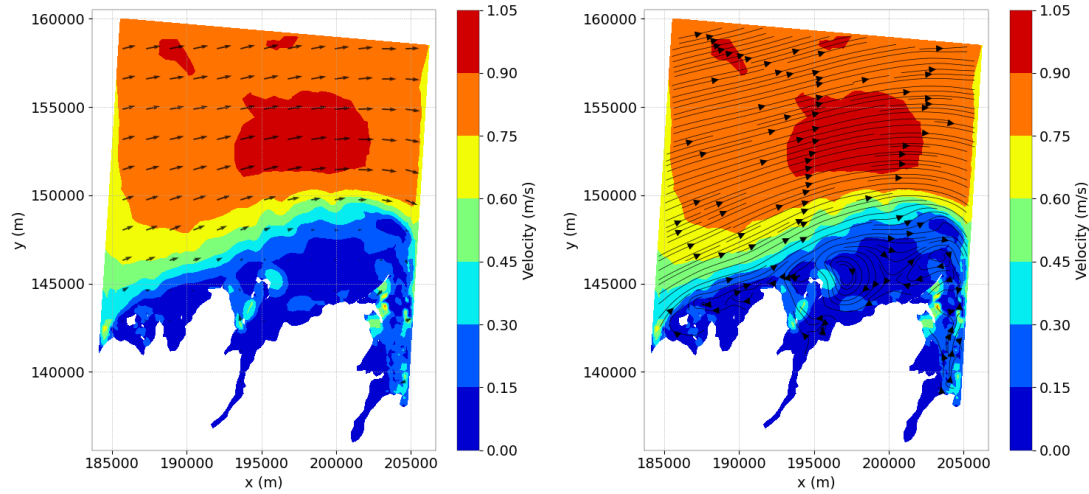


Figure 34.4: Surface velocity (in m/s) at final time (with vectors on the left and streamlines on the right).

Depth-averaged velocity magnitude, vectors and streamlines can be plotted from the 2D RESULT FILE (see Figure 34.5).

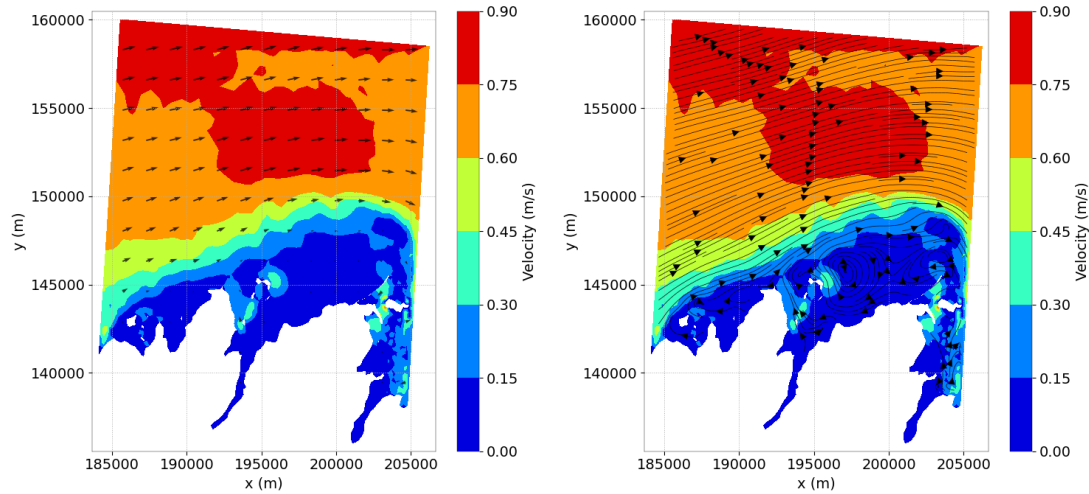


Figure 34.5: Depth-averaged velocity (in m/s) at final time (with vectors on the left and streamlines on the right).

Surface velocity can also be plotted from the 2D RESULT FILE with a mask for tidal flats (see Figure 34.6).

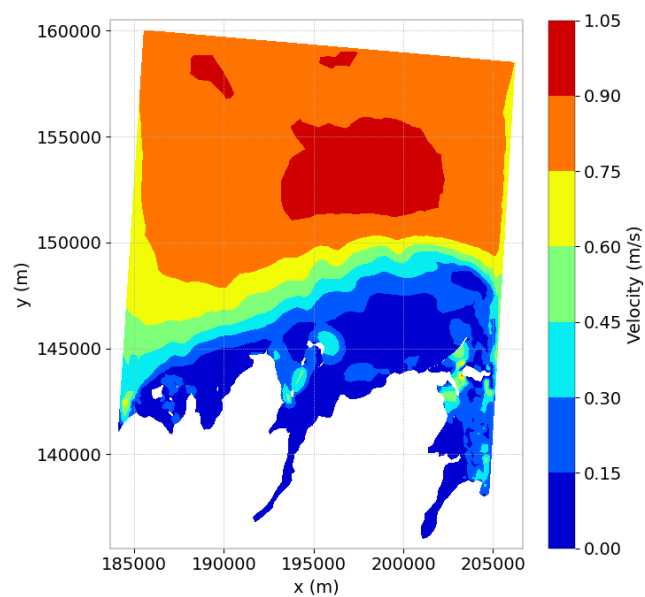


Figure 34.6: Surface velocity (in m/s) at final time with mask for tidal flats.

#### 34.4 Conclusion

TELEMAC-3D is able to model tide in coastal areas.

## 35. Tracer submitted to wetting and drying (tracer\_wet\_dry)

### 35.1 Purpose

This test demonstrates the behaviour of buoyant tracer released from a source in an intertidal environment. The purposes are to ensure tracer mass conservation (particularly under wetting and drying), and to raise a flag if new code developments have modified the advection or diffusion of tracers.

### 35.2 Description

The model domain is a channel 2,000 m long and 100 m wide, with a sloping bed. Buoyant tracer is added to the model from a source at the middle of the domain (unit flow rate and concentration). The tracer rises to the surface and spreads horizontally, as the water level rises and falls, inundating and exposing part of the bed. Water level variations are defined using a sine curve at the offshore boundary. The characteristics of the case are the following:

- maximum streamwise velocity of the offshore boundary during simulation  $U_0 = 0.04 \text{ m.s}^{-1}$ ,
- water depth amplitude of the offshore boundary (sine curve)  $H_0 = 2.0 \text{ m}$ ,
- total duration of the event  $T = 33,300 \text{ s}$ ,
- channel length  $L = 2,000 \text{ m}$ ,
- channel width  $l = 100 \text{ m}$ ,
- Reynolds Number  $R_e = \frac{U_0 \times H_0}{\nu} = 8 \times 10^4$  where  $\nu$  is the kinematic viscosity of water,
- Froude Number  $F_r = \frac{U_0}{\sqrt{g \times H_0}} = 0.009$  where  $g$  is the gravity acceleration.

#### 35.2.1 Geometry and Mesh

The model is a channel of length 2,000 m and width 100 m. A triangular mesh is constructed on the 2D domain with the following characteristics (see Figure 35.1):

- 1,000 triangular elements,
- 606 nodes.

For the 3D Mesh, 6 regularly spaced planes are used.

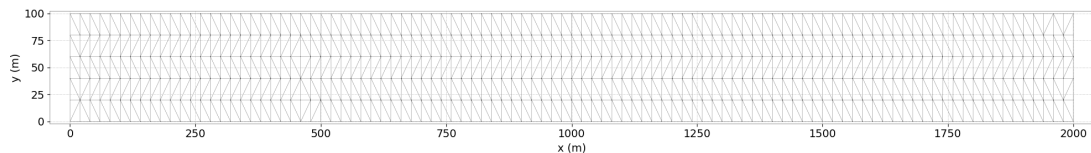


Figure 35.1: 2D Mesh of the Tracer wet/dry case.

### 35.2.2 Bathymetry

The bathymetry is a simple sloped bed with constant gradient from  $z = 0$  m to  $z = 2$  m, as in Figure 35.2.

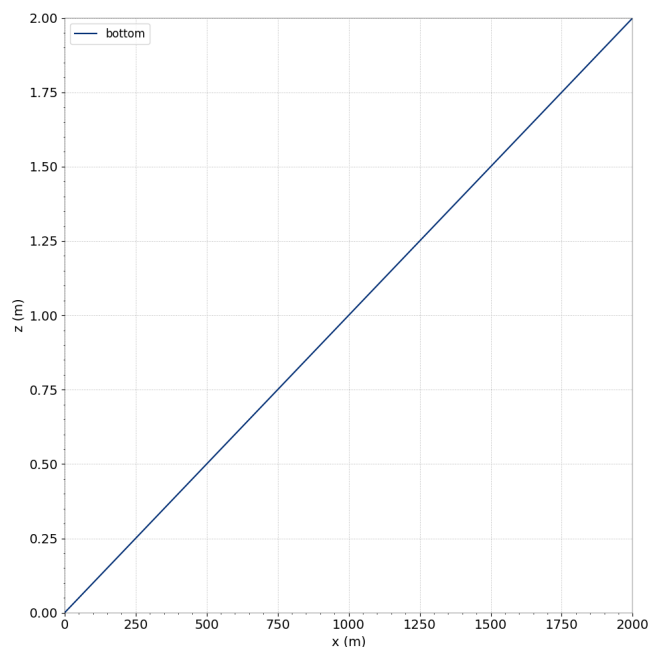


Figure 35.2: Longitudinal bathymetry profile of the Tracer wet/dry test case.

### 35.2.3 Numerical parameters

### 35.2.4 Initial conditions

At the beginning of the simulation, the free surface level is constant and equal to 1.1 m. The water is at rest (zero velocity everywhere) and the tracer value is set to 0.

### 35.2.5 Boundary conditions

The boundaries are solid everywhere, and the bottom friction is calculated using Nikuradse's formula with roughness length of 0.001 m. The elevation and tracer are prescribed with free velocity at offshore boundary ( $z = 0$  m). The tracer source is located in abscissa 1,000 m, ordinate 60 m and elevation 1 m. At its source, the discharge is set to 1.0 m<sup>3</sup>/s and the tracer value to 1.0 g/L (= 1.0 kg/m<sup>3</sup>).

### 35.2.6 Cases

For this test case, three different simulations are run. The following characteristics are common to all cases:

- time step: 10 s,
- simulation duration: 86,400 s (1 day),
- hydrostatic version,
- advection of velocities: Characteristics (default scheme until version 8.0).

The simulation parameters specific to each case are summed up in Table 35.1.

Case	Name	Advection scheme for tracers
1	LEO POSTMA	Leo Postma scheme for tidal flats
2	CHAR	characteristics scheme
3	MURD	N-scheme for tidal flats

Table 35.1: List of the simulation parameters used for the three cases tested in the Tracer wet/dry example.

### 35.2.7 Physical parameters

In the simulations, the Coriolis force and the wind effect are not taken into account. Besides, the viscosity is set as constant and equal to  $0.1 \text{ m}^2/\text{s}$  on horizontal directions and to  $10^{-6} \text{ m}^2/\text{s}$  on the vertical directions.

For the tracer, a constant diffusion is considered. The diffusivity coefficient value is set to  $0.01 \text{ m}^2/\text{s}$  on horizontal directions and to  $10^{-6} \text{ m}^2/\text{s}$  on the vertical directions. The used tracer density law is the  $\beta$  spatial expansion with a coefficient of  $0.0003 \text{ K}^{-1}$ . The standard value of the tracer is set to 0.

## 35.3 Results

### 35.3.1 First observations

The evolution of water depth on the offshore boundary can be seen in Figure 35.3.

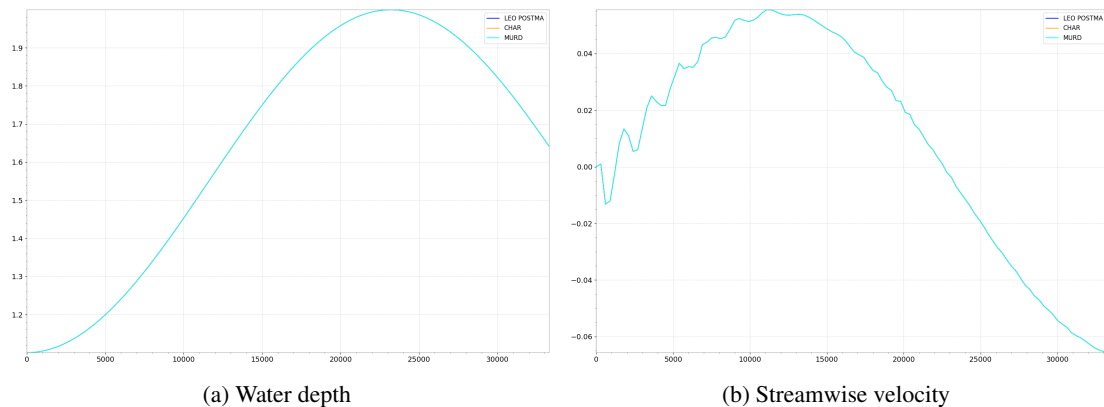


Figure 35.3: Evolution of water depth and velocity on the offshore boundary of the Tracer wet/dry case - Point of coordinates (0 m, 50 m).

On the other hand, the evolution of the tracer can be seen in Figure 35.4, for scheme LEO POSTMA for example.

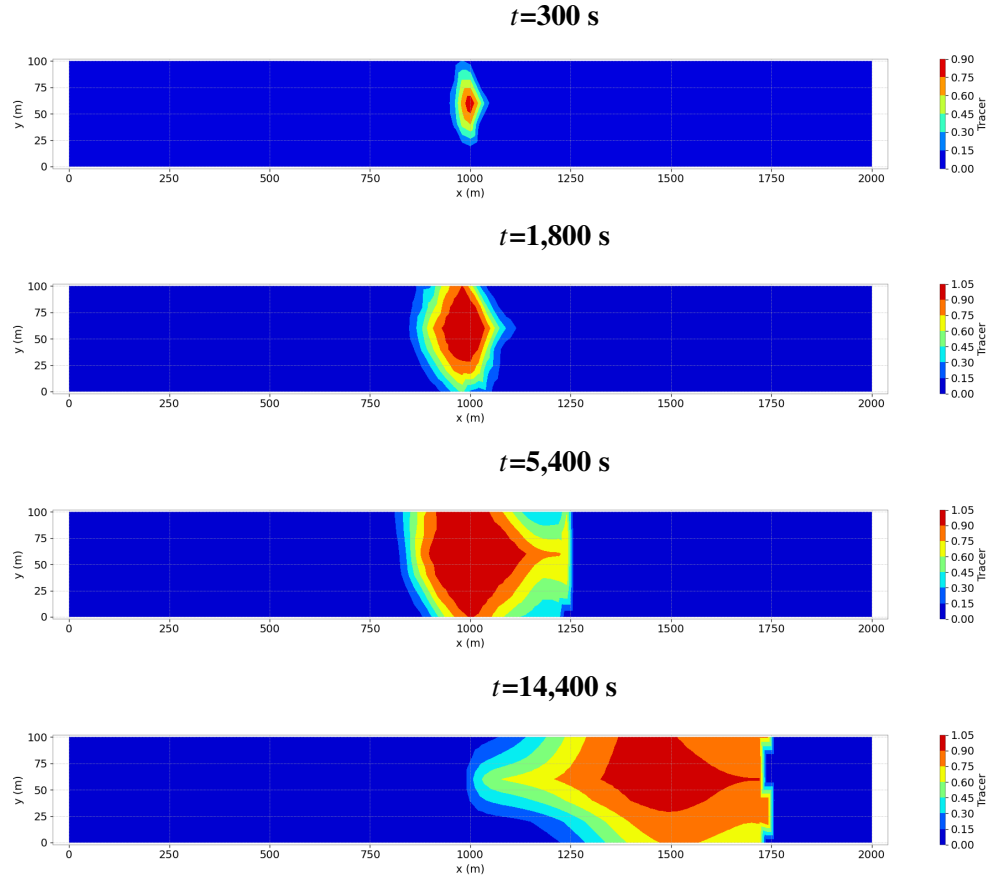


Figure 35.4: Evolution of the tracer at the free surface for case LEO POSTMA on the Tracer wet/dry example.

The buoyant tracer rises and is advected onshore by the currents and rising water levels. The water then recedes, exposing the bank and carrying the plume offshore.

The simulation demonstrates that:

- a source of buoyant tracer behaves as expected (tracer rises to the surface, is advected with the ambient currents, and pools near the source during periods of weak current),
- the value of tracer on a dry node is retained from the last time the node was wet.

### 35.3.2 Comparison of schemes

#### Performance

Performance tests are conducted on the cases. The studied variable here is the water depth.

Simulation times for each of these cases with sequential and parallel runs (using 4 processors) are shown in the Table 35.2<sup>1</sup>.

---

<sup>1</sup>Keep in mind that these times are specific to the validation run and the type of the processors that were used for this purpose.

CPU Time	LEO POSTMA	CHAR	MURD
Sequential	0 M 26 S	0 M 28 S	0 M 30 S
Parallel	0 M 10 S	0 M 10 S	0 M 10 S

Table 35.2: Time of simulation for different cases of the Tracer wet/dry example.

Sequential and parallel simulations results are compared for each case in the Table 35.3. That allows to quantify the loss of information that goes along with the partitioning of the mesh.

	$\ \varepsilon\ _{L^1}$	$\ \varepsilon\ _{L^2}$	$\ \varepsilon\ _{L^\infty}$
LEO POSTMA	0.000e+00	0.000e+00	0.000e+00
CHAR	0.000e+00	0.000e+00	0.000e+00
MURD	0.000e+00	0.000e+00	0.000e+00

Table 35.3: Sequentiel VS Parallel - Errors on water depth values of the Tracer wet/dry case.

### Accuracy

The comparison of the impact of the chosen scheme on the advection of tracer can be seen in Figure 35.5.

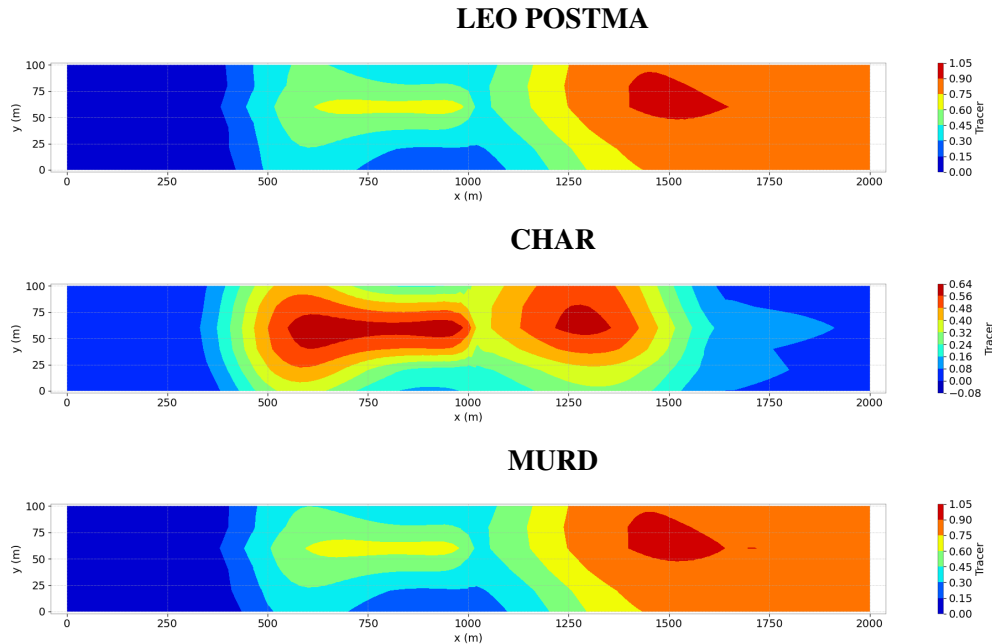


Figure 35.5: Comparison of tracer at last time step at the free surface all cases on the Tracer wet/dry example.

The behaviours of schemes LEO POSTMA and MURD are comparable. CHAR scheme gives different results. In order to check if the values of tracer are physical, the maximum and minimum values during the simulation for each scheme are shown resp. in the Tables 35.4 and 35.5.

Schemes	LEO POSTMA	CHAR	MURD
Minimim H [m]	0.00E+00	-4.11E-01	0.00E+00

Table 35.4: Minimum value of tracer through the simulation for each case of the Tracer wet/dry example.

Schemes	LEO POSTMA	CHAR	MURD
Minimim H [m]	1.00E+00	1.05E+00	1.00E+00

Table 35.5: Maximum value of tracer through the simulation for each case of the Tracer wet/dry example.

### Positivity

Furthermore, the positivity of the used scheme can be checked for all cases. In order to achieve this, the minimum value of the water depth during the whole simulation, and on all the points of the mesh, is transcribed in Table 35.6.

Schemes	LEO POSTMA	CHAR	MURD
Minimim H [m]	0.00E+00	0.00E+00	0.00E+00

Table 35.6: Minimum value of water depth through the simulation for each case of the Tracer wet/dry example.

### Mass conservation

The mass conservation can be checked by calculating the volume in the domain during time (as the density is constant in time and space). Lost volume is calculated as  $V_{initial} - V_{final}$ .

		LEO POSTMA	CHAR	MURD
Sequential	Lost volume [ $m^3$ ]	1.60E-10	-1.89E-10	2.91E-11
	Relative error	<b>2.65E-15</b>	<b>-3.13E-15</b>	<b>4.81E-16</b>
Parallel	Lost volume [ $m^3$ ]	-1.89E-10	1.60E-10	-4.37E-11
	Relative error	<b>-3.13E-15</b>	<b>2.65E-15</b>	<b>-7.22E-16</b>

Table 35.7: Volume loss and relative error for different schemes of the Tracer wet/dry example.

The evolution of water volume is shown in Figure 35.6.

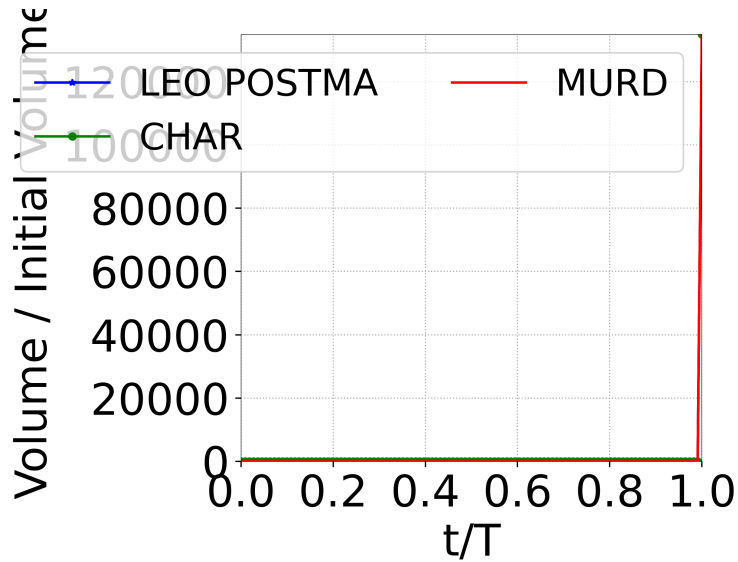


Figure 35.6: Evolution of water volume for the tested schemes on the Tracer wet/dry case.

There is in fact a volume creation because a free surface evolution is imposed at the upstream boundary via a liquid boundaries file (sine curve). In order to have a real check of mass conservation, the difference between the volume and the created volume generated by the flux can be plotted, in Figure 35.7.

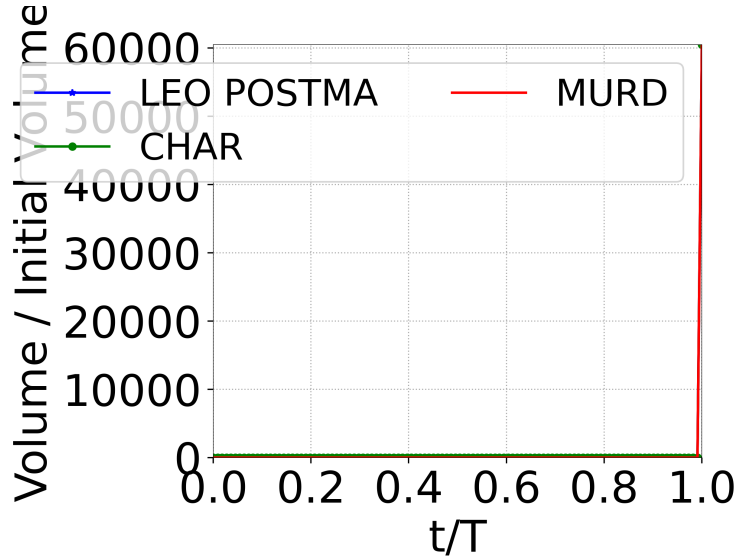


Figure 35.7: Evolution of the initial water volume for the tested schemes on the Tracer wet/dry case.

The three studied schemes conserve the mass of water. On the other hand, analysis of the tracer mass shows a constant increase because of the presence of a source in the middle of the channel (Figure 35.8).

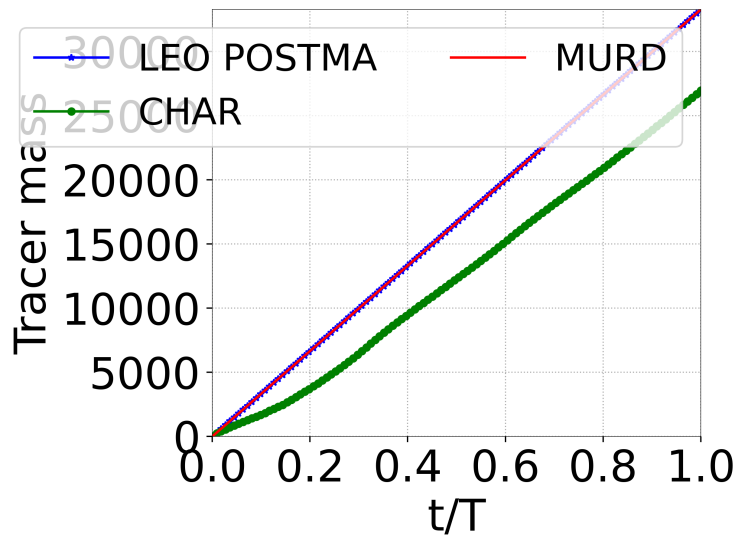


Figure 35.8: Evolution of tracer mass for the tested schemes on the Tracer wet/dry case.

There is a difference between the behaviour of MURD and LEO POSTMA schemes on one side, and the CHAR scheme on the other. In order to check if no spurious tracer mass is created, we can check the evolution of the difference between the tracer mass and the created tracer mass generated by the source (Figure 35.7). This shows a behaviour of the characteristics scheme that is unwanted. The LEO POSTMA and MURD schemes behave perfectly.

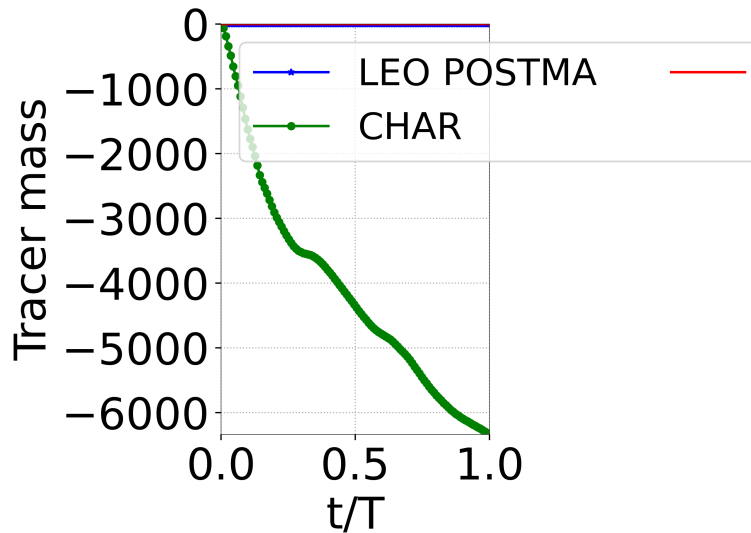


Figure 35.9: Evolution of the initial tracer mass for the tested schemes on the Tracer wet/dry case.

## 35.4 Conclusion

TELEMAC-3D correctly simulates the buoyancy of an active tracer, with a good tracer and water mass conservation. In order to achieve this kind of simulations, one should use the recommended schemes: LEO POSTMA or MURD.

## 36. Solitary wave propagation over an uneven bottom (uneven)

### 36.1 Purpose

This test demonstrates the availability of TELEMAC-3D to propagate a wave over an uneven seabed.

### 36.2 Description

The configuration is a rectangular channel (600 m long and 6 m wide) with a solitary wave that propagates over an uneven seabed.

A piecewise affine bathymetry only dependent on the abscissa coordinate  $x$  is defined (see Figure 36.1):

$$\begin{cases} \text{if } x < 160, & z = -10, \\ \text{if } 160 \leq x < 260, & z = -10 - 0.05(160 - x), \\ \text{if } x \geq 260, & z = -5. \end{cases}$$

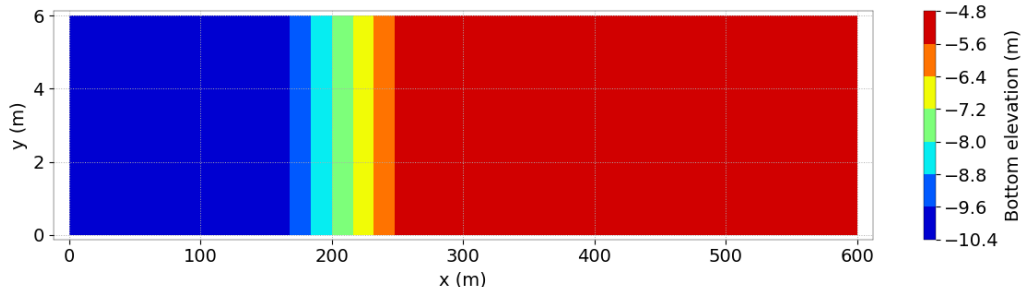


Figure 36.1: Bottom elevation.

#### 36.2.1 Initial and Boundary Conditions

An analytical solution of solitary wave is used as initial condition for the water depth and the horizontal velocity components.

The boundary conditions are only closed boundaries:

- For the solid walls, a slip condition on channel banks is used for the velocities,
- No bottom friction.

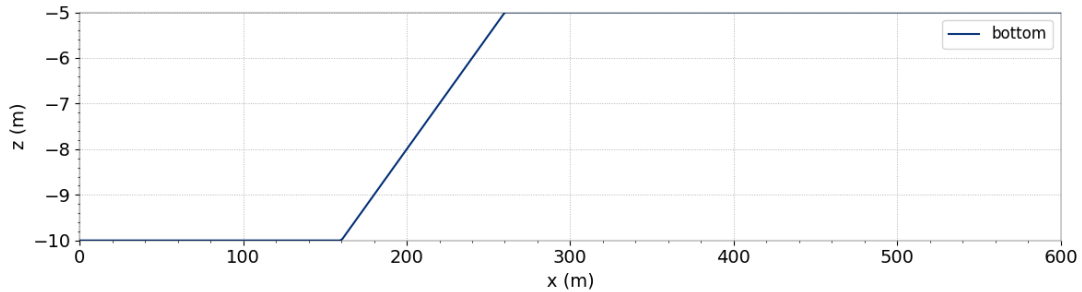


Figure 36.2: Profile.

### 36.2.2 Mesh and numerical parameters

The 2D mesh (Figure 36.3) is made of 7,206 triangular elements (4,210 nodes).

3 planes are regularly spaced in the vertical direction (see Figure 36.4).

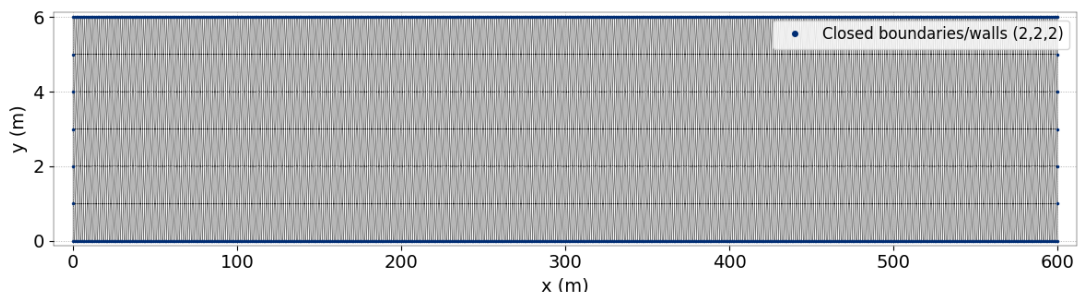
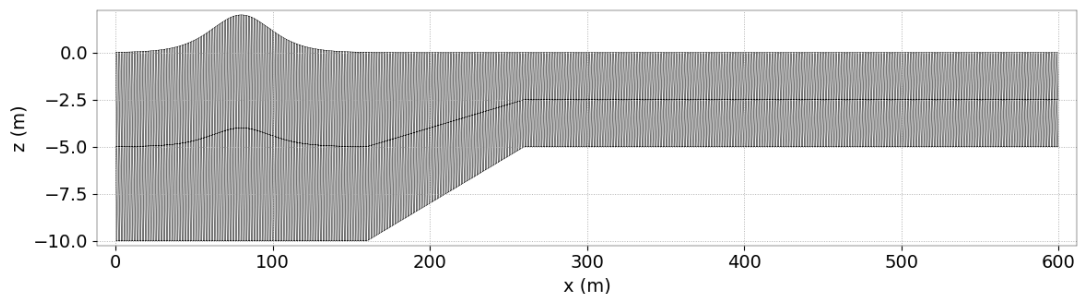


Figure 36.3: Horizontal mesh.

Figure 36.4: Initial vertical mesh along  $y = 1$  m.

The non-hydrostatic version of TELEMAC-3D is used.

To solve the advection, the method of characteristics is used for velocities.

The time step is 0.25 s for a simulated period of 25 s.

### 36.2.3 Physical parameters

No diffusion is considered.

### 36.3 Results

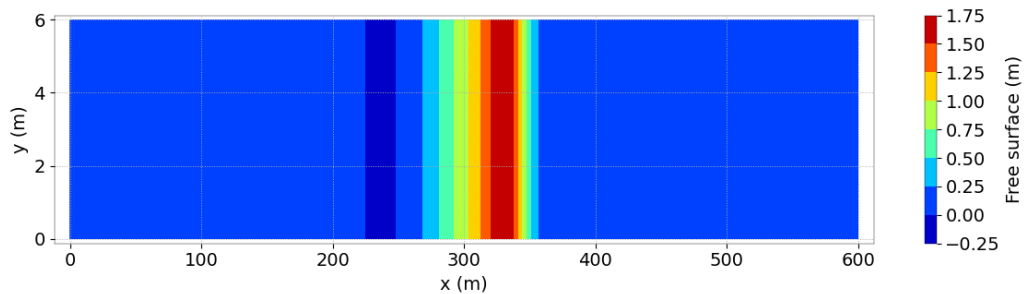


Figure 36.5: Free surface at final time step.

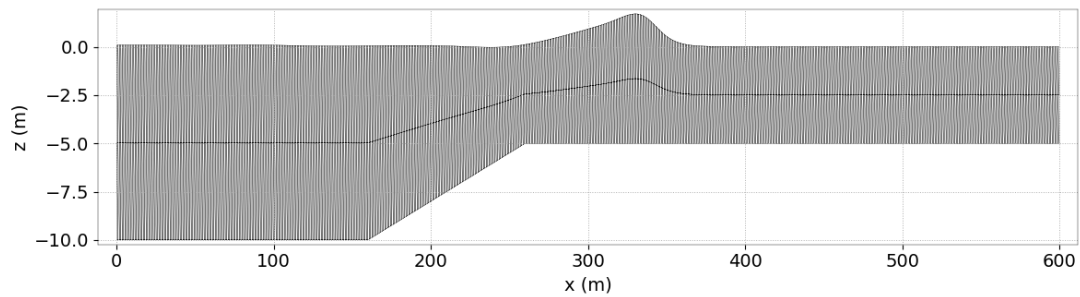


Figure 36.6: Vertical section of free surface at final time step.

## 37. Uncovering of a beach (vasque)

### 37.1 Purpose

This test demonstrates the ability of TELEMAC-3D to model water retention in a bowed beach during ebbing tide.

### 37.2 Description

A beach profile presenting a bowl is considered. Its extent is a channel of size  $46 \text{ m} \times 9 \text{ m}$ . The water level is initially at high tide level, covering the entire domain (see Figure 37.1).

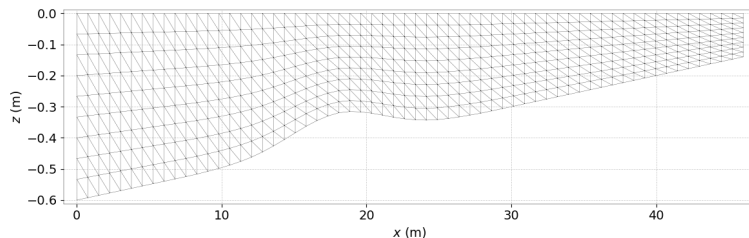


Figure 37.1: Initial free surface elevation and bottom elevation.

The ebbing tide is simulated with the seaward final water level below the beach bowl.

#### 37.2.1 Geometry and mesh

The bathymetry is a beach profile starting at  $z = -0.14 \text{ m}$ , presenting a bowl, and ending at  $z = -0.6 \text{ m}$ . It is defined by  $z = -0.6 + 0.01x + 0.1e^{\frac{-(x-19)^2}{20}}$ , see Figure 37.2.

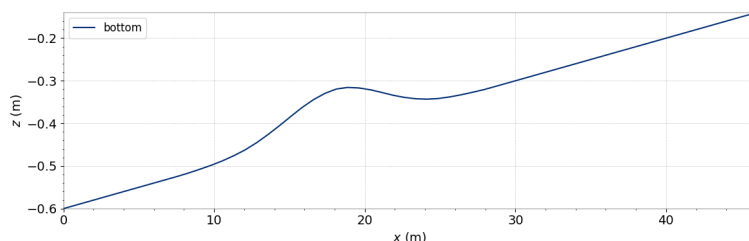


Figure 37.2: Bathymetry.

The bowed beach profile is specified in the `USER_T3D_CORFON` subroutine.

The mesh is regular. It is made of squares split into two triangles (see Figure 37.3) with the following characteristics:

- 828 triangular elements,
- 470 nodes,
- Maximum size range:  $\sqrt{2}$  m.

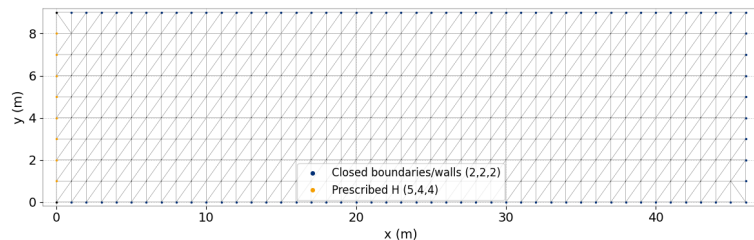


Figure 37.3: Horizontal mesh.

10 planes are regularly spaced on the vertical (see Figure 37.4 for the initial distribution).

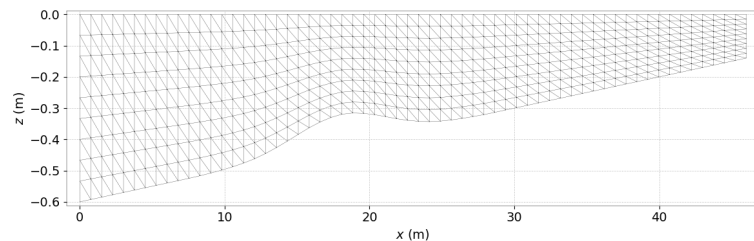


Figure 37.4: Vertical mesh at initial time step.

### 37.2.2 Physical parameters

A constant viscosity of  $0.1 \text{ m}^2/\text{s}$  is used in both directions. A Strickler law with coefficient equal to  $40 \text{ m}^{1/3}/\text{s}$  is used to model bottom friction.

### 37.2.3 Initial and boundary conditions

Constant free surface level at  $z = 0 \text{ m}$  corresponding to high tide and no velocity are used as initial conditions.

The boundary conditions are:

- Shoreline: solid wall with slip condition (closed boundaries on sides and landward),
- Seaward boundary controlling decreasing water depth (ebbing tide) with `USER_SL3` function:  $z = 0.275 (\cos(\frac{2\pi}{600}t) - 1)$  is imposed,
- Lateral boundaries: solid walls with slip condition in the channel.

### 37.2.4 Numerical parameters

The non-hydrostatic version of TELEMAC-3D is used. To solve the advection, the method of characteristics (scheme #1) is used for velocities. The time step is 0.5 s for a simulated period of 300 s.

## 37.3 Results

Figures 37.5 and 37.6 present longitudinal cross profiles of water level at initial and final times of the simulation. The water level decreases regularly over the beach. At final time, the bowl is filled of water and the water level is completely horizontal, while the seaward water level is below the bowl position (see Figures 37.6 and 37.7).

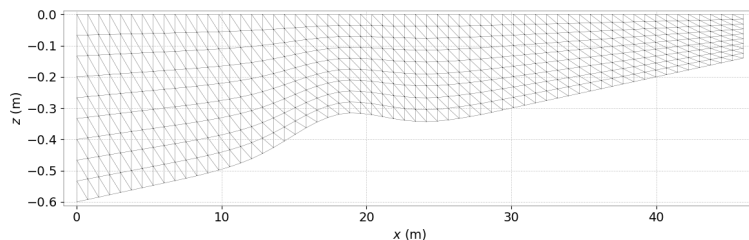


Figure 37.5: Free surface elevation at initial time.

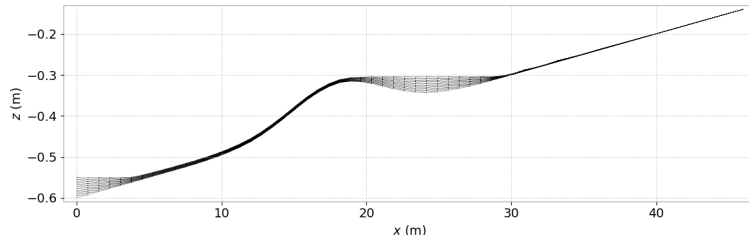


Figure 37.6: Free surface elevation at final time (= 300 s).

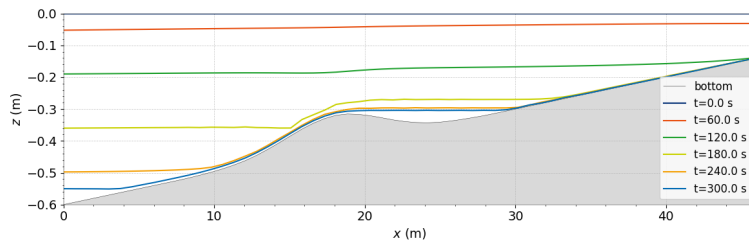


Figure 37.7: Evolution of the free surface elevation in time.

## 37.4 Conclusion

TELEMAC-3D is capable to model water retention in bathymetry bowls.

## 38. Flow in a channel submitted to wind (vent)

### 38.1 Description

This test, a rectangular channel submitted to a wind, demonstrates the availability of TELEMAC-3D to represent the currents induced by wind blowing at the surface of a closed channel. More precisely, this case allows verifying that a linear decrease of the mixing length model at the bottom and at the surface is able to reproduce such circulation. Moreover, this test allows verifying the proper implementation of the sources terms and external forces as the wind.

The geometry dimensions of rectangular channel is 500 m long and 100 m wide, with horizontal bed at depth -10 m. At the initial state, the channel is submitted to a constant  $10 \text{ m} \cdot \text{s}^{-1}$  wind. The wind generates a slope of the free surface and a vertical two-dimensional circulation. Tsanis [1] has made an inventory of existing laboratory or in-situ measurements and has plotted these values on a non-dimensional graph. He deduced a characteristic vertical velocity profile (Figure 38.1), which will be compared to the numerical results of this test case. Tsanis mixing length turbulence model is so used for the vertical turbulence model.

The turbulent viscosity has the following expression:

$$\nu_t = l^2 \sqrt{\frac{1}{2} \left[ \frac{\partial u_i}{\partial x_j} + \frac{\partial u_j}{\partial x_i} \right]^2},$$

where  $l$  is mixing length and  $h$  the water depth.

On the other hand, the horizontal viscosity for velocity is constant and equal to  $0.1 \text{ m}^2 \cdot \text{s}^{-1}$ .

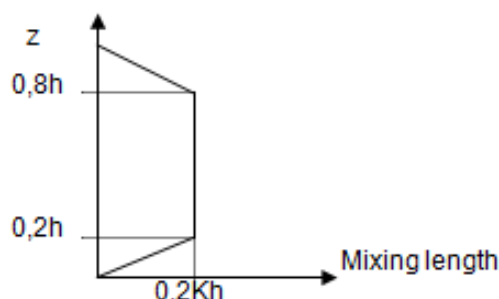


Figure 38.1: Characteristic vertical velocity profile, where  $K$  is Karman constant equal to 0.40.

Wind induces a wind stress ( $\tau$ ) at the free surface of channel. The wind stress is written as follows:

$$\tau = \rho_{air} K_F \mathbf{w} |\mathbf{w}|,$$

With:

$$\mathbf{w} = 10 \text{ m} \cdot \text{s}^{-1} \text{ Velocity of wind,}$$

$$K_F = \frac{(-0.12 + 0.137 \|\mathbf{w}\|)}{1000}.$$

### 38.1.1 Initial and Boundary Conditions

The initial water level is 0 m and the velocity is null.

The boundary conditions are:

- For the solid walls, a slip condition on the channel banks is used for the velocity,
- On the bottom, a friction stress due to mixing length is taken into account.

For the wind, the conditions are :

- A wind velocity equal to  $10 \text{ m} \cdot \text{s}^{-1}$ ,
- The coefficient of wind influence is  $a_{wind} \frac{\rho_{air}}{\rho_{water}} = 1.625 \cdot 10^{-6}$  with  $\rho_{air}$ ,  $\rho_{water}$  which are respectively the air density and the water density and with  $a_{wind}$  an addimentional coefficient,
- Shear stress wind is taken account on the surface water.

### 38.1.2 Mesh and numerical parameters

The mesh (Figures 38.2, 38.3 and 38.4) is composed of 543 triangular elements (315 nodes) with 15 planes irregularly spaced on the vertical, to form prism elements.

The time step is 10 s for a simulated period of 20,000 s (5 h 33 min 20 s).

This case is computed with the hydrostatic pressure hypothesis. To solve advection, the LIPS scheme is used for the velocities and Diagonal preconditioning is used for propagation (default option). The resolution accuracy is  $10^{-8}$  for the diffusivity velocity and  $10^{-8}$  for the propagation (default values). The implicitation coefficients for depth and velocities are equal to 0.6.

## 38.2 Results

The mass balance is the following:

INITIAL MASS	:	500000.0
FINAL MASS	:	500000.0
MASS LEAVING THE DOMAIN (OR SOURCE)	:	0.000000
MASS LOSS	:	-0.2517768E-03

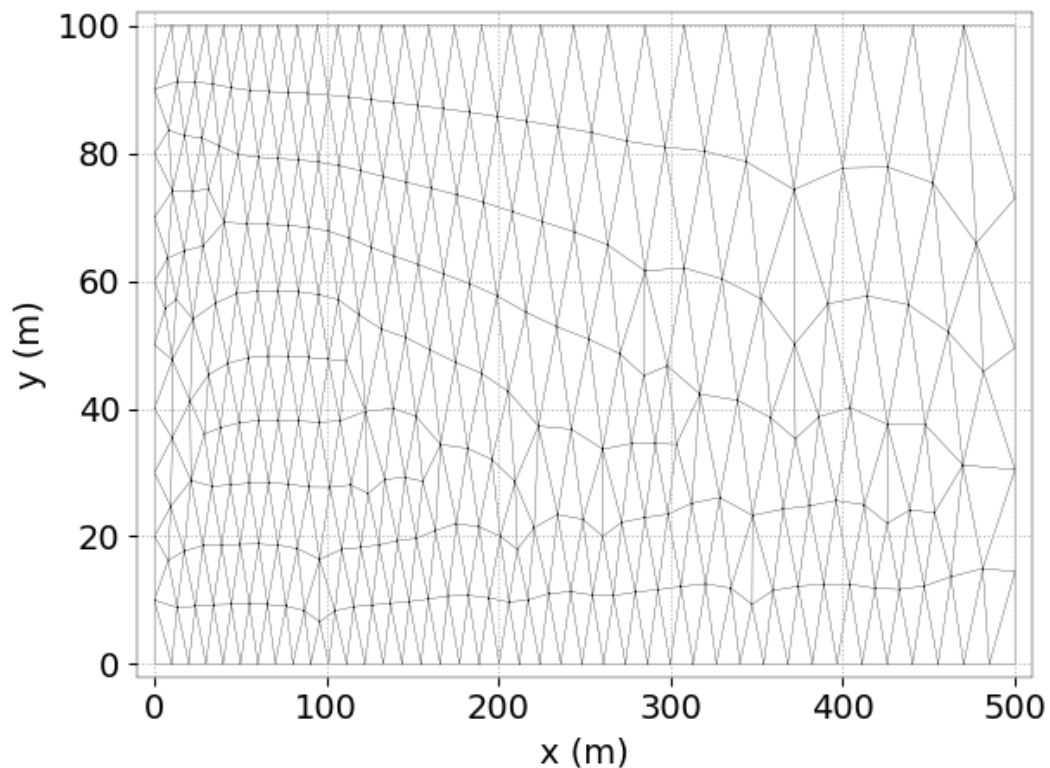


Figure 38.2: Horizontal mesh.

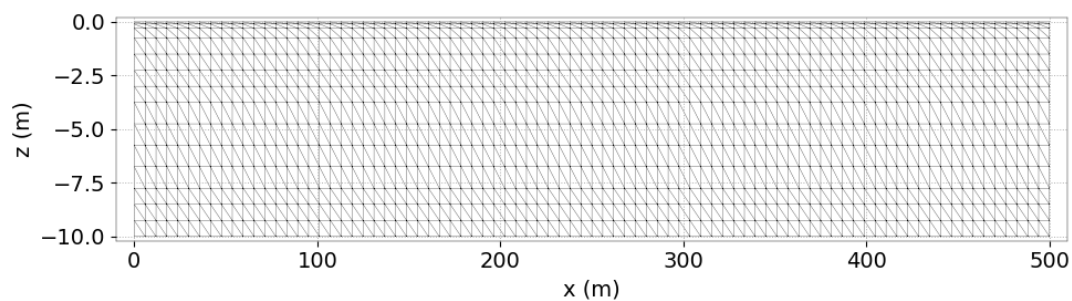


Figure 38.3: Full vertical mesh.

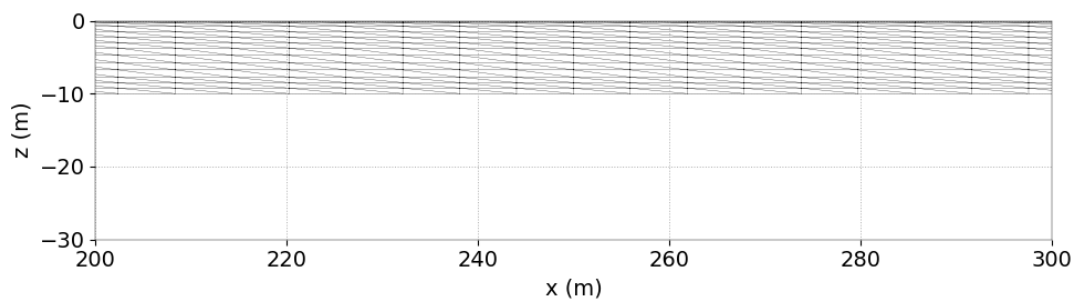


Figure 38.4: Zoom on vertical mesh close to the surface.

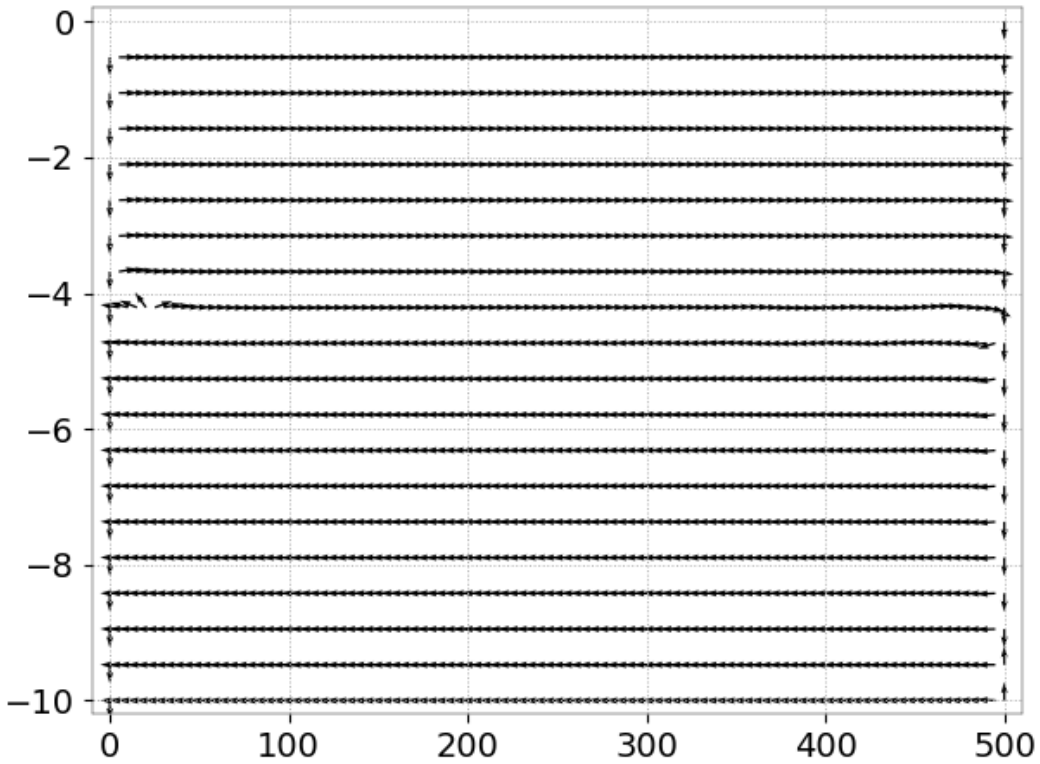


Figure 38.5: The vertical circulation induced by the wind.

Thus, the mass balance is consistent with the accuracy asked (from  $10^{-8}$  to  $10^{-6}$  depending on the system to solve, for the diffusion of velocities or propagation). Figure 38.5 shows the vertical circulation induced by the wind.

The velocity at the surface is  $0.18 \text{ m} \cdot \text{s}^{-1}$  and the return current reaches a maximum value of  $0.058 \text{ m} \cdot \text{s}^{-1}$  (Figure 38.6). However, it must be pointed out that the velocity at the surface depends on the refinement near the surface because the velocity gradient is very high in this area. A distance between the two first vertical points of  $0.50 \text{ m}$  instead of  $0.10 \text{ m}$  induced a velocity at the surface of  $0.12 \text{ m} \cdot \text{s}^{-1}$ , but the velocity field below  $1 \text{ m}$  under the surface was only slightly modified. J. Wu [2] proposed for the velocity  $\mathbf{u}_s$  us at the surface the expression:

$$\mathbf{u}_s = 0.55 \left( \frac{\tau}{\rho_{air}} \right)^{1/2}.$$

This gives  $\mathbf{u}_s = 0.19 \text{ m} \cdot \text{s}^{-1}$ . Then, the velocity computed with a mesh of  $0.10 \text{ m}$  is very close to this theoretical value. Figure 38.7 shows the non-dimensional plot of the vertical velocity profile. The numerical results fit the measurements reasonably well. The upper part of the profile, where the velocities have the same orientation as the wind, is close to measured profiles, but the lower part is smoothed. This could mean that the turbulence intensity is stronger in nature. The slope of the free surface presented in figure 38.8 is equal to  $1.58 \cdot 10^{-6}$  (between  $x = 100 \text{ m}$  and  $x = 400 \text{ m}$ ). The computation of the slope, assuming that the flow is homogeneous on the vertical, gives a slope equal to  $1.66 \cdot 10^{-6}$ . This value is in agreement with the value given by TELEMAC-3D.

The velocity field produced by TELEMAC-3D using the standard mixing length is correct. Near

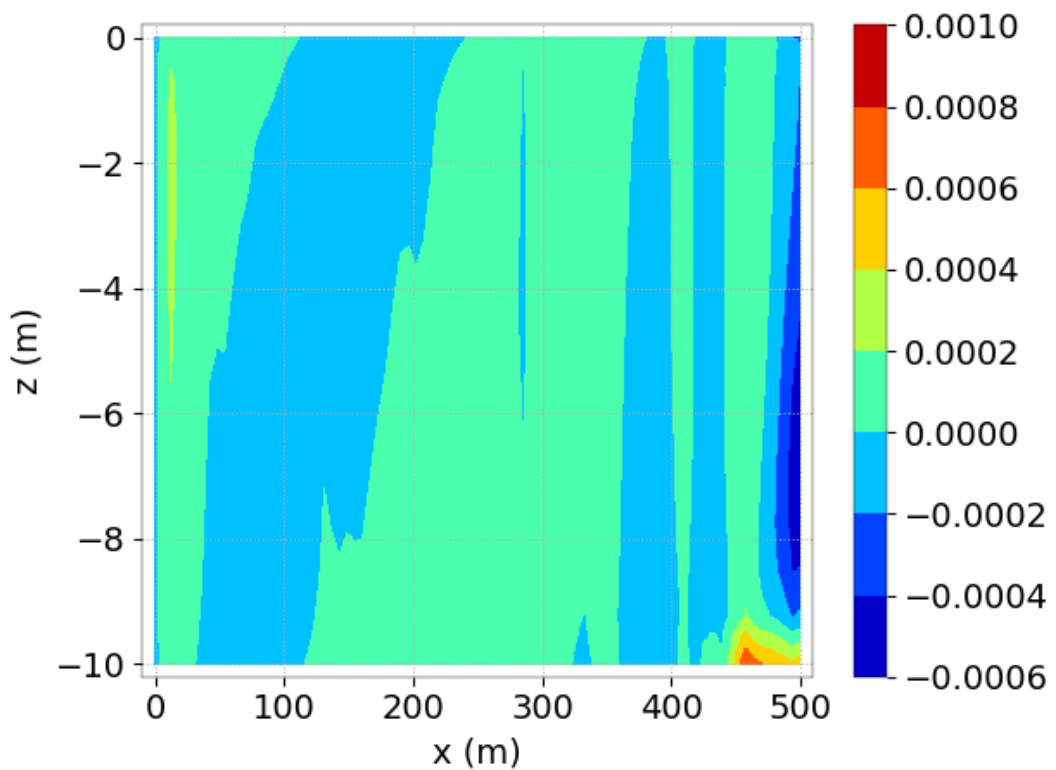


Figure 38.6: Velocity field on the vertical.

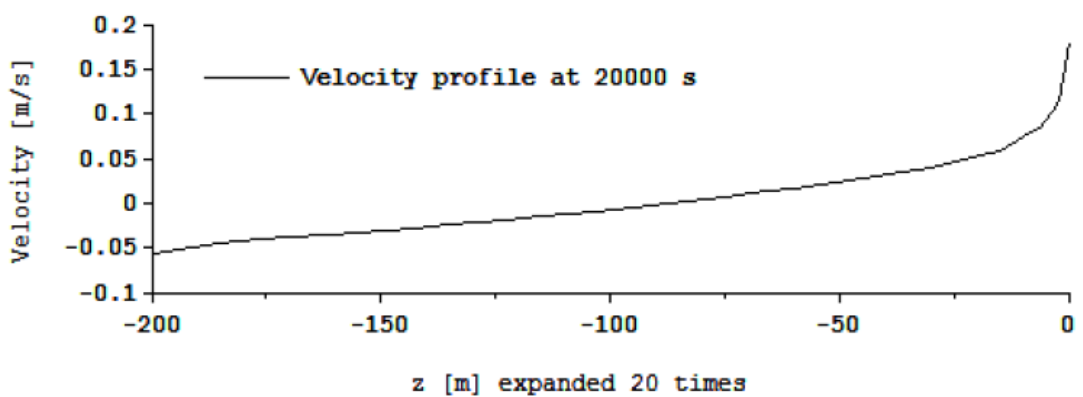


Figure 38.7: Vertical profile of velocity.

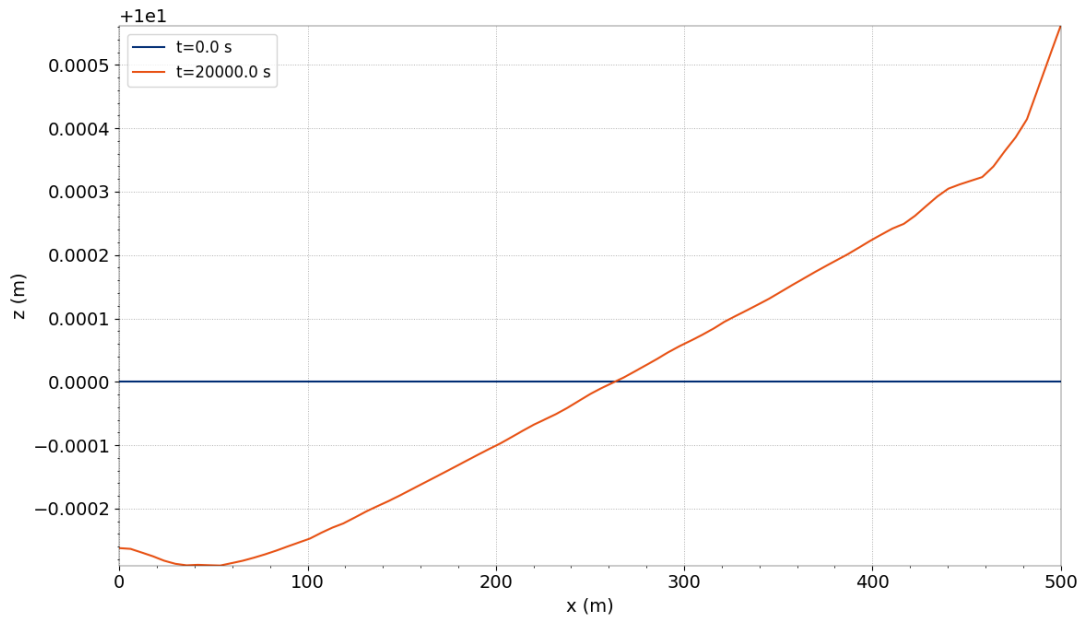


Figure 38.8: Free surface.

the surface, the quality of the results depends on the vertical resolution near the surface. The second level of the vertical mesh should be fixed 0.10 m below the surface for a good result. In the deeper part, the profile is a little bit more smoothed. Taking into account the effect of the wind directly into the turbulence model may improve this result.

### 38.3 Reference

- [1] TSANIS I., Simulation of wind-induced water currents, Journal of Hydraulic Engineering, Vol.115, n 8, 1989, pp 1113-1134.
- [2] WU J., Prediction of near-surface drift currents from wind velocity, Journal of Hydraulic Division, 99, 1973, pp 1291-1302.

- [1] C. Adduce, G. Sciortino, and S. Proietti. Gravity currents produced by lock exchanges: Experiments and simulations with a two-layer shallow-water model with entrainment. *Journal of Hydraulic Research*, 138(2), 2012.
- [2] D. Barr. Densimetric exchange flow in rectangular channels. III. large scale experiments. *La Houille Blanche*, (22):619–632, 1967.
- [3] T. Benjamin. Gravity currents and related phenomena. *Journal of Fluid Mechanics*, 31 (2):209–248, 1968.
- [4] M. Benoit. Projet clarom-ecomac (fiche cep&m m06101.99). modélisation non-linéaire par les équations de boussinesq de la propagation des vagues non-déferlantes en zone côtière. Technical Report HP-75/01/069, EDF R&D-LNHE, 2001.
- [5] M. W. Dingemans. Comparison of computations with boussinesq-like models and laboratory measurements. Technical Report MAST-G8M note, H1684, 32 pp., Delft Hydraulics note, 1994.
- [6] Audusse E., Bristeau M.-O., Pelanti M., and Sainte-Marie J. Approximation of the hydrostatic navier–stokes system for density stratified flows by a multilayer model. kinetic interpretation and numerical solution. *Journal of Computational Physics*, 230:3353–3478, 2011.
- [7] J-M. HERVOUET. *Hydrodynamics of free surface flows. Modelling with the finite element method*. John Wiley & Sons, Ltd, Paris, 2007.
- [8] J.-M. Hervouet and C. Villaret. Profil de rouse modifié, une solution analytique pour valider telemac-3d en sédimentologie. Technical Report HP-75/04/013/A, EDF R&D LNHE, 2004.
- [9] J.A. Jankowski. *A non-hydrostatic model for free surface flows*. PhD thesis, Universität Hannover, 1999. Bericht Nr. 56/1999, Institut für Strömungsmechanik und ERIB.
- [10] Abbas L. Analyse des besoins pour le logiciel de simulation numérique telemac-3d. Technical Report H-P74-2015-05098-FR, Laboratoire d’Hydraulique Saint-Venant, 2015.
- [11] E. V. Laitone. The second approximation to cnoidal and solitary waves. *Journal of Fluid Mechanics*, 9:430–444, 1960.
- [12] Pelanti M. and Salencon M.-J. Simulation of wind-induced phenomena in stratified water bassin by two-dimensienal thermo-hydrodynamic model. Technical report.

- [13] B. Ramaswamy. Numerical simulation of unsteady viscous free surface flow. *Journal of Computational Physics*, 90:396–430, 1990.